NUC TP 393

GLASS OR CERAMIC SPHERICAL-SHELL WINDOW ASSEMBLY FOR 20,000-PSI OPERATIONAL PRESSURE

by

Jerry D. Stachiw

Ocean Technology Department

May 1974

NAVAL UNDERSEA CENTER, SAN DIEGO, CA. 92132

AN ACTIVITY OF THE NAVAL MATERIAL COMMAND

ROBERT H. GAUTIER, CAPT, USN
Commander

Wm. B. McLEAN, Ph.D.
Technical Director

ADMINISTRATIVE STATEMENT

The research covered by this report was conducted in the Ocean Technology Department of the Naval Undersea Center from June 1971 to December 1973 and was funded by the Director of Naval Laboratories under the program for Independent Research and Independent Exploratory Development.

SUMMARY

PROBLEM

Optical systems for search and recovery missions in the deep ocean require pressure-resistant windows that will transmit images without distortion. This can be readily accomplished utilizing a spherical-shell sector as the window shape. But in order for the spherical-shell window to satisfy all of the optical requirements it must also be fabricated from a transparent material that will undergo only very minute displacement and virtually no deformation under hydrostatic loadings encountered at abyssal depths in the ocean.

Although acrylic plastic spherical shell sectors have been utilized widely in manned submersibles, they have not been found adequate for precision optical systems because they experience large displacement and deformation when subjected to high hydrostatic pressure.

APPROACH

Spherical shell sectors with 150-degree included spherical angles were fabricated from optical glass, chemically surface-compressed glass, or transparent ceramic and mounted on a compliant, metallic flange with a plane conical window seat covered by a fiber-reinforced epoxy-plastic bearing gasket. Because the angles on the bearing surface of the window and on the flange window seat matched closely, stress concentrations in the window were minimized. The bearing gasket sandwiched between the window and the flange decreased stress concentrations further.

RESULTS

Extensive testing has shown that chemically surfaced-compressed glass or ceramic spherical-shell windows with a 150-degree included spherical angle and a ratio of thickness to inner radius (t/R_i) of 0.33 will perform reliably for at least 300 long-term cycles to an external hydrostatic pressure of 20,000 psi. At lesser operational pressure the minimum cyclic life is significantly larger.

Spherical shell windows made from annealed optical glass were found to have a cyclic life of only 200 long-term cycles to 20,000-psi pressure.

RECOMMENDATION

It is recommended that the NUC-developed 150-degree spherical-shell window-flange assembly utilizing a chemically surface-compressed glass or ceramic window be employed in unmanned submersible systems for abyssal depths. It is postulated with reasonable assurance that a submersible system equipped with such windows can operate to any ocean depth with a minimum projected fatigue life of 1,000 cycles.

CONTENTS

INTRODUCTION

The Naval Undersea Center (NUC), working with a spherical-shell window with a 150-degree spherical angle and a matching compliant flange, has developed a window-flange assembly that utilizes a glass or ceramic window and is suitable for operational pressures up to 20,000 psi. This paper describes the design, fabrication, and testing of the assembly and presents recommendations for the engineer who may wish to pattern similar assemblies after the NUC prototype.

BACKGROUND

Pressure-resistant optical windows are required both on land and in the sea. On land, they are incorporated into internal pressure vessels serving as deep-ocean simulators and hyperbaric chambers. In the sea, they are employed in the external pressure hulls of manned and unmanned submersibles. In either case, it is desirable that the window-flange assembly, consisting of the window and flange, should take up a minimum of space in the hull while providing a maximum field of view and pressure resistance.

Optical man-rated windows have been developed over the years (references 1-11) to meet operational requirements in the pressure range from −15 to 20,000 psi and the temperature range from −40 to 150° F. Almost without exception, they have been made of methyl metacrylate plastic (acrylic plastic). These windows have been found to be reliable and inexpensive. Because of the acrylic plastic's low strength and tendency to creep, however, window-flange assemblies incorporating acrylic plastic windows are very bulky, particularly those designed for the 10,000- to 20,000-psi pressure range. For example, the ratio of thickness to minor diameter of a 90-degree conical frustum acrylic window for abyssal depths is at least 2.0.

Glass windows have also been used, but as a rule only for low-pressure applications in the chemical processing industry, or for high-pressure applications in deep−submergence photographic systems. In both cases, the windows have been thick, circular, flat disks of small diameter with a thickness-to-diameter ratio approaching or equaling that of flat-disc acrylic plastic windows.

Some spherical-shell glass windows were also built and used on a experimental basis, but their structural performance was in most cases less than successful when

they were subjected to hydrostatic pressures in excess of 10,000 psi. As a rule, their failure was initiated at the window-flange interface through the formation of circumferential cracks that propagated parallel to the curved shell surface (references 12-15). But, despite the documented failures, research on spherical-shell windows made of glass continued, as this approach was known to assure a larger field of vision and, theoretically, to offer the maximum potential pressure resistance for any given membrame shell shape. The NUC window-flange assembly described in this report represents the successful conclusion to this research.

THEORETICAL CONSIDERATIONS

OBJECTIVE

The objective of the research study was to develop a proven glass or ceramic window-flange assembly with panoramic vision for operational pressures up to 20,000 psi. In order for the window-flange assembly to be adaptable without changes to many potential undersea applications, it was to be designed as a self-sufficient structural element independent of the pressure hull on which it would be mounted.

APPROACH

The approach taken to satisfying the objectives of the study was to use the spherical-shell configuration for the window shape, plane conical bearing surfaces for mating the window to the support flange, fiber-reinforced epoxy for the bearing gasket, and transparent glass ceramic or chemically surface-compressed glass for the window. This approach was based on the results of past studies conducted by the author and the published data of other investigators.

The spherical-shell configuration was chosen because both theoretical considerations and experimental findings (reference 3) have proven beyond doubt that this shape is structurally and optically superior to flat-disc and conical-frustum windows. Structurally, it distributes compressive stresses in the window without major concentrations; while optically its convex-concave lens effect gives a larger and truer view of objects in hydrospace. The 150-degree spherical angle was chosen because it provides almost the same field of view as a complete hemisphere while retaining the advantages associated with the fabrication and mounting of smaller spherical sectors. Also, a previous experimental study with acrylic spherical-shell sectors under external hydrostatic loading has shown that the 150-degree spherical-shell sector undergoes smaller shear and tensile stresses at the interface of the sector and flange than does a 90-degree sector.

The plane-conical bearing surfaces on the edges of the shell and the flange were deemed adequate for the bearing stresses predicted and were less expensive

than toroidal- or spherical-conical surfaces. They also make mass-produced windows and flanges interchangeable in the field.

The fiber-reinforced epoxy gasket was considered to possess sufficient compliance for cushioning the point contacts resulting from an imperfect match between the window and the flange while offering adequate strength to withstand the 80,000-psi axial bearing stress predicted for some locations on the window-flange interface.

Transparent glass ceramic and chemically surface-compressed* glass were chosen because they offer superior resistance to the tensile and flexural stresses often encountered in spherical shell windows at the window-flange interface. In addition, ordinary glass and acrylic plastic windows were included in the study to compare their structural performance with that of the ceramic and chemically surface-compressed glass windows.

DESIGN

During the design of the window-flange assembly, three parameters were to be met: (1) the assembly was to be a self-contained structural subsystem independent of the stress levels and deformations of the hull, (2) concentrations of compressive stresses and presence of tensile stresses were to be avoided in the window, and (3) all components were to be interchangeable from one assembly to another in the field.

To make the assembly a self-contained structural subsystem (Appendix A), the window was designed to rest on a flange and be retained by rings that do not form a part of the hull structure (figure 1). Since the flange mounting-ring that bolts to the hull is not rigidly attached to the flange, the latter is free to contract radially under the influence of hydrostatic pressure. The sliding friction between the flange and the hull imposes some restraint on the flange; but this is minor and, in addition, the frictional constraint between two flat surfaces does not readily transmit bending moments from the hull to the flange. The mounting ring also, although bolted to the hull, is not subjected to high stresses by the hull because it is made of DELRIN plastic with a significantly lower modulus of elasticity than that of a typical metallic hull.

All tensile stresses and the concentration of compressive stresses in the window were to be avoided through the use of a flange that would contract radially at a rate approximately matching that of the window and would possess sufficient axial flexibility to insulate the window from rotational moments in the reinforcing boss around the penetration in the hull. Several designs and fabrication materials for the flange were studied exhaustively before the final choice was made.

Of great help here was the finite element analysis applied to the proposed flange configurations by Mr. K. Nishida of the Naval Ship Research and Development Center (NSRDC). This analysis is reported in Appendix B. Although the simplifying assumptions used in the analysis (unrestrained slippage between the window and the

---

*Chemically surface-compressed glass denotes in this paper a glass whose surface has been precompressed by an ion-exchange process.

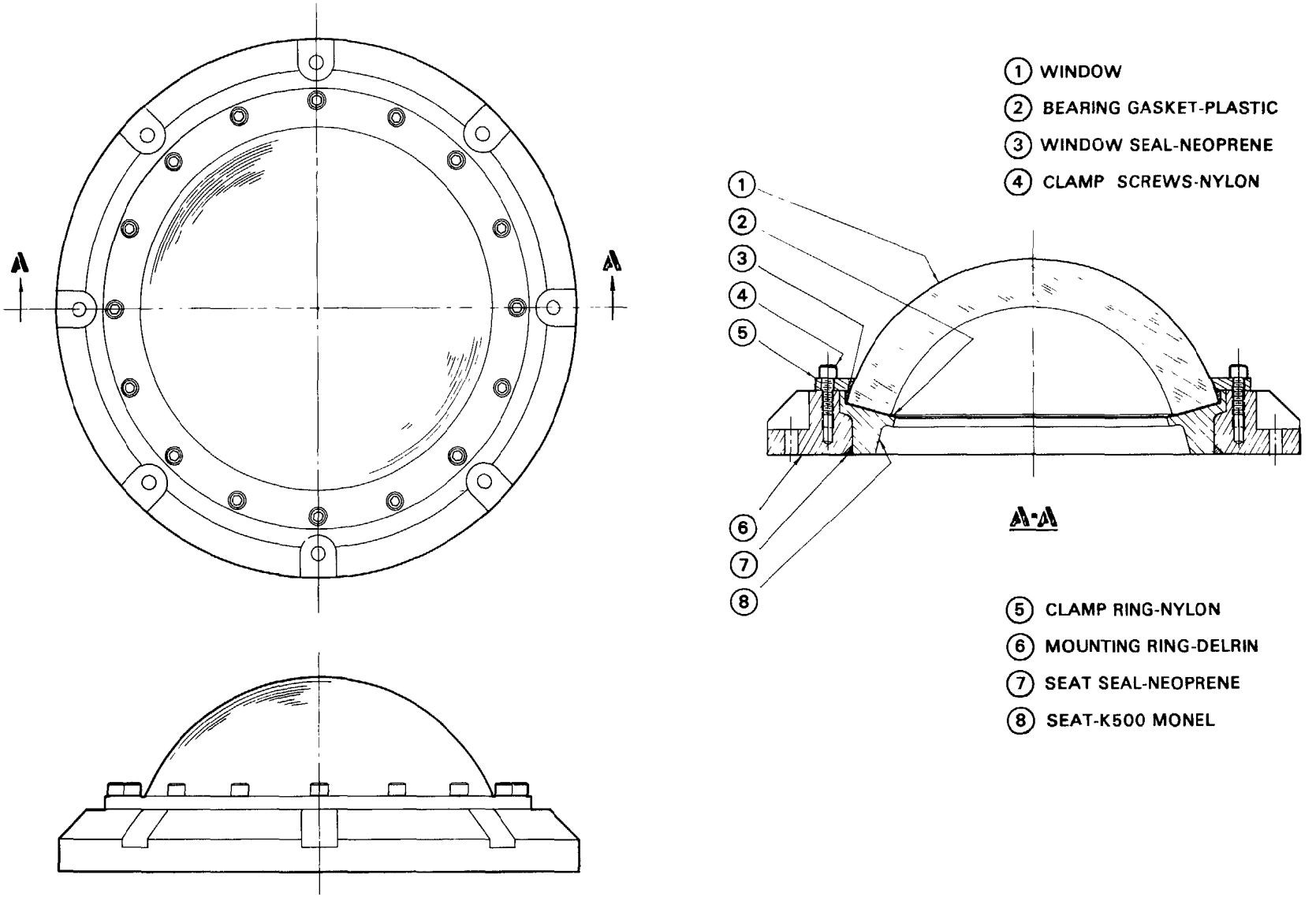

Figure 1. NUC spherical-shell window-flange assembly with 150-degree included spherical angle for service to 20,000-psi hydrostatic pressure.

gasket and between the flange and the hull) make the calulated stress values (figure 2) diverge somewhat from actual values, the finite element analysis showed that (1) the chosen flange configuration does not generate tensile stresses in the glass or glass ceramic window and that (2) flange material with a modulus of elasticity somewhat in excess of 30 x 10^6 psi was needed to match the radial rigidity of the flange to that of the window. Since it is known that the coefficient of static friction between two metal parts is in the 0. 3-to-0.5 range, a flange material with a modulus of elasticity somewhat less than 30 x 10^6 would be just right for this application. The family of Monel alloys fall into this range of elastic moduli, and they were considered prime candidates for the flange.

Monel K-500 was chosen for the flange because (1) it possesses the required resistance to corrosion, (2) it minimizes the galvanic corrosion that occurs when dissimilar metals are mounted on a steel hull, (3) its strength is adequate, and (4) the radial deformation of a Monel K-500 flange under hydrostatic loading matches more closely the deformation of glass or glass ceramic window than would that of a titanium or aluminum flange.

FABRICATION

FLANGE

The flange was machined from Monel K-500 plate hot-finished and aged to C-30 hardness so that a minimum yield point of 100,000 psi could be achieved. The angle of the plane-conical bearing surface was within ±5 minutes of the specified 150-degree included conical angle (figure 1).

WINDOWS

Windows were fabricated from several materials (figure1). The primary material was an Owens-Illinois Cer-Vit glass composition that could be used in the glassy phase (SSC-201) or converted to a ceramic state (C-101) that also was transparent.

The windows remaining in the glassy phase were subjected to ion-exchange treatment that placed their surfaces into compression. The windows which had the glassy phase converted by heat treatment into the ceramic state received no surface-compression treatment. This was considered advantageous as it permitted an experimental comparison of two techniques for imparting additional tensile strength to a given material. Because of impurities both the glass and ceramic had a yellow tint.

Secondary window materials were Schotts annealed BK-7 borosilicate crown glass and Rohm and Haas Plexiglas G acrylic plastic. These materials were chosen because they represent the structural performances of a typical unstrengthened optical glass and typical plastic transparent material used today in pressure-resistant undersea windows.

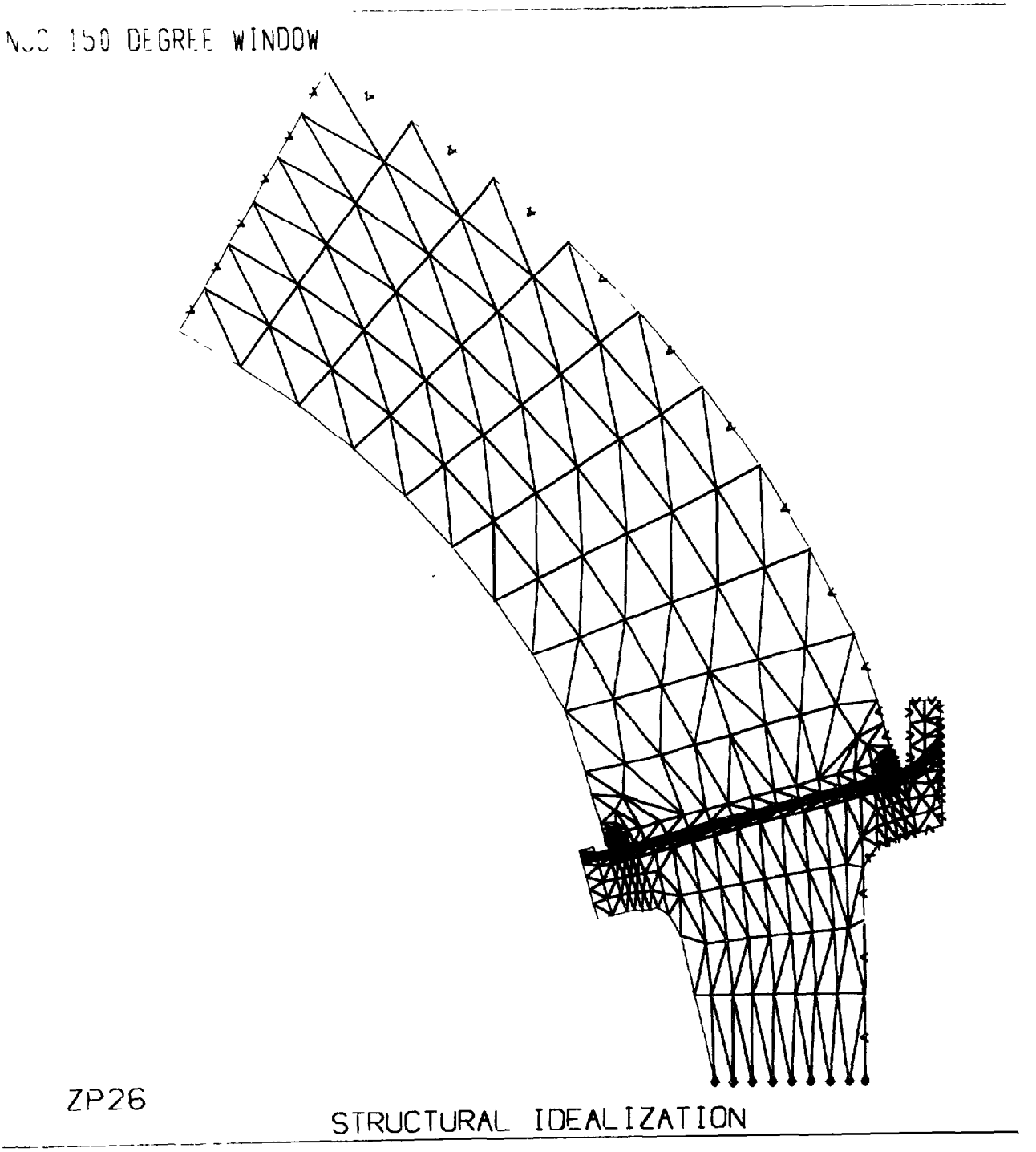

Figure 2. Finite element stress analysis of the NUC window-flange assembly subjected to external hydrostatic pressure; a glass window was supported by a Monel K-500 flange on an epoxy-coated PRD-49 cloth gasket. (sheet 1 of 10)

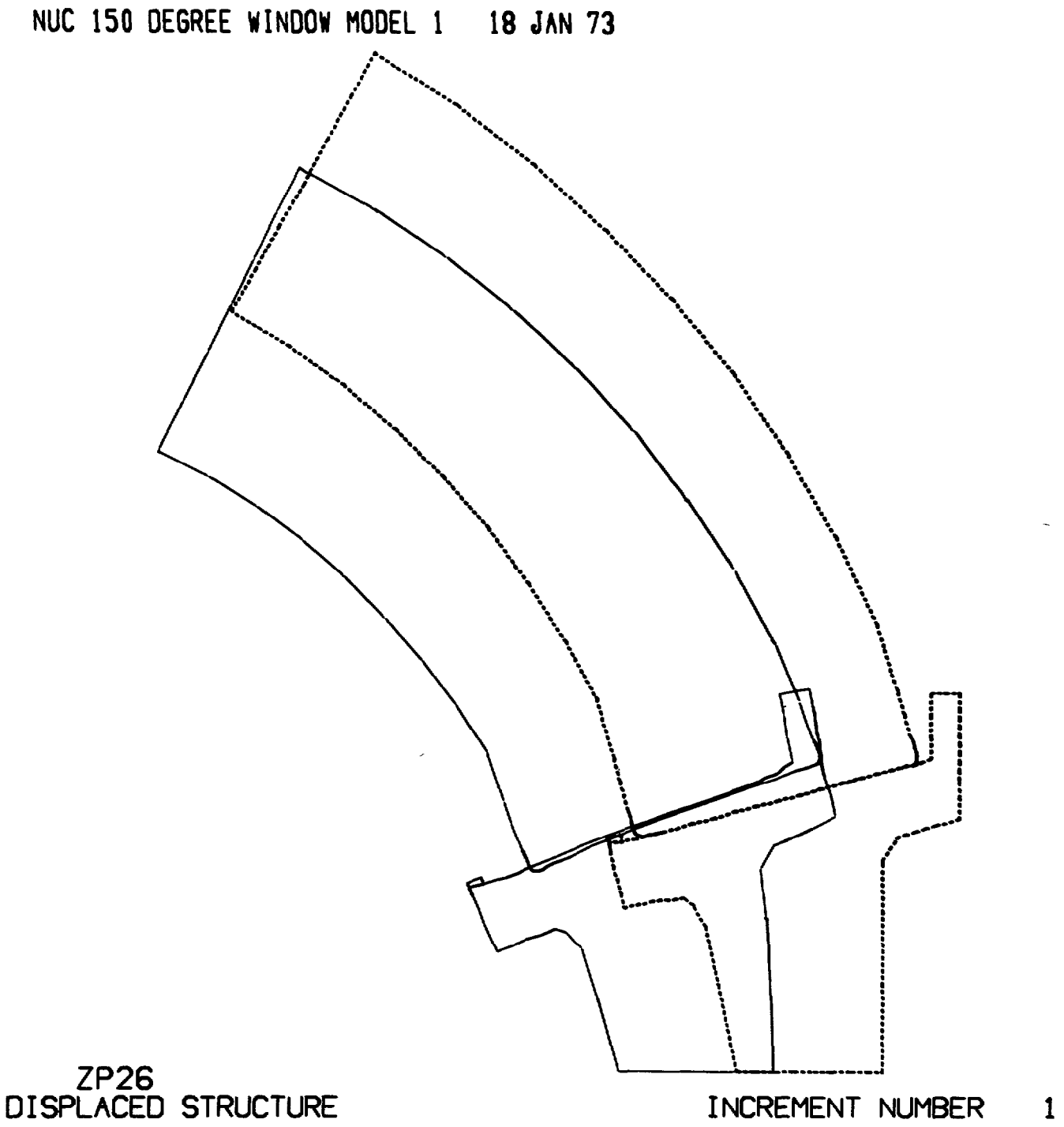

Figure 2. Finite element stress analysis of the NUC window-flange assembly subjected to external hydrostatic pressure; a glass window was supported by a Monel K-500 flange on an epoxy-coated PRD-49 cloth gasket. (sheet 2 of 10)

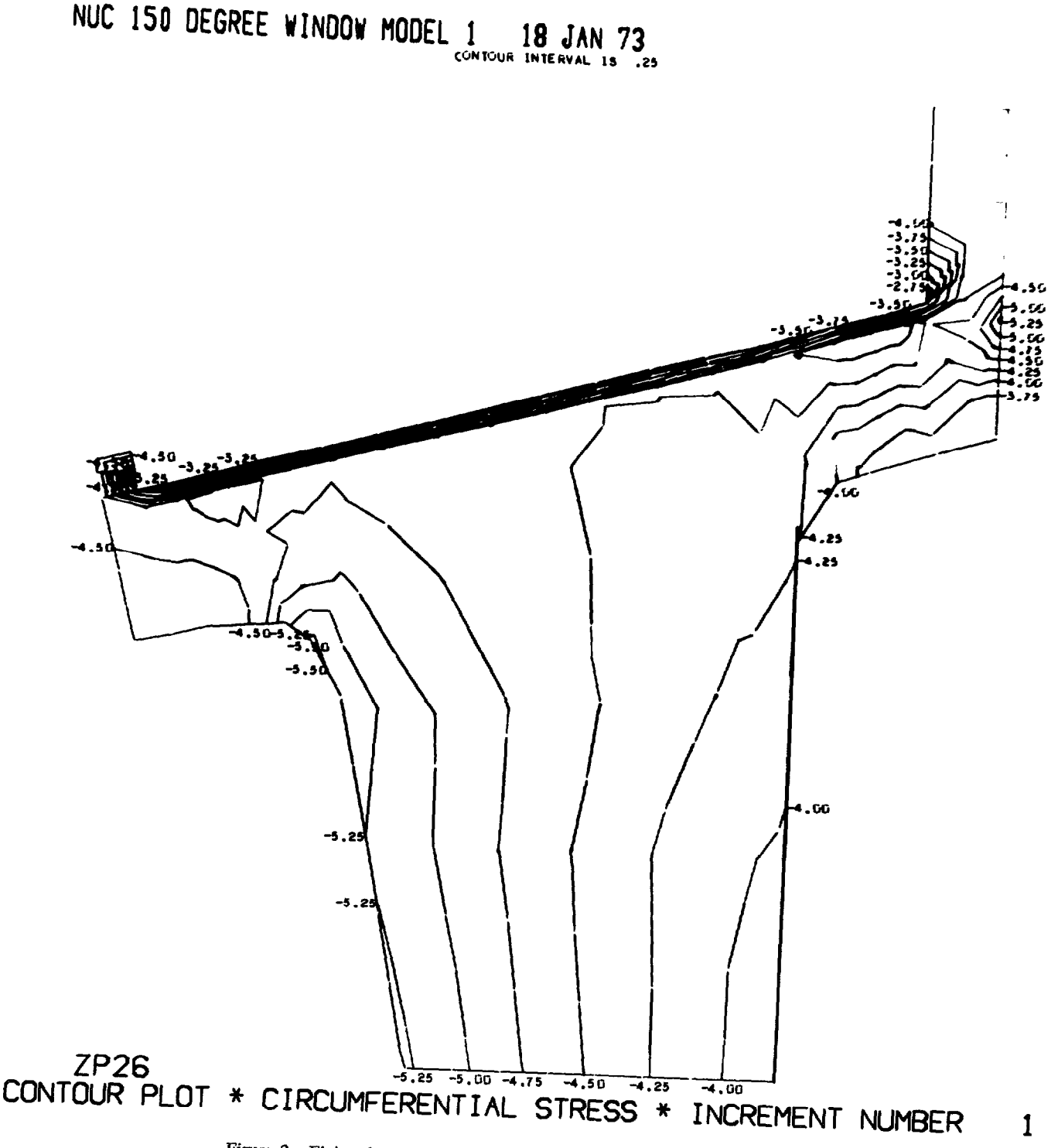

Figure 2. Finite element stress analysis of the NUC window-flange assembly subjected to external hydrostatic pressure; a glass window was supported by a Monel K-500 flange on an epoxy-coated PRD-49 cloth gasket. (sheet 3 of 10)

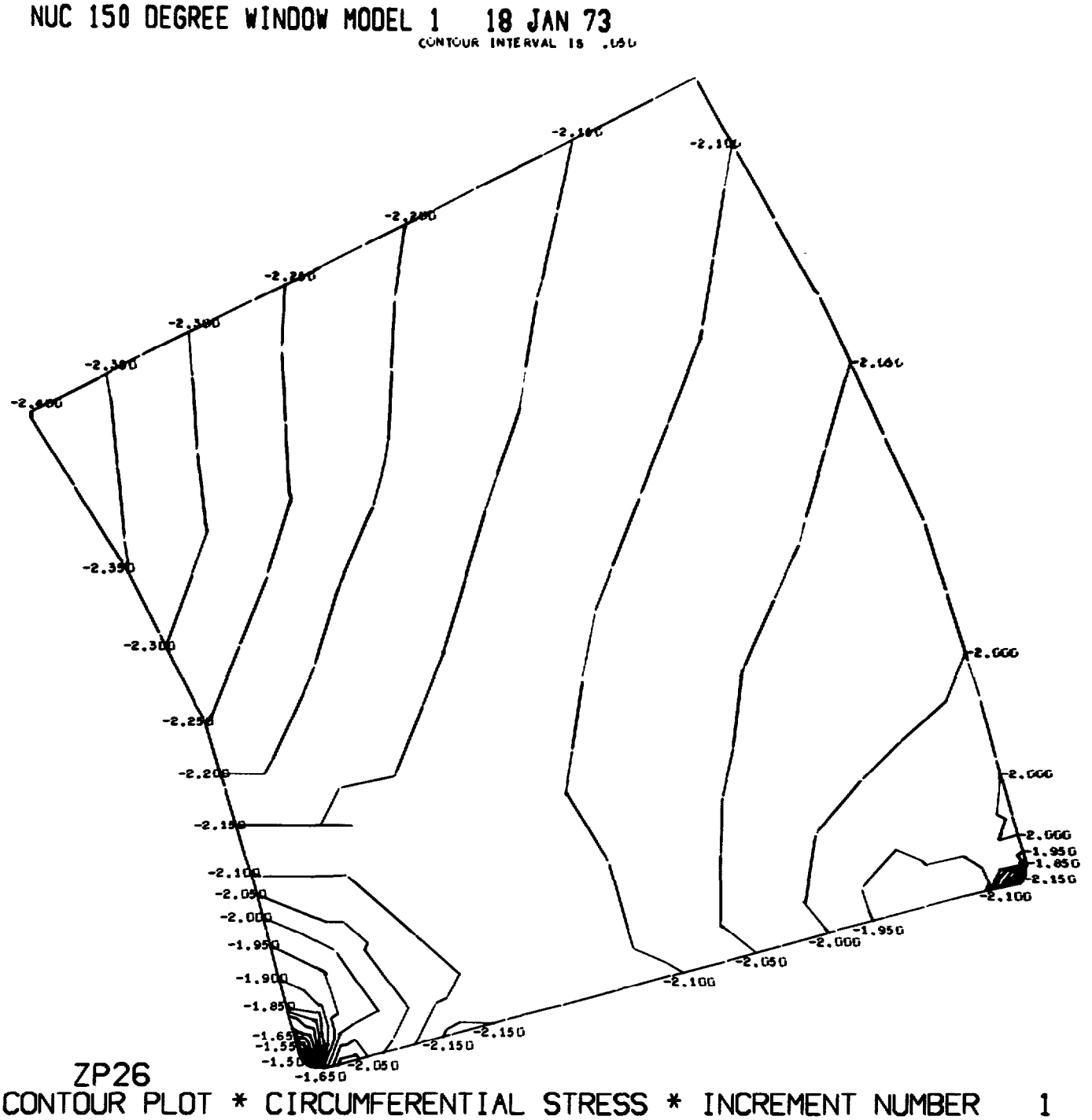

Figure 2. Finite element stress analysis of the NUC window-flange assembly subjected to external hydrostatic pressure; a glass window was supported by a Monel K-500 flange on an epoxy-coated PRD-49 cloth gasket. (sheet 4 of 10)

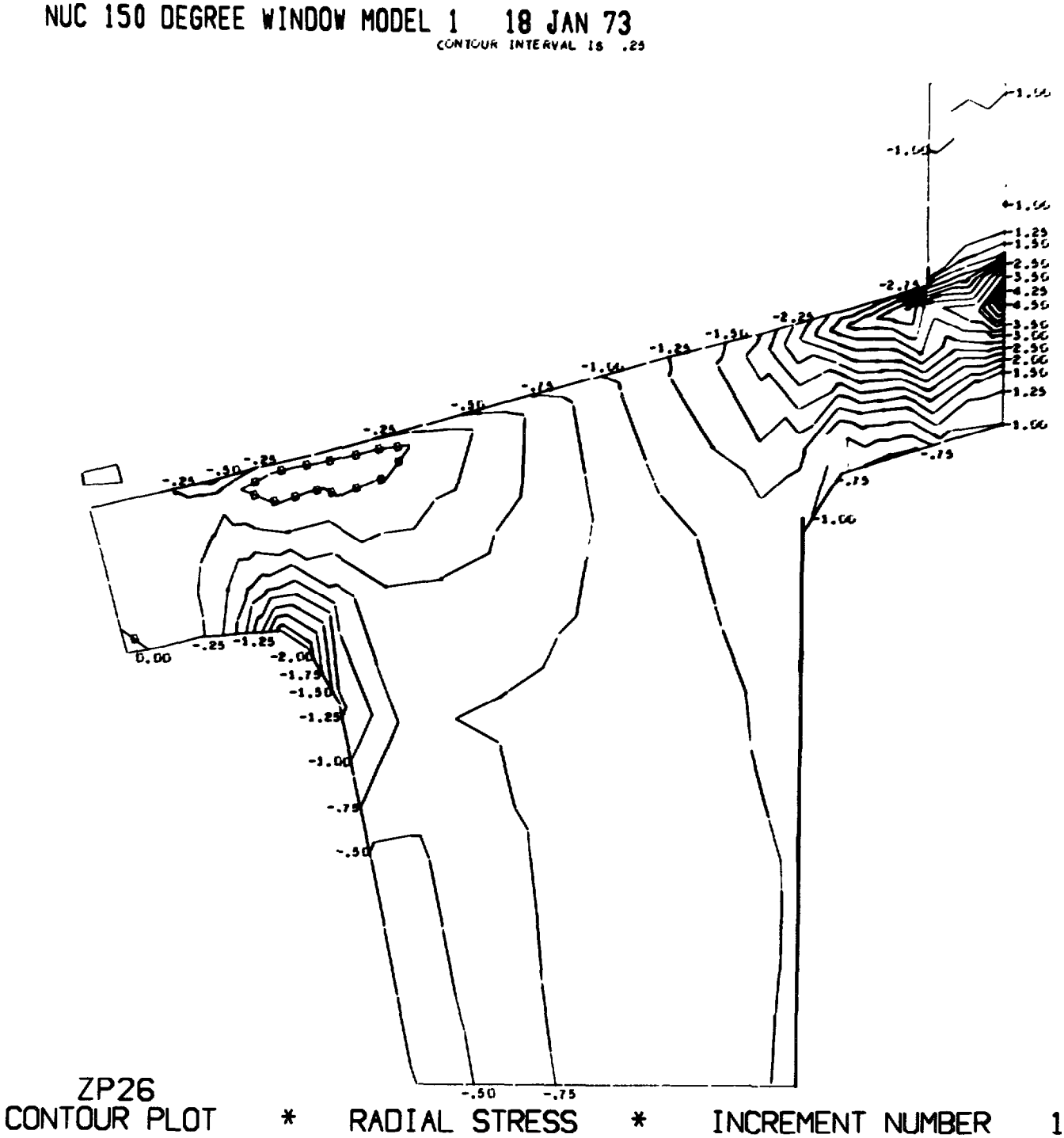

Figure 2. Finite element stress analysis of the NUC window-flange assembly subjected to external hydrostatic pressure; a glass window was supported by a Monel K-500 flange on an epoxy-coated PRD-49 cloth gasket. (sheet 5 of 10)

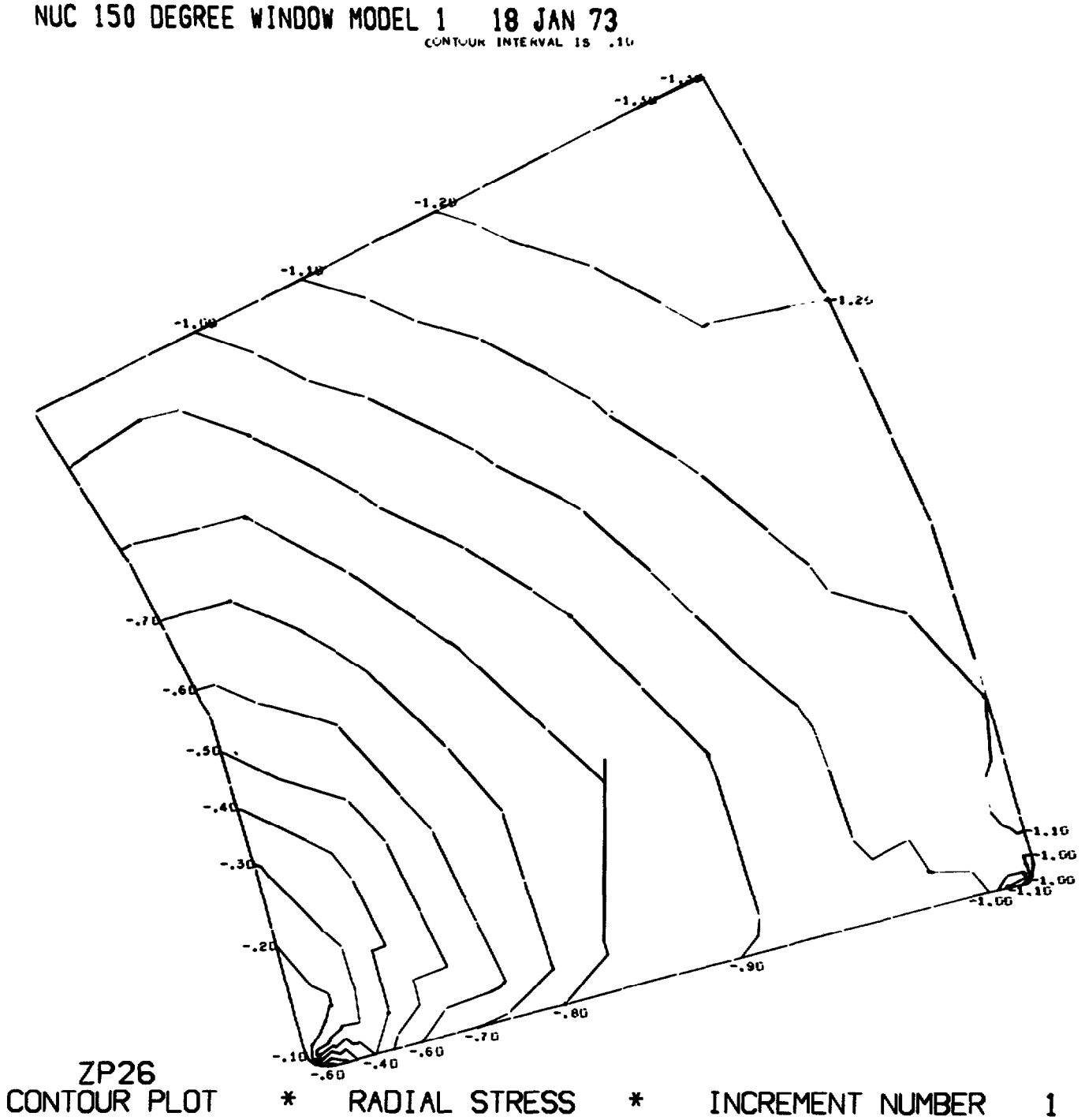

Figure 2. Finite element stress analysis of the NUC window-flange assembly subjected to external hydrostatic pressure; a glass window was supported by a Monel K-500 flange on an epoxy-coated PRD-49 cloth gasket. (sheet 6 of 10)

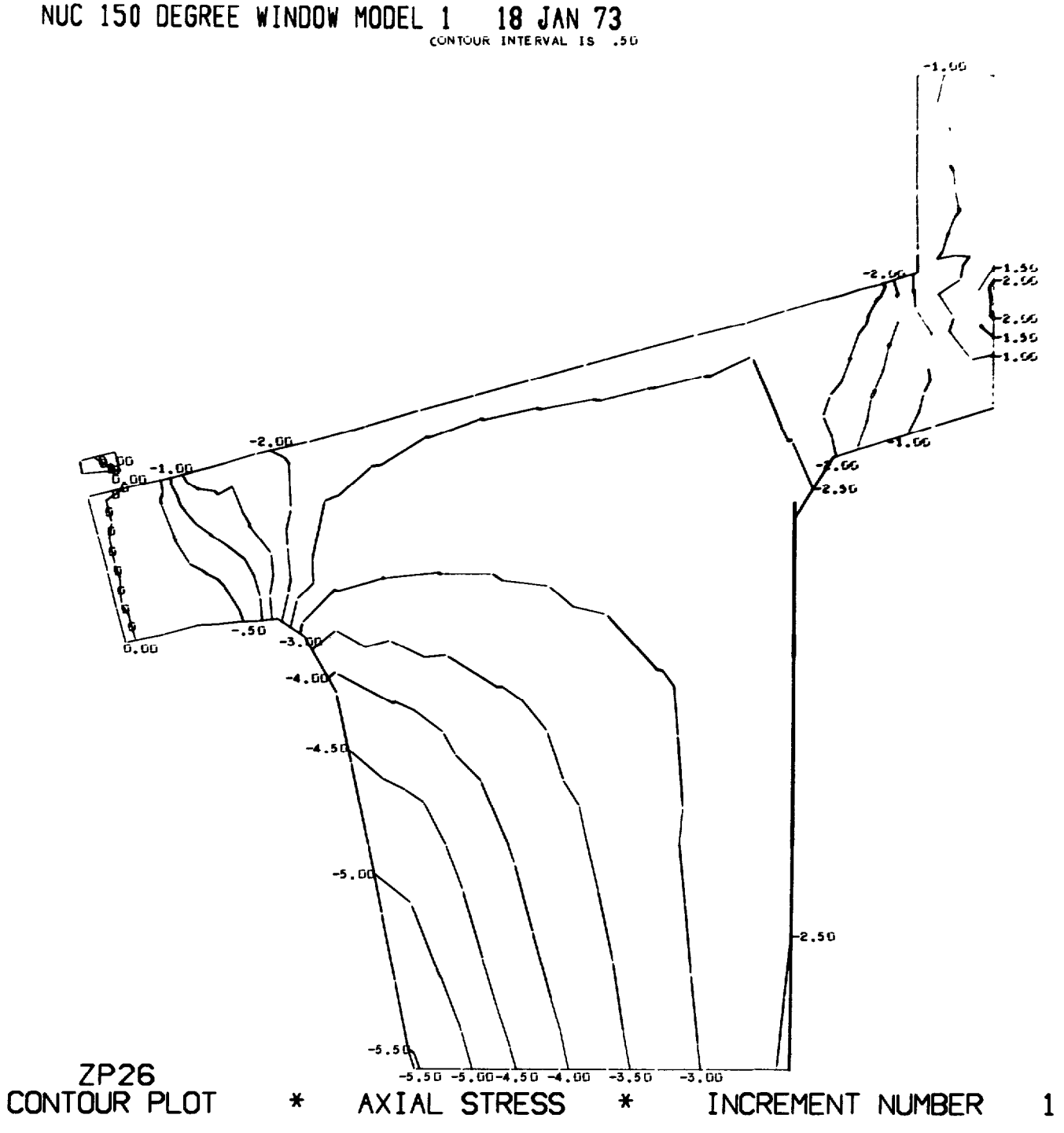

Figure 2. Finite element stress analysis of the NUC window-flange assembly subjected to external hydrostatic pressure; a glass window was supported by a Monel K-500 flange on an epoxy-coated PRD-49 cloth gasket. (sheet 7 of 10)

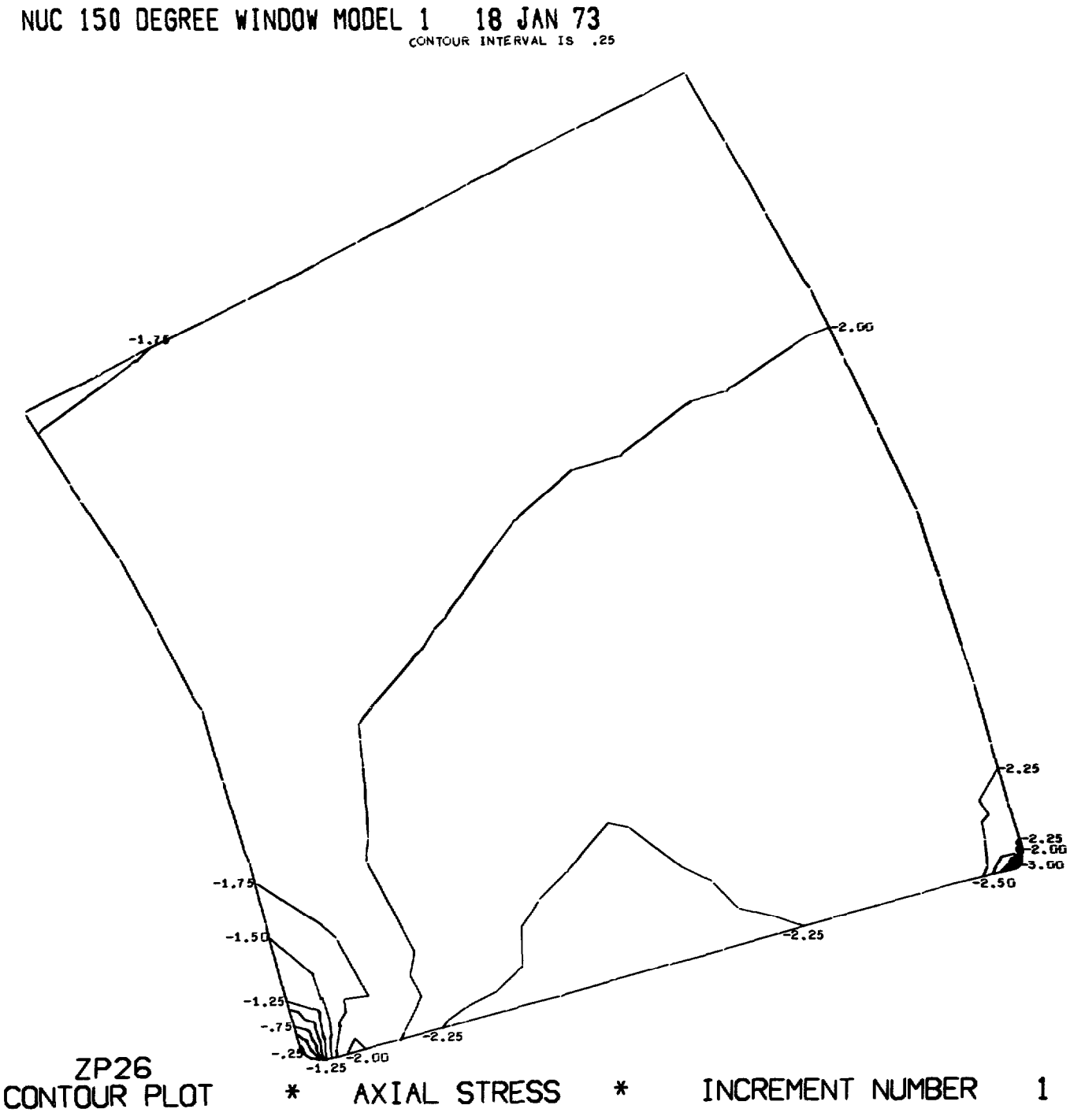

Figure 2. Finite element stress analysis of the NUC window-flange assembly subjected to external hydrostatic pressure; a glass window was supported by a Monel K-500 flange on an epoxy-coated PRD-49 cloth gasket. (sheet 8 of 10)

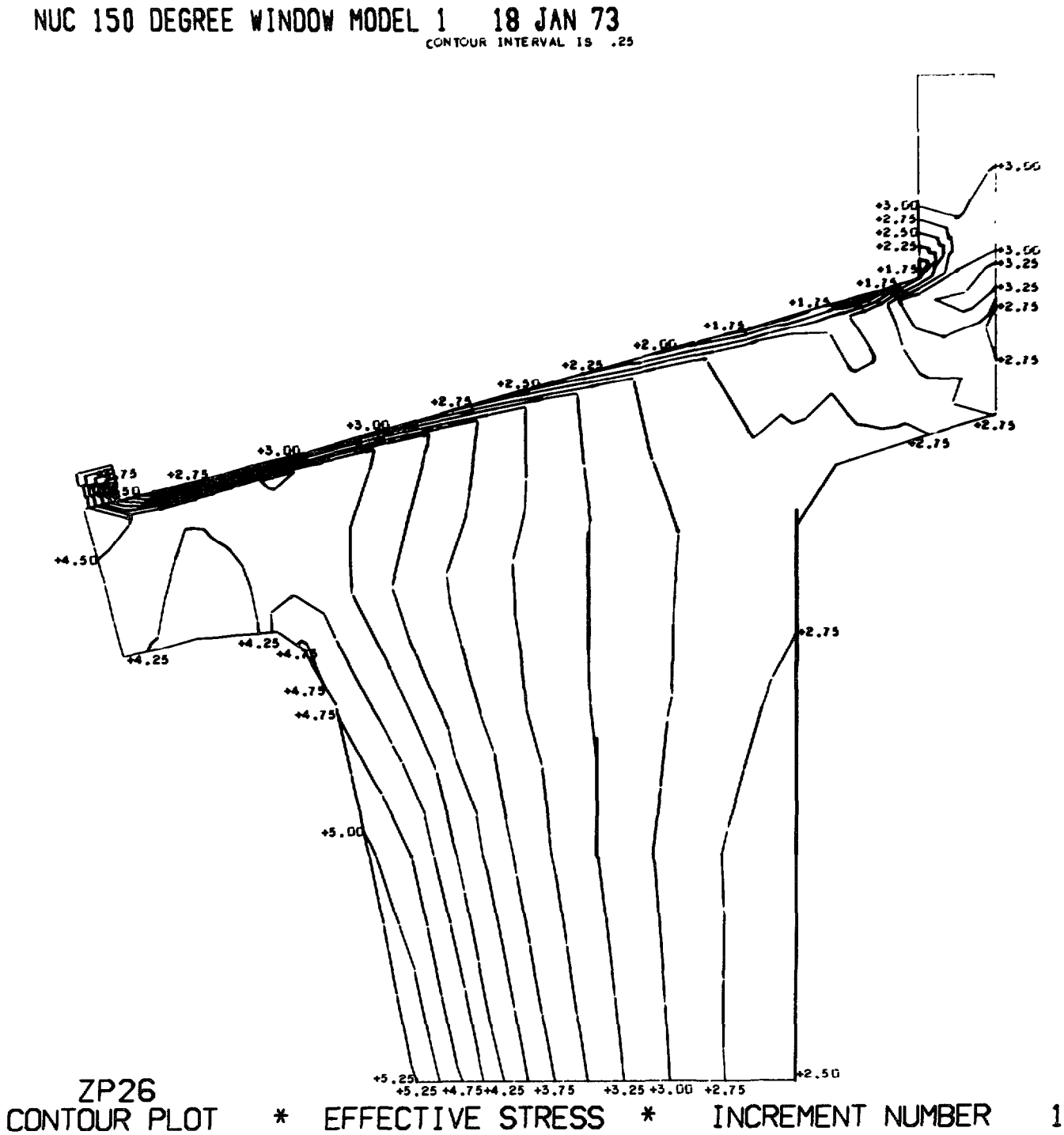

Figure 2. Finite element stress analysis of the NUC window-flange assembly subjected to external hydrostatic pressure; a glass window was supported by a Monel K-500 flange on an epoxy-coated PRD-49 cloth gasket. (sheet 9 of 10)

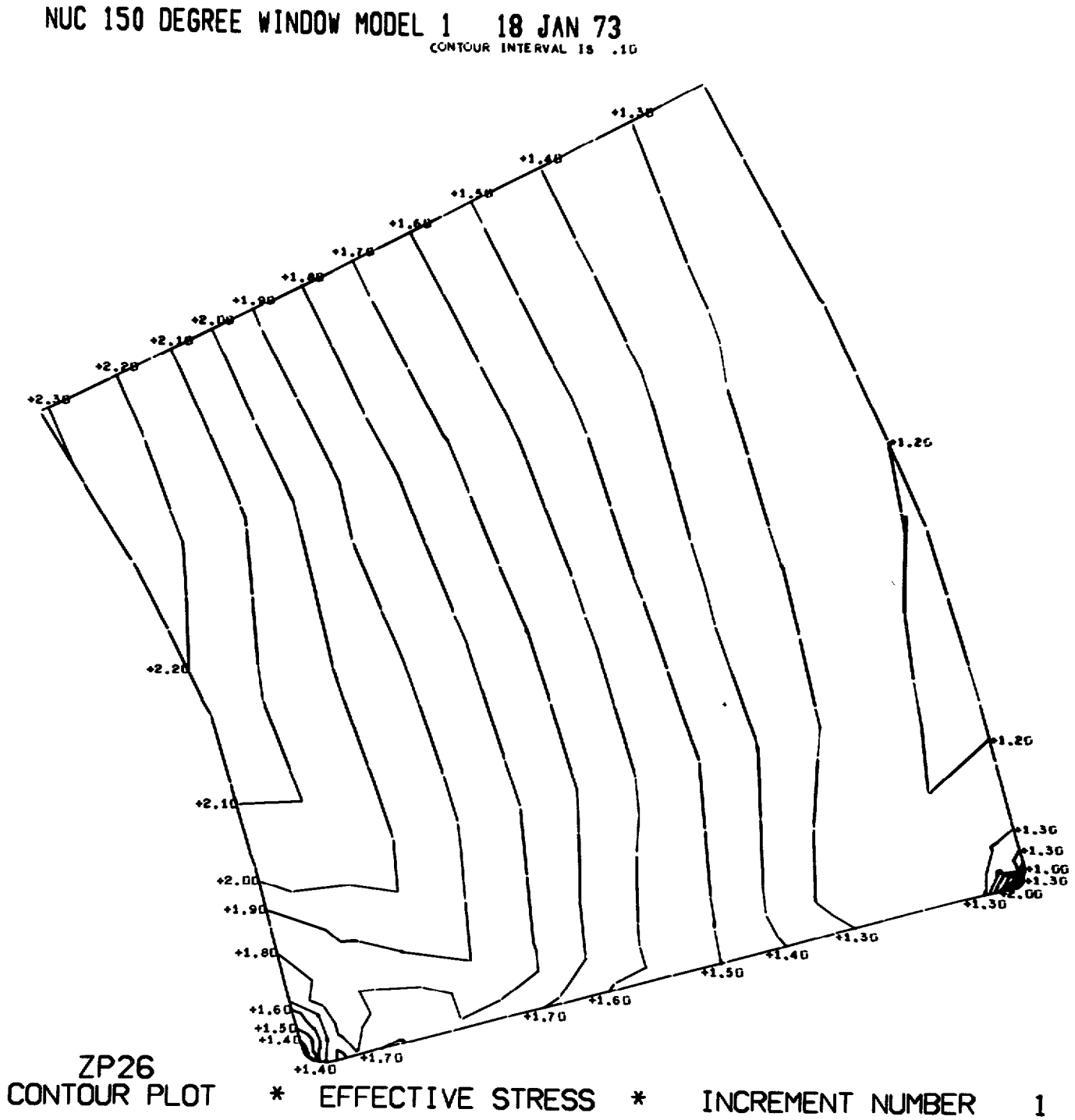

Figure 2. Finite element stress analysis of the NUC window-flange assembly subjected to external hydrostatic pressure; a glass window was supported by a Monel K-500 flange on an epoxy-coated PRD-49 cloth gasket. (sheet 10 of 10)

The Cer-Vit SSC-201 and C-101 windows were fabricated by hot-pressing oversize hemispheres and subsequently grinding them down on all surfaces to the specified size (Appendix C). The ground Cer-Vit SSC-201 windows were later subjected to ion-exchange treatment that chemically compressed the window surfaces. The fabrication of borosilicate crown glass and acrylic plastic windows consisted of grinding the hemispherical shapes from oversize glass and plastic castings.

To insure interchangeability between the 20 window specimens and 5 flanges used in the study, the spherical angle of the window's plane-conical bearing surface was maintained within ±1 minute. The dimensions of the convex and concave surfaces were kept within ±0. 020 inch and the finish on the surfaces was of optical quality.

BEARING GASKET

The bearing gasket was formed in a permanent mold by laminating two layers of DuPont PRD-49* cloth with epoxy resin. The resulting product was 0.020 inch thick and had a 150-degree included conical angle to match the bearing surface of the window (figure 1).

RETAINING RINGS

The clamp ring for holding the window in the flange and the mounting ring for the attachment of the flange to the hull were made from Nylon and Delrin, respectively. Plastics were chosen for this application because of their compliance to hull deformation and superior corrosion resistance (figure 1).

TESTING PROGRAM

The testing program focused primarily on the experimental evaluation of the spherical window-flange assembly developed during the study. Secondary goals were the evaluation of bearing gaskets for the window, and the material quality control for the window material.

BEARING GASKET

Since the predicted bearing stresses on the gasket were to be in the 40,000- to 80,000-psi range, it was deemed important to select gasket material capable of withstanding such high stresses repeatedly. Bearing materials were tested using a hardened tool-steel plunger 0.975 inch in diameter which pushed against a flat anvil of similar material.

---

*The new trade name for PRD-49 is KEVLAR-49.

The following gasket materials were tested (figure 3):

DuPont's Fairprene 5722A	0.022 inch thick
Rasbestos Manhattan A56	0.018 inch thick
Armstrong Accobest AN 8012	0.015 inch thick
Fiberglas cloth, epoxy-coated (1 layer of cloth)	0.012 inch thick
Fiberglas cloth, epoxy-laminated (2 layers of cloth)	0.020 inch thick
DuPont's PRD-49 cloth, epoxy-coated (1 layer of cloth)	0.012 inch thick
DuPont's PRD-49 cloth, epoxy-laminated (2 layers of cloth)	0.020 inch thick

After 10 applications of a 40,000-psi bearing stress to the materials it was found that only the neoprene-coated nylon-cloth Fairprene 5722A and epoxy-coated PRD-49 cloth were undamaged. When the bearing stress was increased to 80,000 psi, only the gasket made by impregnating two layers of PRD-49 cloth with epoxy was found to be free of damage. Thus, the only gasket considered reliable for service in the window-flange assembly under cyclic hydrostatic pressure loading to 20,000 psi was the laminate composed of two PRD-49 cloth layers impregnated with epoxy resin. For service to hydrostatic pressure in the 0- to 10,000-psi range, the Fairprene 5722A material is considered quite adequate.

The gasket testing program showed also that if no bevel is present on the plunger applying the bearing stress, the gasket will be severely damaged at a fraction of the load that it could carry if the edge of the plunger were beveled. Consequently, a slight bevel was specified for the edges of the glass and ceramic windows.

MATERIAL QUALITY CONTROL

The testing of window materials attempted to answer two important questions: (1) What are the mechanical properties of the materials, and (2) what is the effect of inclusions like bubbles on their compressive strength? Since the study focused on Cer-Vit C-101 and SSC-201 transparent materials, the bulk of the tests addressed themselves to these materials.

Mechanical properties of the window materials were determined by testing material coupons cast from the same material and subjected to the same thermal and chemical treatment as were the windows. Two types of tests were applied to the test specimens. The four-point loading flexure test was applied to 0.25-inch-diameter, 5.5-inch-long rods to determine the modulus of rupture (MOR), while the uniaxial loading test was used on 0.5-inch-diameter, 1-inch-long rods to find the ultimate compressive strength.

The rate of loading was sufficiently high to load the test specimens to failure in less than a minute. To make the tests more realistic, the surfaces of some specimens were abraded, and during tests to determine compressive strength the end conditions

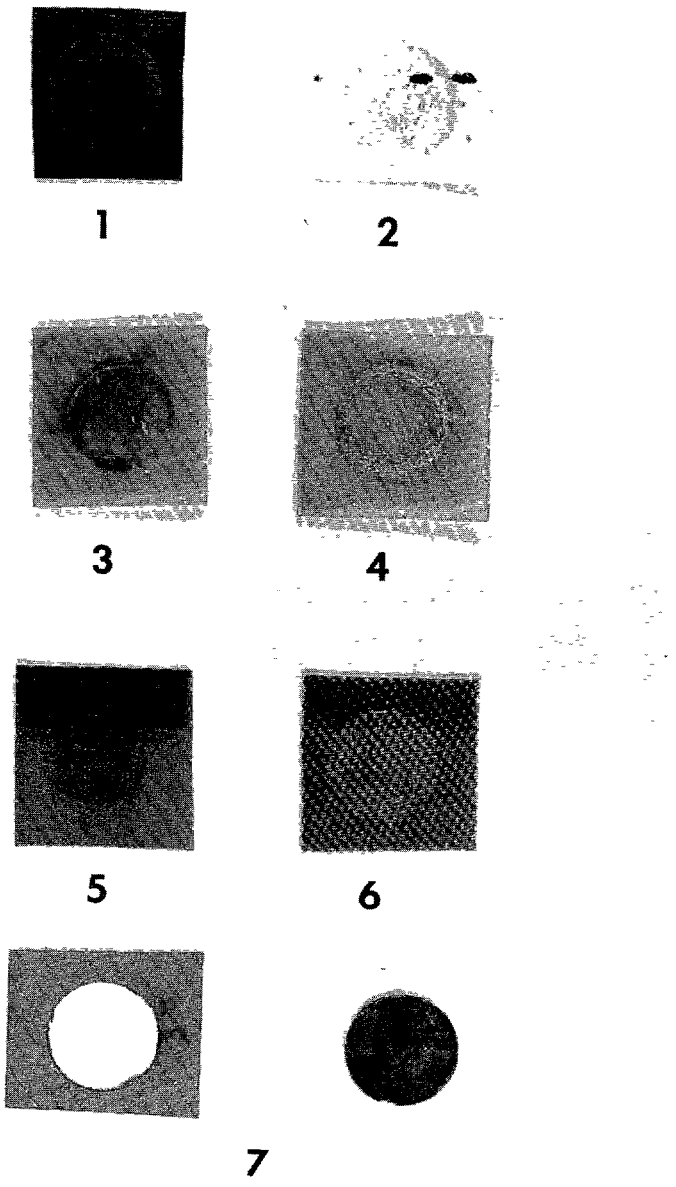

Figure 3. The following gasket materials were evaluated for use in the NUC window-flange assembly; (1) DuPont's Fairprene 5722A; (2) Rasbestos Manhattan A56; (3) Fiberglas cloth, epoxy-coated; (4) Fiberglas cloth, 2 layers laminated with epoxy; (5) DuPont's PRD-49 cloth, epoxy-coated; (6) Dupont's PRD-49 cloth, 2 layers laminated with epoxy; and (7) Armstrong Accobest AN 8012.

were varied to introduce the effect of bearing surface hardness and gasket extrusion. On the basis of test data and visual observations the following findings have been made:

The modulus of rupture in flexure for abraded Cer-Vit SSC-201 surface compressed glass is significantly superior to that of abraded Cer-Vit C-101 ceramic (60,900 psi average and $\bar{x}$ = 3,700 psi versus 14,500-psi average and $\bar{x}$ = 2,100 psi)*. Still, the modulus of rupture for Cer-Vit C-101 ceramic is somewhat higher (Table 1) than that of a typical glass composition (reference 14) (14,500-psi average and $\bar{x}$ = 2,100 psi versus 6,500-psi average and $\bar{x}$ = 700 psi) widely employed in the manufacture of deep-submergence glass buoys.

The ultimate compressive strength of abraded Cer-Vit SSC-201 surface compressed glass and Cer-Vit C-101 ceramic rods tested between identical hardened tool-steel anvils (figure 4) was approximately the same (173,000-psi average; $\bar{x}$ = 12,780 psi for SSC-201; versus 174,000-psi average; $\bar{x}$ = 3,740 psi for C-101). The compressive strength of these materials (Table 2) is only moderately superior to that of glass compositions used in deep-submergence buoys (134,818-psi average; $\bar{x}$ = 13,243 psi).

The effect of bubbles on the ultimate compressive strength of both Cer-Vit C-101 and SSC-201 was found to be significant. For C-101 the difference between the average strength of perfect specimens (174,000-psi average; $\bar{x}$ = 3,740 psi) and that of specimens with bubbles (155,117-psi average; $\bar{x}$ = 11,700 psi) was about 19,000 psi. For SSC-201 the difference in average strength between perfect specimens (173,000-psi average; $\bar{x}$ = 12,780 psi) and those with bubbles (164,000-psi average; $\bar{x}$ = 14,000 psi) was similar to that of C-101.

The specimens with bubbles (figure 5) failed at lower loading than did perfect specimens because the bubbles served as crack initiators. As a rule, the cracks would appear on the surfaces of bubbles (figure 6) before the ultimate failure load was reached. Cracks were initiated by large bubbles at approximately 30 percent of ultimate loading, by small bubbles at about 60 percent. The cracks originated at the poles of bubbles facing the ends of the compressive test specimen.

The effect of gaskets on the ultimate compressive strength of the specimens was very significant. In all cases the specimens resting on a gasket failed at lower compressive loading than did those resting on bare steel. In this respect, the worst gasket was Rasbestos Manhattan A56, with an average ultimate stress of 72,000 psi, while the best gaskets were epoxy-laminated PRD-49 and Fairprene 5722A, with an average ultimate stress of 83,000 psi.

The effect of the test jig configuration on the ultimate compressive strength was also significant. During the tests on Cer-Vit C-101 specimens, in which the diameter of the anvil matched that of the test specimens (figure 4), the average ultimate compressive loading at failure was higher (203,666 psi; $\bar{x}$ = 21,400 psi) than that measured during tests in which the diameter of the anvil was several times larger (174,000 psi; $\bar{x}$ = 3,740 psi). At the termination of tests for which

---

*x = standard deviation

Table 1. Modulus of Rupture for Test Specimens Under Flexural Loading.

Material	Specimen	Maximum stress (psi)
Cer-Vit C-101	1	12,600
Cer-Vit C-101	2	13,200
Cer-Vit C-101	3	11,800
Cer-Vit C-101	4	14,100
Cer-Vit C-101	5	11,700
Cer-Vit C-101	6	13,400
Cer-Vit C-101	7	10,400
Cer-Vit C-101	8	13,100
Cer-Vit C-101	9	16,500
Cer-Vit C-101	10	15,100
Cer-Vit C-101	11	15,300
Cer-Vit C-101	12	14,300
Cer-Vit C-101	13	17,100
Cer-Vit C-101	14	12,300
Cer-Vit C-101	15	16,800
Cer-Vit C-101	16	17,700
Cer-Vit C-101	17	15,400
Cer-Vit C-101	18	14,700
Cer-Vit C-101	19	14,100
Cer-Vit C-101	20	16,700
Cer-Vit C-101	21	15,100
Cer-Vit C-101	22	18,000

Average modulus of rupture = 14,500 psi
Standard deviation = 2,100 psi

Material	Specimen	Maximum stress (psi)
Cer-Vit SSC-201	23	50,000
Cer-Vit SSC-201	24	63,900
Cer-Vit SSC-201	25	57,700
Cer-Vit SSC-201	26	57,900
Cer-Vit SSC-201	27	59,400
Cer-Vit SSC-201	28	62,000
Cer-Vit SSC-201	29	62,600
Cer-Vit SSC-201	30	63,200
Cer-Vit SSC-201	31	58,600
Cer-Vit SSC-201	32	59,100
Cer-Vit SSC-201	33	56,100
Cer-Vit SSC-201	34	62,800
Cer-Vit SSC-201	35	59,800
Cer-Vit SSC-201	36	61,300
Cer-Vit SSC-201	37	62,900
Cer-Vit SSC-201	38	64,100
Cer-Vit SSC-201	39	63,400
Cer-Vit SSC-201	40	62,100
Cer-Vit SSC-201	41	65,700
Cer-Vit SSC-201	42	65,200

Average modulus of rupture = 60,900 psi
Standard deviation = 3,700 psi

NOTE:
1. All specimens were 5.5 inches long with a 0.250-inch nominal diameter.
2. The surface of all specimens was abraded by tumbling them in a ball mill with 240-grit silicon carbide.
3. Flexural load was applied with a four-point test jig.

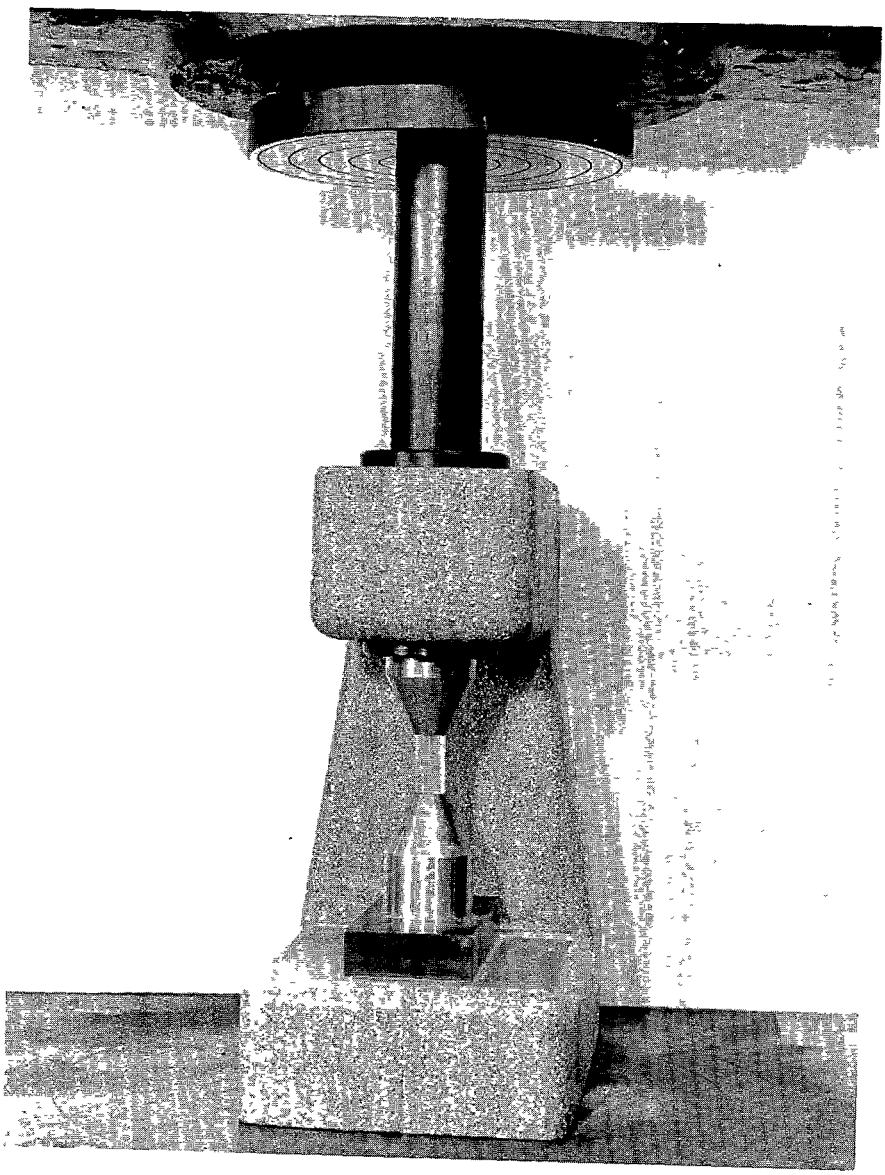

Figure 4. Test apparatus for determining the uniaxial compressive strength of glass and ceramic.

Table 2. Ultimate Compressive Strength
of Test Specimens Under Uniaxial Compressive Loading.

TEST CONDITION A

Material	Specimen	Finish	Total no. of bubbles	Size of bubbles	Location of bubbles	Nominal stress (psi)
Cer-Vit C-101	1	Polished	0	-	–	170,000 U
Cer-Vit C-101	2	Polished	0	-	–	179,000 U
Cer-Vit C-101	3	Polished	2	T	Internal	117,000 C, 173,000 U
Cer-Vit C-101	4	Polished	1	T	Internal	106,000 C, 154,000 U
Cer-Vit C-101	5	Polished	5	T	Internal	123,000 C, 188,000 U
Cer-Vit C-101	6	Polished	0	-	–	119,000 C, 173,000 U
Cer-Vit C-101	7	Polished	1	T	Internal	98,000 C, 152,000 U
Cer-Vit C-101	8	Polished	6	T,S,M	Internal	141,000 C, 165,000 U
Cer-Vit C-101	9	Polished	1	L	Internal	61,000 C, 143,000 U
Cer-Vit C-101	10	Polished	2	T,L	Internal	53,800 C, 145,000 U
Cer-Vit C-101	11	Polished	1	S	Internal	133,000 C, 160,000 U
Cer-Vit C-101	12	Polished	1	M	Internal	138,000 C, 157,000 U
Cer-Vit C-101	13	Polished	3	S	Internal, one at edge	107,000 C, 151,000 U
Cer-Vit C-101	14	Polished	1	S	Internal	148,000 C, 157,000 U
Cer-Vit C-101	15	Polished	1	L	Internal	60,000 C, 142,000 U
Cer-Vit C-101	16	Polished	2	S,L	Internal	59,000 C, 140,000 U
Cer-Vit C-101	17	Polished	2	S	Internal	129,000 C, 151,000 U
Cer-Vit C-101	18	Polished	1	M	Internal	107,000 C, 146,000 U
Cer-Vit C-101	19	Polished	5	T,S	Internal, one at edge	110,000 C, 161,000 U
Cer-Vit C-101	20	Polished	1	M	Internal	138,000 C, 152,000 U
SSC-201	21	Ground	0	–	–	167,000 U
SSC-201	22	Ground	0	–	–	187,000 U
SSC-201	23	Ground	0	–	–	182,000 U*

Table 2. Ultimate Compressive Strength
of Test Specimens Under Uniaxial Compressive Loading. (Continued).

TEST CONDITION A (Continued)						
SSC-201	24	Ground	0	–	–	167,000 U*
SSC-201	25	Ground	0	–	–	148,000 U*
SSC-201	26	Ground	0	–	–	174,000 U*
SSC-201	27	Ground	1	M (axial)	Internal	178,000 U*
SSC-201	28	Ground	1	M (axial)	Internal	150,000 U
SSC-201	29	Ground	0	–	–	186,000 U*
TEST CONDITION B						
Cer-Vit C-101	30	Ground	0	–	–	202,000 U
Cer-Vit C-101	31	Ground	0	–	–	230,000 U
Cer-Vit C-101	32	Ground	0	–	–	174,000 U
Cer-Vit C-101	33	Ground	0	–	–	204,000 U
Cer-Vit C-101	34	Ground	0	–	–	182,000 U
Cer-Vit C-101	35	Ground	0	–	–	230,000 U
TEST CONDITION C				Gasket Material		
Cer-Vit C-101	36	Ground	0	Fairprene 5722A		95,000 U
Cer-Vit C-101	37	Ground	0	Fairprene 5722A		90,000 U
Cer-Vit C-101	38	Ground	0	Fairprene 5722A		67,000 U
Cer-Vit C-101	39	Ground	0	PRD-49 Epoxy Laminate		89,000 U
Cer-Vit C-101	40	Ground	0	PRD-49 Epoxy Laminate		92,000 U
Cer-Vit C-101	41	Ground	0	PRD-49 Epoxy Laminate		84,500 U
Cer-Vit C-101	42	Ground	0	Rasbestos Manhattan A56		77,000 U
Cer-Vit C-101	43	Ground	0	Rasbestos Manhattan A56		79,000 U
Cer-Vit C-101	44	Ground	0	Rasbestos Manhattan A56		61,500 U
Cer-Vit C-101	45	Ground	0	Armstrong Accobest		74,000 U

Table 2. Ultimate Compressive Strength
of Test Specimens Under Uniaxial Compressive Loading. (Continued).

TEST CONDITION C (Continued)

Cer-Vit C-101	46	Ground	0	Armstrong Accobest	89,500 U
Cer-Vit C-101	47	Ground	0	Armstrong Accobest	82,000 U

NOTES:

1. Test Condition A: Loading anvils are 1.500-inch-diameter hardened-steel cylinders.
2. Test Condition B: Loading anvils are conical steel frustums with 50-degree included angle and 0.550-inch minor and 1.500-inch major diameters.
3. Test Condition C: Loading anvils are 1.500-inch-diameter hardened-steel cylinders covered with nonmetallic bearing gaskets consisting of

   DuPont Fairprene 5722A, 0.020 inch thick;
   Rasbestos Manhattan A56, 0.016 inch thick;
   Armstrong Accobest AN 8012, 0.0156 inch thick;
   and PRD-49 Epoxy Laminate (DuPont), 0.020 inch thick.
4. T,S,M, and L designate sizes of bubbles inside the test specimen:

   T = tiny (approximately 0.2 mm); S = small (approximately 1.0 mm); M = medium (approximately 2.0 mm); and L = large (approximately 4.0 mm).
5. Test specimen is 0.5 inch in diameter and 1.0 inch in length.
6. Rate of load application is 200,000 psi/minute.
7. *Specimen previously tested to 50,000- and 75,000-psi compressive stress level.
8. C indicates that crack initiation was observed at this nominal stress level, while U designates uniaxial nominal stress level at catastrophic failure.

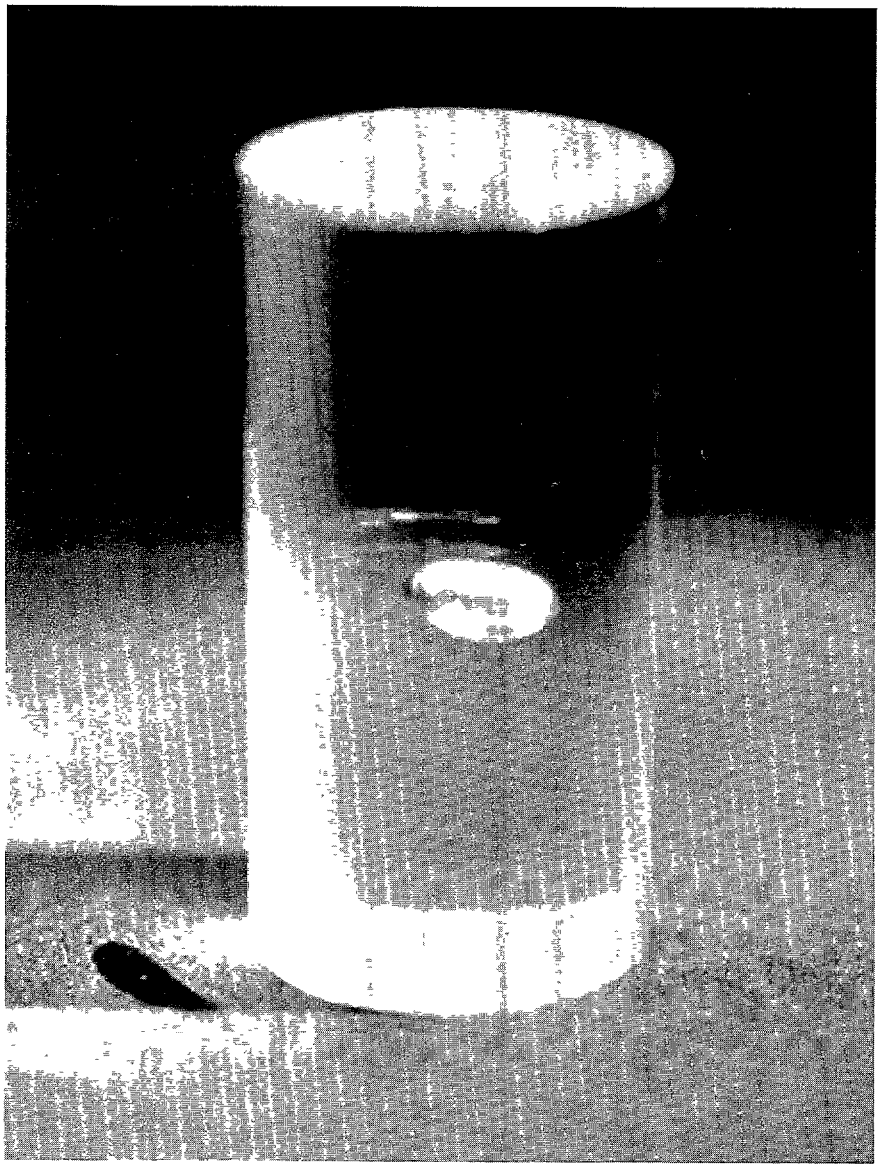

Figure 5. Typical Cer-Vit C-101 glass ceramic specimen with a large air bubble in its interior.

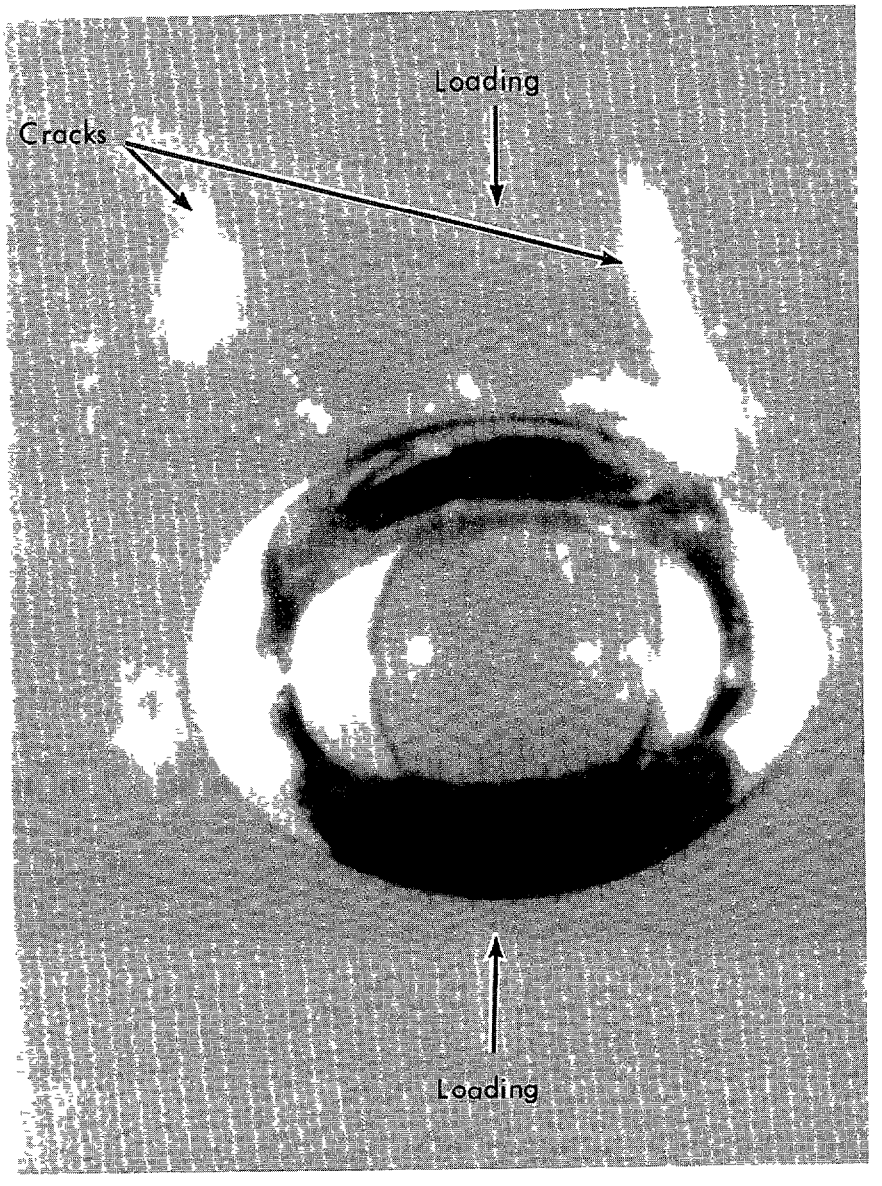

Figure 6. Cracks initiated at the boundary of a bubble located in a Cer-Vit C-101 glass ceramic test specimen under uniaxial compressive loading.

specimens resting between wide anvils were loaded to no more than 50 percent of their ultimate strength, cracks were observed in the bearing surfaces of the specimens when the load was decreased to zero.

These conclusions were drawn from testing of material specimens: (1) chemical precompression of the surface improves the ultimate tensile but not compressive strength of glass; (2) Cer-Vit C-101 glass ceramic has only a moderate mechanical strength advantage over typical glass whose surface is not chemically precompressed; (3) nonmetallic bearing gaskets should be employed only where their use is absolutely necessary, as they will cause the glass or ceramic specimen to fail at a lower compressive stress than is observed when the specimen rests on an elastically matched metal block.

HYDROSTATIC TESTING OF WINDOWS

Hydrostatic testing of window assemblies explored three questions. (1) How deep can the NUC spherical window assembly operate without failure? (2) What is the cyclic fatigue life of the window assembly at different depths? (3) How resistant are the window assemblies to underwater shock?

For all of the hydrostatic tests, the window assemblies were bolted to individual, 5-inch-thick steel plates. Great care was taken during mounting to center the window in the flange and keep grease off the window's bearing surface. The assemblies (figure 7 a,b) were tested at the Southwest Research Institute in a pressure vessel with a diameter of 10 inches and an internal pressure capability of 20,000 psi (figure 8). The assemblies were externally pressurized with oil at room temperature. Underwater shock tests were conducted in a pressure vessel 30 inches in diameter and 180 inches long. Water was used as the medium and the shock was generated by explosive charges (figure 9). Pressure pulses set up by the explosive charges were measured at the test assemblies and recorded using the instrumentation shown in figure 10. Some of the windows were instrumented with electric-resistance strain gages and sensitive transducers (figure 11) to measure strains and acoustic emissions generated by the window undergoing hydrostatic pressurization (Appendix D).

EVALUATION OF WINDOW ASSEMBLIES

The window assemblies were evaluated in two series of hydrostatic tests. Each series attempted to answer a different set of questions that might be asked by a potential user of NUC spherical-shell, glass or glass-ceramic windows.

Long-term cyclic tests (Table 3) were performed to give the user evidence that the window assembly will without any doubt perform satisfactorily for at least 300 cycles at any chosen hydrostatic pressure in the 0- to 20,000-psi range. To make the tests realistic, the length of each cycle was set at 8 hours, of which 4 hours were under pressure and 4 without pressure. This cycle was thought to approximate the typical dive profile of a submersible system.

Acoustic emissions (Appendix D) recorded during several pressurizations of Cer-Vit C-101 and SSC-201 windows to a pressure of 20,000 psi indicate that C-101 ceramic is a good acoustic emitter while SSC-201 glass is a very poor one.

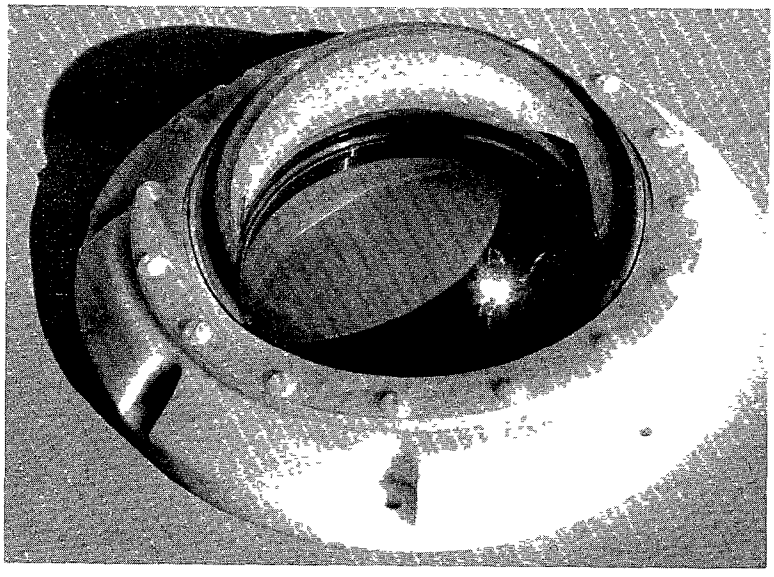

(a) Top

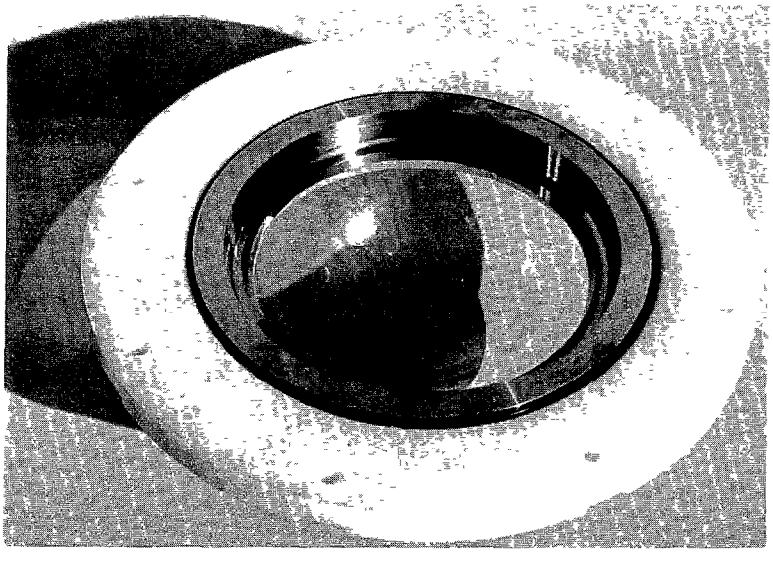

(b) Bottom

Figure 7. The NUC 150-degree spherical-shell window-flange assembly.

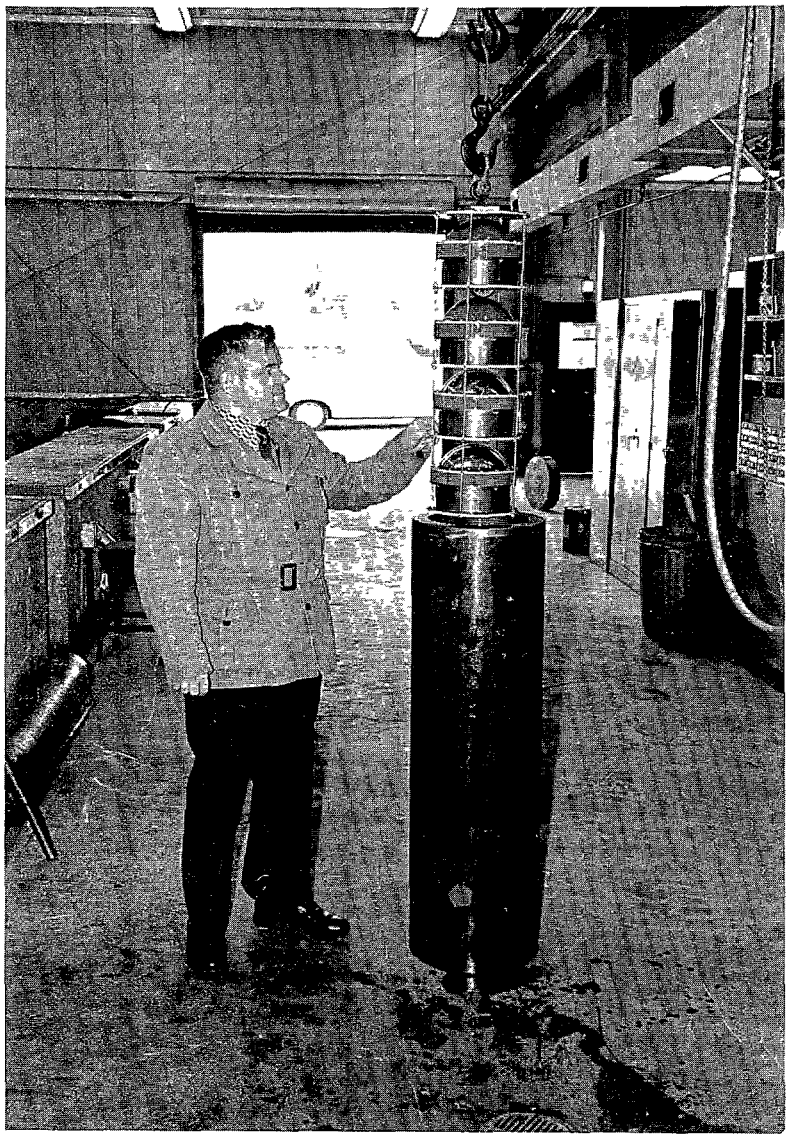

Figure 8. Holding jig for static and cyclic pressure testing of NUC window-flange assemblies in the 20,000-psi pressure vessel of the Southwest Research Institute.

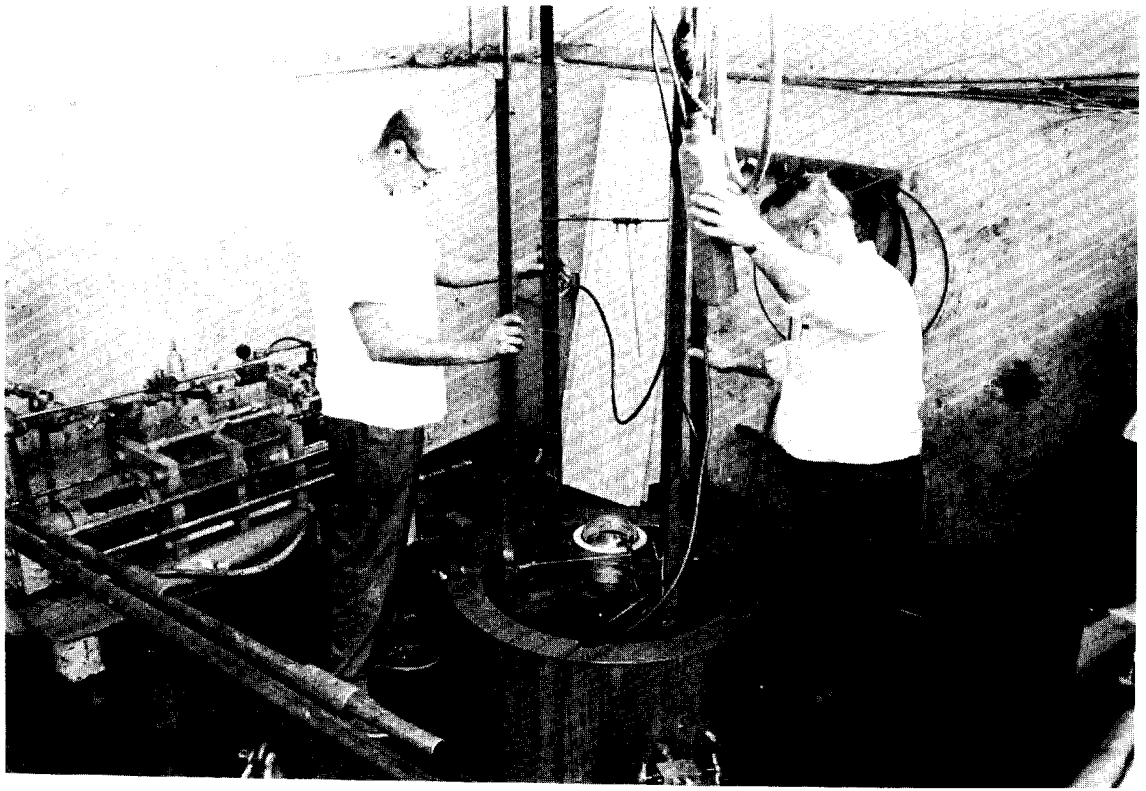

Figure 9. Holding jig for hydrodynamic impulse testing of NUC window-flange assemblies in the 30-inch-diameter pressure vessel at the Southwest Research Institute.

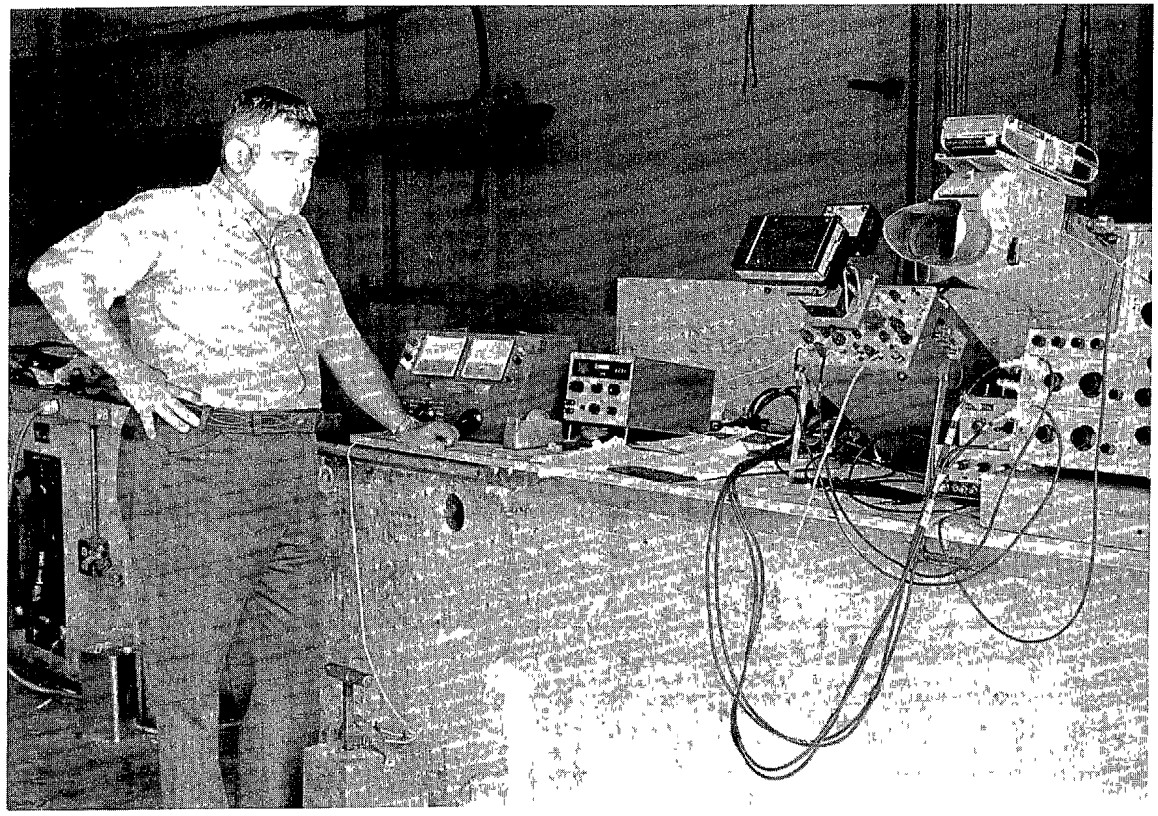

Figure 10. Instrumentation used to record pressure pulses at the test specimen after an explosive charge was set off inside the pressure vessel.

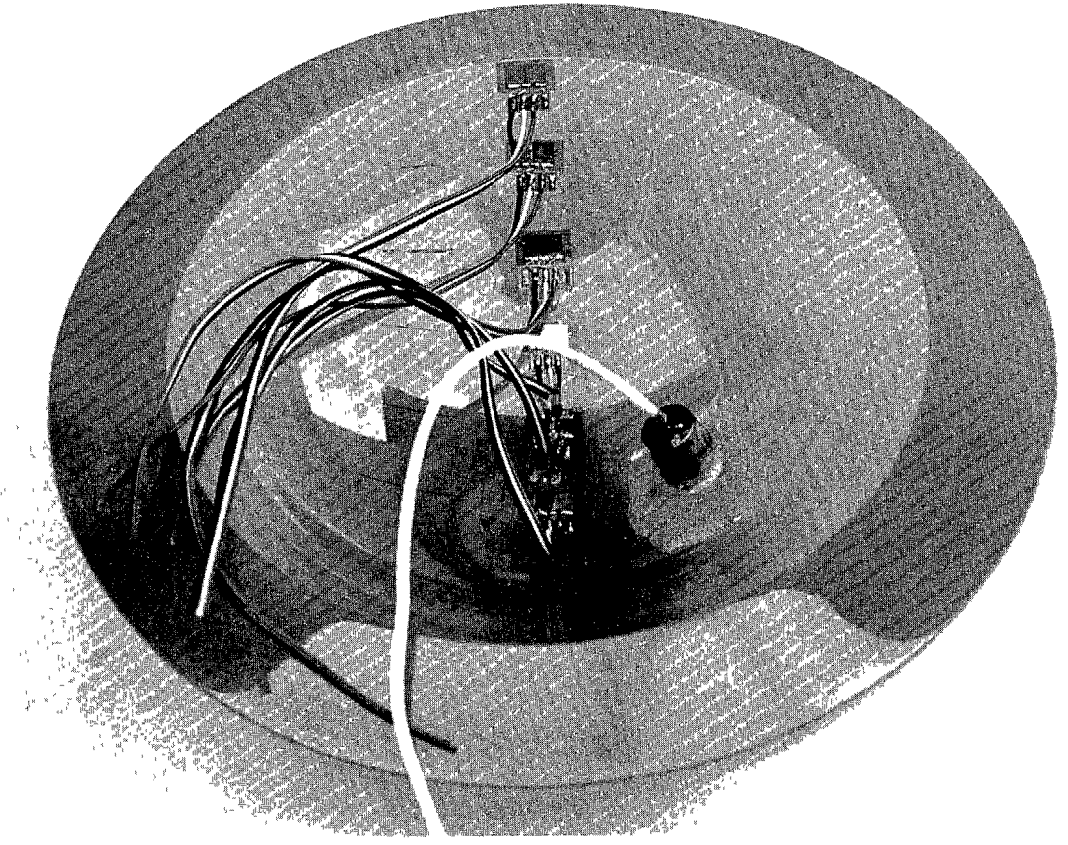

Figure 11. Instrumentation used to record strain and acoustic emissions of 150-degree spherical-shell window subjected to hydrostatic loading.

Table 3. Long-Term Hydrostatic Cycling of Windows.

Pressure range	Specimen number	Material type	Material condition	Gasket type	Number of cycles	Test results
0 to 4,500 psi	1	C-101	B	FP	128	no cracks
	3	C-101	B	FP	128	no cracks
	14	SSC-201	D	EL	128	no cracks
	20	acrylic plastic	A	FP	128	no cracks
0 to 9,000 psi	4	C-101	C	FP	137	no cracks
	5	C-101	C	EL	137	no cracks
	11	SSC-201	A	EL	137	no cracks
	13	SSC-201	A	FP	137	no cracks
0 to 13,500 psi	5	C-101	C	EL	113	no cracks
	7	C-101	B	EL	113	no cracks
	16	SSC-201	C	EL	113	no cracks
	15	SSC-201	D	EL	113	no cracks
0 to 20,000 psi	2	C-101	B	EL	300	no cracks
	8	C-101	B	EL	300	no cracks
	12	SSC-201	B	EL	300	no cracks
	17	SSC-201	B	EL	300	no cracks
	18	BK-7	AA	EL	207	catastrophic failure

Note: 1. Duration of a typical cycle: 4 hours under load and 4 hours at zero pressure.
2. Rate of pressurization and depressurization: approximately 1,000 psi/min.
3. FP = Fairprene 5722A, 0.02 inches thick; EL = 2 layers of PRD-49 cloth (Style 181; 5.0 oz/yd^2) laminated with epoxy, 0.02 inches thick.
4. AA = excellent specimens with no bubbles.
A = very good specimens with bubble size < 1 mm, quantity < 10.
B = good specimen with bubble size < 2 mm, quantity < 10.
C = fair specimen with bubble size < 2 mm, quantity < 40.
D = poor specimen with bubble size < 2 mm, quantity < 40; very extensive striae.

Furthermore, C-101 very definitely displays the Kaiser effect during repeated pressurizations; thus, acoustic emissions can be used to detect the initiation and growth of cracks in the transparent glass ceramic material.

During these tests separate groups of windows were subjected to cyclic tests over the pressure ranges from 0 to 4,500; 0 to 9,000; 0 to 13,500; and 0 to 20,000 psi. In this manner, if the specimens were found to fail in service at a pressure of 20,000 psi, it would be known for what lesser pressure service they are acceptable. Dupont PRD-49 and Fairprene 5722A fiber-reinforced gaskets were used for the cyclic tests to 4,500 and 9,000 psi to establish their prospective rates of wear at these pressures. For the 13,500- and 20,000-psi cyclic tests, only the PRD-49 epoxy-laminate gasket was utilized, although the Fairprene 5722A gasket was evaluated in a single 2-cycle test to 20,000 psi.

None of the 19 Cer-Vit C-101 glass ceramic and SSC-201 chemically surface-compressed glass windows failed, nor were any cracks initiated during the long-term cyclic tests. This was true even for windows that contained striae and many bubbles (about 20 bubbles in the 1- to 3-mm size, figures 12 and 13). The PRD-49 fiber-reinforced gaskets were found to show very little wear even after 300 long-term cycles to a hydrostatic pressure of 20,000 psi, while the Fairprene 5722A gasket began to show wear after 130 cycles to a pressure of 9,000 psi.

Experimentally measured circumferential strains on the flange and adjoining glass ceramic window were found to differ considerably (Appendix E), indicating that sliding of the window on the gasket-covered flange took place. Also, the strains show that the free sliding which was assumed in the finite element analysis to occur between the flange and the steel bulkhead was decreased significantly by friction (table 4).

The window made from annealed BK-7 optical glass failed after 207 pressure cycles to 20,000 psi of internal hydrostatic pressure. The failure was catastrophic resulting in a complete disintegration of the window. Origin of failure was located to be on the bearing surface of the window (figures 14 and 15).

The acrylic plastic window was found to perform successfully for 100 cycles at a hydrostatic pressure of 4,500 psi even though the bearing stresses were in the 9,000-psi range. This is amazing when one considers that the cyclic pressure was approximately equal to 50 percent of the short-term failure pressure for such a window (reference 3). This can be explained only by the fact that the loading in each pressure cycle lasted only 4 hours, a Fairprene 5722A gasket was used to eliminate shear stress at the bearing surface, and only 100 cycles were applied to the window.

Shock Tests were conducted to establish a qualitative comparison of the resistances of the four transparent materials to underwater shock. Four NUC spherical window assemblies equipped with acrylic plastic, Cer-Vit SSC-201 surface-compressed glass, Cer-Vit C-101 glass ceramic, and BK-7 optical glass windows were chosen for the tests (table 5).

The tests were conducted at a 450-psi static pressure simulating a 1,000-foot depth. This depth was chosen for the tests because it (a) represented only a

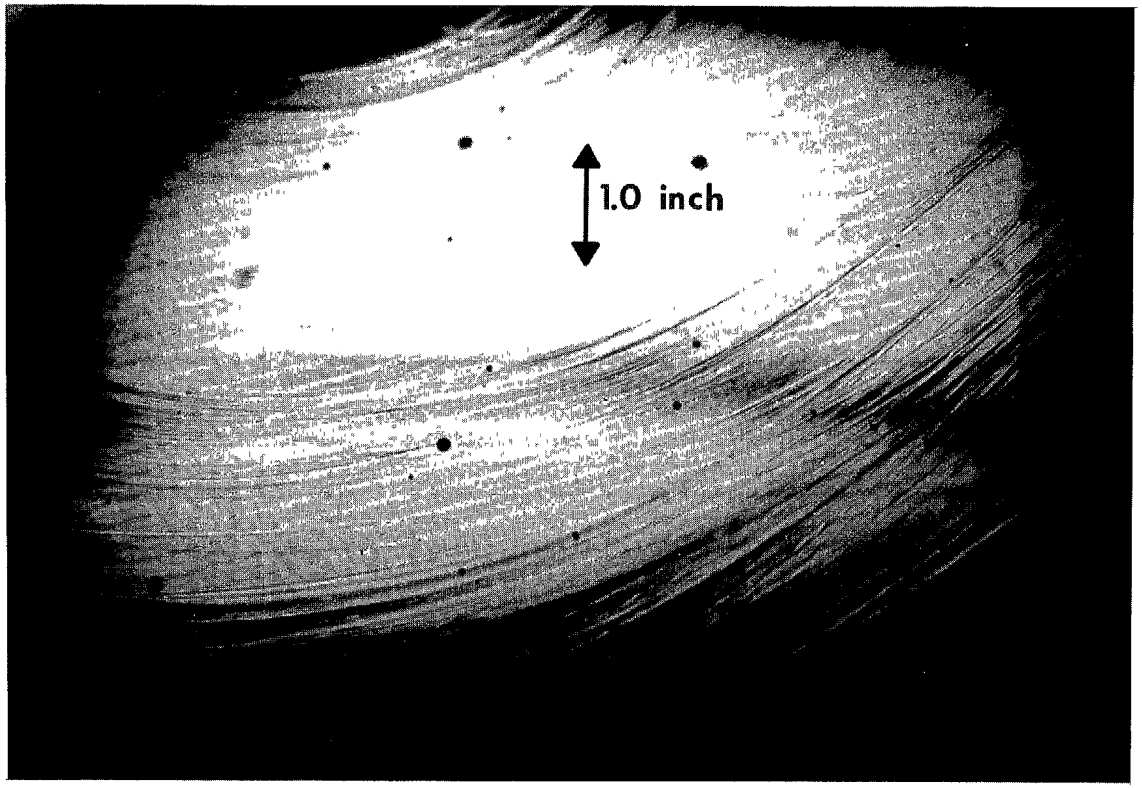

Figure 12. Typical window with many air bubbles and striae; specimen shown is window 15 fabricated from Cer-Vit SSC-201 glass.

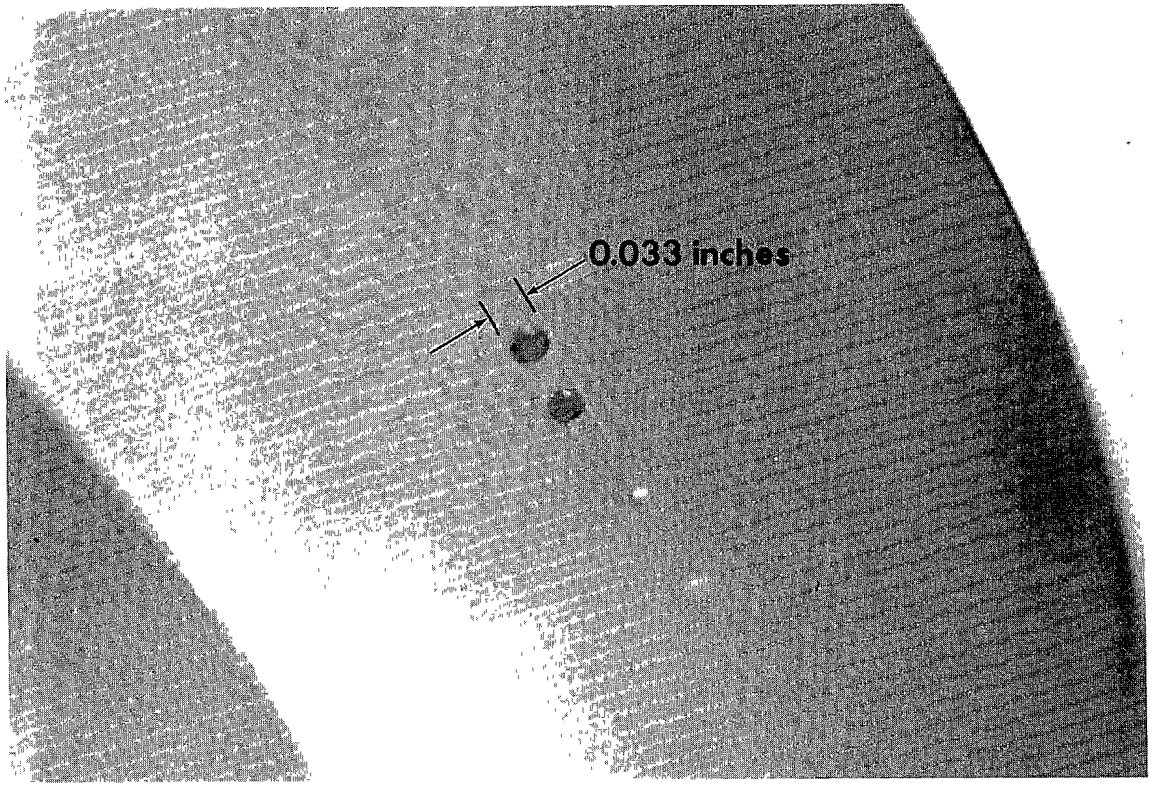

Figure 13. Typical window with air bubbles intersecting the bearing surface. specimen shown is window 3 fabricated from Cer-Vit C-101 glass ceramic.

Table 4. Actual Strains and Stresses in NUC Spherical Window Assembly at 20,000-psi External Hydrostatic Loading.

Location	Axial strains	Circumferential strains	Axial stresses	Circumferential stresses
Apex	–3300	–3300	–59,000	–59,000
75-deg Elevation (Window)	–3200	–3300	–57,500	–58,500
60-deg Elevation (Window)	–3000	–3200	–54,500	–56,500
45-deg Elevation (Window)	–2700	–3000	–49,500	–52,500
30-deg Elevation (Window)	–2400	–2700	–44,000	–47,000
15-deg Elevation (Window)	+100	–1900	– 5,300	–27,000
5-deg Elevation (Flange)	–3000	–400	–90,000	–33,400

NOTE:

1. All strain gages were located on the interior surface of the window assembly, which used a C-101 glass ceramic window.

2. Strains are given in microinches/inch.

3. Constants used in conversion of strains to stresses were $E = 13.4 \times 10^6$ psi, $\mu = 0.25$ for Cer-Vit C-101; and $E = 26 \times 10^6$ psi, $\mu = 0.32$ for K-500 Monel.

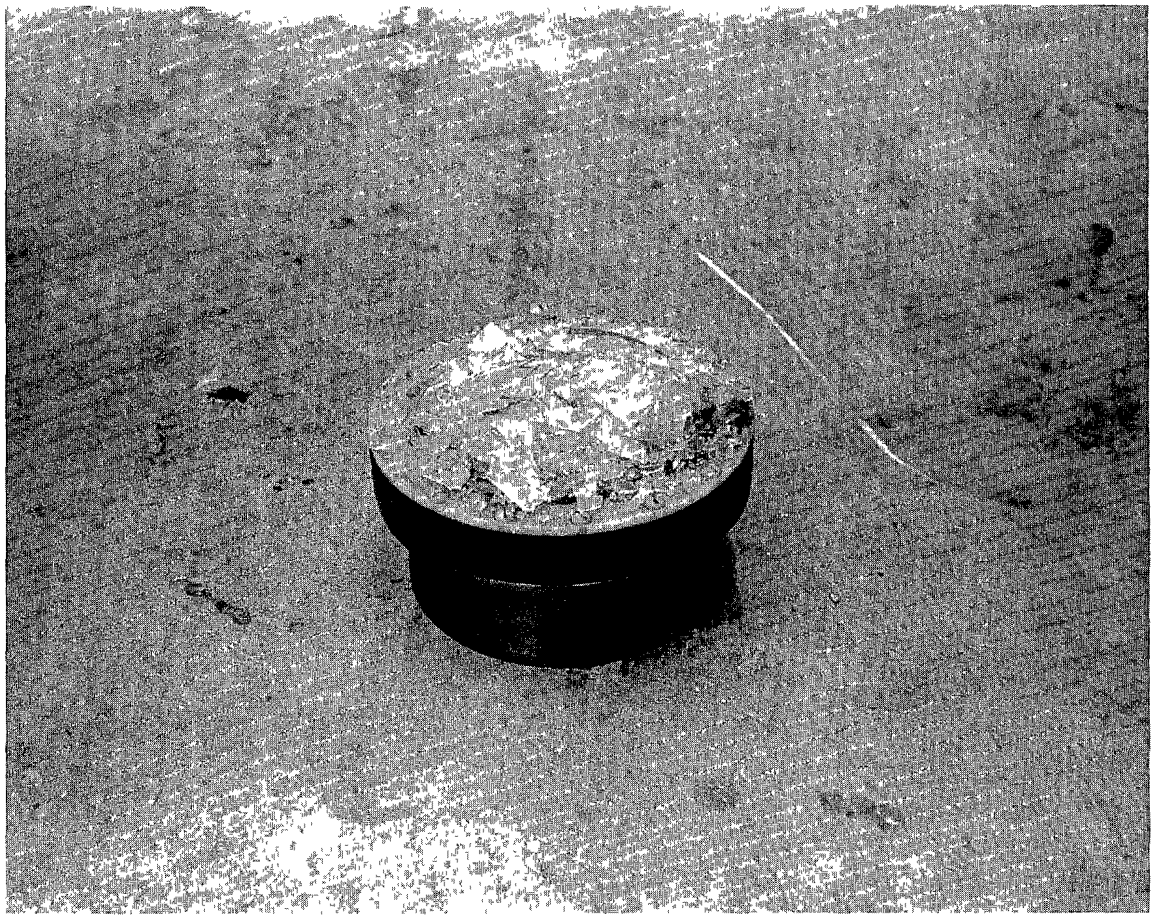

Figure 14. Failed BK-7 window after 207 pressure cycles from 0 to 20,000 psi with 4-hour sustained loading at each pressure application.

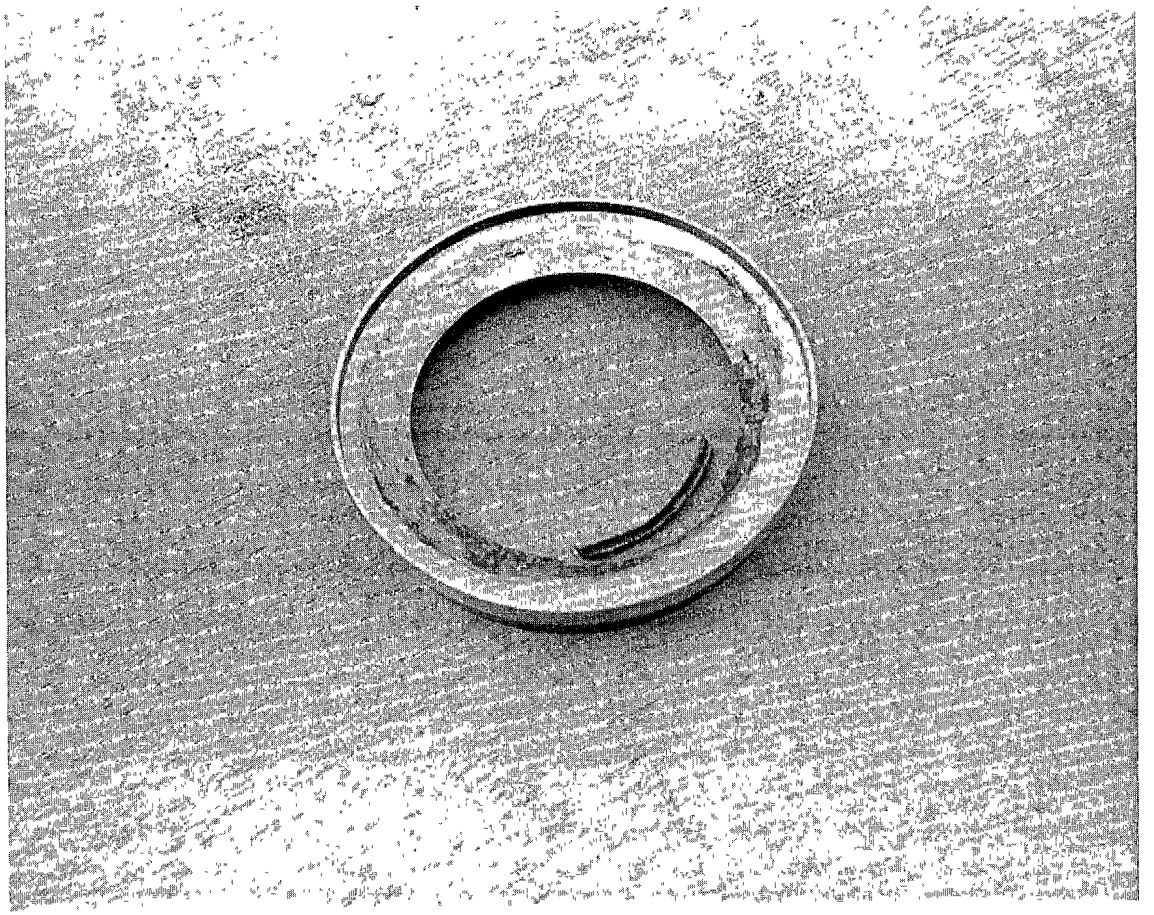

Figure 15. Window-flange from the failed BK-7 window assembly shown in figure 14.
Note the deep scars in the bearing surface from repeated cycling of window with bearing cracks.

Table 5. Resistance of Windows to Dynamic Pressure Impulses at a Simulated Depth of 1,000 feet.

Size of charge	Acrylic plastic specimen no. 19	Cer-Vit SSC-201 chemically surface-strengthened glass specimen no. 6	Cer-Vit C-101 glass ceramic specimen no. 9	BK-7 borosilicate crown glass specimen no. 10
1.1 grams	48 inches	48 inches	48 inches	48 inches
1.1 grams	36 inches	36 inches	36 inches	36 inches
1.1 grams	24 inches	24 inches	24 inches	24 inches
1.1 grams	12 inches	12 inches	12 inches[c]	12 inches[d]
4.6 grams	48 inches	48 inches[b]		
4.6 grams	36 inches			
4.6 grams	24 inches			
4.6 grams	12 inches			
8.2 grams	48 inches			
8.2 grams	36 inches			
8.2. grams	24 inches			
8.2 grams	12 inches[a]			

Note: 1. The standoff is measured between the tip of the charge and the outer surface of the window.
2. The explosive used is a mixture of 50 percent PETN, 50 percent TNT.

a No cracks
b Few cracks
c Many cracks
d Fracture, everywhere

fraction of the window's potential static depth capability and thus its brittle failure under a given shock loading would be a measure of material brittleness rather than static strength; and yet (b) it represented a depth at which the failure of a window due to shock loading would be disastrous to a manned vehicle because the crew could not escape alive after their breathing atmosphere was suddenly compressed from 0 to 450 psi.

During the tests each window was subjected individually to a series of hydrodynamic shock tests generated by small explosive charges inside a pressure vessel. The distance of the windows from the explosive charges was varied from 48 to 12 inches, while the size of the charge was varied from 1.1 to 8.2 grams.

All of the windows save that fabricated of acrylic plastic failed under hydrodynamic shock (figures 16 and 17). The glass and ceramic windows were found to be several orders of magnitude weaker than the acrylic plastic windows; of those the most resistant to shock was made of chemically surface-compressed glass Cer-Vit SSC-201, while the least resistant was made of annealed BK-7 optical glass (figure 18 a,b; 19; 20 a,b; 21; 22).

FINDINGS

1. NUC 150-degree spherical-shell window-flange assembly utilizing chemically surface-compressed glass or transparent glass ceramic, with a thickness-to-inner-radius ratio of at least 0.333 has a proven minimum fatigue life of 300 cycles consisting of 4-hour pressurizations to a hydrostatic pressure of 20,000-psi.
2. Similar windows fabricated from annealed BK-7 optical glass have shown to have a proven fatigue life of only 200 pressure cycles from 0- to 20,000-psi hydrostatic pressure.
3. Similar windows fabricated from acrylic plastic have a proven minimum fatigue life of 100 cycles consisting of 4-hour pressurizations to a hydrostatic pressure of 4,500 psi.
4. Epoxy-laminated PRD-49 cloth and neoprene-impregnated nylon cloth Fairprene 5722A are acceptable bearing gaskets for the NUC 150-degree spherical-shell window-flange assembly providing that the hydrostatic pressure does not exceed 20,000-psi. The cyclic fatigue life of epoxy-laminated PRD-49 bearing gaskets appears to be an order of magnitude longer than that of Fairprene 5722A under a bearing stress of 40,000-psi on the gasket.
5. Chemically surface-compressed glass Cer-Vit SSC-201 is significantly superior in structural applications to annealed glass and transparent glass ceramic Cer-Vit C-101 when the structure is subjected to tensile stresses, but possesses only moderate advantages when the structure is subjected to compressive stresses only.
6. Transparent glass ceramic Cer-Vit C-101 is only moderately superior in structural applications to annealed glass regardless of whether the structure is subjected to tensile or compressive stresses.

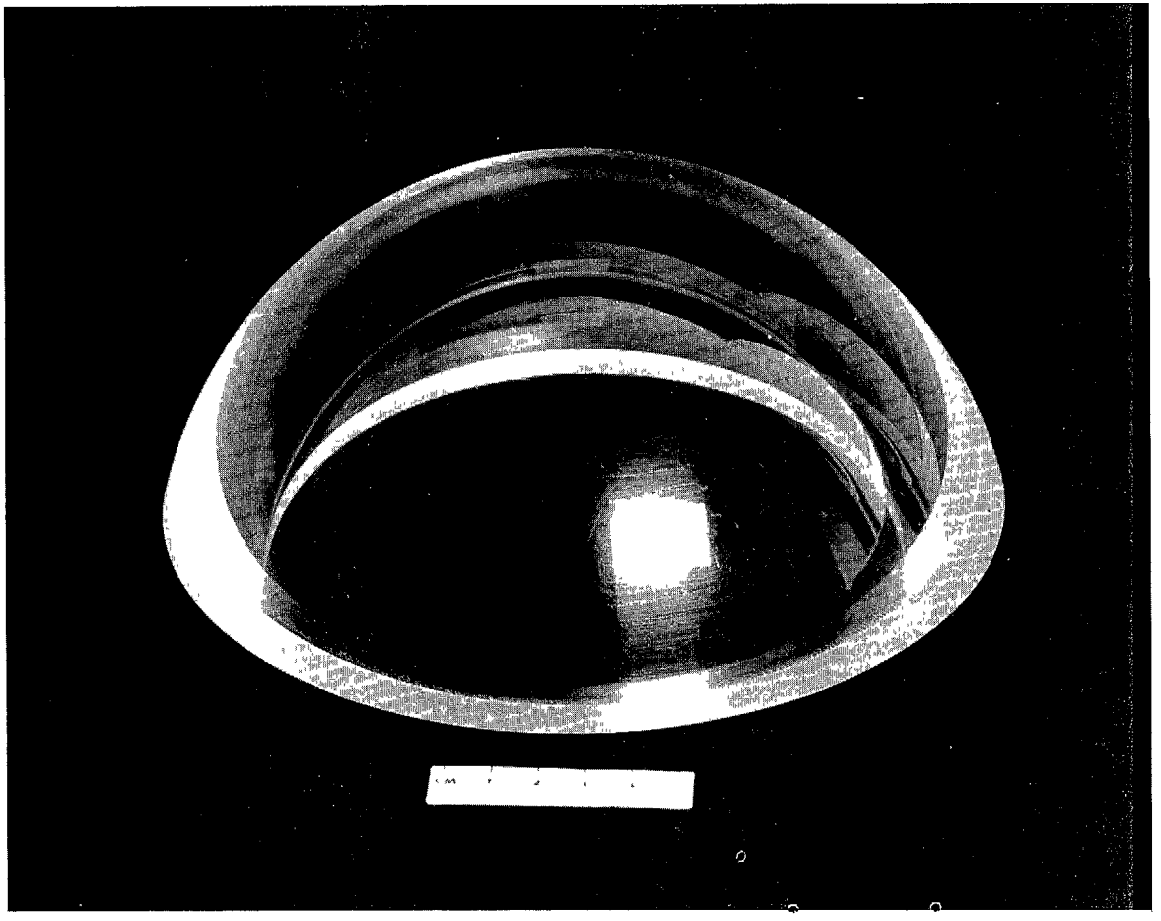

Figure 16. Plexiglas G acrylic plastic window did not fail even under the hydrodynamic impulse of an 8.2-gram explosive charge set off at a 12-inch standoff and a simulated 1,000-foot depth.

Gage 1 .2v/div

Gage 3 .2v/div

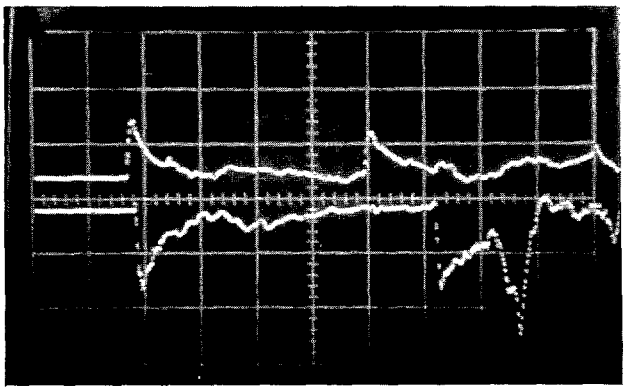

50 μsec/div

	Gage 1	Gage 2	Calculated
Peak Shock Overpressure, psi:	5,020	3,250	4,950 psi
Unit Impulse, psi-sec:	.244	.138	0.140 psi sec
Duration, μsec:	150	160	150

Figure 17. These data were recorded for the Plexiglas G acrylic plastic window subjected to hydrodynamic impluse testing.

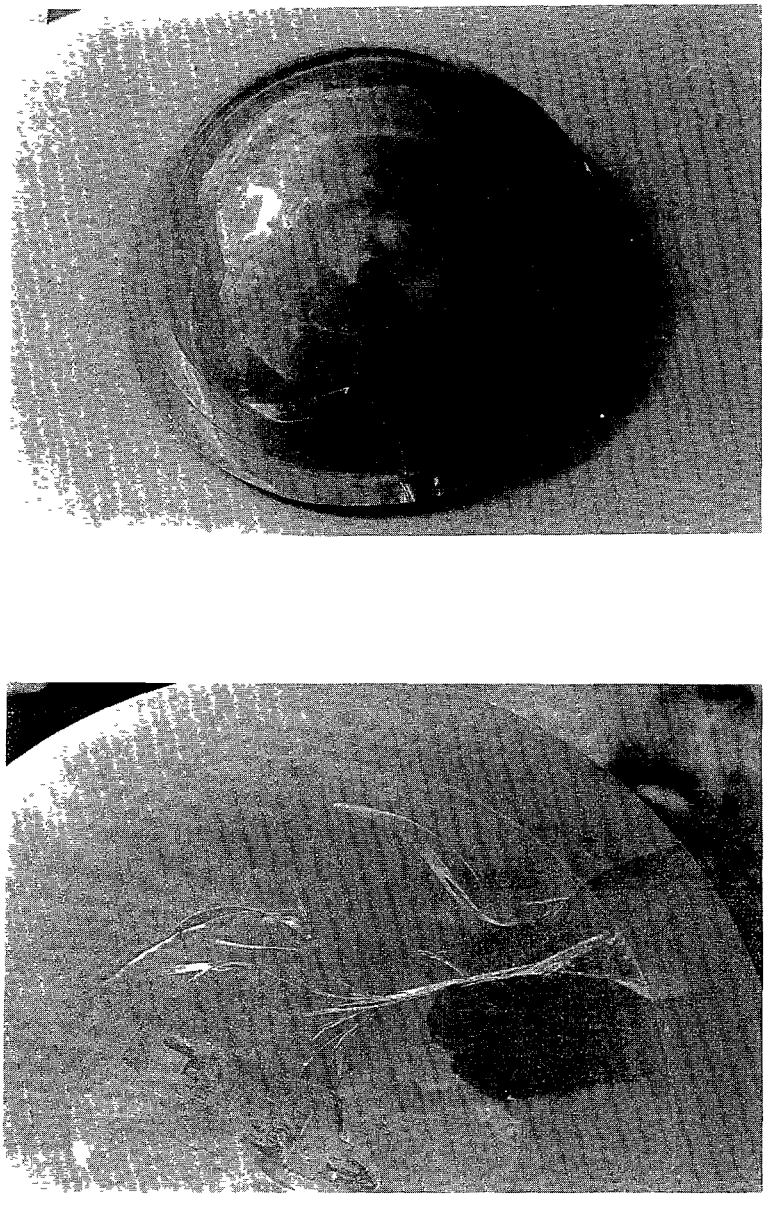

Figure 18. Cer-Vit C-101 window failed when subjected to the hydrodynamic impulse of a 1.1-gram charge set off at a 12-inch standoff and a simulated 1,000-foot depth.

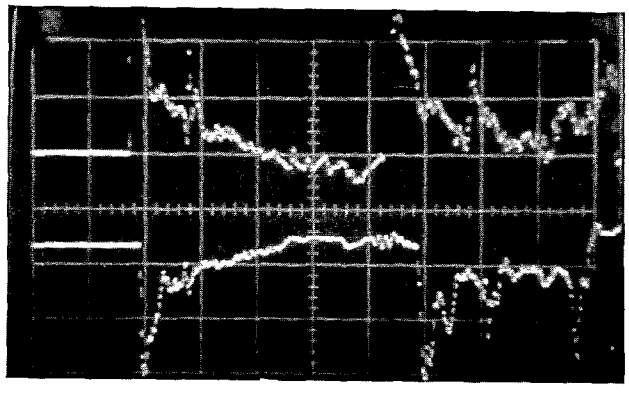

	Gage 1	Gage 2	Calculated
Peak Shock Overpressure, psi:	NA	2,350	2,290
Unit Impulse, psi-sec:	NA	.0682	.0358
Duration, μsec:	120	120	NA

Notes: (1) Model failed.

Figure 19. These data were recorded for the Cer-Vit C-101 window subjected to hydrodynamic impulse testing.

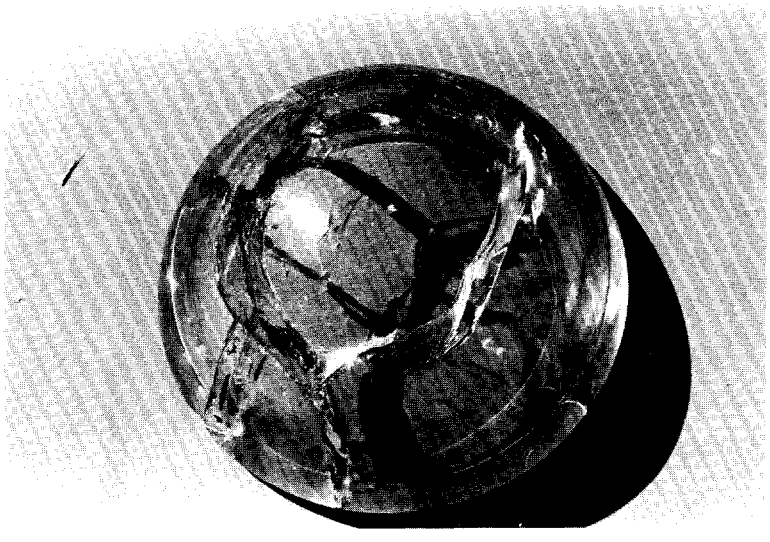

(a)

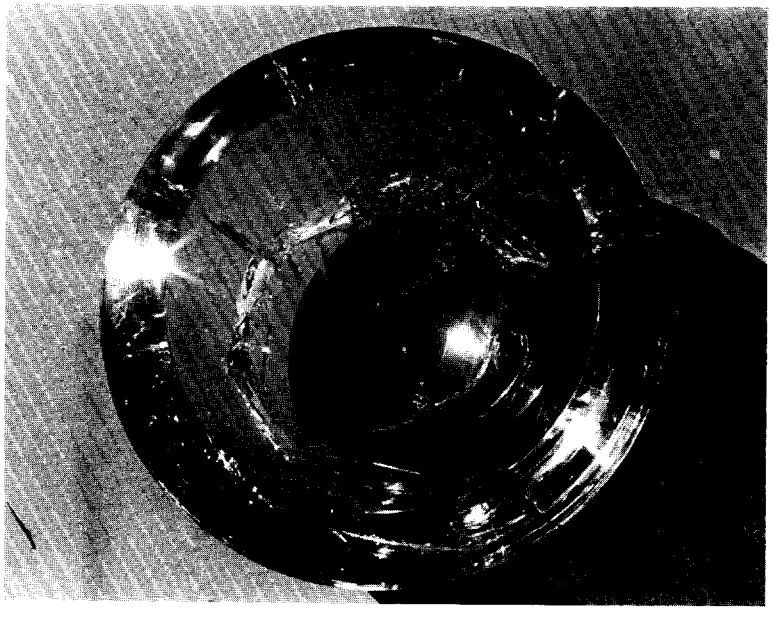

(b)

Figure 20. Cer-Vit SSC-201 chemically surface-compressed glass window failed when subjected to the hydrodynamic impulse of a 4.6-gram explosive charge set off at a 48-inch standoff and a simulated 1,000-foot depth.

Gage 1
Gage 2

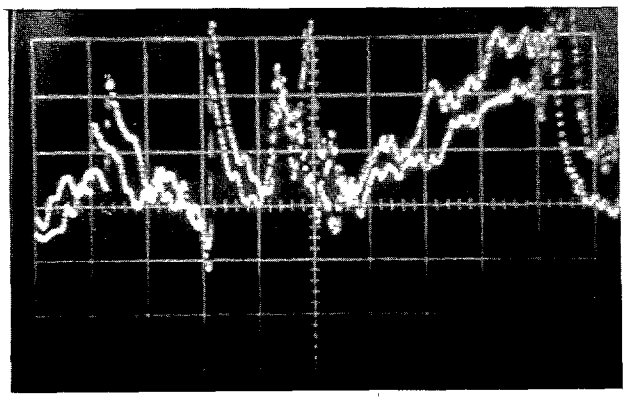

50 mv/div

t 50 μsec/div

	Gage 1	Gage 2	Calculated
Peak Shock Overpressure, psi:	1,360	1,270	835
Unit Impulse, psi-sec:	.0382	.0364	.0216
Duration, μsec:	700	800	NA

Note: Model failed.

Figure 21. These data were recorded for the Cer-Vit SSC-201 chemically surface-compressed glass window subjected to hydrodynamic impulse testing.

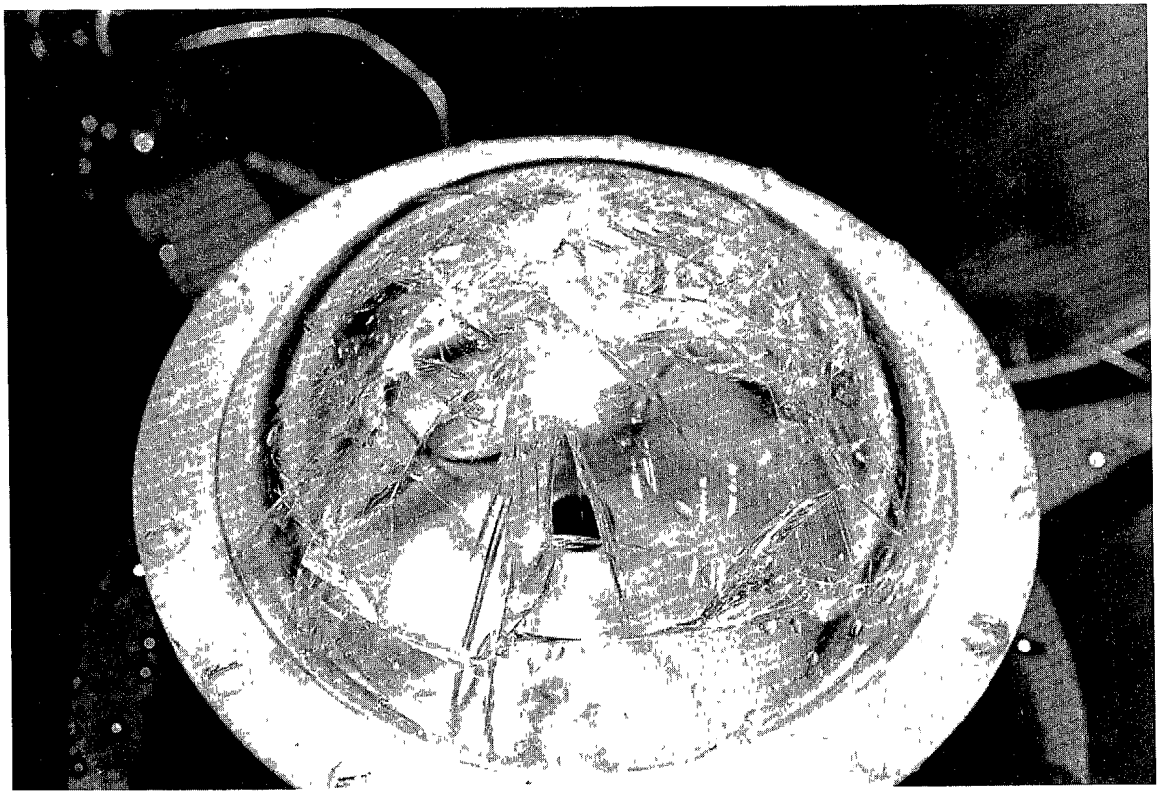

Figure 22. BK-7 glass window failed under the hydrodynamic impulse of a 1.1-gram explosive charge set off at a 12-inch standoff and a simulated 1,000-foot depth.

CONCLUSIONS

Spherical-shell sectors with a 150-degree included angle and a plane conical bearing surface have been found to serve successfully as windows with abyssal ocean depth capability if (a) fabricated from transparent glass ceramic Cer-Vit C-101, chemically surface-compressed glass Cer-Vit SSC-201 or annealed optical glass, (b) mounted in the compliant NUC window-mounting flange, and (c) cushioned by an epoxy-impregnated PRD-49 cloth or neoprene-impregnated nylon Fairprene 5722A cloth bearing gaskets. For maximum fatigue life the chemically surface-compressed glass or transparent glass ceramic Cer-Vit C-101 are preferred to annealed optical glass.

DESIGN RECOMMENDATIONS

Since some of the design parameters entering into the successful performance of NUC 150-degree spherical window assembly are not very well understood, some precautions must be taken if successful performance is to be assured from window assemblies patterned after the NUC prototype.

WINDOW ASSEMBLY

1. When the NUC design is copied in every detail the resulting window assembly will have a 100-percent assurance of successful performance to an external pressure of 20,000 psi.
2. When the NUC design dimensions are scaled up but the material, finish, and dimensional tolerance specifications are retained, the resulting window assembly may have an estimated 90- to 99-percent assurance of successful long fatigue life to an external pressure of 20,000 psi.
3. When only the key features of NUC design are retained including the (a) 150-degree included spherical angle, (b) plane-conical bearing surface, (c) laminated PRD-49 or Fairprene 5722A gasket material, (d) chemically surface-compressed glass with a minimum 50,000-psi precompression stress on the surface, glass ceramic with a minimum 12,000-psi MOR in abraded test condition, and (e) mounting flange with radial deformation theoretically matching that of window, the resulting assembly may have an estimated 60- to 70-percent assurance of successful long fatigue life to 20,000-psi.

Thus, it appears to be highly desirable for users of glass or glass ceramic spherical windows to pattern their designs as closely as possible on the NUC design so that the performance of their window assemblies is essentially the same as described in this paper. Annealed optical glass BK-7 may be used instead of the mechanically superior transparent ceramic or chemically surface-compressed glass providing the user is will to accept the shorter cyclic fatigue life of this material.

PRESSURE HULL

In addition to the precautions that should be observed during the design, fabrication and assembling of the window assembly, certain minimum conditions must be met also by the pressure hull on which the assembly is to be mounted:

1. The flange seat on the hull must be initially flat and should remain flat after the hull is subjected to its proof test depth.
2. The flange-seat diameter on the hull should decrease under hydrostatic loading at a rate that is equal to or less than that calculated for the window flange.
3. The finish of the flange seat should be in the 32 to 63 rms range.

OPERATIONAL RECOMMENDATIONS

There are several operational procedures that should be followed to insure successful performance of the window assemblies:

1. The bearing surface of the window, gasket, and flange *should be wiped completely dry of water and grease* prior to assembling them.

2. If the Fairprene 5722A gasket is utilized, it should be bonded to glass with Pliobond or equivalent contact cement. The joint in the gasket should be radial and without overlapping.
3. Two O-rings instead of a single one should be wedged between the window and the window flange (figure 1, item 3). Using two 1/8-inch-thick O-rings helps to center the window in the seat and keeps it from working loose during handling on the deck.
4. The bottom surface of the flange, which rests on the pressure hull, should be wiped clean and well greased, prior to mounting the flange on the pressure hull.

If these procedures are followed every time that the window assembly is put together, the integrity of the assembly will be assured to 20,000 psi and the premature appearance of cracks in the window's bearing surface will be prevented.

REFERENCES

1. J.D. Stachiw and K.O. Gray. Windows for External or Internal Hydrostatic Pressure Vessels, Part I: Conical Acrylic Windows Under Short Term Pressure Application. Technical Report R-512, Naval Civil Engineering Laboratory, Port Hueneme, California, January 1967.

2. J.D. Stachiw, G.M. Dunn, and K.D. Gray. Windows for External or Internal Hydrostatice Pressure Vessels, Part II: Flat Acrylic Windows Under Short Term Pressure Application. Technical Report R-527, Naval Civil Engineering Laboratory, Port Hueneme, California, May 1967.

3. J.D. Stachiw and F. Brier. Windows for External or Internal Hydrostatic Pressure Vessels, Part III: Spherical Shell Acrylic Windows Under Short Term Pressure Application. Technical Report R-631, Naval Civil Engineering Laboratory Port Hueneme, California, June 1969.

4. J.D. Stachiw. Windows for External or Internal Hydrostatic Pressure Vessels, Part IV: Conical Acrylic Windows Under Long Term Pressure Application at 20,000 psi. Technical Report R-645, Naval Civil Engineering Laboratory, Port Hueneme, California, October 1969.

5. J.D. Stachiw and W.A. Moody. Windows for External or Internal Hydrostatic Pressure Vessels, Part V: Conical Acrylic Windows Under Long Term Pressure Application at 10,000 psi. Technical Report R-708, Naval Civil Engineering Laboratory, Port Hueneme, California, December 1970.

6. J.D. Stachiw and K.O. Gray. Windows for External or Internal Hydrostatic Pressure Vessels, Part VI: Conical Acrylic Windows Under Long Term Pressure Application of 5000 psi. Technical Report R-747, Naval Civil Engineering Laboratory, Port Hueneme, California, November 1971.

7. J.D. Stachiw and J.R. McKay. Windows for External or Internal Hydrostatic Pressure Vessels, Part VII: Effect of Temperature and Flange Configuration on Critical Pressure of 90 Degree Conical Acrylic Windows Under Short Term Loading. Technical Report R-773, Naval Civil Engineering Laboratory, Port Hueneme, California, August 1972.

8. J.D. Stachiw. Development of Spherical Acrylic Plastic Pressure Hull for Hydrospace Application. Technical Report R-676, Naval Civil Engineering Laboratory, Port Hueneme, California, April 1970.

9. J.D. Stachiw and K.O. Gray. Procurement of Safe Viewports for Hyperbaric Chambers. American Society of Mechanical Engineers, Journal of Engineering For Industry, November 1971.

10. J.D. Stachiw. Acrylic Plastic Hemispherical Shells for NUC Undersea Elevator. NUC Technical Report TP 315, Naval Undersea Center, San Diego, California, September 1972.

11. J.R. Maison and J.D. Stachiw. Acrylic Pressure Hull for Johnson-Sea-Link Submersible. American Society of Mechanical Engineers, Paper 71-WA/Unt-6, December 1971.

12. J.F. Proctor. Stresses in Shallow Glass Domes with Constrained Edges. Technical Report TR 66-46, Naval Ordnance Laboratory, White Oak, Silver Springs, Maryland, June 1966.

13. D.W. Murphy. Development and Testing of a 56-inch Diameter Jointed Glass Pressure Hull. American Society of Mechanical Engineers, Paper 69-WA/Unt-2, New York, December 1969.

14. J.J. Lones. Deep Submergence Windows for Optical Systems. Society of Photo-Optical Instrumentation Engineers, Proceedings, March 1971.

15. R.E. Wilson, H.A. Perry, and F.J. Koubek. Salt Water Resistance of Surface Compression Strengthened Glass. Technical Report TR-71-56, Naval Ordnance Laboratory, White Oak, Silver Springs, Maryland, October 1971.

APPENDIX A

ASSEMBLY OF THE WINDOW-FLANGE SUBSYSTEM

The window-flange subsystem has been designed to be assembled independently of the submersible system on which it will be used from interchangeable, mass produced parts. This reduces to a minimum the number of parts to be stocked by the supplier as well as the operational delay – and thus the cost – required to replace a damaged window-flange assembly in the field.

Assembly of the subsystem entails fastening together five components in a specific sequence. The components should be laid out on a work bench in an orderly sequence and kept free of grease (figure A.1). First, the window-flange mounting ring (figure A.2) is fitted over the flange (figure A.3). Second, the window-bearing gasket (figure A.4) is place atop the flange and the window (figure A.5) is set upon it. Third, an O-ring is carefully inserted into the annular space between the convex surface of the window and the window flange lip (figure A.6). Finally, the window retainer (figure A.7) is slipped over the window and fastened to the mounting ring with screws (figure A.8). Tightening of the screws completes assembly (figure A.9).

Only after the window-flange subsystem is assembled can grease be liberally applied to the bearing surface of the window flange that will be mated to the submersible's hull. The grease will prevent corrosion on the mating surfaces, which slide over one another, and will substantially aid the lower O-ring in sealing the interface between the hull and the window flange. After the insertion of the O-ring into the groove located in the bearing surfaces of the window-flange subsystem (figure A.10), it can be mated to the submersible's hull.

Scale drawings of the window-flange subsystem and its components are presented in figures A.11 through A.15 in order of assembly.

Figure A.1. Components of the window-flange subsystem.

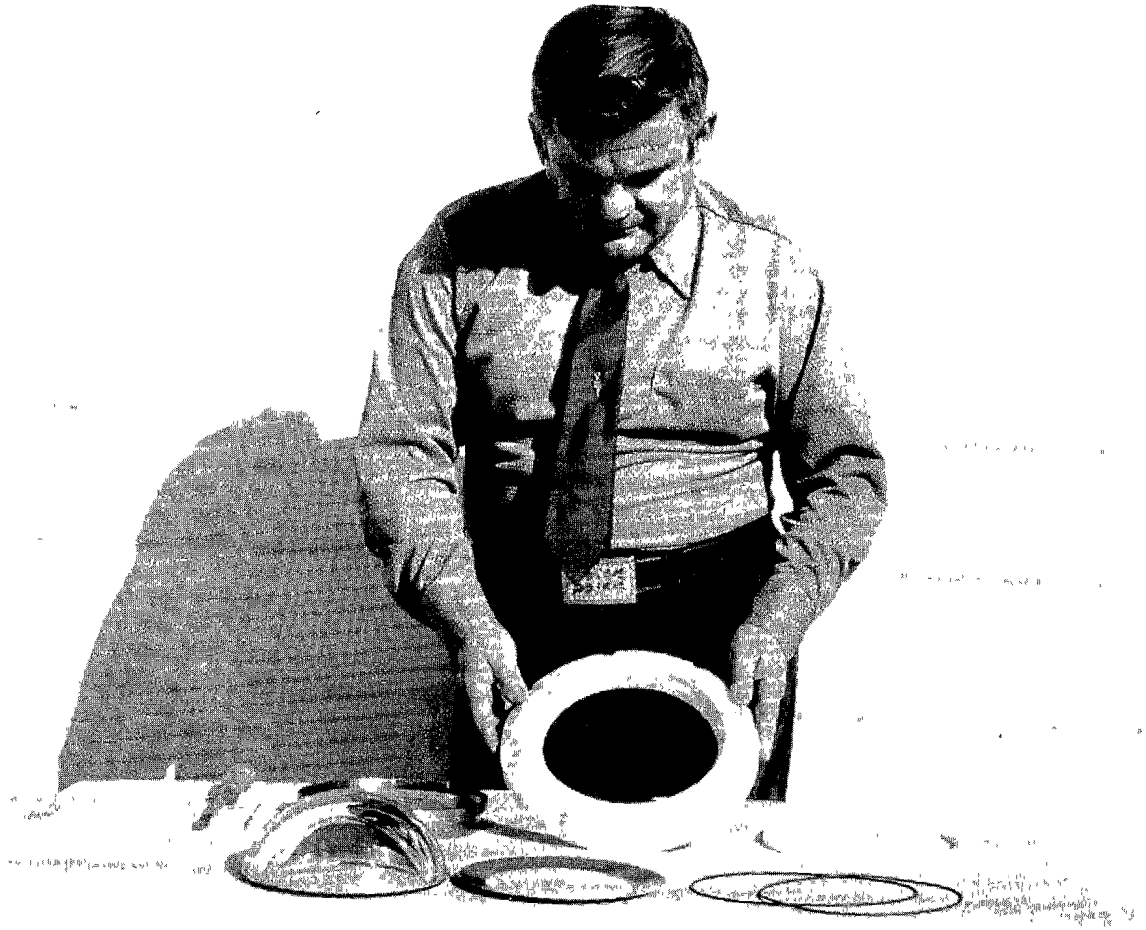

Figure A.2. Window-flange mounting ring.

Figure A.3. Flange (K-500 Monel).

Figure A.4. Window-bearing gasket (two layers of PRD-49 fiber cloth laminated with epoxy resin).

Figure A.5. Window (acrylic, glass, or ceramic).

Figure A.6. Placement of the upper O-ring into the annular space between the convex surface of the window and the inner surface of the flange lip.

Figure A.7. Window retainer (Nylon).

Figure A.8. Window retainer screws (Nylon).

Figure A.9. Tightening of the screws.

Figure A.10. Placement of the lower O-ring into the groove in the bearing surface of the window-flange subsystem.

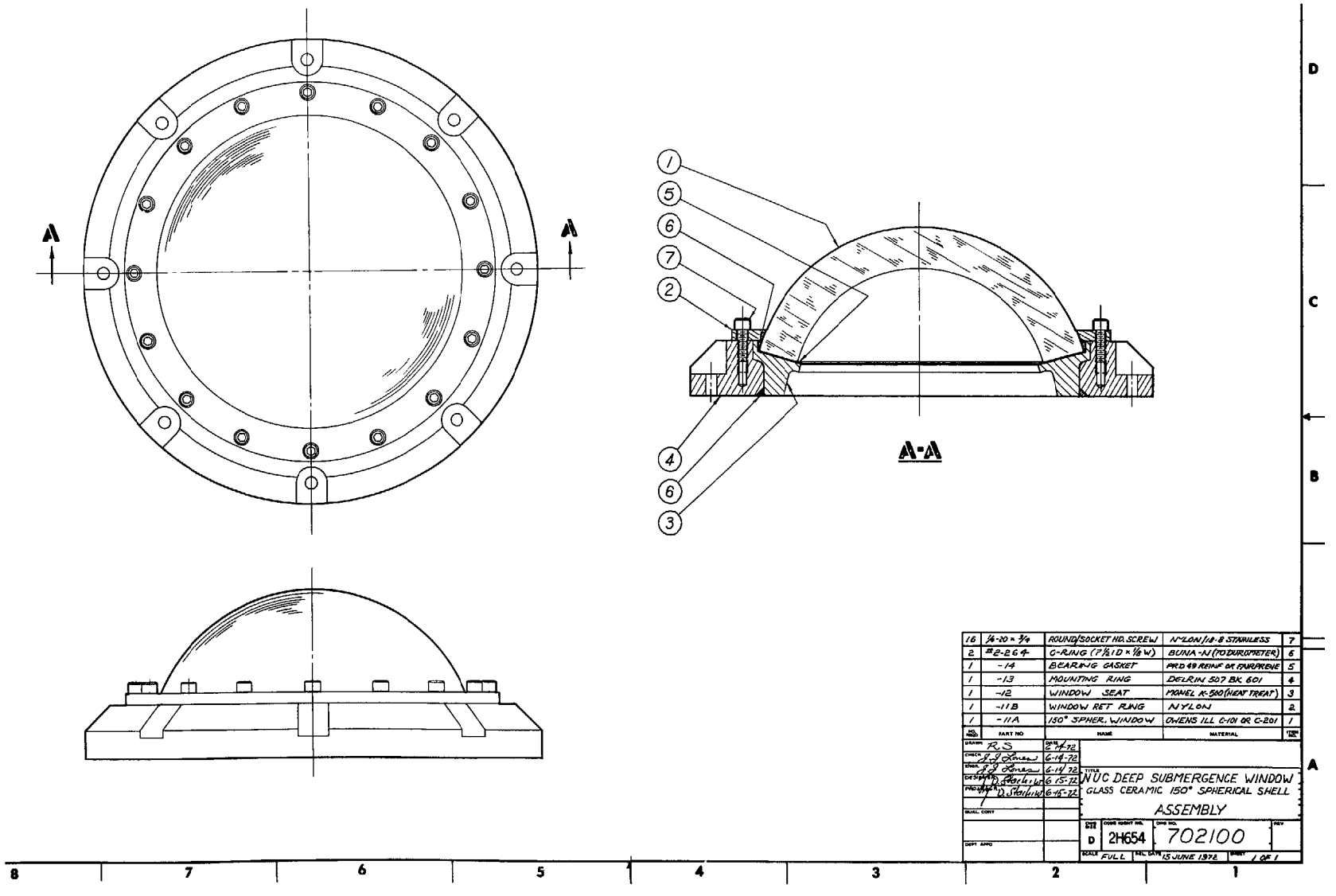

Figure A.11. Scale drawing of the window-flange subsystem.

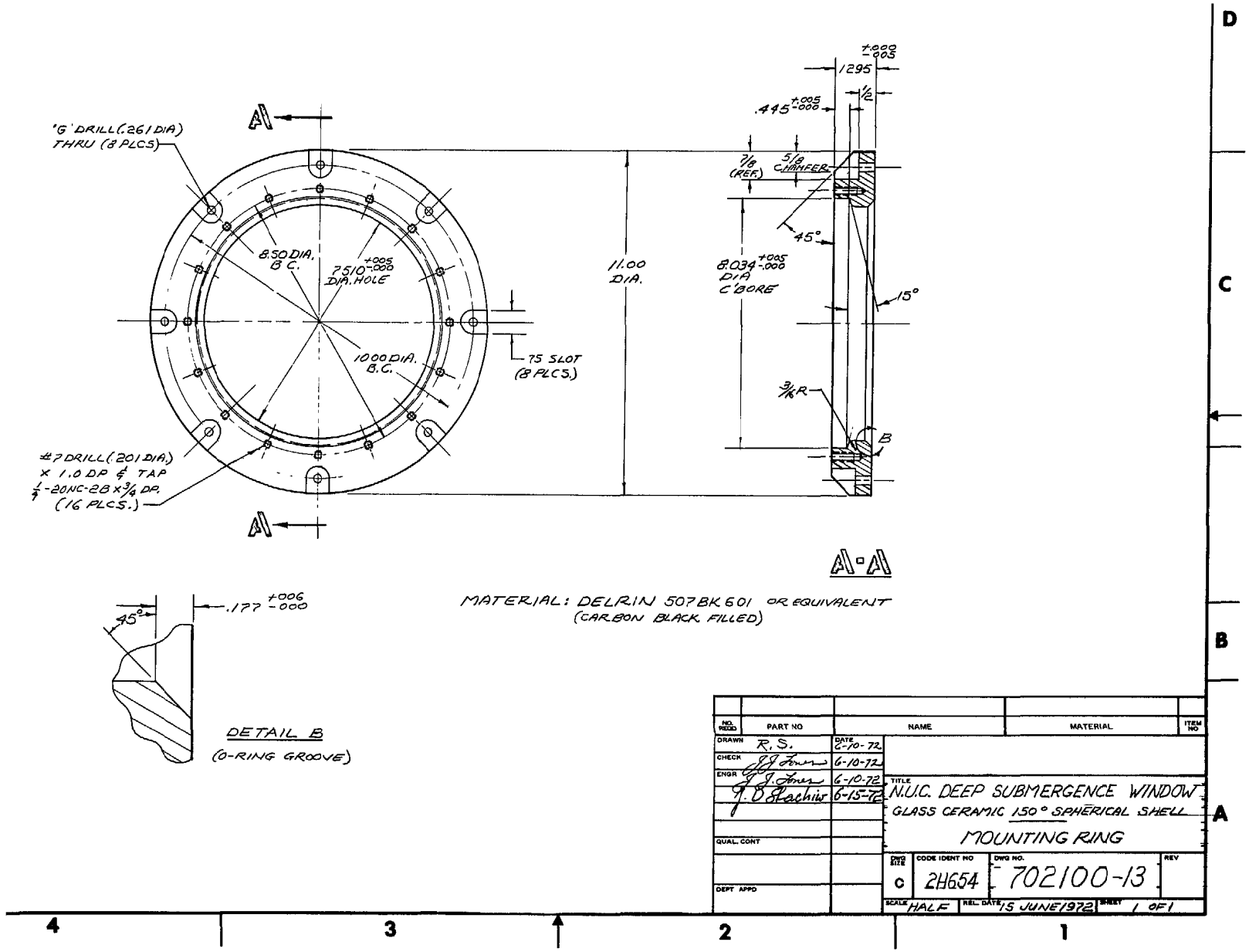

Figure A.12. Scale drawing of the window-flange mounting ring.

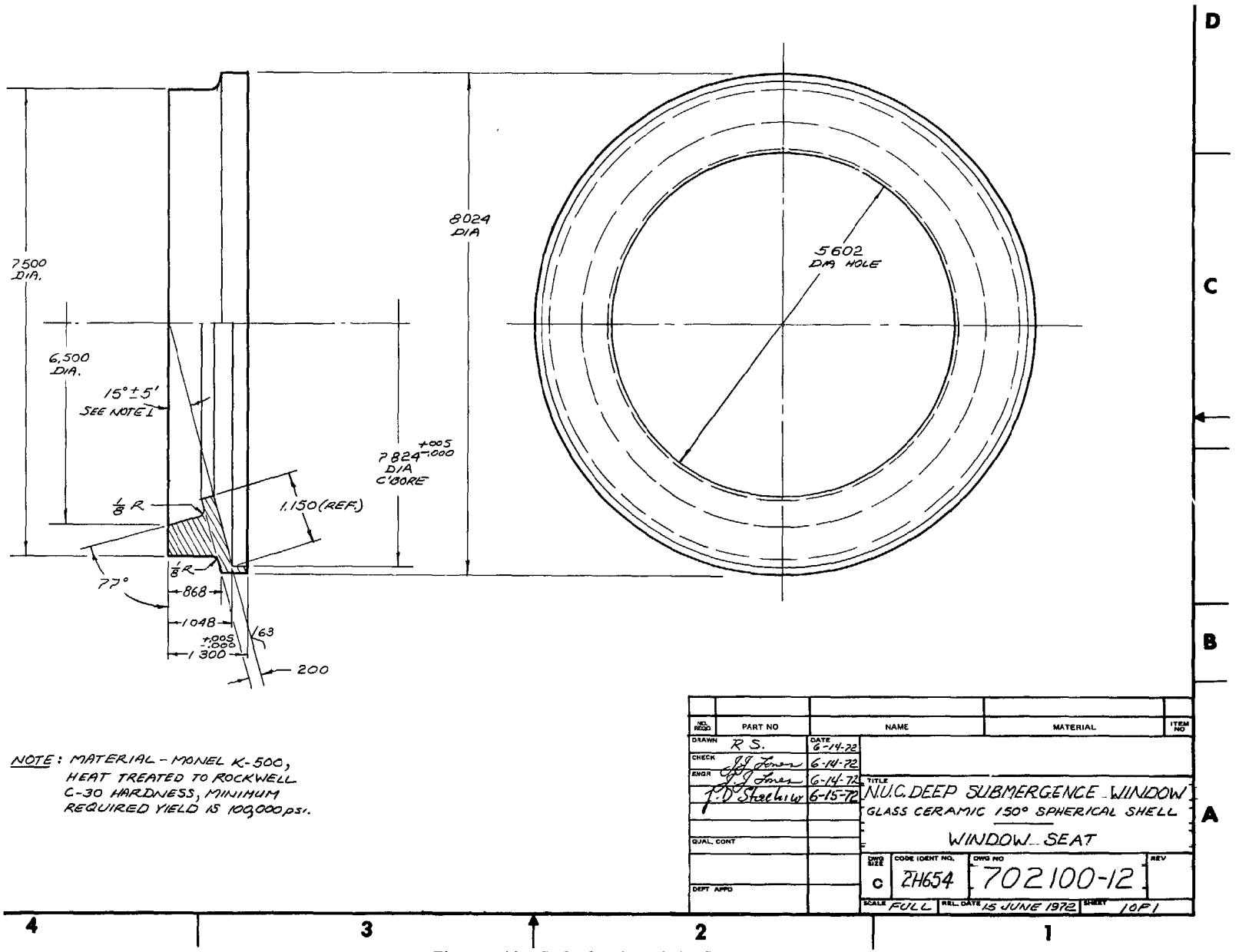

Figure A.13. Scale drawing of the flange.

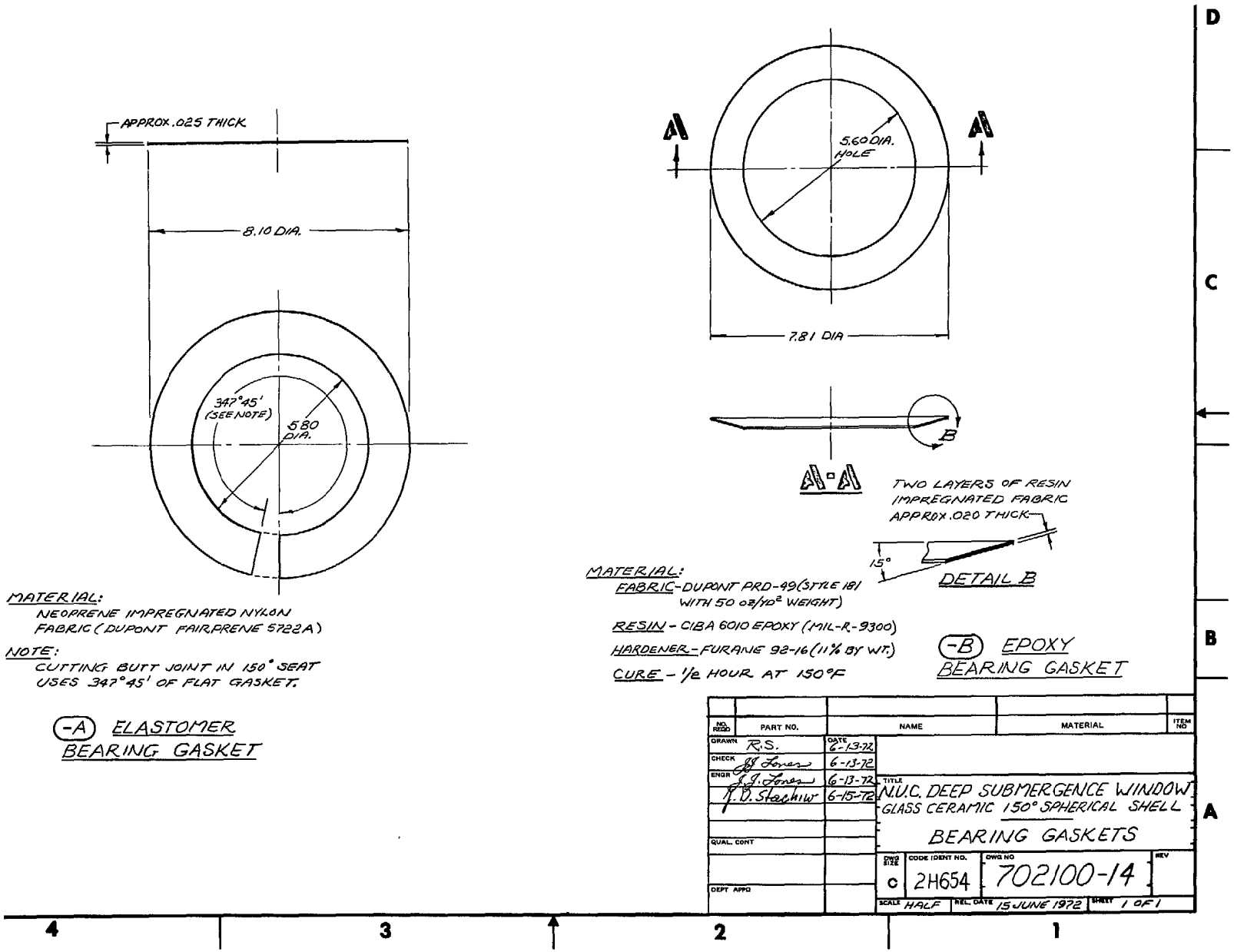

Figure A.14. Scale drawing of the window-bearing gasket.

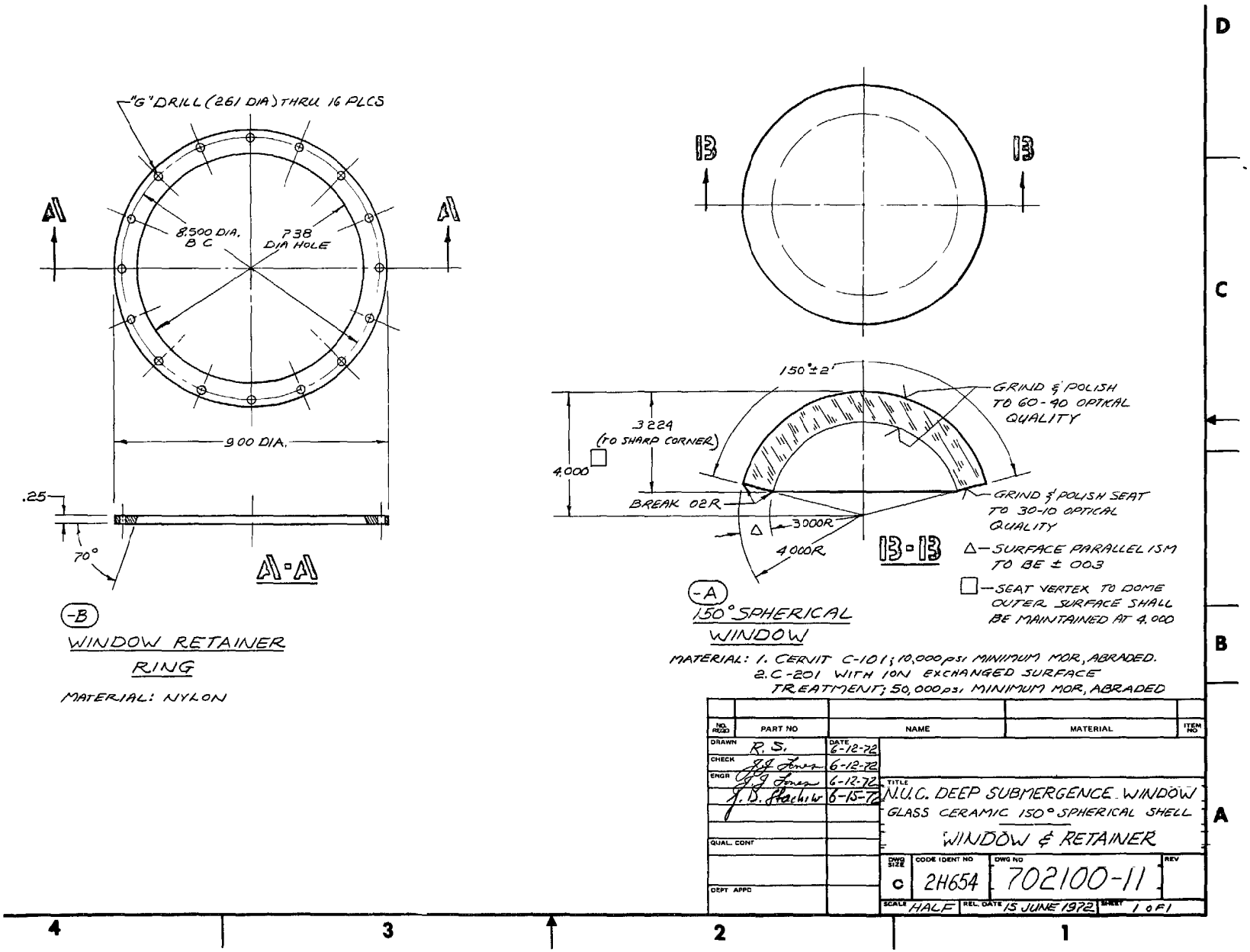

Figure A.15. Scale drawing of the window and window retainer.

APPENDIX B

FINITE ELEMENT STRESS ANALYSIS OF NUC SPHERICAL-SHELL WINDOWS

by

Kanehiro Nishida
Naval Ship Research and Development Center (NSRDC)

DESCRIPTION OF PROBLEM

Two window-flange assembly configurations were submitted by the Naval Undersea Center to the Naval Ship Research and Development Center for stress analysis. Each specified a spherical glass ceramic window with an included angle of 150 degrees and a metallic support flange. The two assembly configurations differed solely in the cross-sectional area of the support flange. All other structural parameters such as the included angle, window seat, window dimensions, and method of sealing were identical for both.

The following boundary conditions were specified for this stress analysis:

1. Slipping would occur at the interface between the window and the gasket.

2. The metallic flange was free to move only radially at the equator on roller supports with no axial displacement allowed.

Only the combinations of material properties shown in Table B.1, where E = Young's modulus and Y = Poisson's ratio, were to be analyzed.

APPROACH TO THE PROBLEM

The finite element technique was applied to the two window-flange assembly configurations. This method, as utilized by NSRDC, requires three basic steps: (1) the generation of the structural idealization, (2) the running of the finite element computer program, and (3) the plotting of results. The structural idealizations for both window assembly configurations are shown in figures B.3 and B.4. The two basic idealizations were generated by a computer program written by Rockwell and Pincus (reference B.1). In both cases the meshes consisted of 342 nodes and 545 elements. The finite element computer program utilized for this work was written by Gifford (reference B.2). It utilizes triangular ring elements and can be applied to any axisymmetric problem. It will handle nonlinear effects of the contact problem and nonlinear effects of material properties like plastic deformation.

Table B.1. Summary of Material Parameters

Problem number	Configuration	Flange		Gasket		Window	
		E	μ	E	μ	E	μ
101	A	30×10^6	0.3	20×10^6	0.3	13.4×10^6	0.25
102	A			5×10^6			
103	A			0.5×10^6			
104	A			$.005 \times 10^6$			
104A	A	26×10^6	0.3	5×10^6	0.3	13.4×10^6	0.25
105	A	17×10^6	0.3	20×10^6	0.3	13.4×10^6	0.3
106	A			5×10^6			
107	A			0.5×10^6			
108	A			$.005 \times 10^6$			
109	A	30×10^6	0.3	20×10^6	0.3	10.5×10^6	
110	A			5×10^6			
111	A			0.5×10^6			
112	A			$.005 \times 10^6$			
112A	A	26×10^6	0.3	5×10^6	0.3	10.5×10^6	0.25
113	A	17×10^6	0.3	20×10^6	0.3	10.5×10^6	0.3
114	A			5×10^6			
115	A			0.5×10^6			
116	A			$.005 \times 10^6$			
201	B	30×10^6	0.3	5×10^6	0.3	13.4×10^6	0.25
202	B	17×10^6					
203	B	10×10^6					
204	B	5×10^6					

As shown in Table B.1, a total of 22 computer runs were made, 18 of Configuration A and 4 of Configuration B. For each configuration combinations of materials for the window, flange, and gasket were analyzed. Results of the analysis are presented in graphical form. One plot for each combination shows the structure in the original and deformed state. Other plots show the stresses in the form of contour maps. On these contour maps stresses are given in sensitivities, i.e., the stress for 1 psi of external hydrostatic pressure.

FINDINGS

Configuration A

Changing mechanical properties of the various parts (figure B.5 and B.6) did not have a very significant effect on the stress in the glass ceramic windows mounted in flange Configuration A (Problems 101 through 108). In practically every case the compressive circumferential stress at the bearing surface, however, was slightly lower than the Lame' stress for thick-walled spheres. This indicates that a hoop tensile stress is superimposed on the membrane stress. The deviation from the membrane stress appears to be only about 10 percent and, therefore, should not be a significant factor. The axial stress plots indicate that the major portion of the load is transmitted through the central portion of the bearing surface. At midthickness, the stress sensitivity is about -2.25 psi/psi; at the edges, the sensitivity drops off to about -2 psi/psi. The parabolic stress distribution is caused by the shape of the metal flange web, which has a narrower width than the thickness of the glass ceramic window.

It appears that the steel flange provides a radial displacement (figure B.7) that better approximates the membrane displacement of the glass ceramic window than does the titanium flange. However, it appears that the glass ceramic has a tendency to slide outward from the steel flange. This probably causes the lower hoop stress in the glass ceramic part noted earlier. The titanium flange has a tendency to deflect radially almost twice as much as the glass ceramic window.

Computer problems 109 through 116, which were identical to 101 through 108 except that the window material was a glass with a lower Young's modulus, (10.5×10^6) produced stress distributions which were nearly identical to those in the higher modulus (13.4×10^6) glass ceramic windows. This is mainly due to the basic assumption that slipping occurs at the interface. Although various properties for the gasket were tried, their effect was practically unnoticeable, again because of the slippage assumption.

Configuration B

Changing mechanical properties of the metal flange Configuration B produced change in the stresses in the glass ceramic window (figures B.8, B.9, and B.10). It appears that as the stiffness of the flange was decreased by lowering Young's modulus, a very local increase in the circumferential and axial stress was created at the inner edge of the glass ceramic bearing surface. Although this stress is compressive, it should nevertheless be viewed with caution.

The manner in which the glass ceramic window and flange move relative to one another should be carefully considered (figure B.11). It should be noted that slipping between window and flange may not occur in the actual case. This would cause shear stresses at the interface and possibly local tensile stresses at flaws in the window. It would, therefore, appear that a good choice for a flange material would be aluminum since it deflects in approximately the same manner as the window. This minimizes the effect of shear stresses between the window and the flange.

CONCLUSIONS

Steel appears to be suitable as the construction material *for flange Configuration A* while *aluminum and titanium* appear still to be suitable *for flange Configuration B.* The local contact stresses at the inner edge of the aluminum and titanium flanges of Configuration B and the relative outward movement of the glass ceramic window with respect to the steel ring of Configuration A should be noted, as they may become sources of window assembly failure.

REFERENCES

1. Rockwell, R. D. and Pincus, D. S., "Computer Aided Input and Output for Use with the Finite Element Method of Structural Analysis" NSRDC Report 3204 (August 1970).

2. Gifford, L. N., "Finite Element Analysis for Arbitrary Axisymmetric Structures," NSRDC Report 2641 (March 1968).

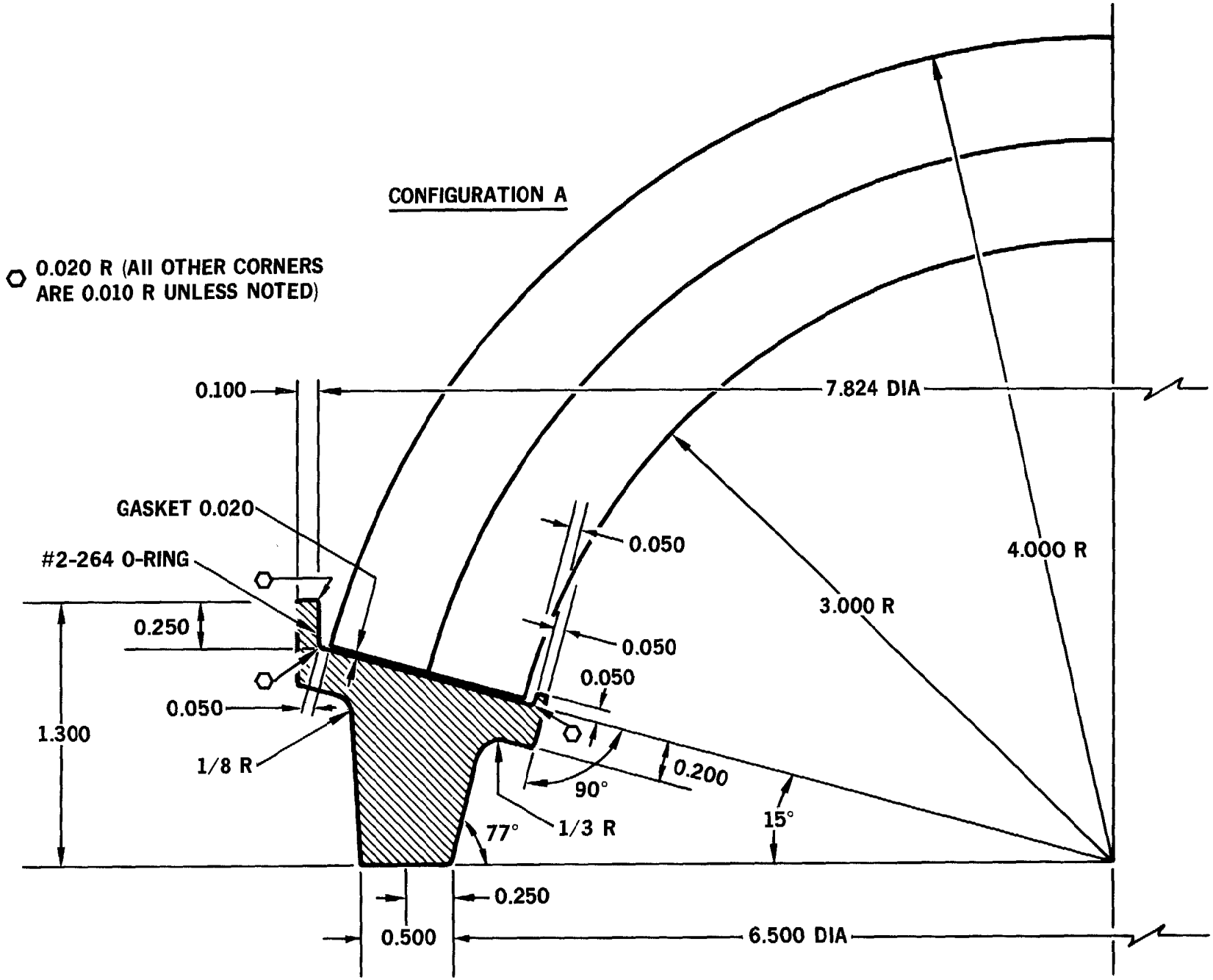

Figure B.1. NUC spherical-shell window-flange assembly Configuration A.
The inner lip on the flange was removed from the design prior to fabrication.

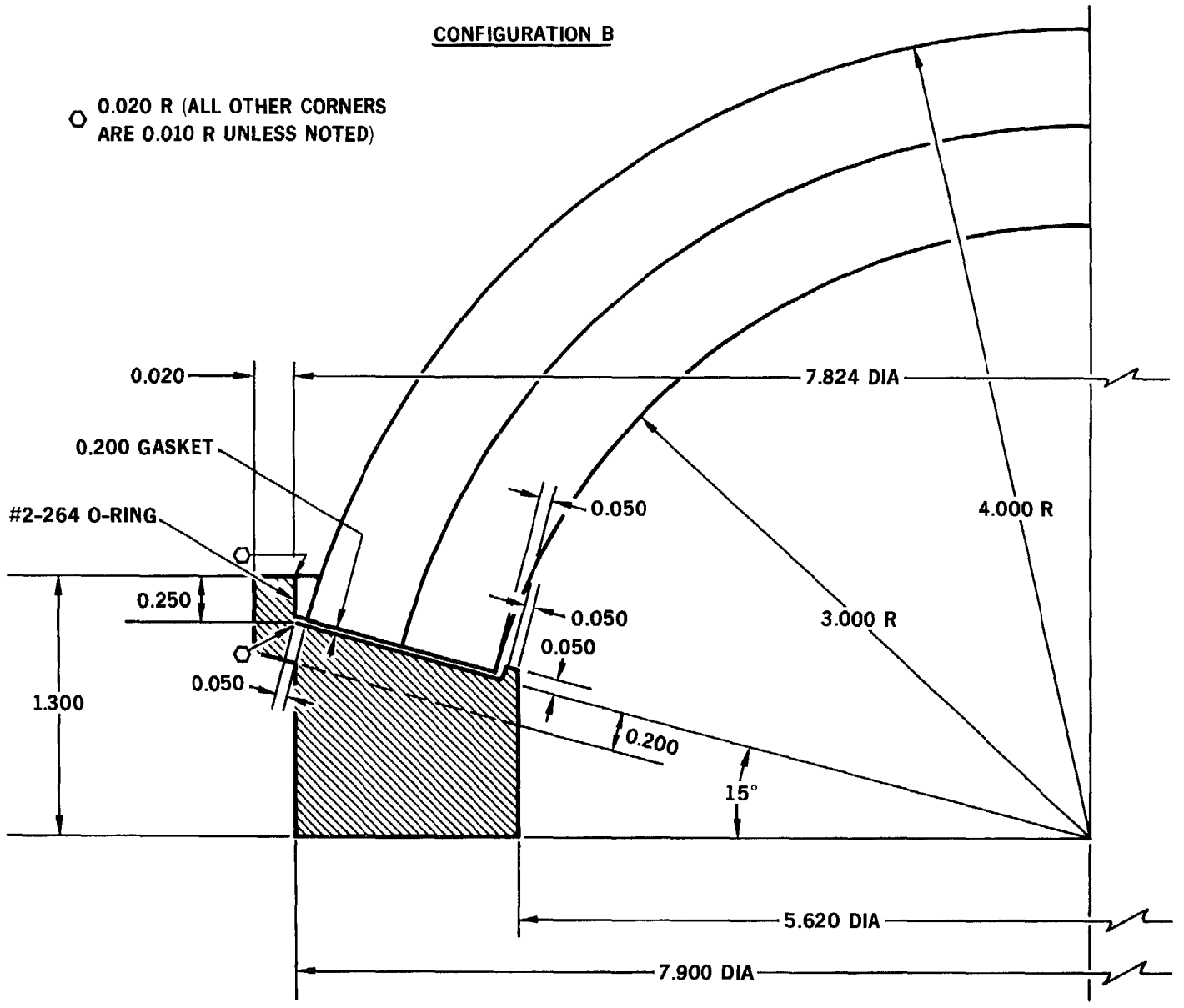

Figure B.2. NUC spherical-shell window-flange assembly configuration B.

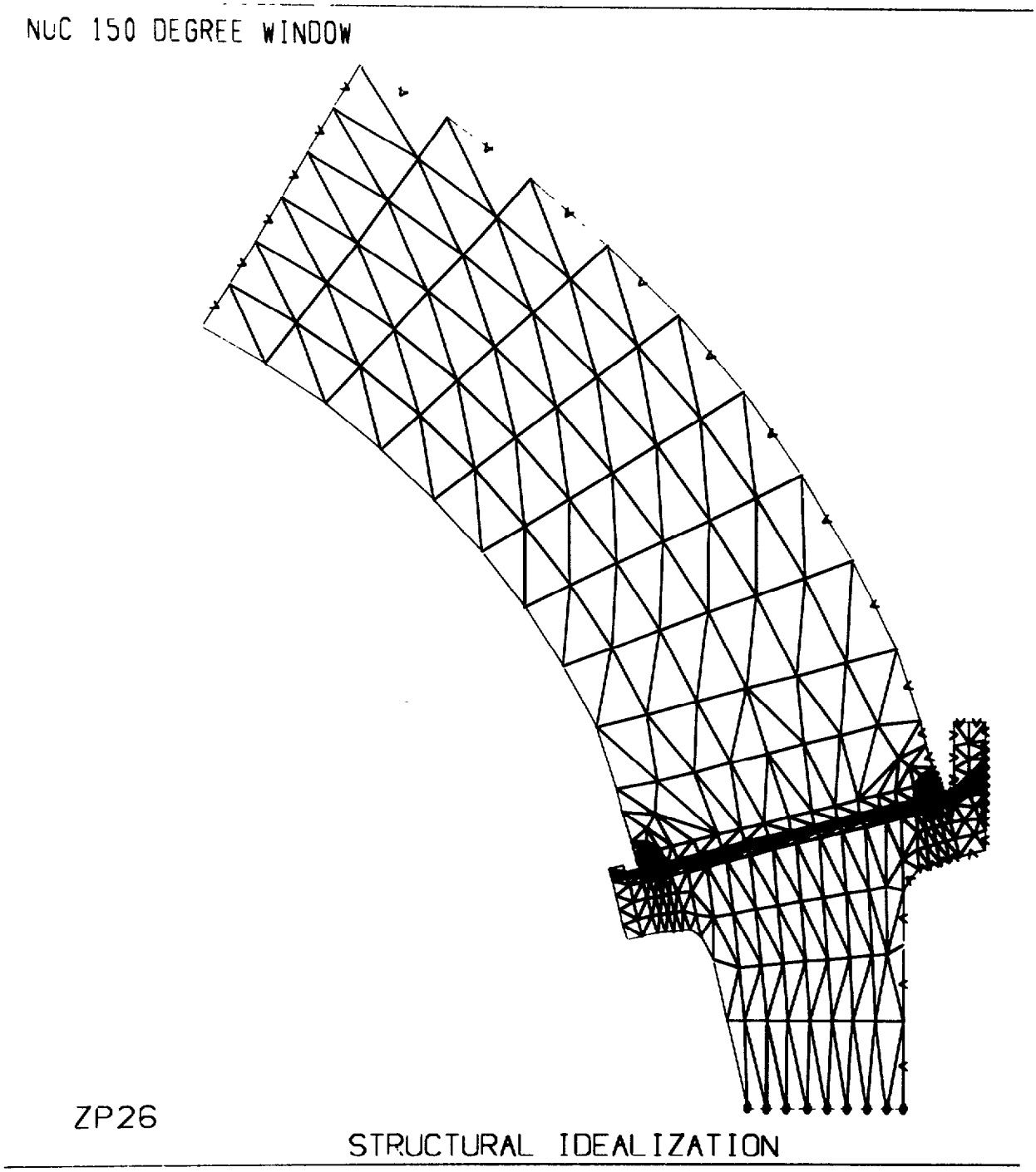

Figure B.3. Structural idealization of Configuration A.

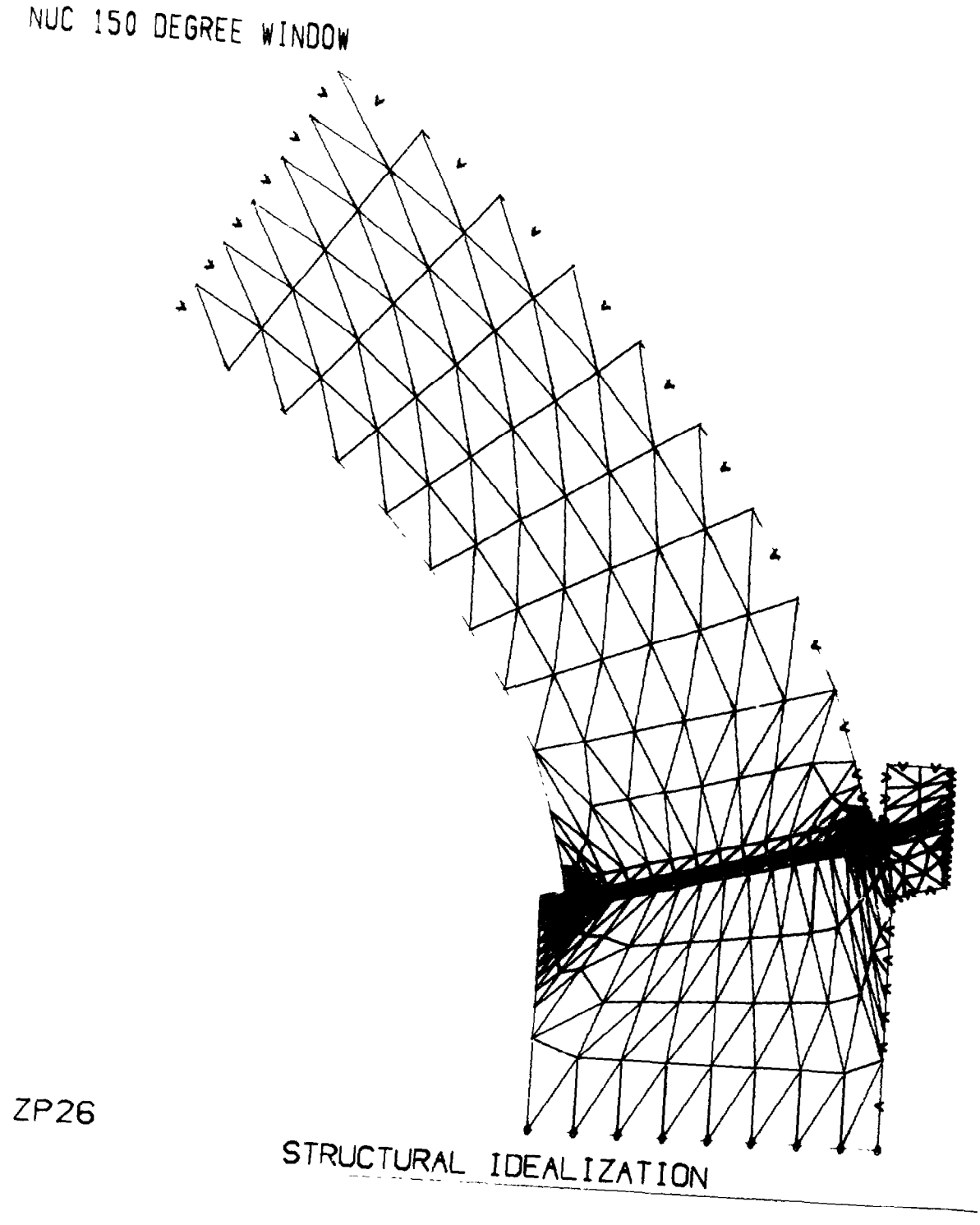

Figure B.4. Structural idealization of Configuration B.

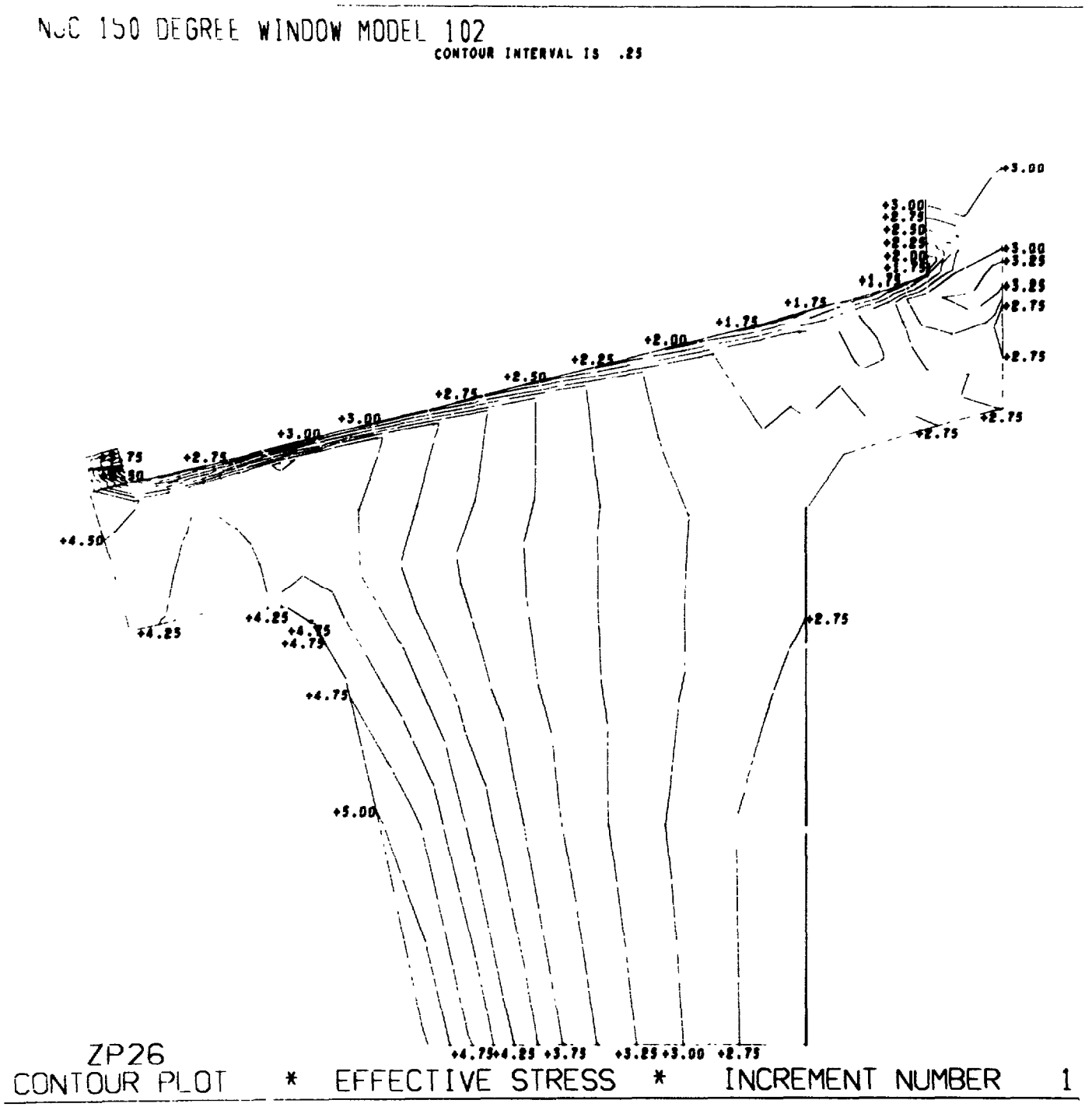

Figure B.5. Magnitude and distribution of stresses in window-flange assembly Configuration A utilizing a steel flange, fiber-reinforced-epoxy gasket, and glass ceramic window (problem 102). (sheet 1 of 7)

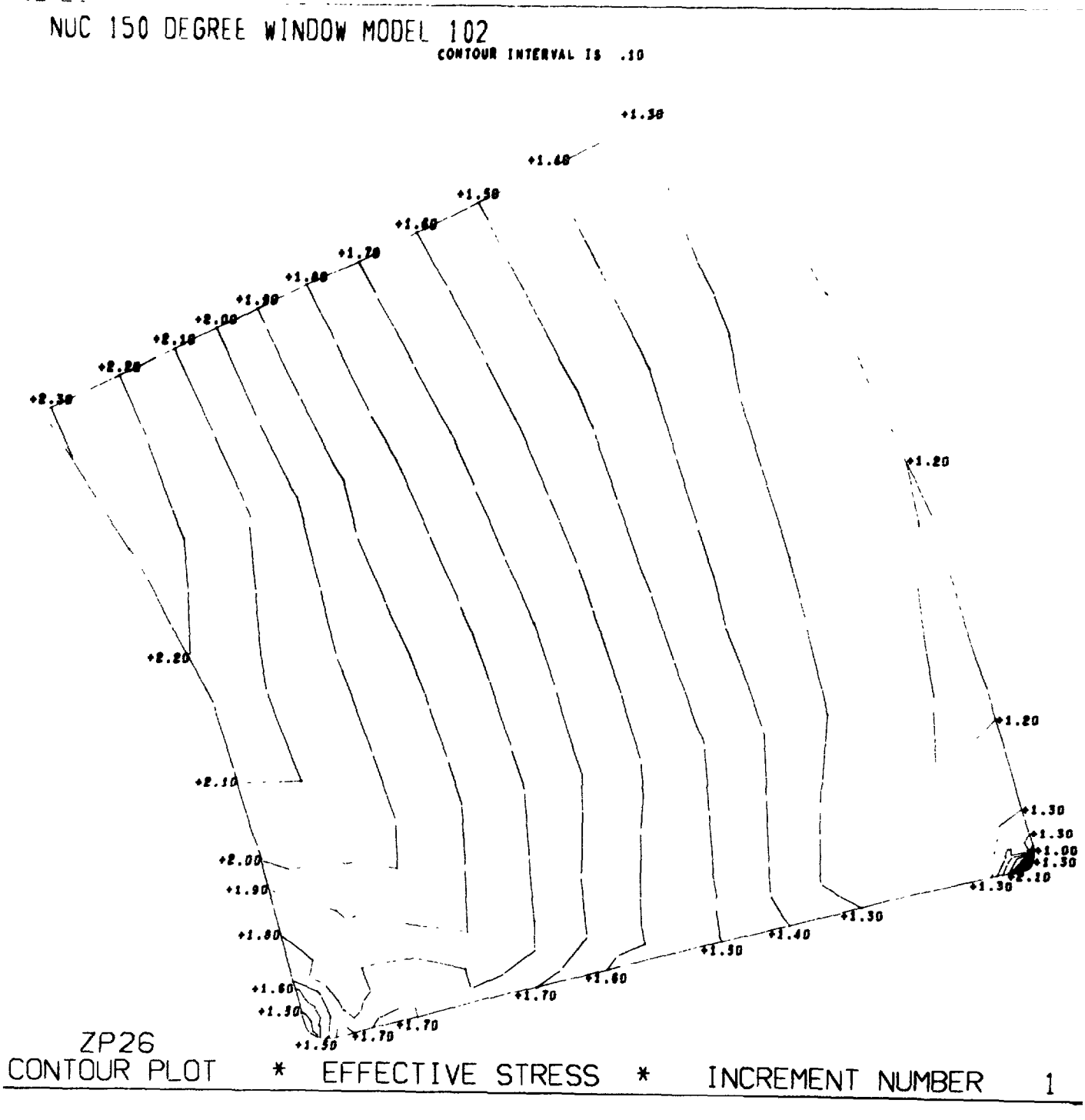

Figure B.5. Magnitude and distribution of stresses in window-flange assembly Configuration A utilizing a steel flange, fiber-reinforced-epoxy gasket, and glass ceramic window (problem 102). (sheet 2 of 7)

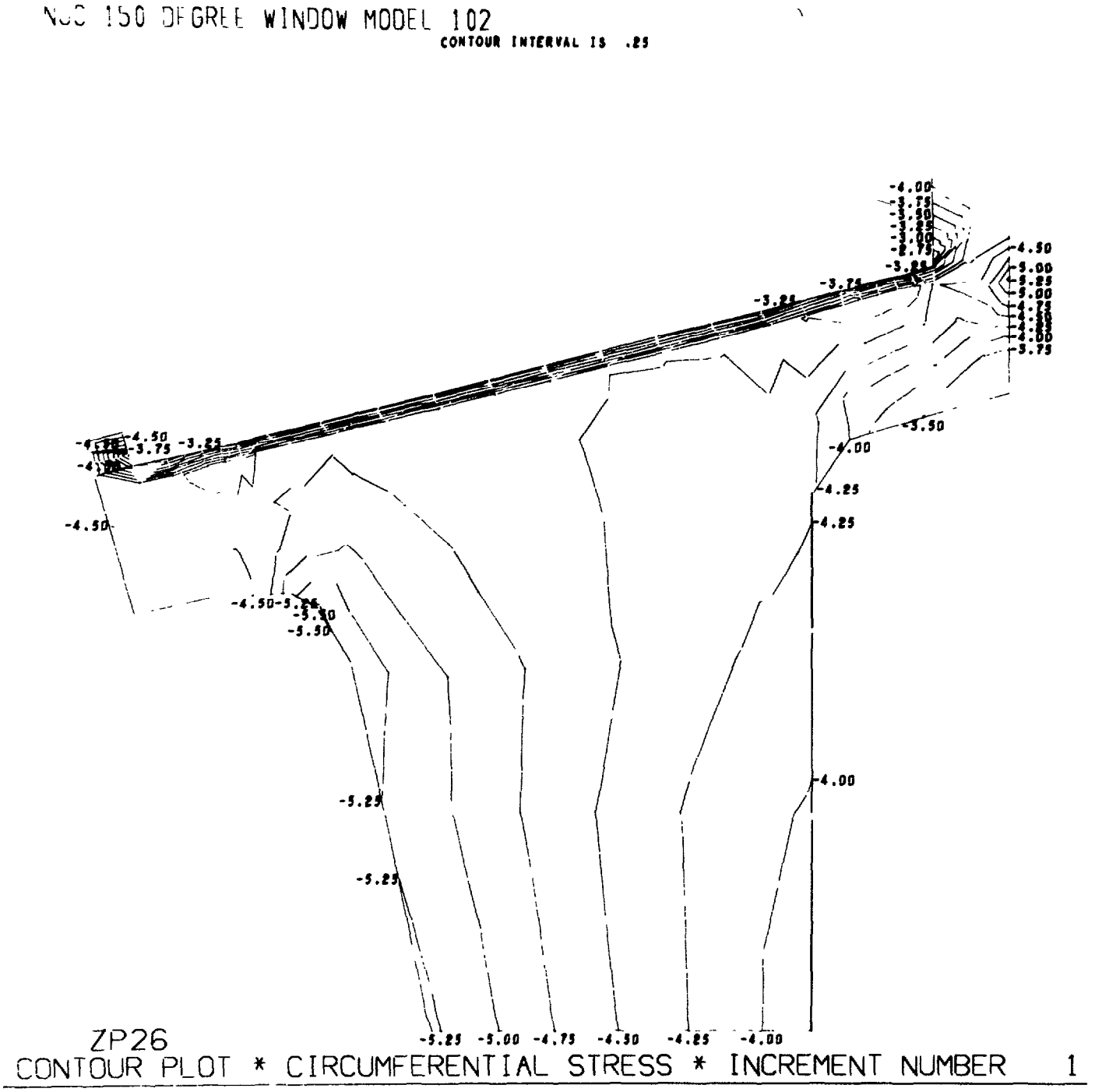

Figure B.5. Magnitude and distribution of stresses in window-flange assembly Configuration A utilizing a steel flange, fiber-reinforced-epoxy gasket, and glass ceramic window (problem 102). (sheet 3 of 7)

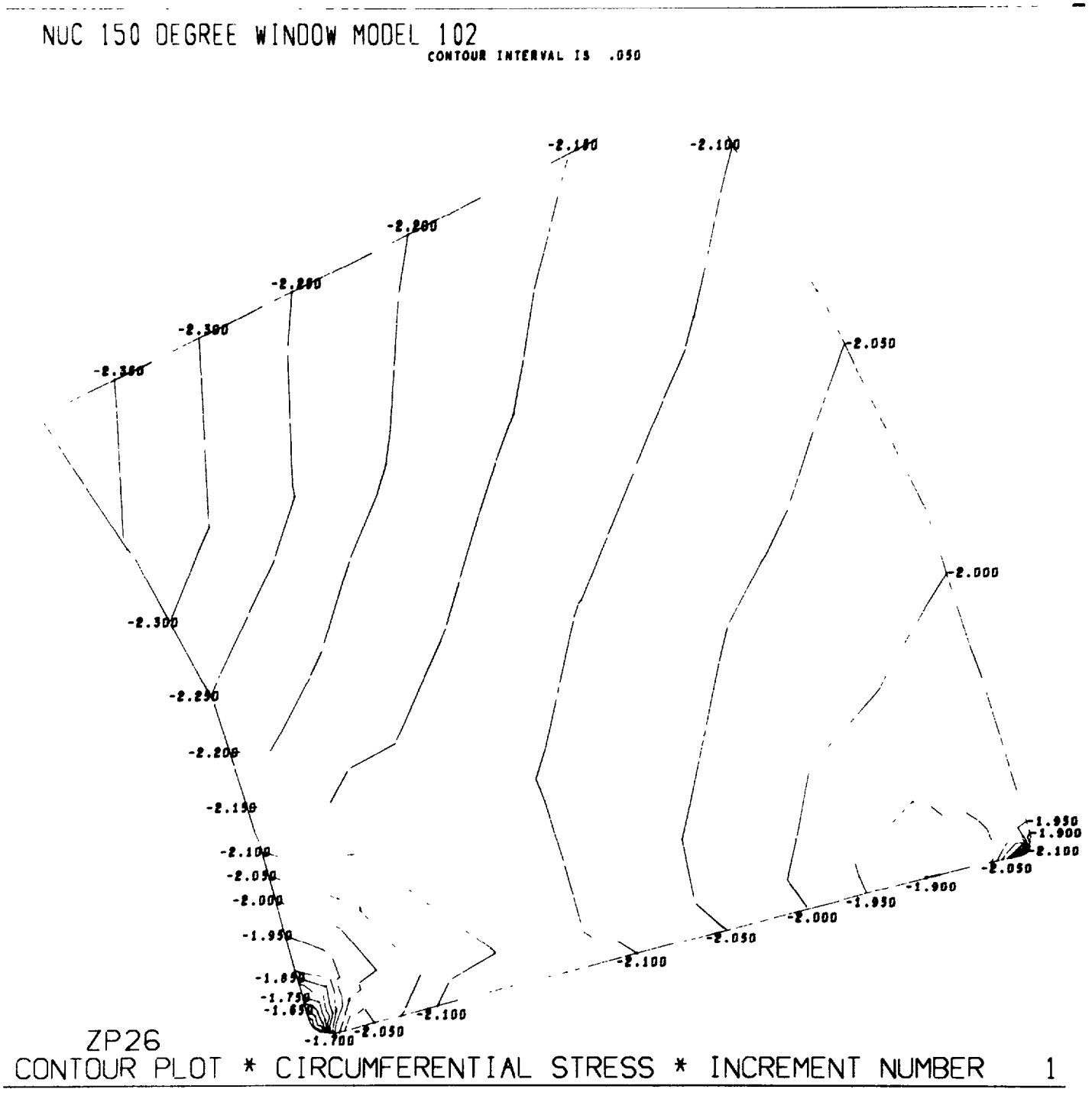

Figure B.5. Magnitude and distribution of stresses in window-flange assembly Configuration A utilizing a steel flange, fiber-reinforced-epoxy gasket, and glass ceramic window (problem 102). (sheet 4 of 7)

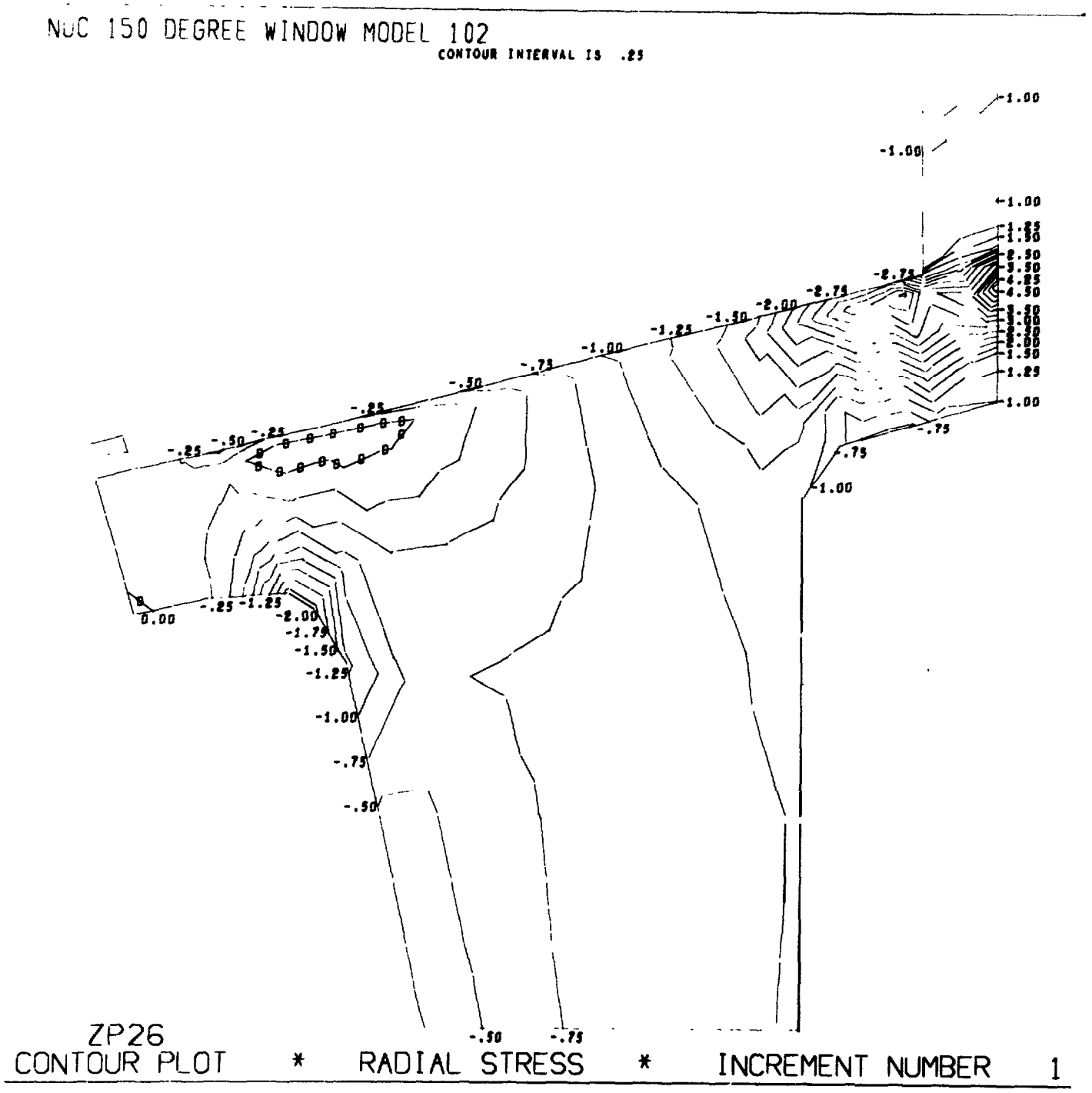

Figure B.5. Magnitude and distribution of stresses in window-flange assembly Configuration A utilizing a steel flange, fiber-reinforced-epoxy gasket, and glass ceramic window (problem 102). (sheet 5 of 7)

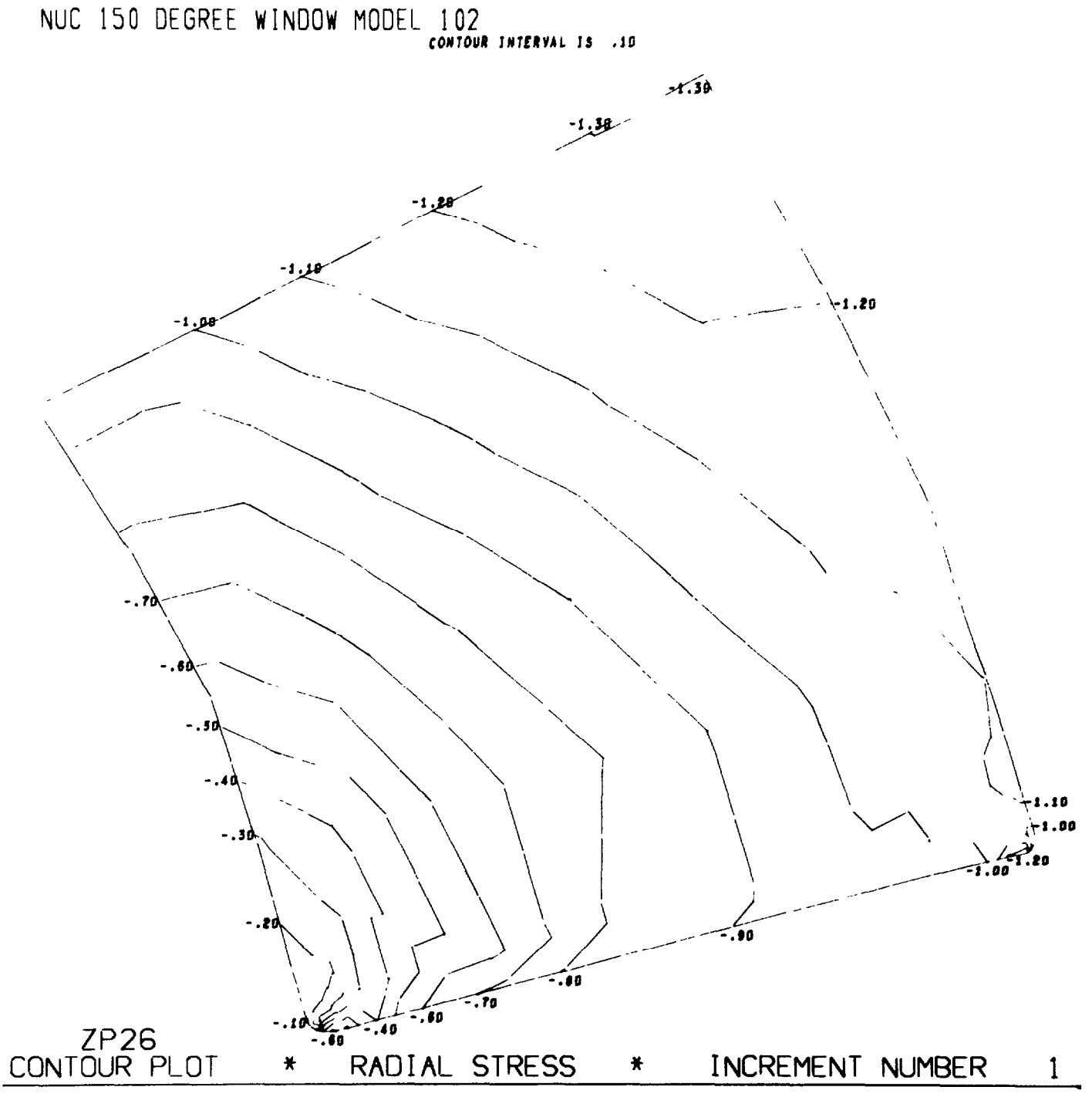

Figure B.5. Magnitude and distribution of stresses in window-flange assembly Configuration A utilizing a steel flange, fiber-reinforced-epoxy gasket, and glass ceramic window (problem 102). (sheet 6 of 7)

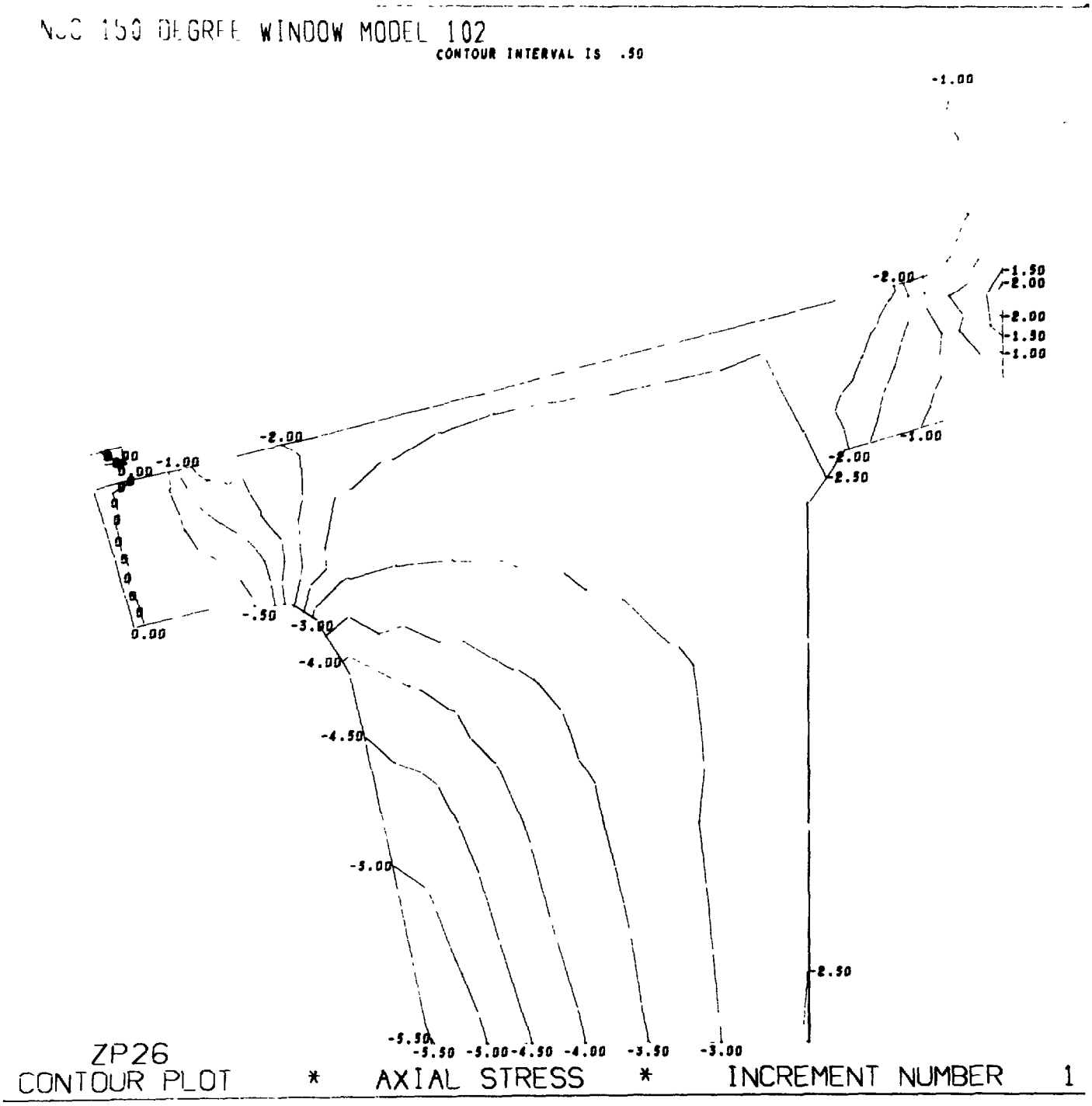

Figure B.5. Magnitude and distribution of stresses in window-flange assembly Configuration A utilizing a steel flange, fiber-reinforced-epoxy gasket, and glass ceramic window (problem 102).(sheet 7 of 7)

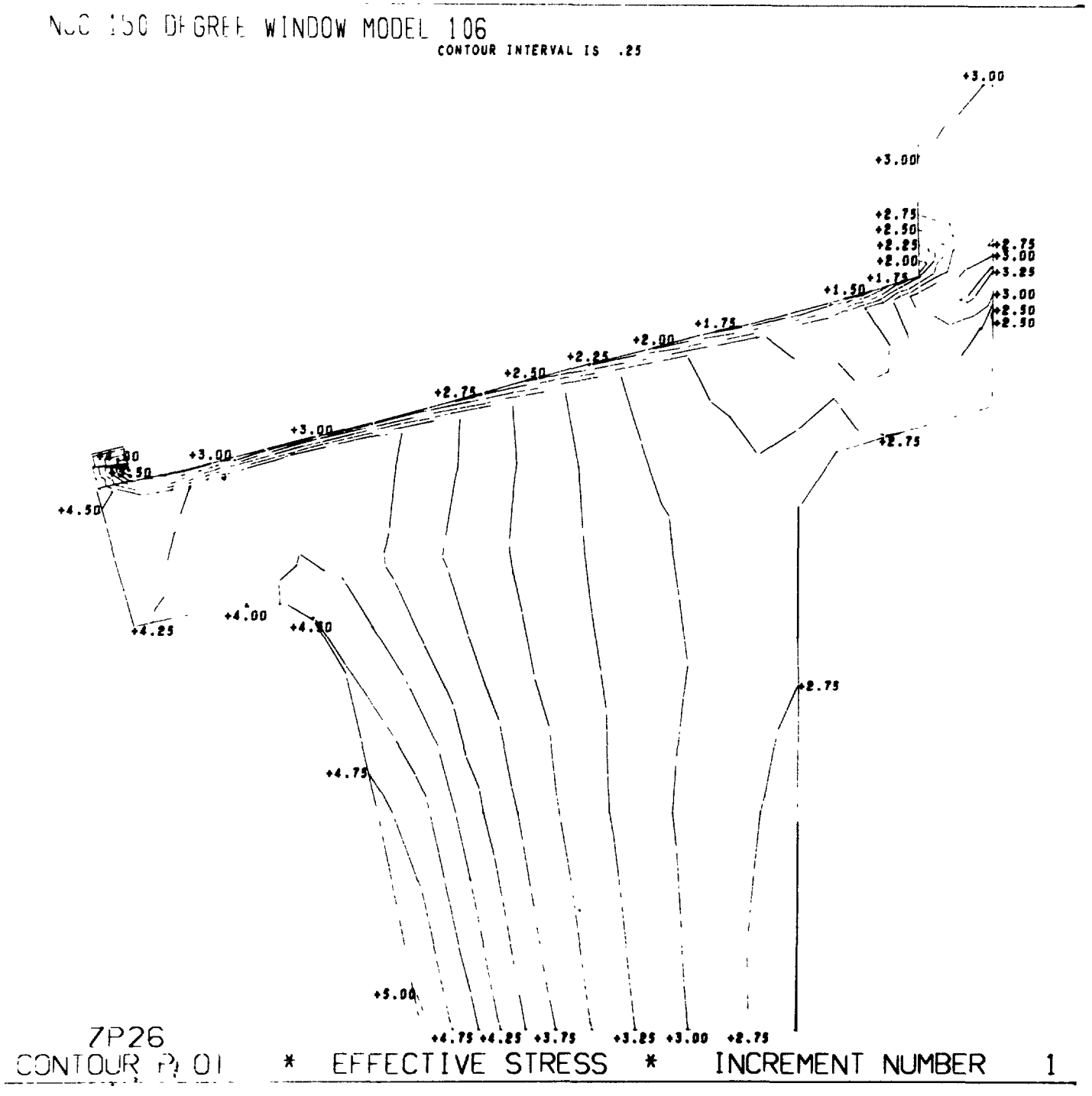

Figure B.6. Magnitude and distribution of stresses in window-flange assembly Configuration A utilizing a titanium flange, fiber-reinforced-epoxy laminate gasket and glass ceramic window (problem 106). (sheet 1 of 8)

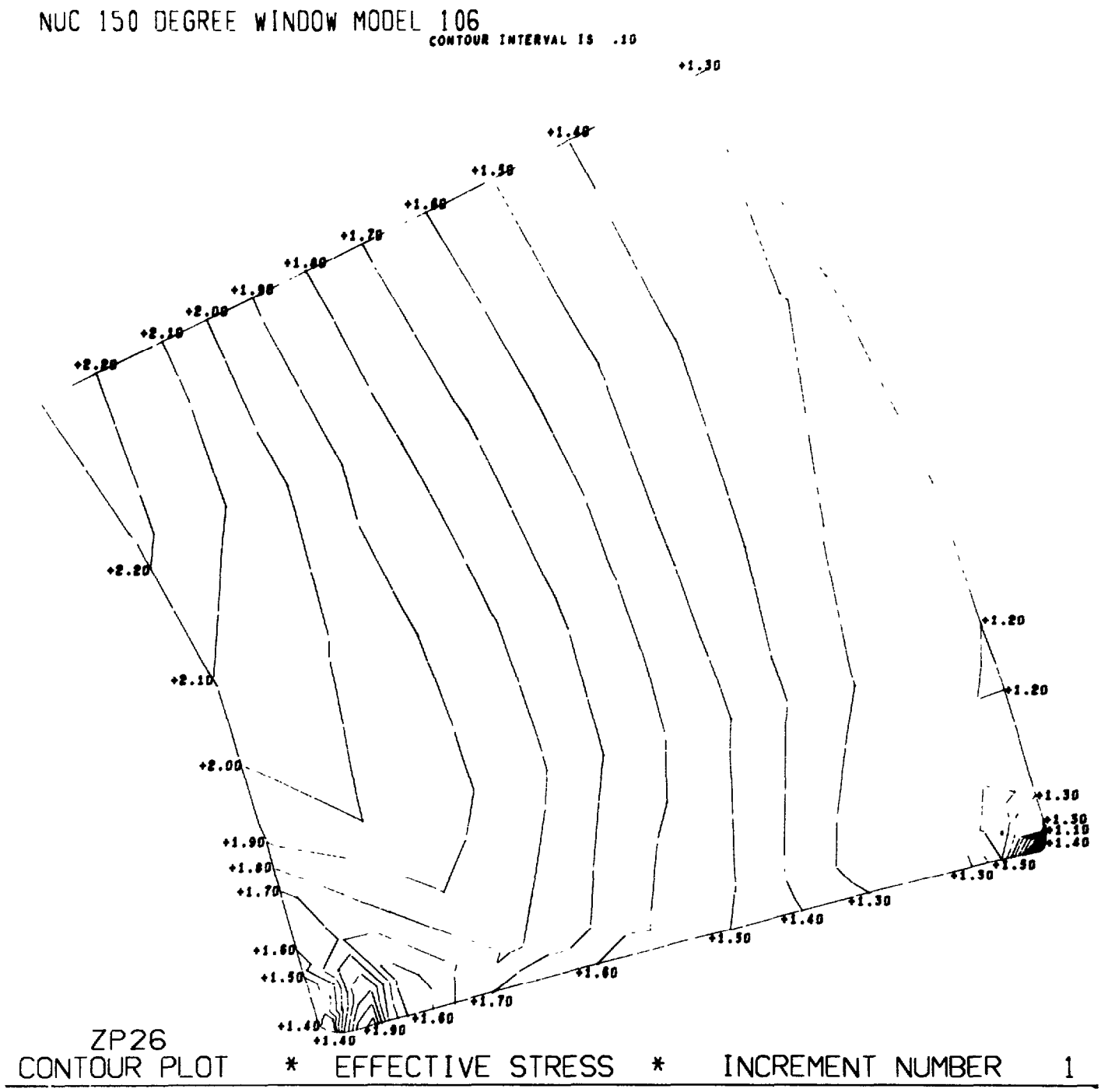

Figure B.6. Magnitude and distribution of stresses in window-flange assembly Configuration A utilizing a titanium flange, fiber-reinforced-epoxy laminate gasket and glass ceramic window (problem 106). (sheet 2 of 8)

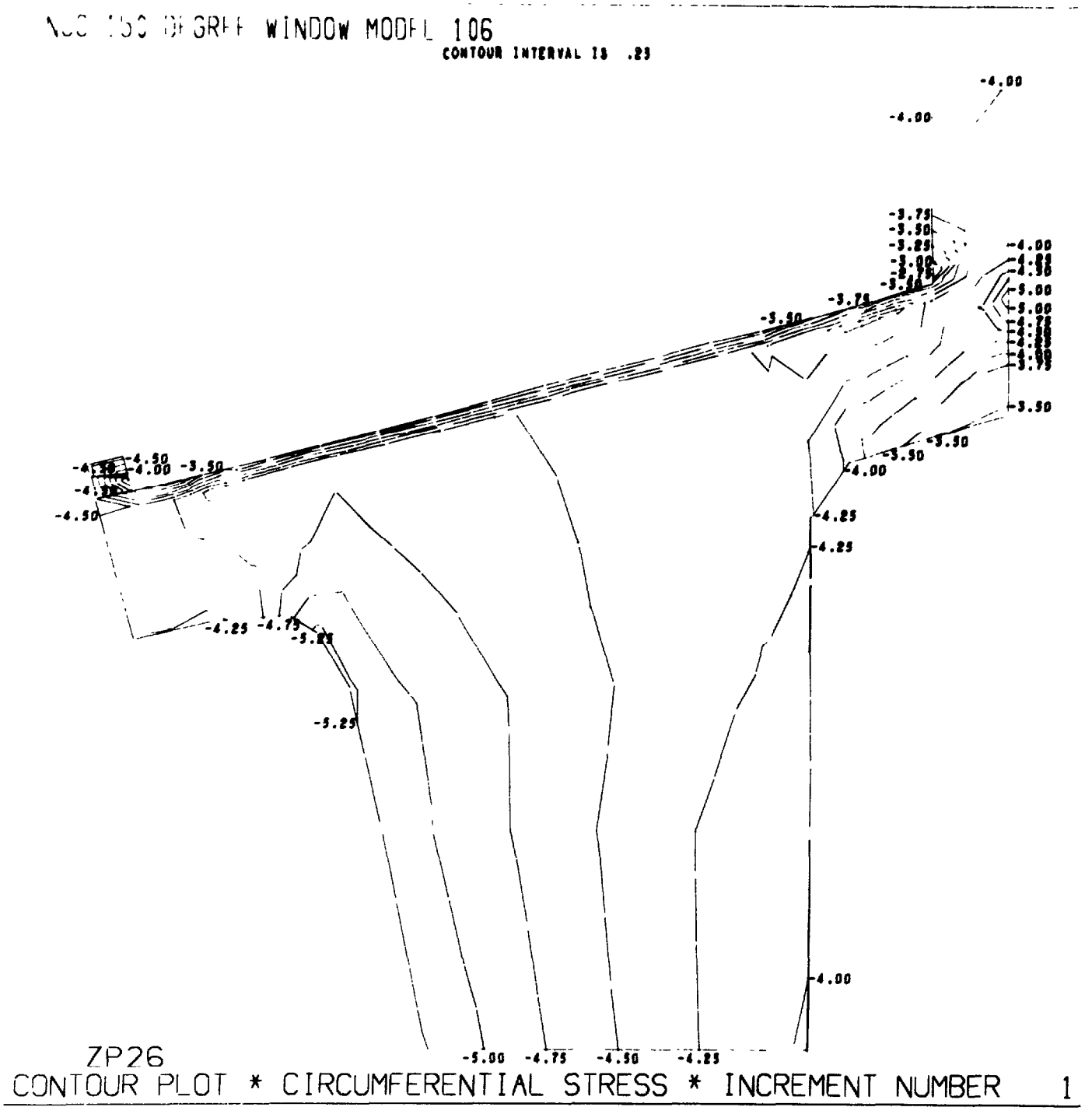

Figure B.6. Magnitude and distribution of stresses in window-flange assembly Configuration A utilizing a titanium flange, fiber-reinforced-epoxy laminate gasket and glass ceramic window (problem 106). (sheet 3 of 8)

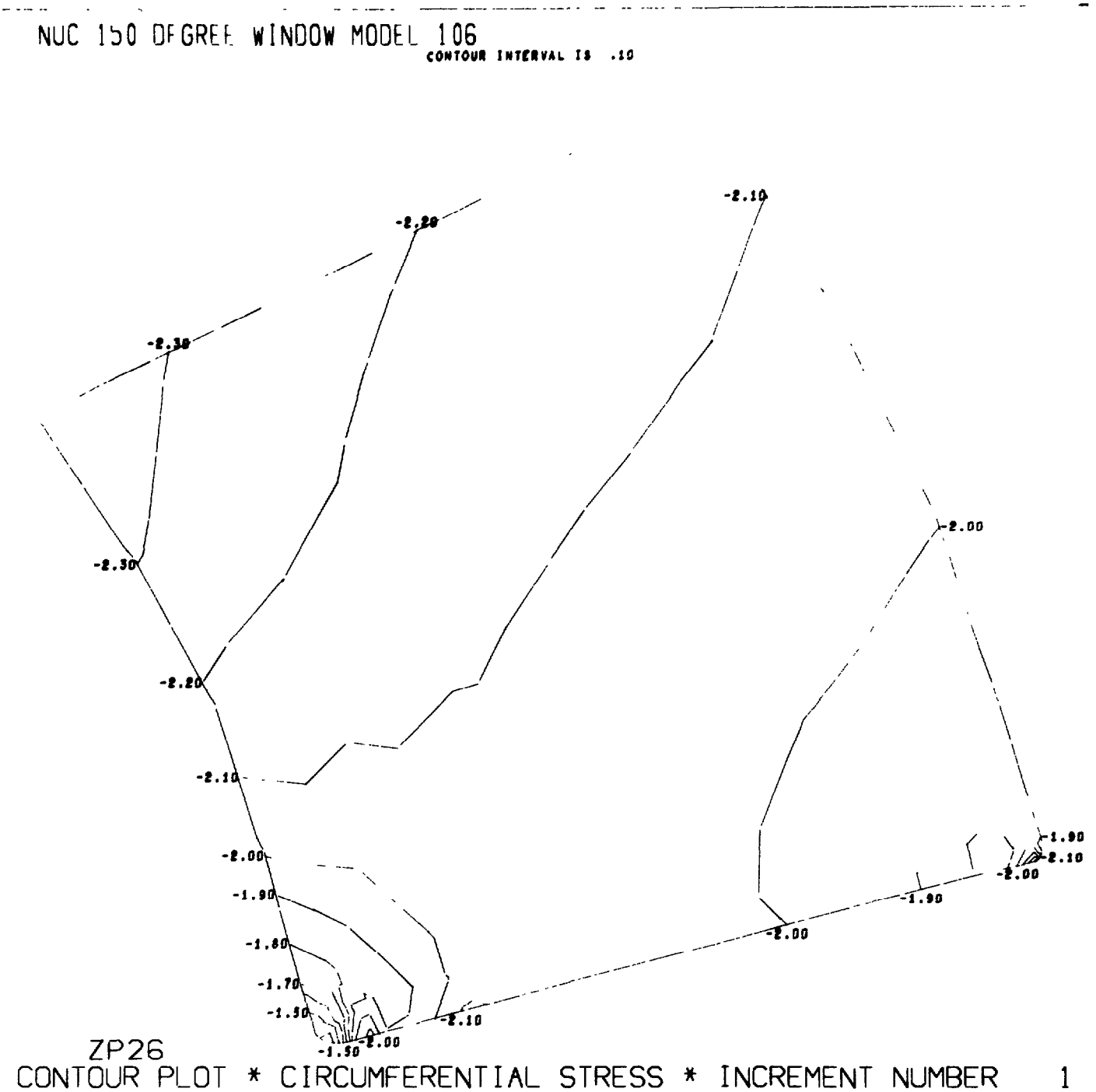

Figure B.6. Magnitude and distribution of stresses in window-flange assembly Configuration A utilizing a titanium flange, fiber-reinforced-epoxy laminate gasket and glass ceramic window (problem 106). (sheet 4 of 8)

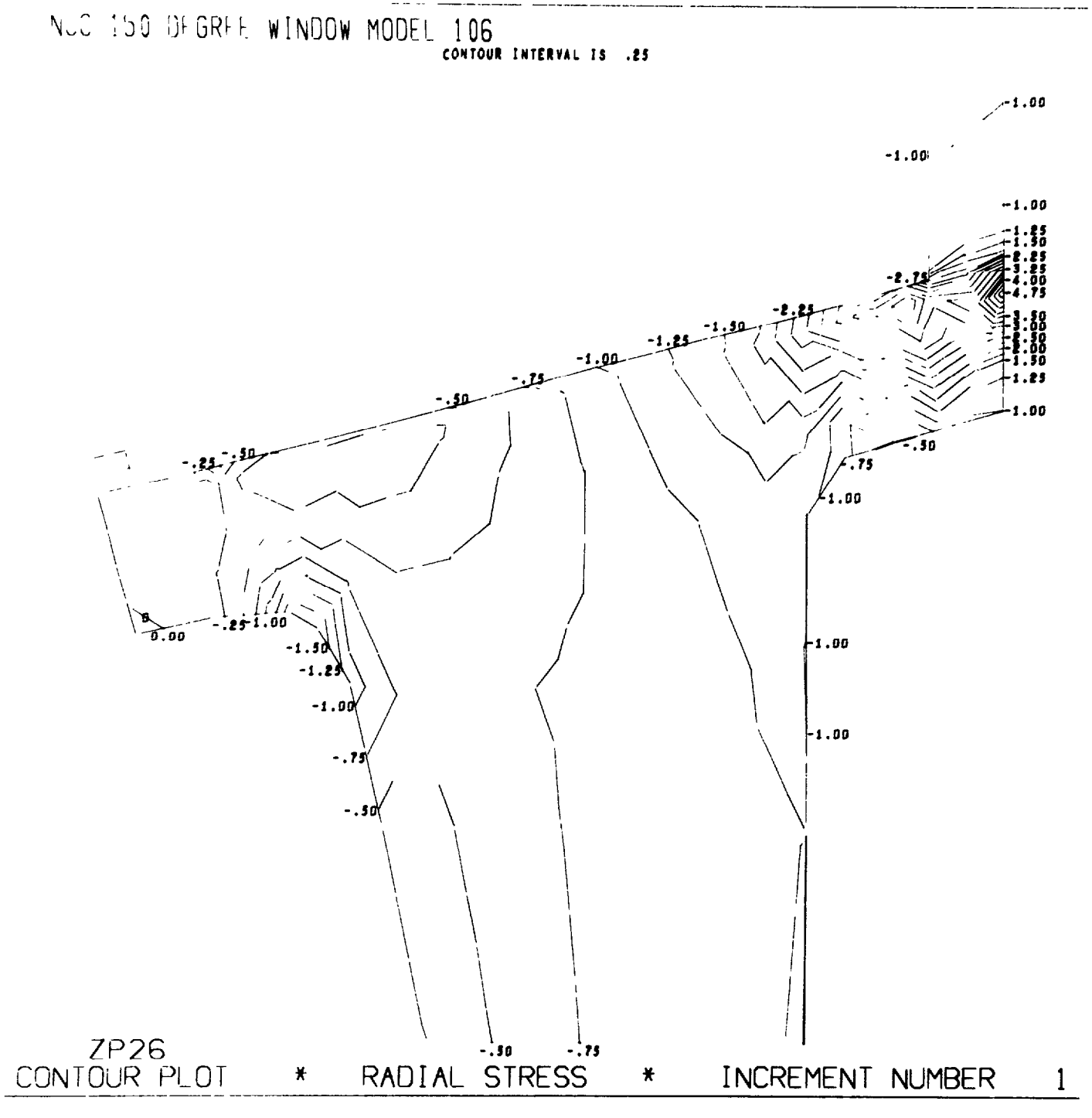

Figure B.6. Magnitude and distribution of stresses in window-flange assembly Configuration A utilizing a titanium flange, fiber-reinforced-epoxy laminate gasket and glass ceramic window (problem 106). (sheet 5 of 8)

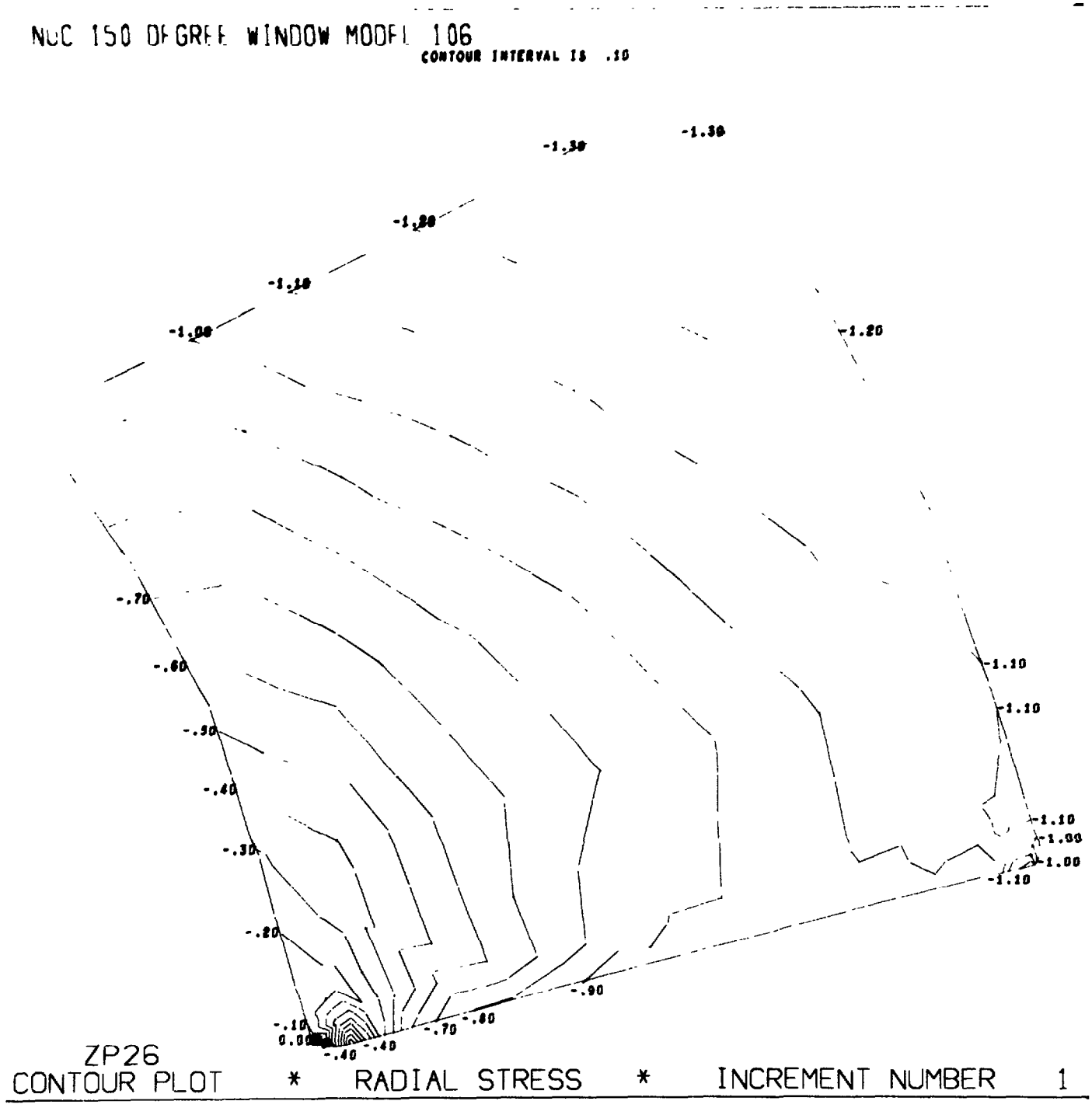

Figure B.6. Magnitude and distribution of stresses in window-flange assembly Configuration A utilizing a titanium flange, fiber-reinforced-epoxy laminate gasket and glass ceramic window (problem 106). (sheet 6 of 8)

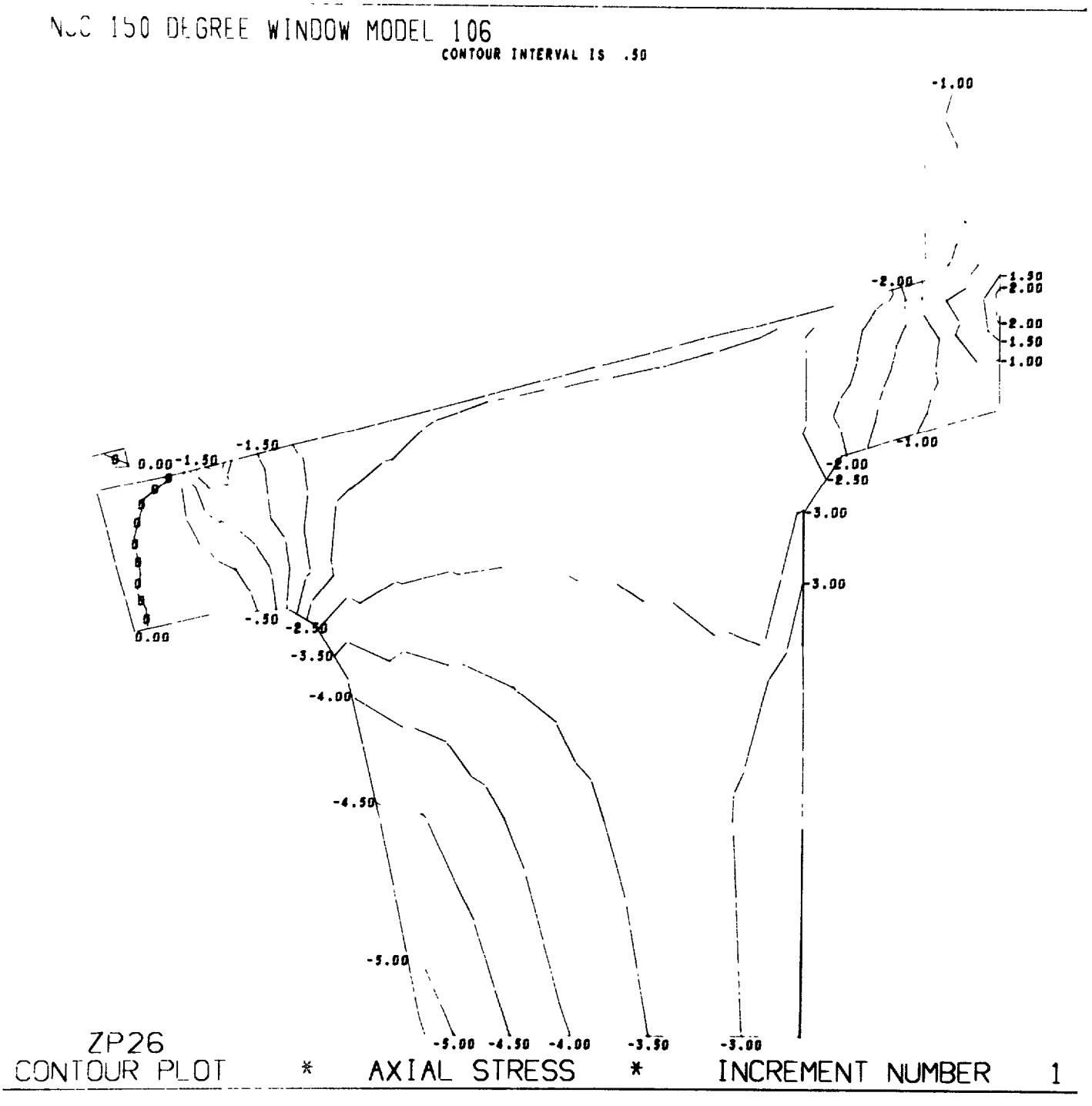

Figure B.6. Magnitude and distribution of stresses in window-flange assembly Configuration A utilizing a titanium flange, fiber-reinforced-epoxy laminate gasket and glass ceramic window (problem 106). (sheet 7 of 8)

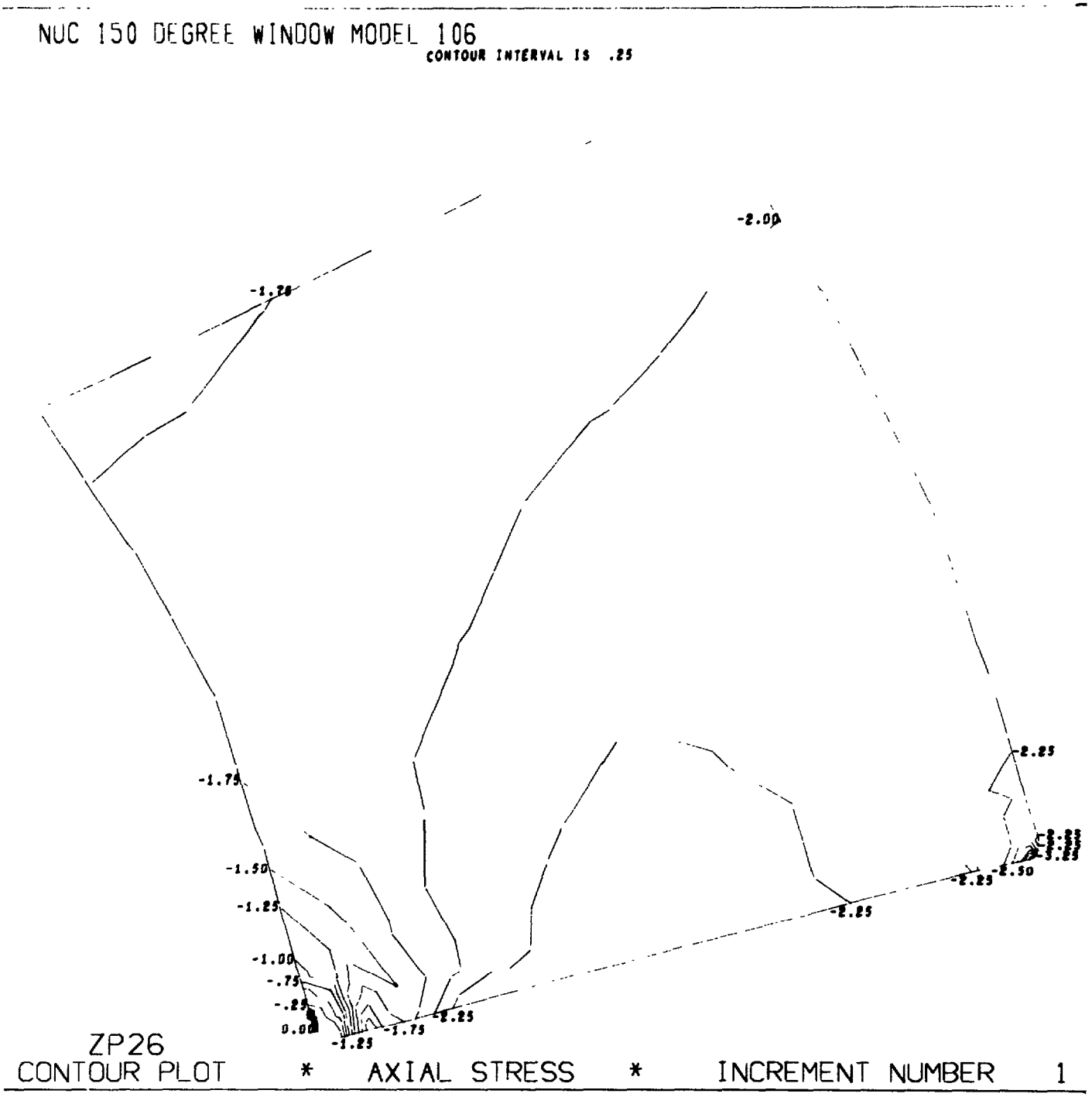

Figure B.6. Magnitude and distribution of stresses in window-flange assembly Configuration A utilizing a titanium flange, fiber-reinforced-epoxy laminate gasket and glass ceramic window (problem 106). (sheet 8 of 8)

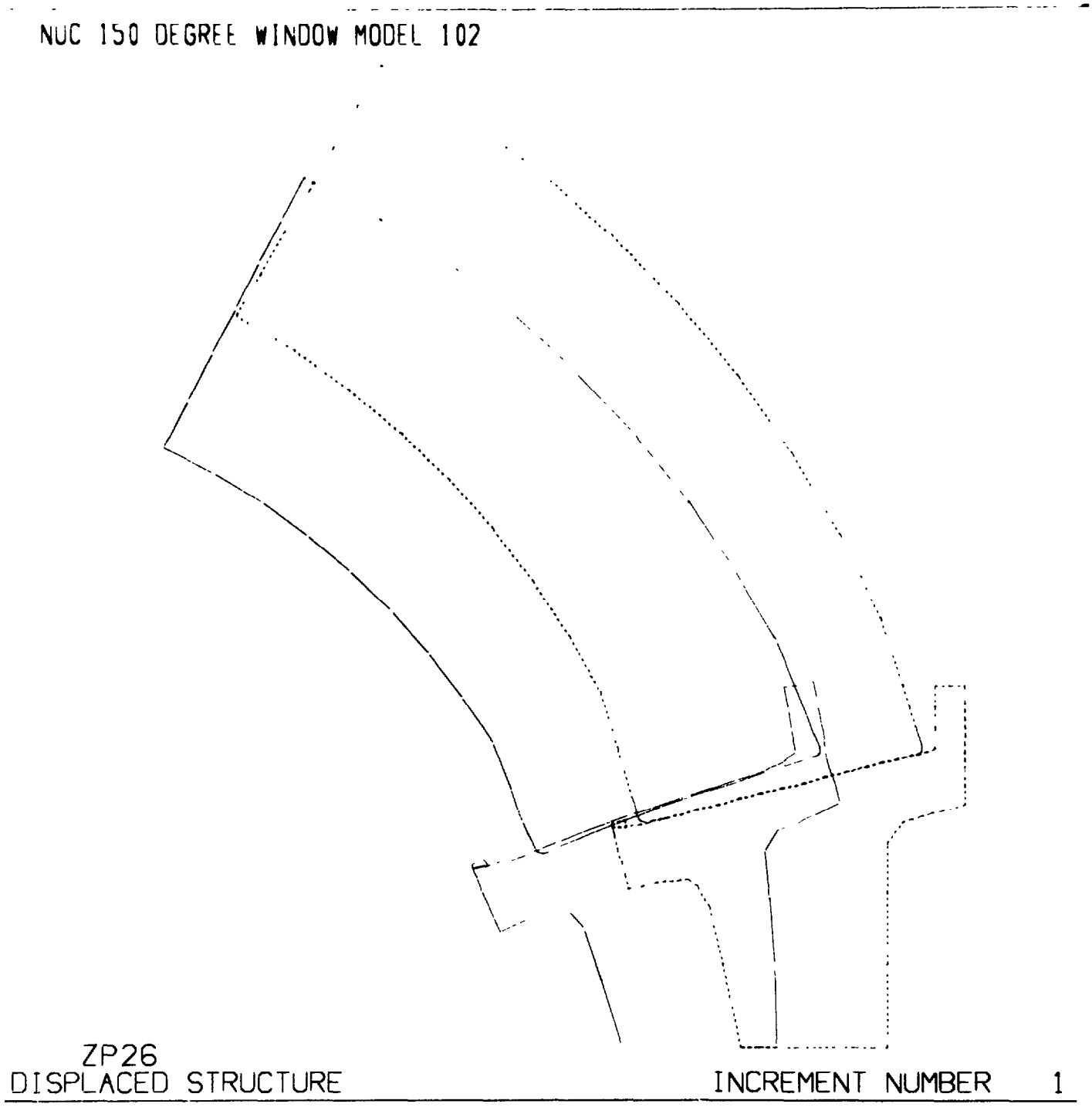

Figure B.7. Radial displacements of window and flange in Configuration A under external hydrostatic loading: problem 102, glass ceramic on steel.

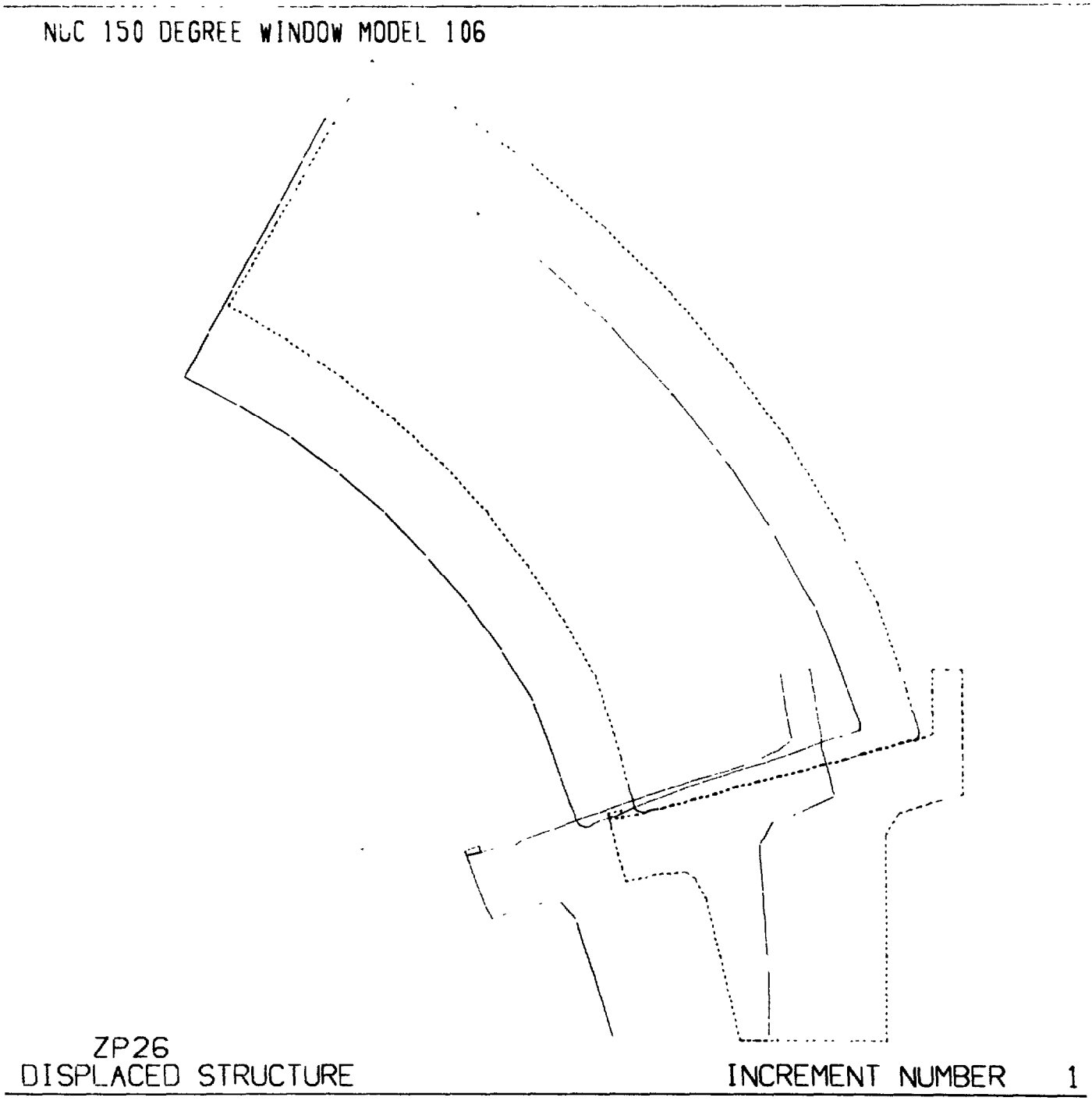

Figure B.7. Radial displacements of window and flange in Configuration A under external hydrostatic loading: problem 106, glass ceramic on titanium.

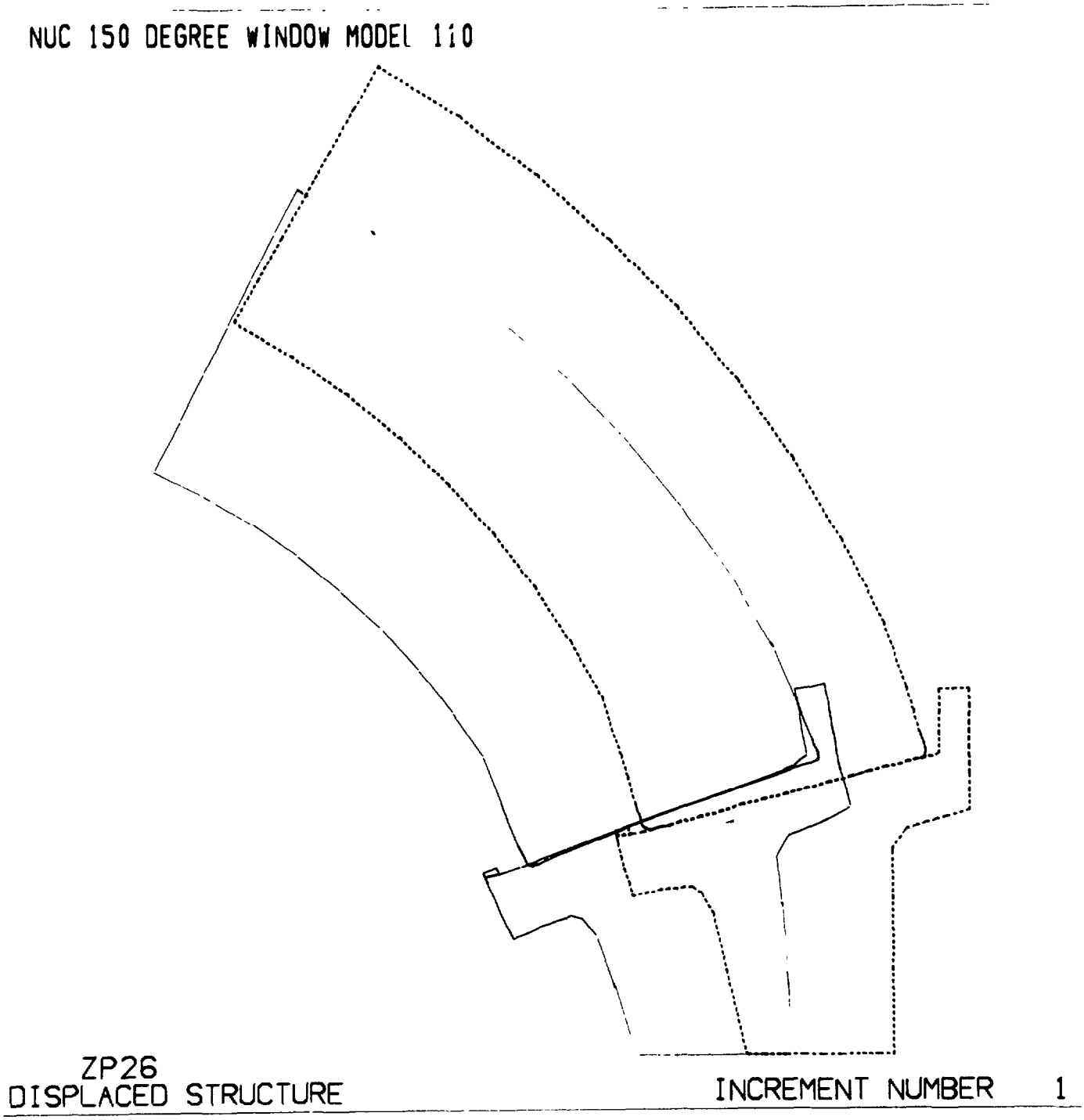

Figure B.7. Radial displacements of window and flange in Configuration A under external hydrostatic loading: problem 110, glass on steel.

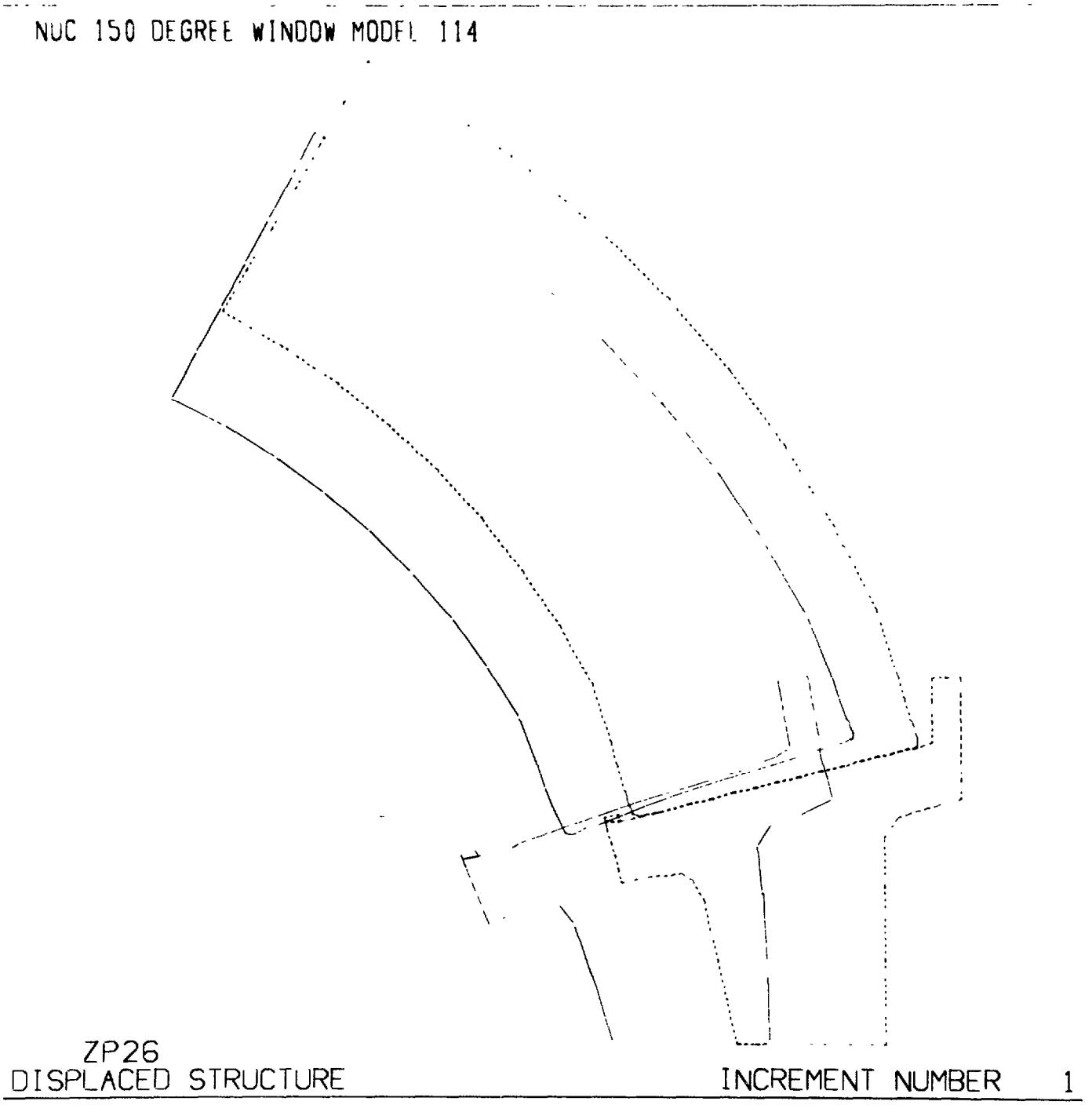

Figure B.7. Radial displacements of window and flange in Configuration A under external hydrostatic loading: problem 114, glass on titanium.

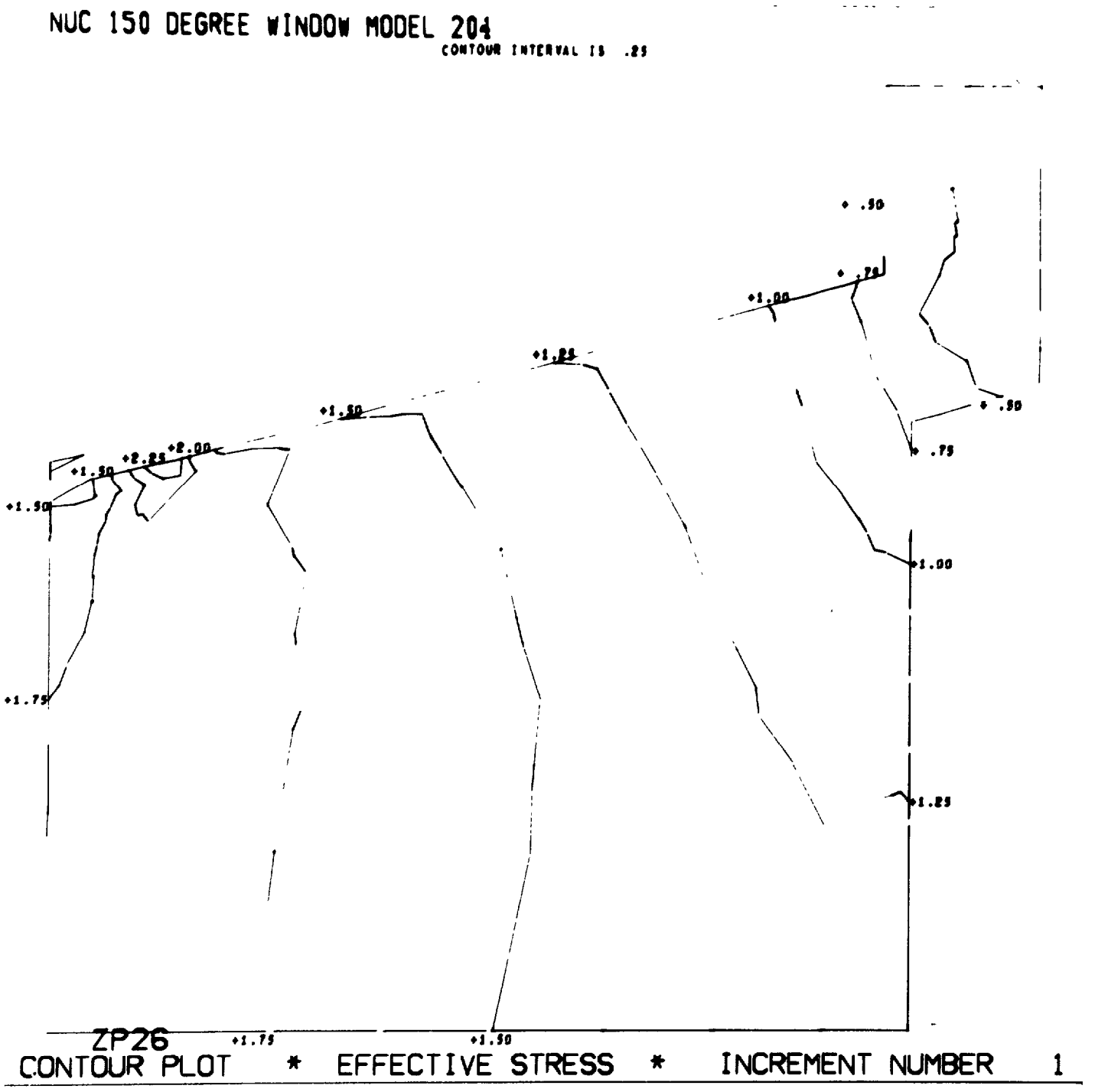

Figure B.8. Magnitude and distribution of stresses in window-flange assembly Configuration B, utilizing a glass-reinforced-plastic flange and glass ceramic window (problem 204). (sheet 1 of 8)

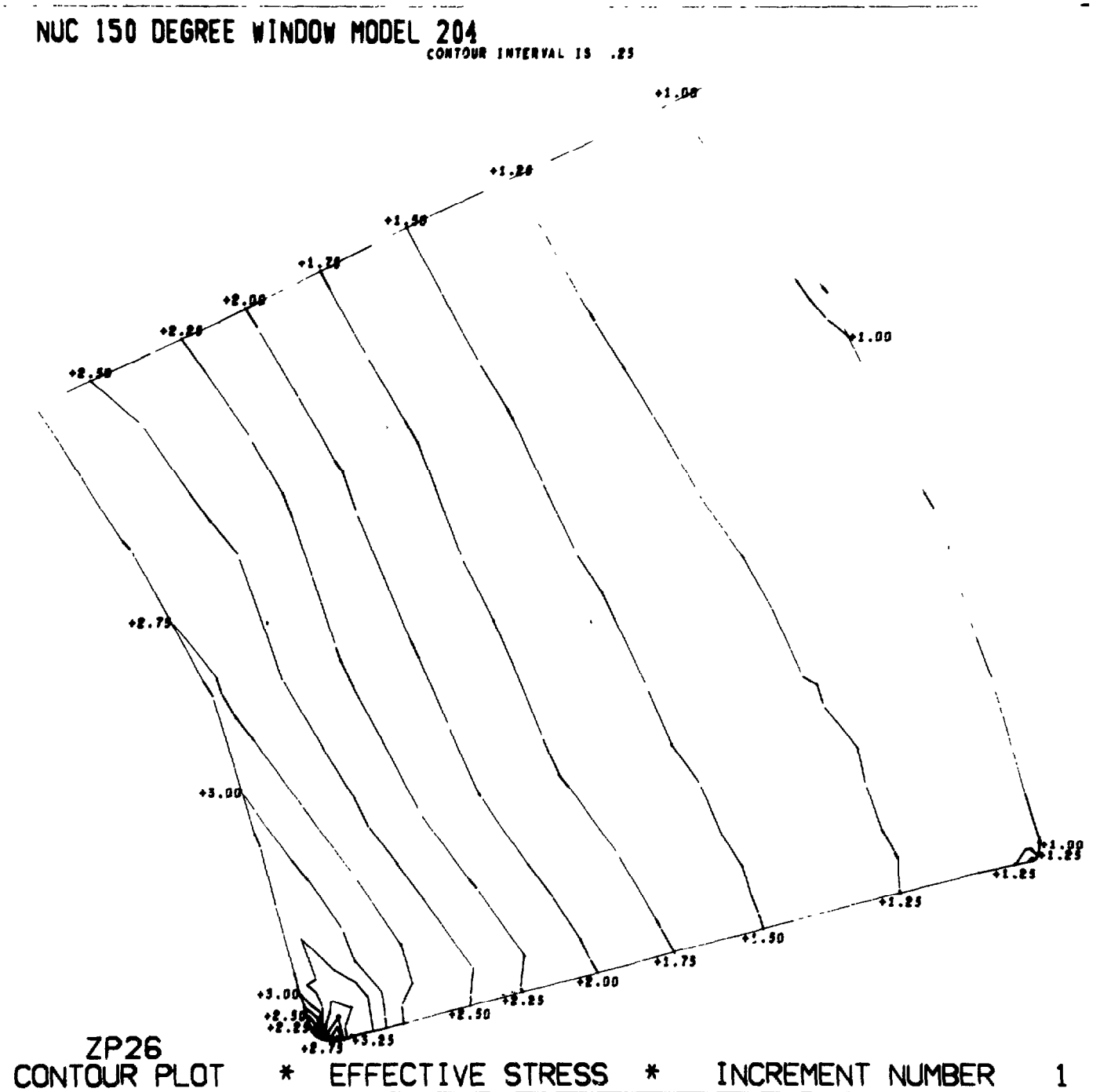

Figure B.8. Magnitude and distribution of stresses in window-flange assembly Configuration B, utilizing a glass-reinforced-plastic flange and glass ceramic window (problem 204). (sheet 2 of 8)

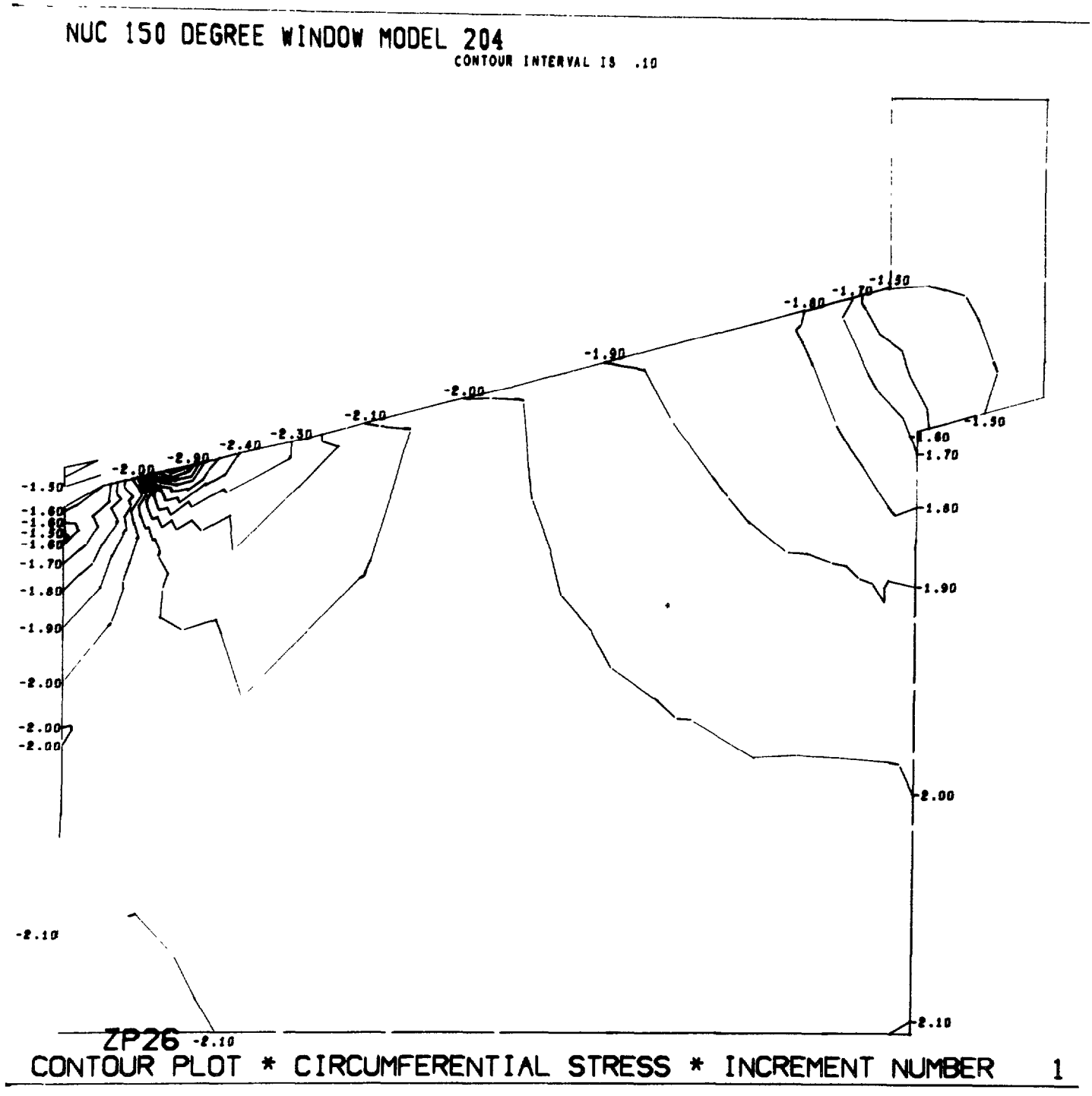

Figure B.8. Magnitude and distribution of stresses in window-flange assembly Configuration B, utilizing a glass-reinforced-plastic flange and glass ceramic window (problem 204). (sheet 3 of 8)

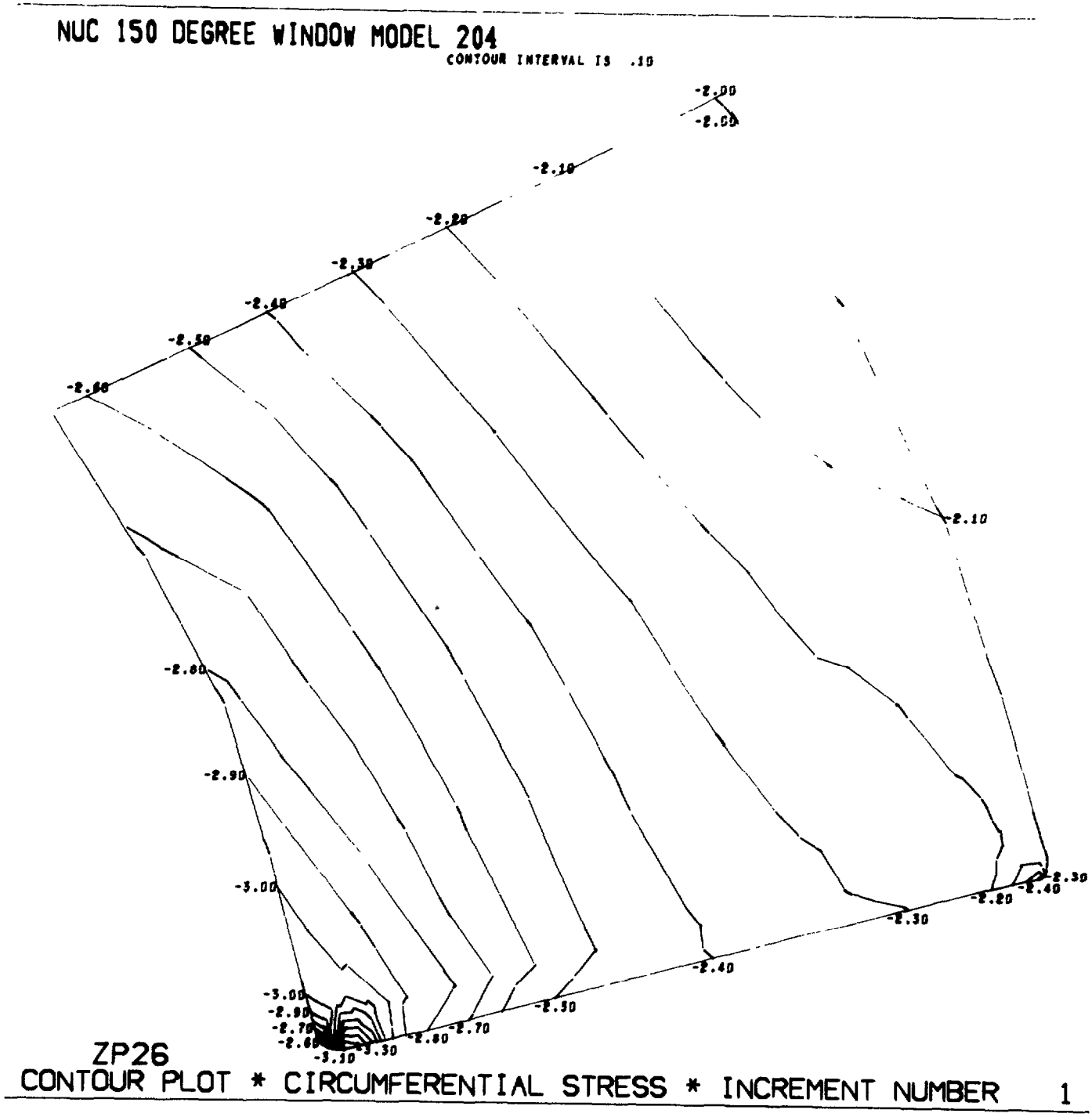

Figure B.8. Magnitude and distribution of stresses in window-flange assembly Configuration B, utilizing a glass-reinforced-plastic flange and glass ceramic window (problem 204). (sheet 4 of 8)

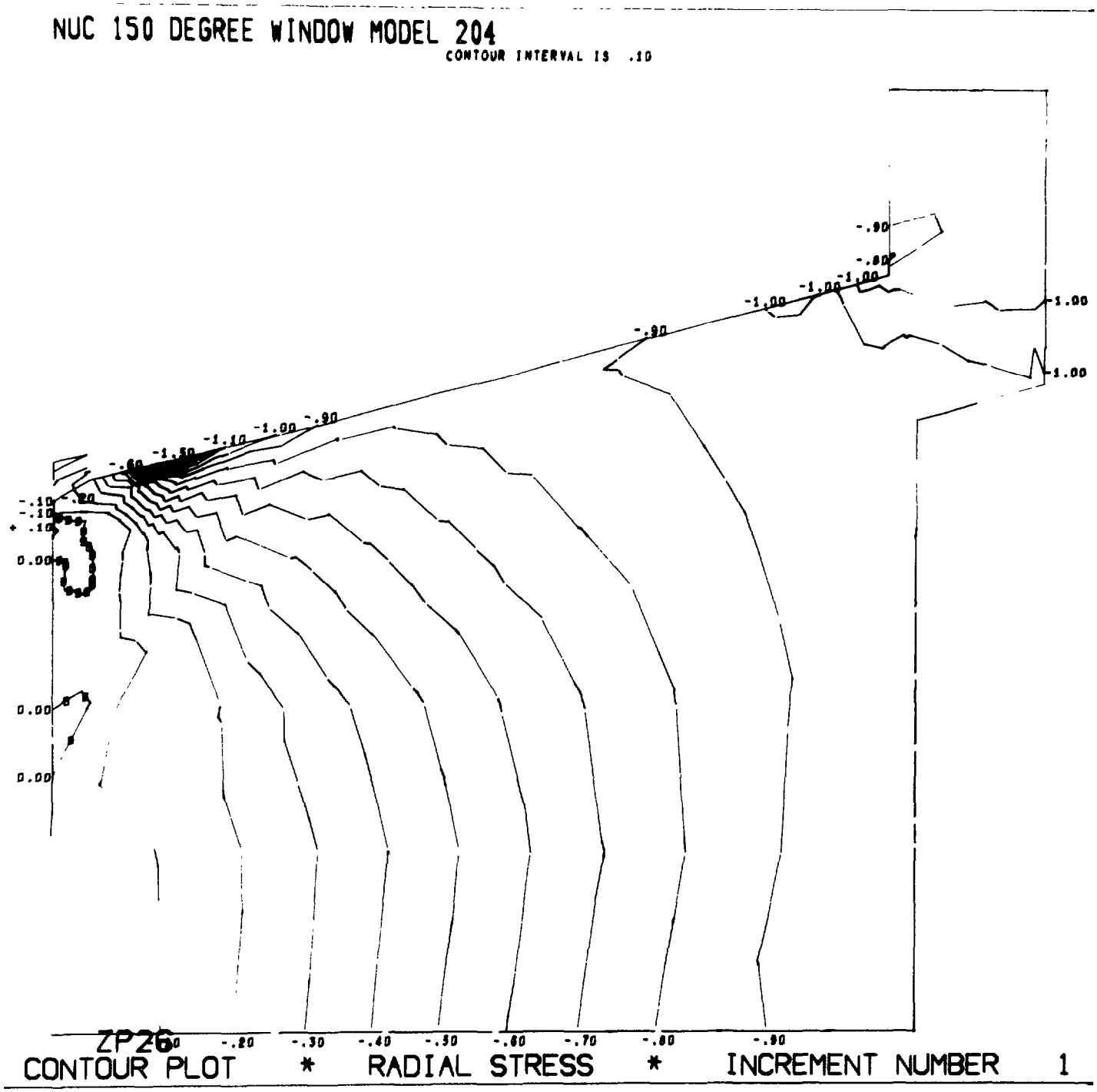

Figure B.8. Magnitude and distribution of stresses in window-flange assembly Configuration B, utilizing a glass-reinforced-plastic flange and glass ceramic window (problem 204). (sheet 5 of 8)

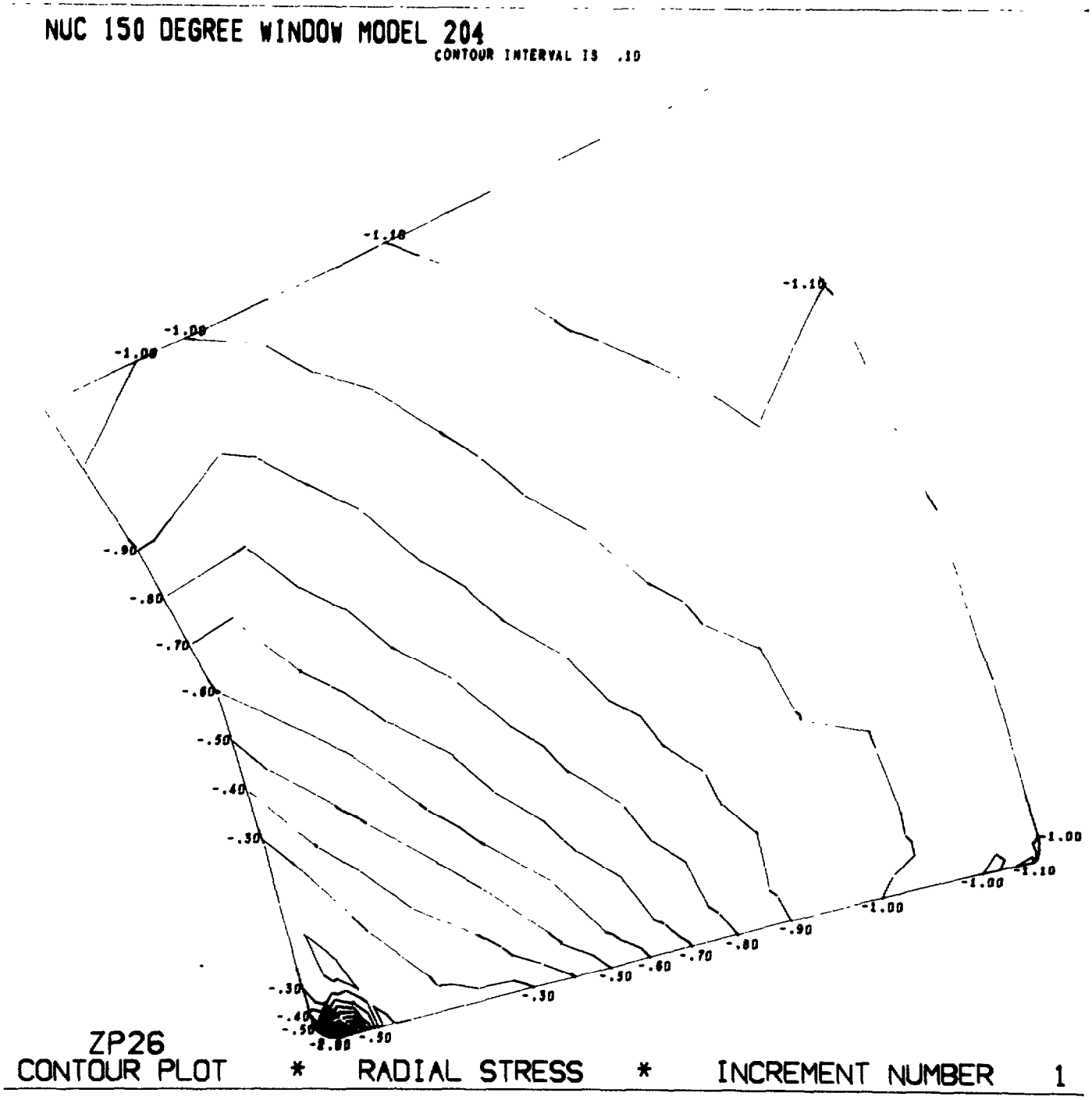

Figure B.8. Magnitude and distribution of stresses in window-flange assembly Configuration B, utilizing a glass-reinforced-plastic flange and glass ceramic window (problem 204). (sheet 6 of 8)

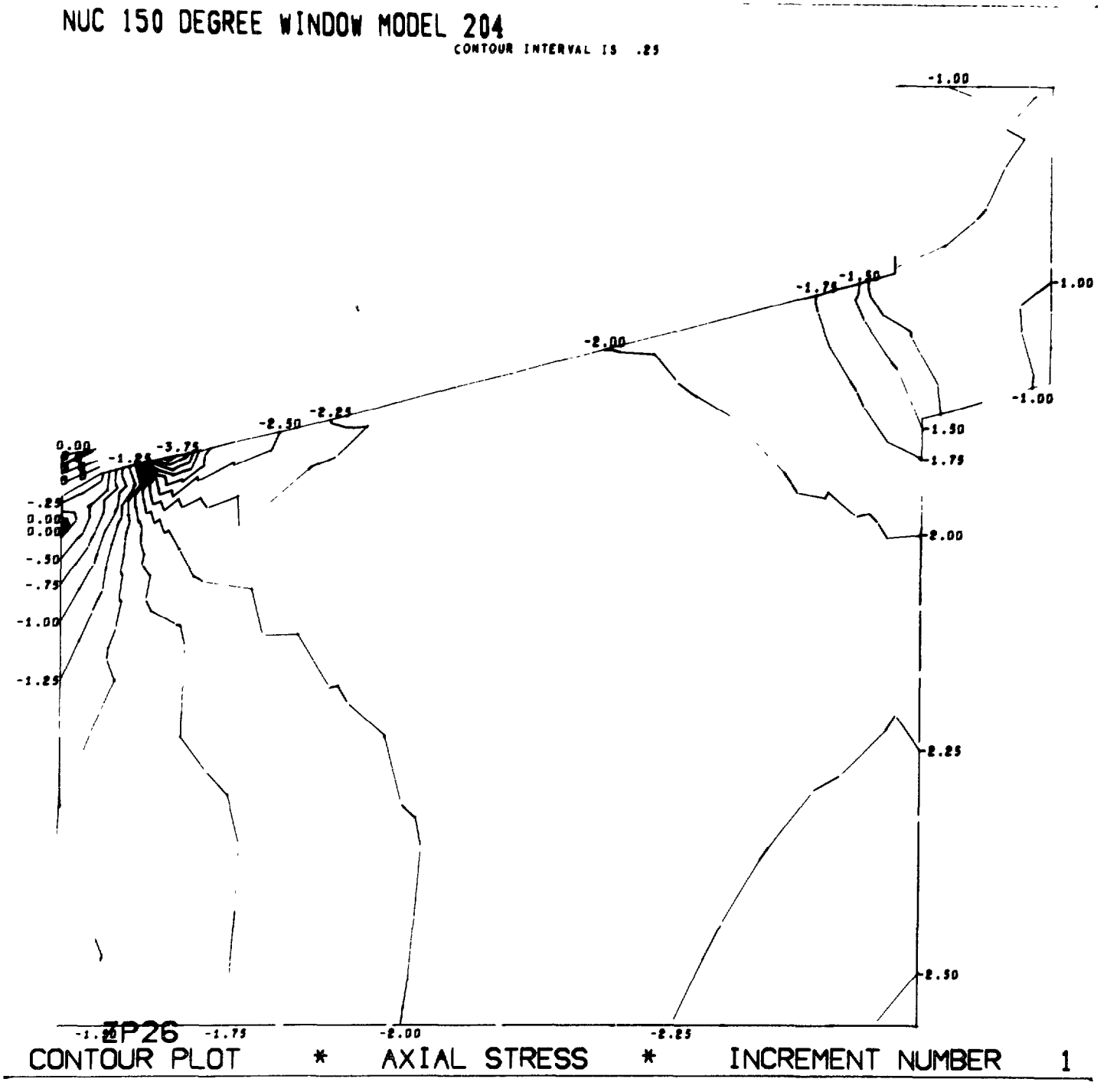

Figure B.8. Magnitude and distribution of stresses in window-flange assembly Configuration B, utilizing a glass-reinforced-plastic flange and glass ceramic window (problem 204). (sheet 7 of 8)

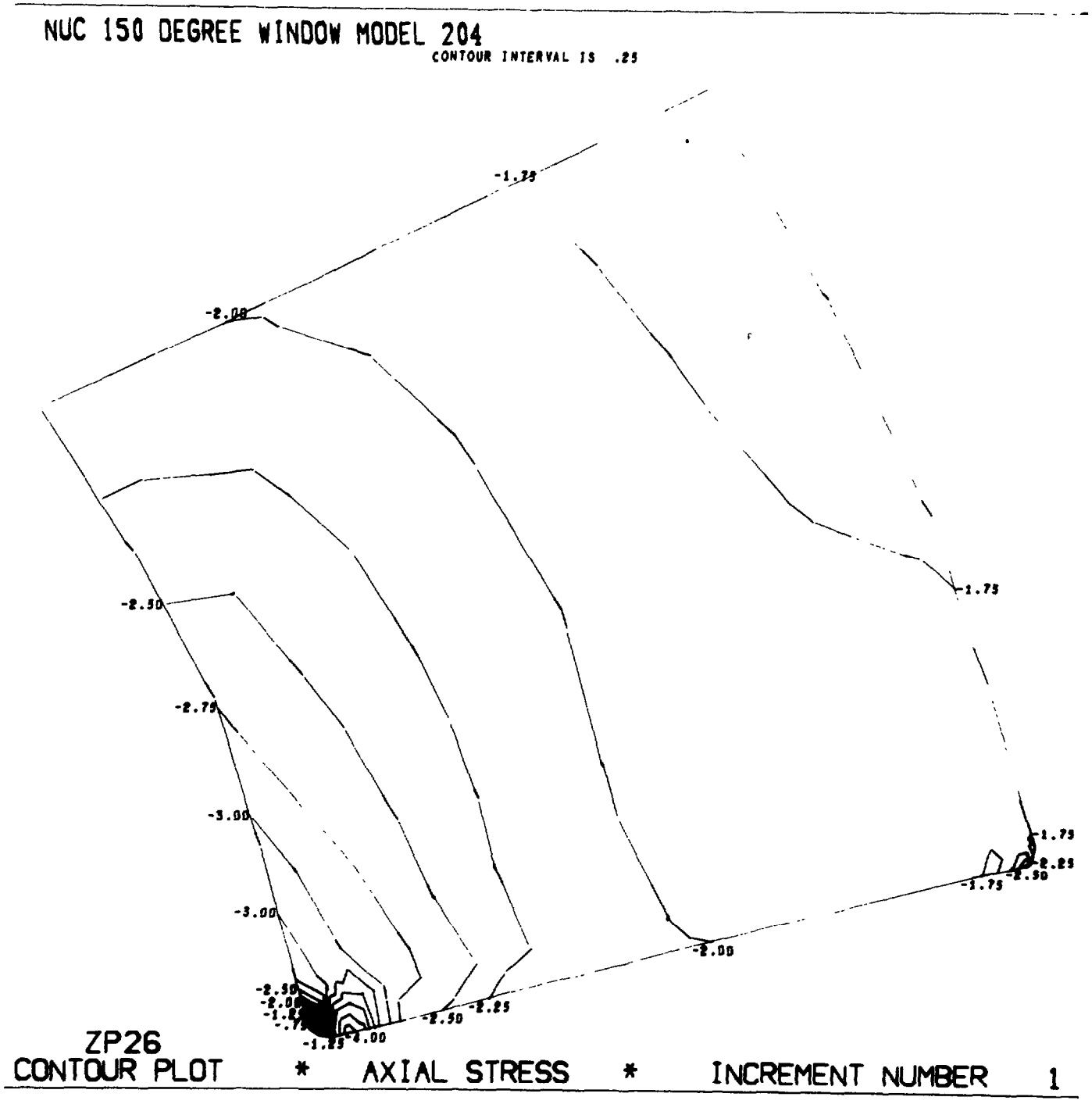

Figure B.8. Magnitude and distribution of stresses in window-flange assembly Configuration B, utilizing a glass-reinforced-plastic flange and glass ceramic window (problem 204). (sheet 8 of 8)

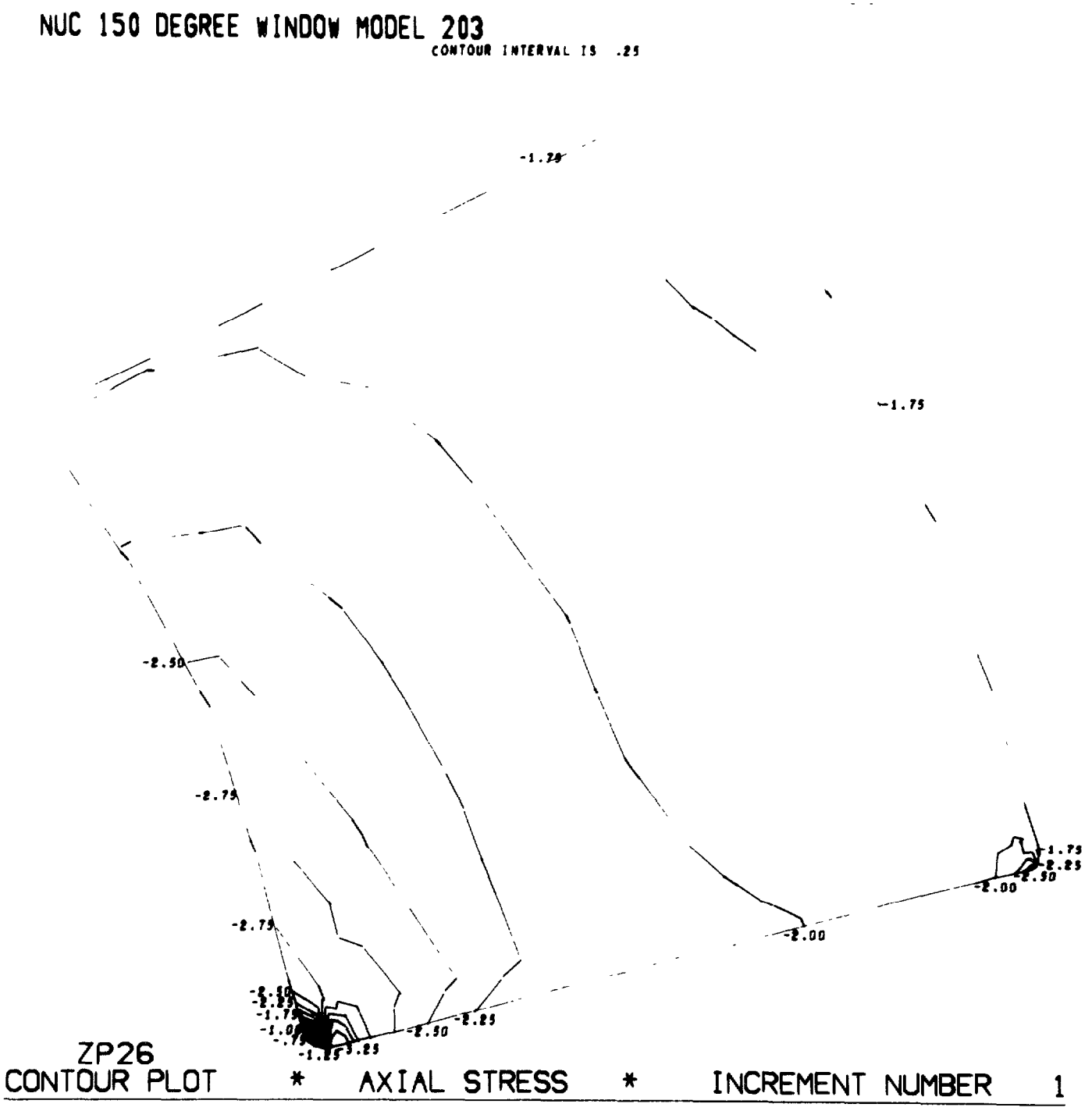

Figure B.9. Magnitude and distribution of stress in window-flange assembly Configuration B utilizing an aluminum flange, fiber-reinforced-epoxy gasket, and glass ceramic window (problem 203). (sheet 1 of 8)

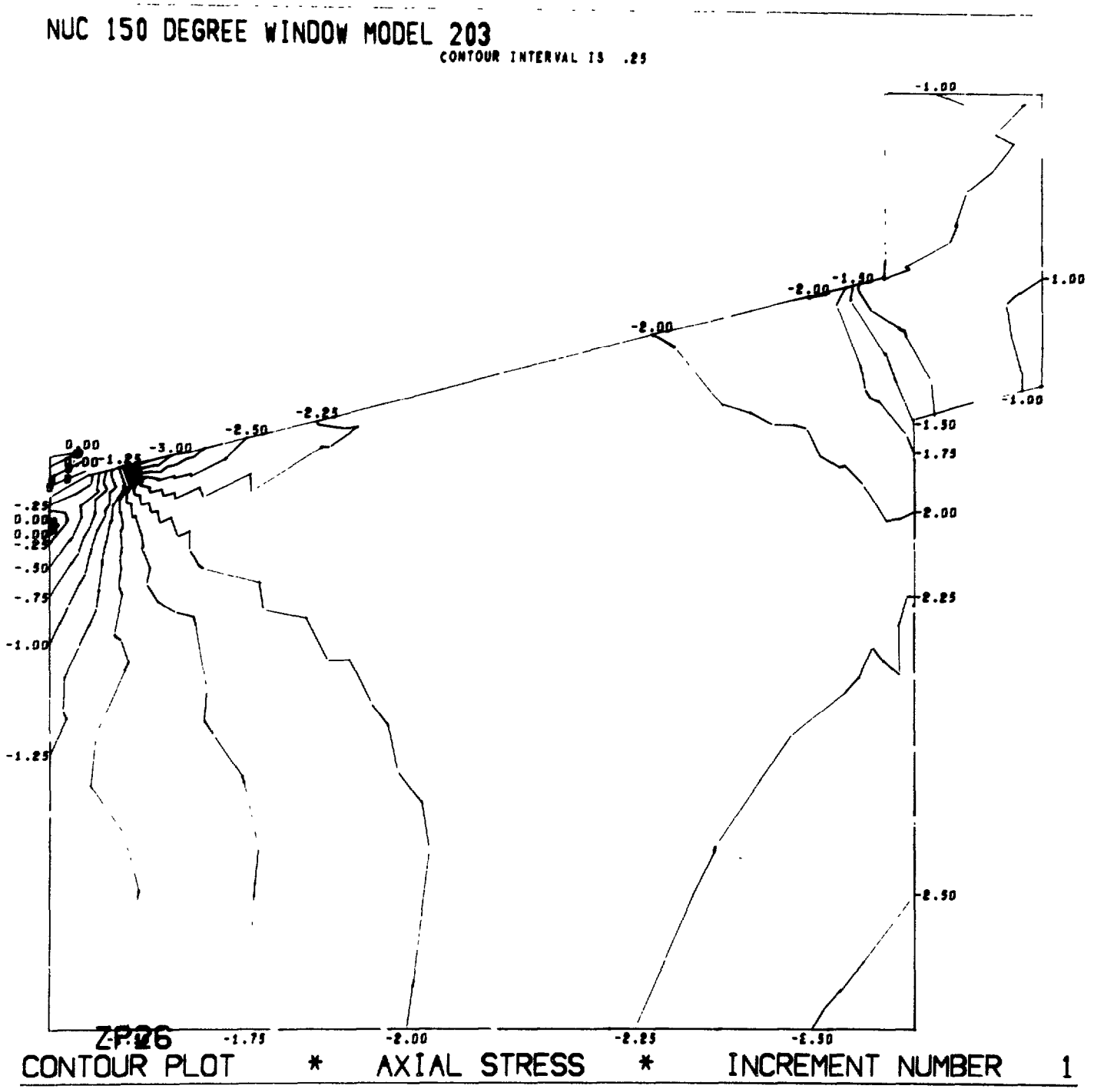

Figure B.9. Magnitude and distribution of stress in window-flange assembly Configuration B utilizing an aluminum flange, fiber-reinforced-epoxy gasket, and glass ceramic window (problem 203). (sheet 2 of 8)

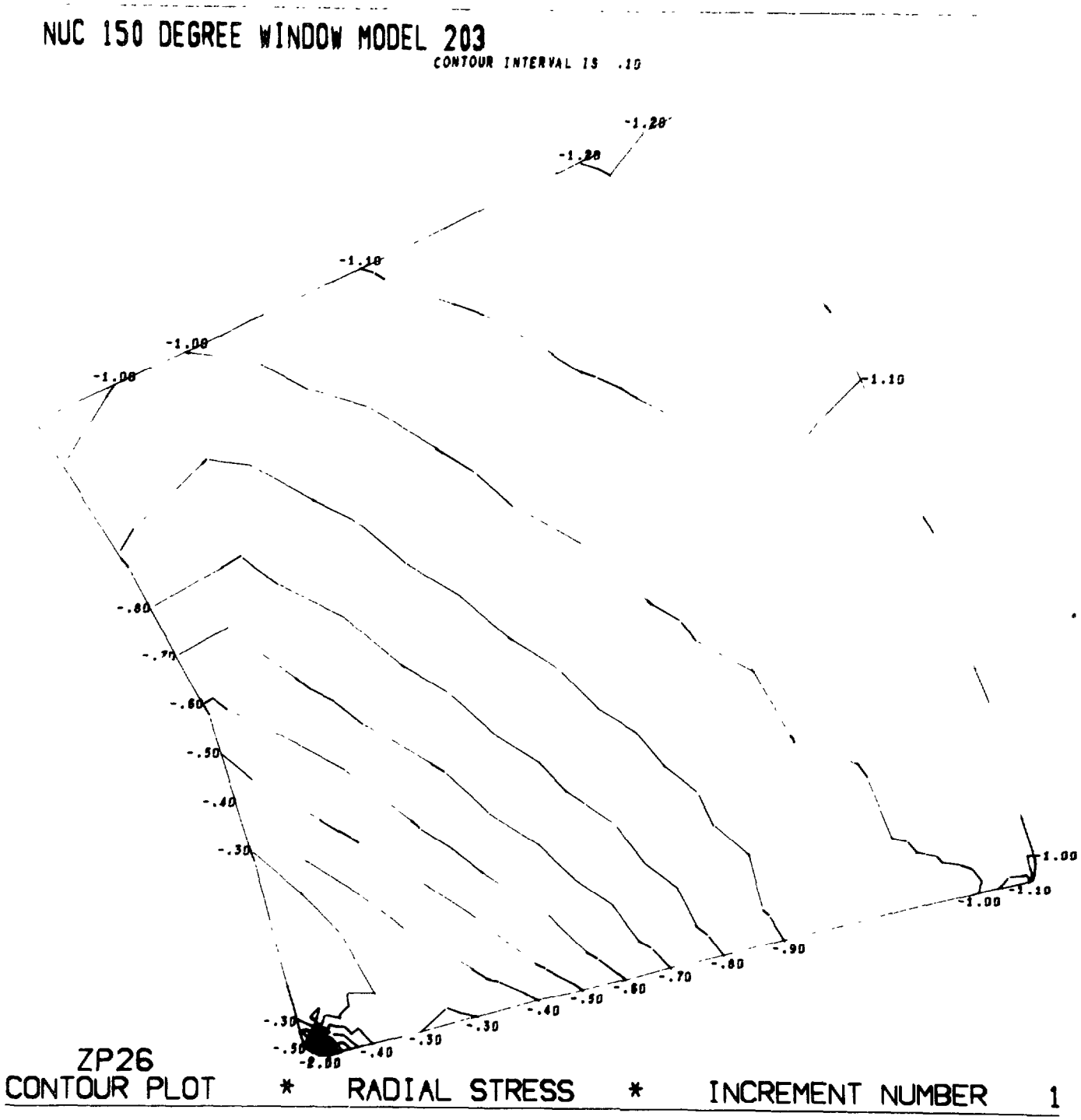

Figure B.9. Magnitude and distribution of stress in window-flange assembly Configuration B utilizing an aluminum flange, fiber-reinforced-epoxy gasket, and glass ceramic window (problem 203). (sheet 3 of 8)

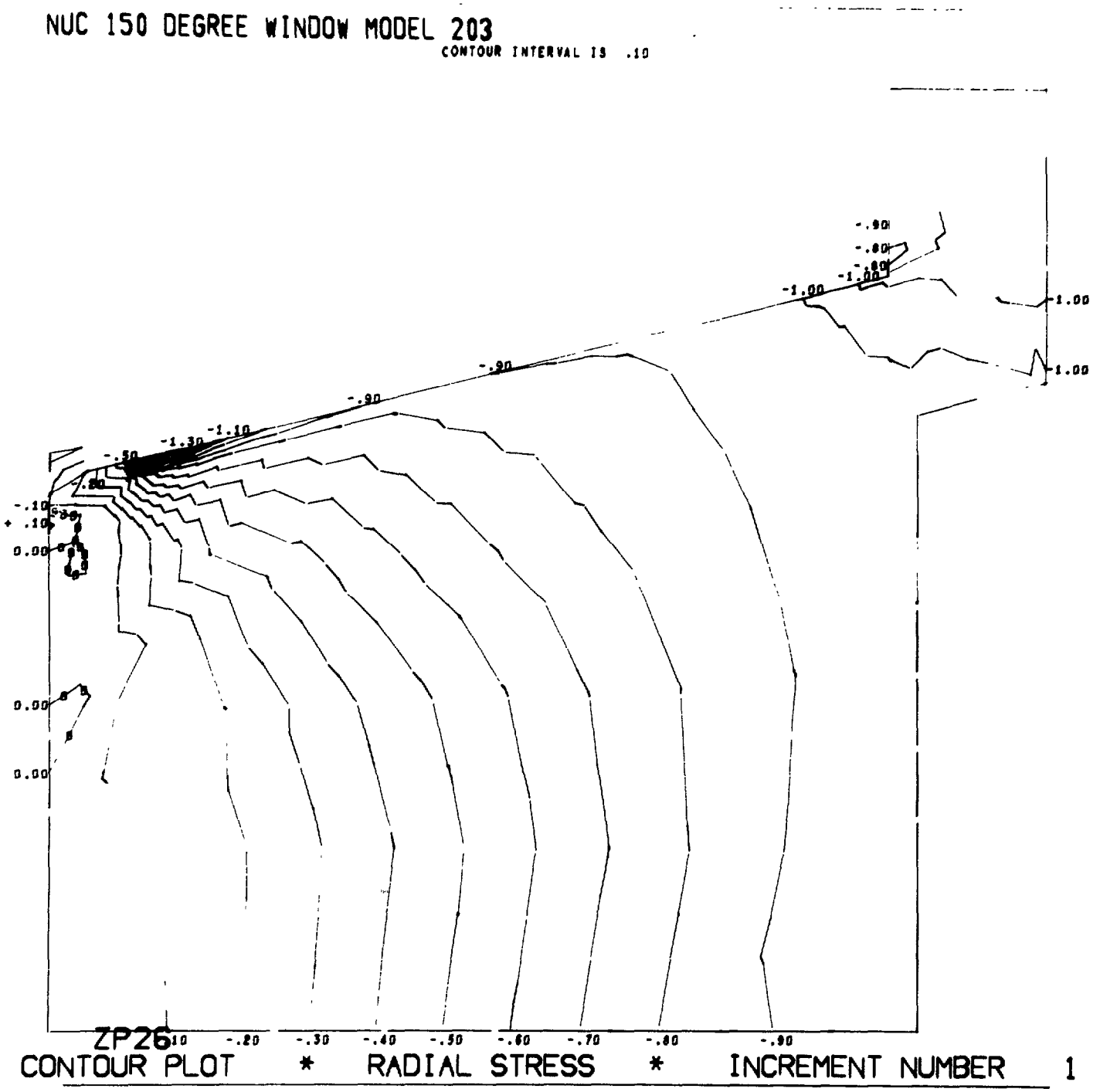

Figure B.9. Magnitude and distribution of stress in window-flange assembly Configuration B utilizing an aluminum flange, fiber-reinforced-epoxy gasket, and glass ceramic window (problem 203). (sheet 4 of 8)

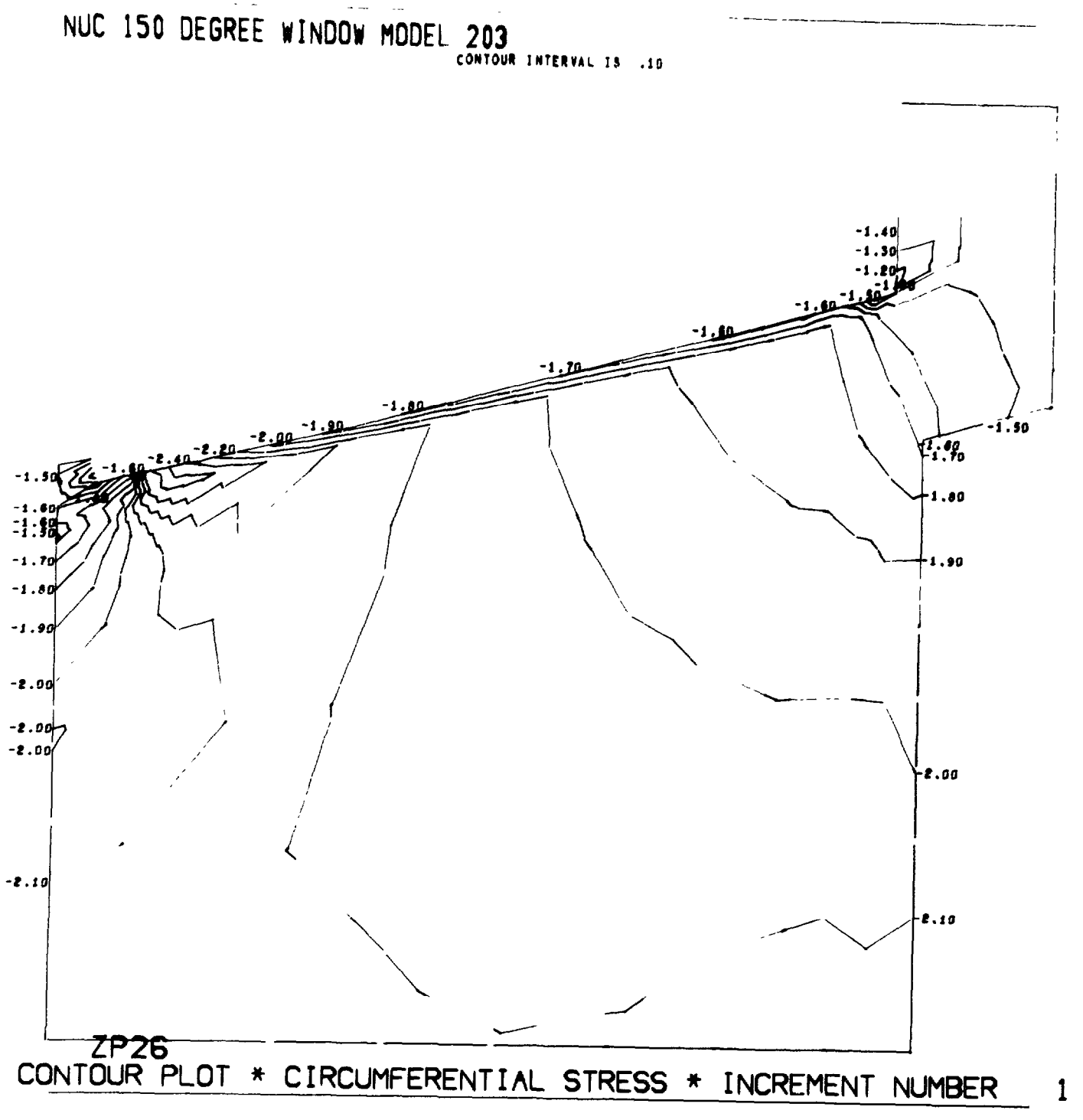

Figure B.9. Magnitude and distribution of stress in window-flange assembly Configuration B utilizing an aluminum flange, fiber-reinforced-epoxy gasket, and glass ceramic window (problem 203). (sheet 5 of 8)

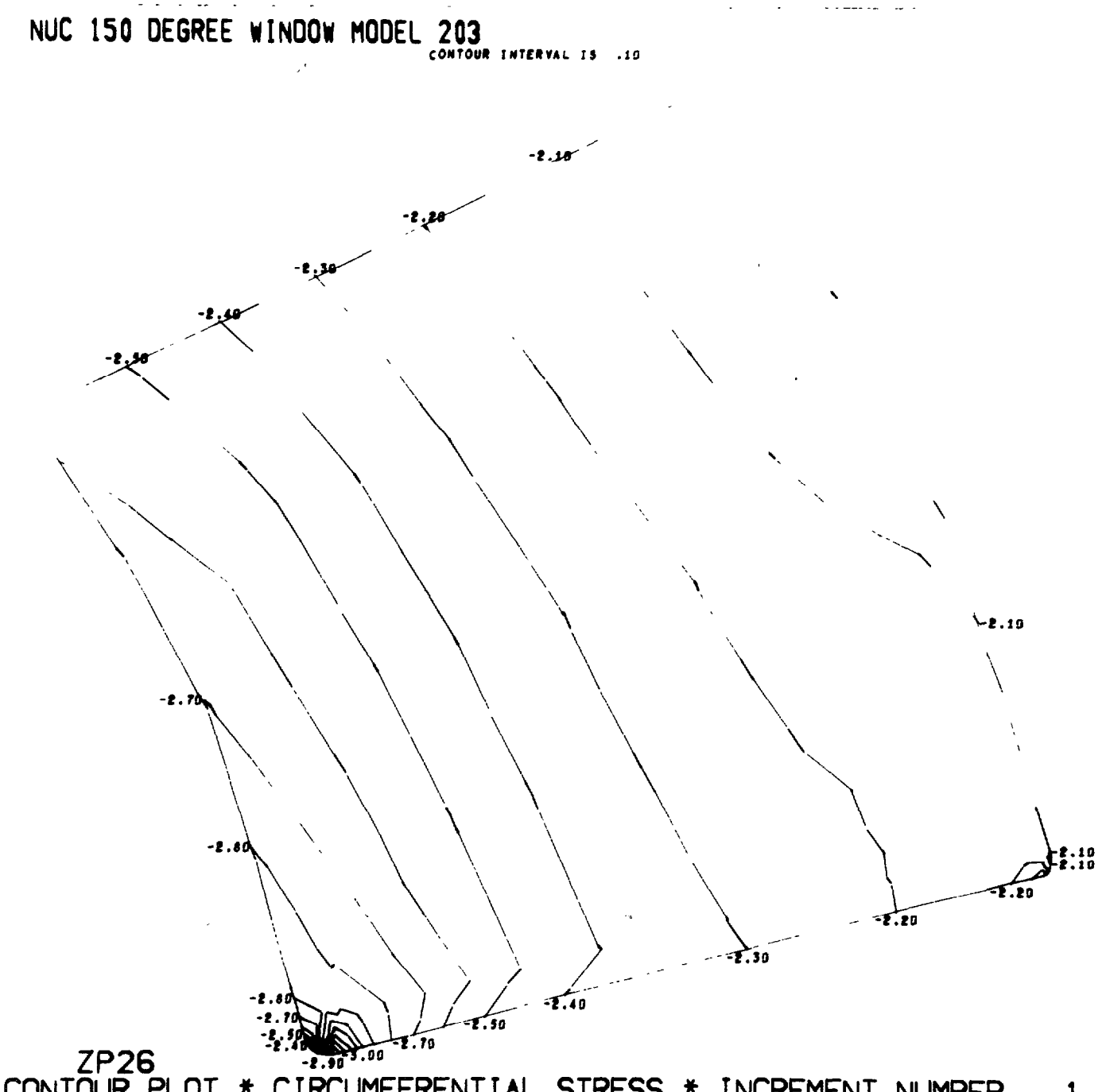

Figure B.9. Magnitude and distribution of stress in window-flange assembly Configuration B utilizing an aluminum flange, fiber-reinforced-epoxy gasket, and glass ceramic window (problem 203). (sheet 6 of 8)

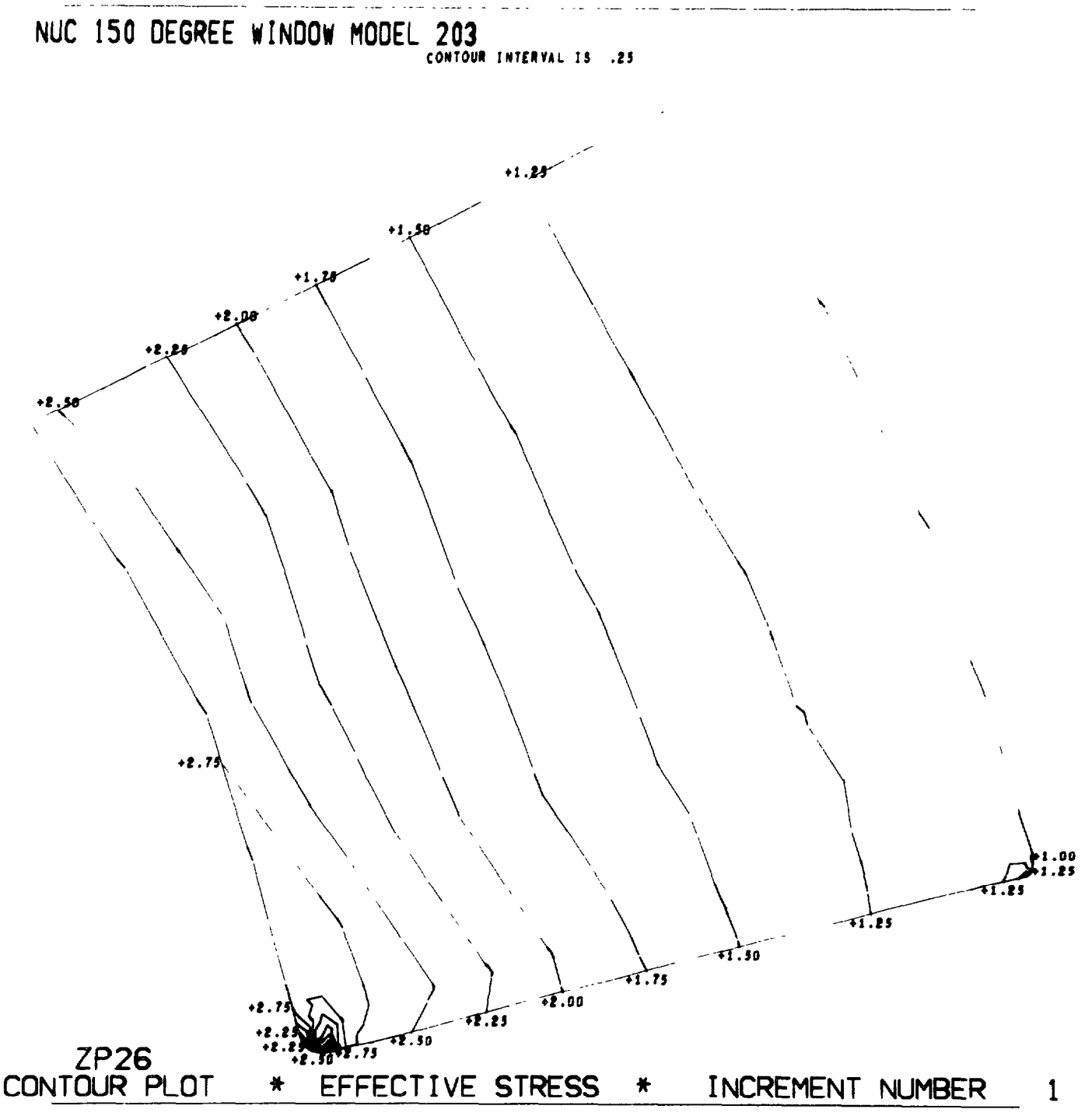

Figure B.9. Magnitude and distribution of stress in window-flange assembly Configuration B utilizing an aluminum flange, fiber-reinforced-epoxy gasket, and glass ceramic window (problem 203). (sheet 7 of 8)

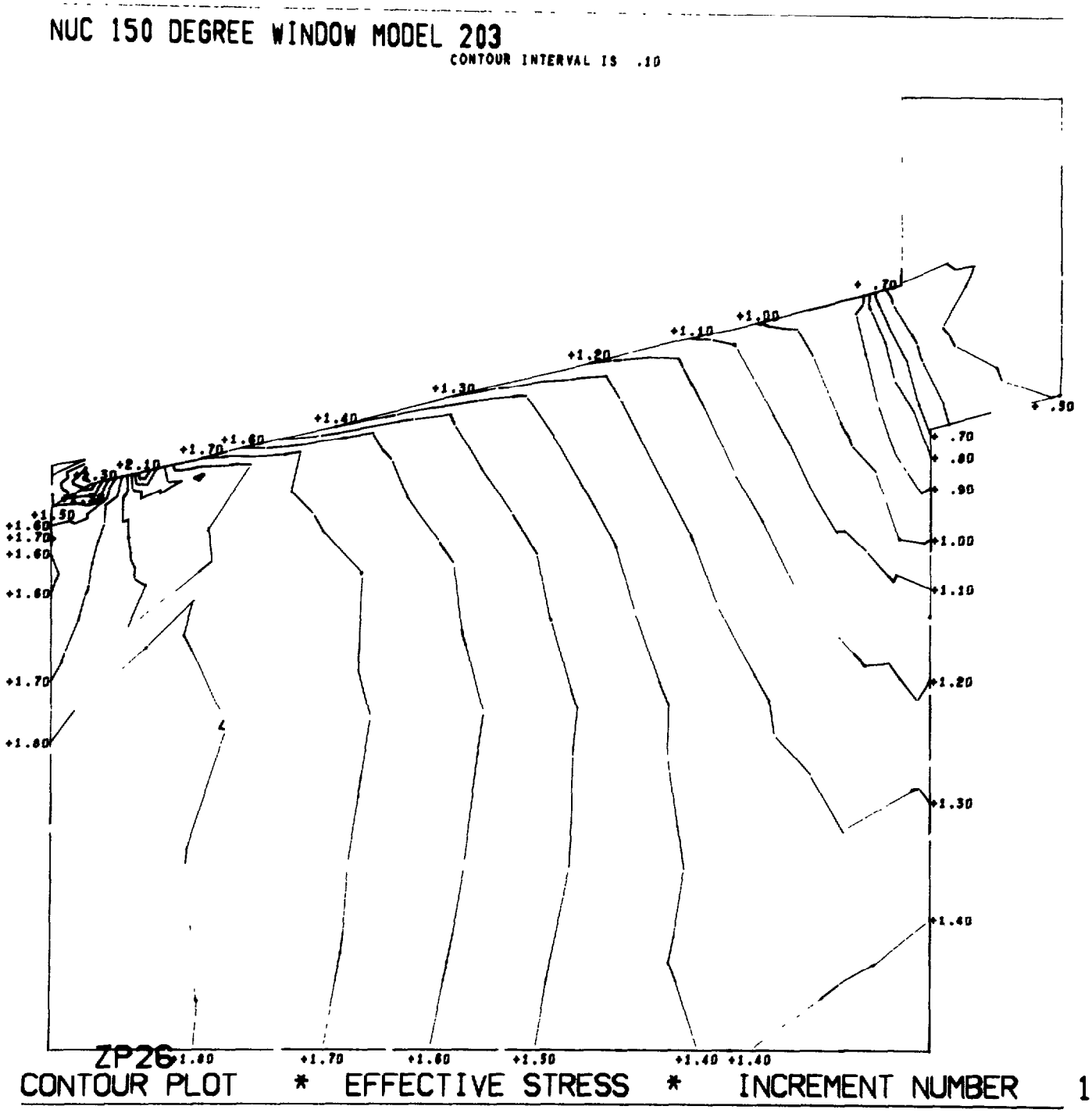

Figure B.9. Magnitude and distribution of stress in window-flange assembly Configuration B utilizing an aluminum flange, fiber-reinforced-epoxy gasket, and glass ceramic window (problem 203). (sheet 8 of 8)

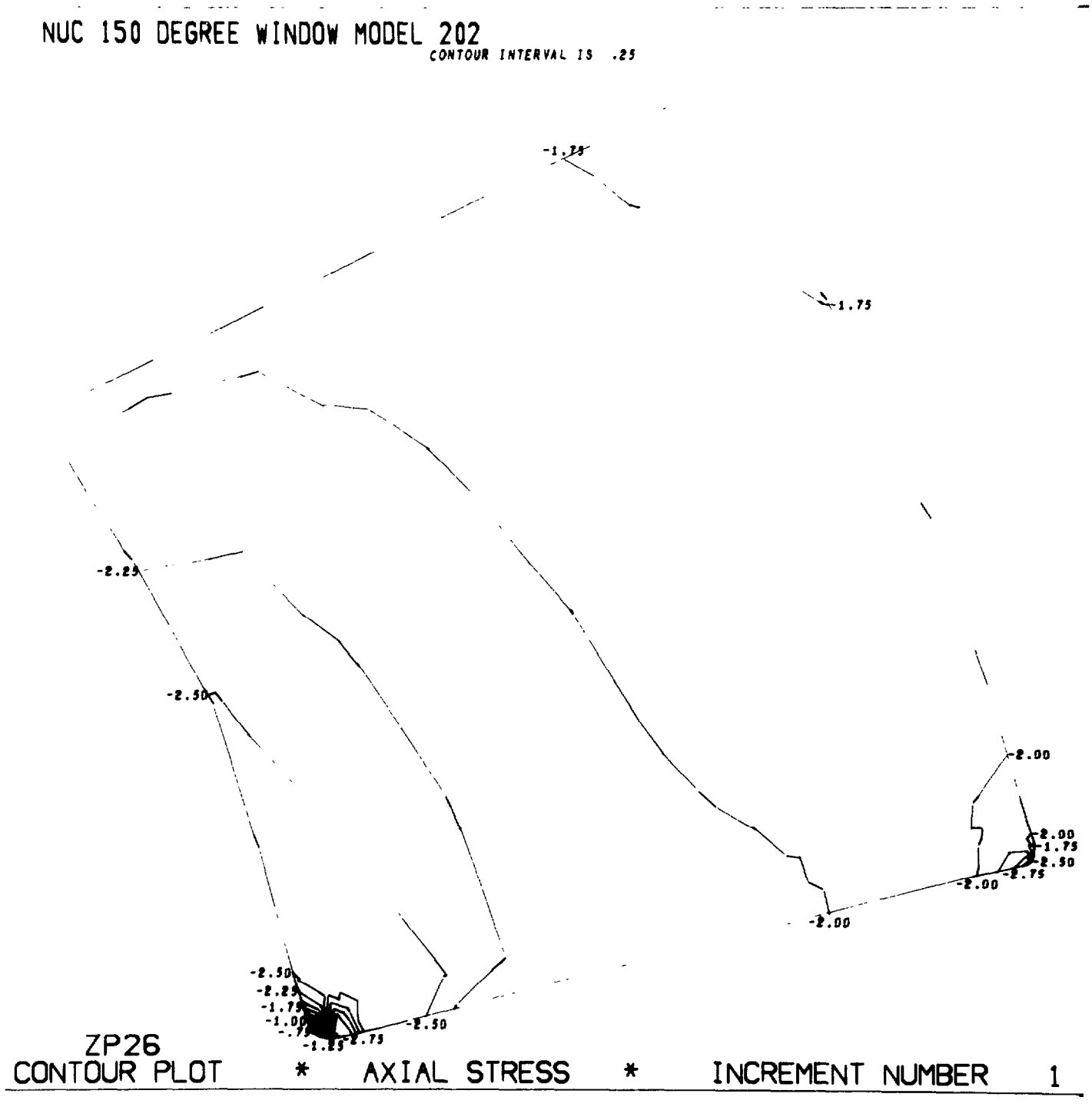

Figure B.10. Magnitude and distribution of stress in window-flange assembly Configuration B utilizing a titanium flange, fiber-reinforced-epoxy gasket, and glass ceramic window (problem 202). (sheet 1 of 8)

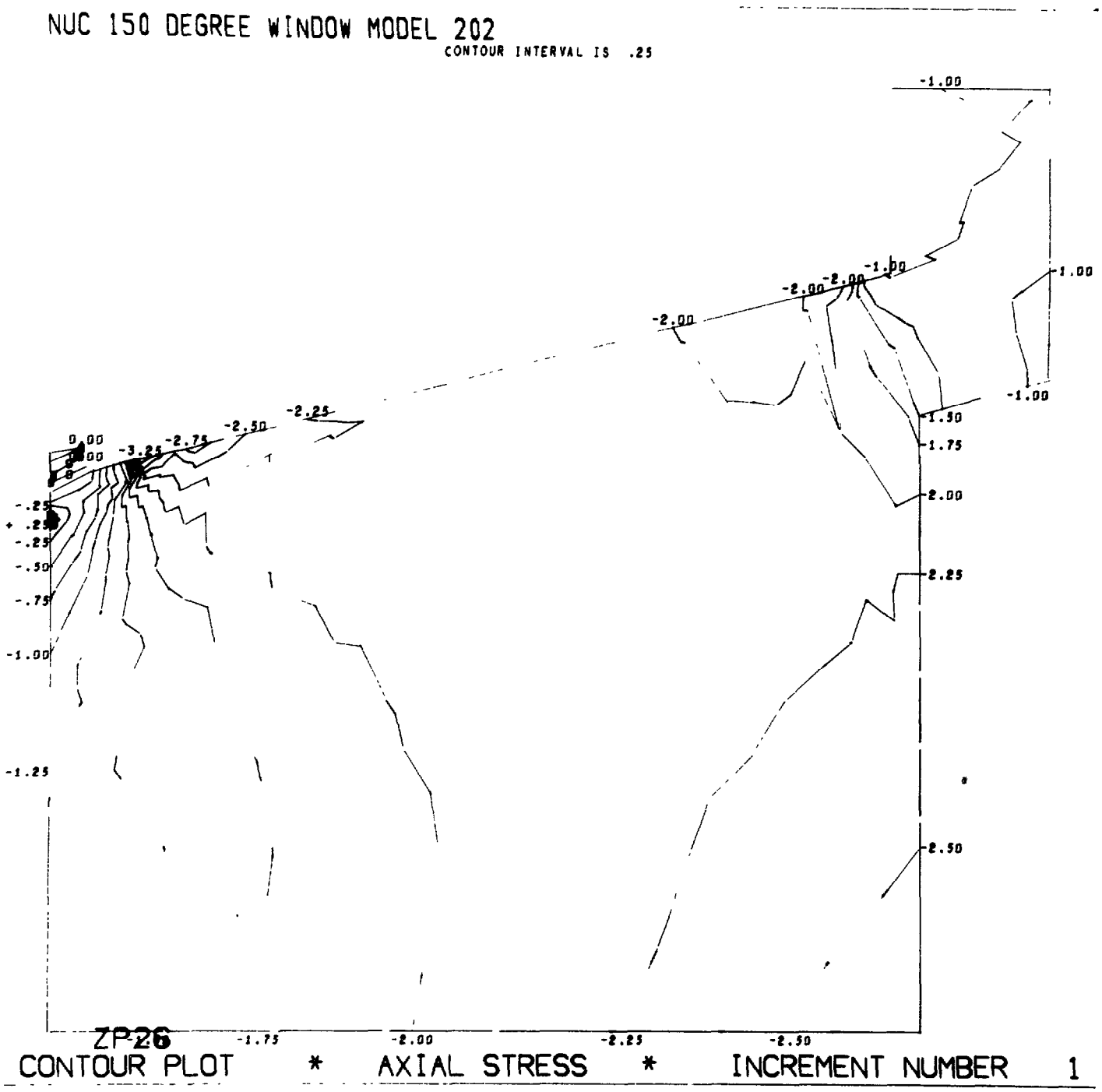

Figure B.10. Magnitude and distribution of stress in window-flange assembly Configuration B utilizing a titanium flange, fiber-reinforced-epoxy gasket, and glass ceramic window (problem 202). (sheet 2 of 8)

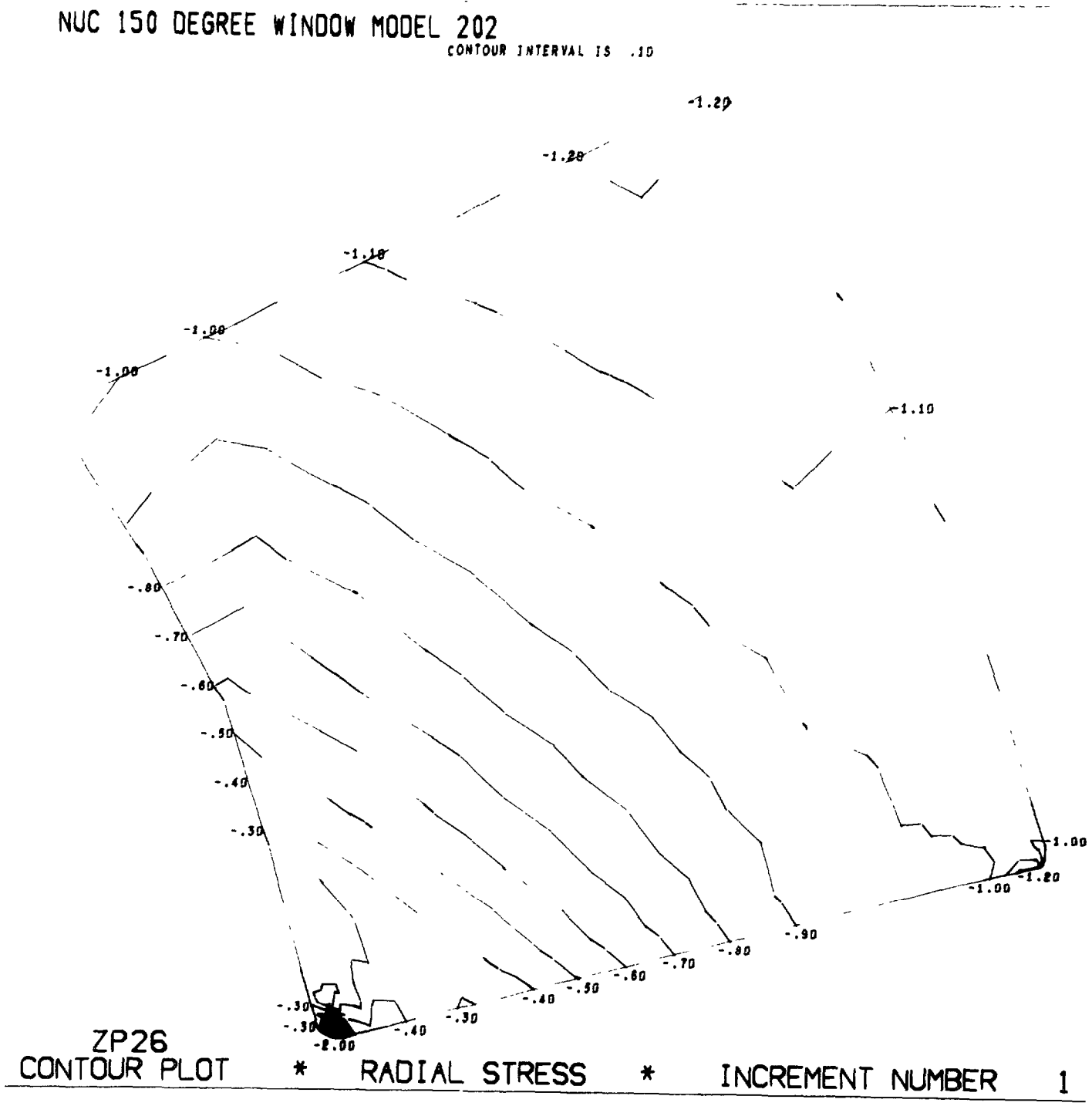

Figure B.10. Magnitude and distribution of stress in window-flange assembly Configuration B utilizing a titanium flange, fiber-reinforced-epoxy gasket, and glass ceramic window (problem 202). (sheet 3 of 8)

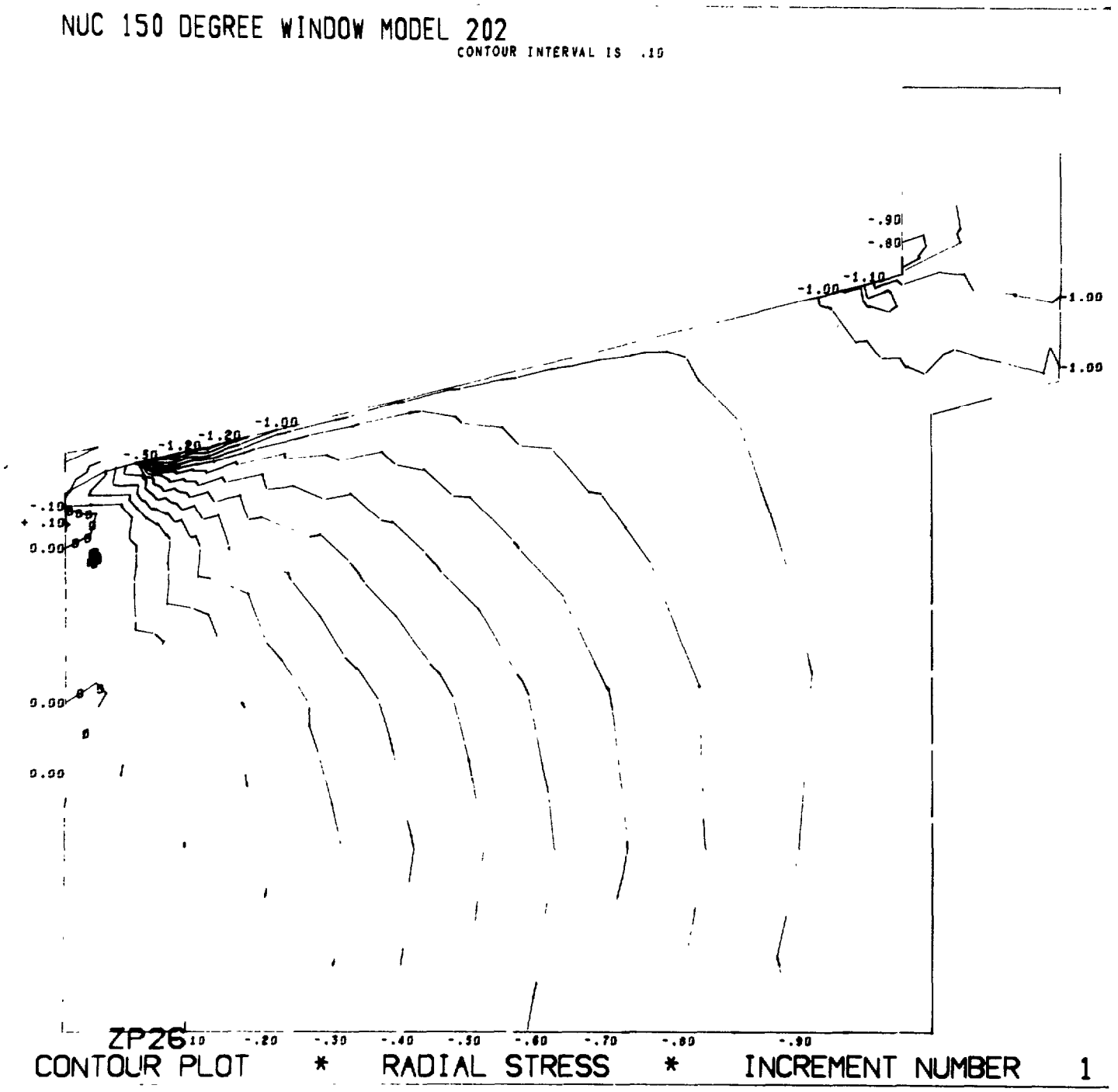

Figure B.10. Magnitude and distribution of stress in window-flange assembly Configuration B utilizing a titanium flange, fiber-reinforced-epoxy gasket, and glass ceramic window (problem 202). (sheet 4 of 8)

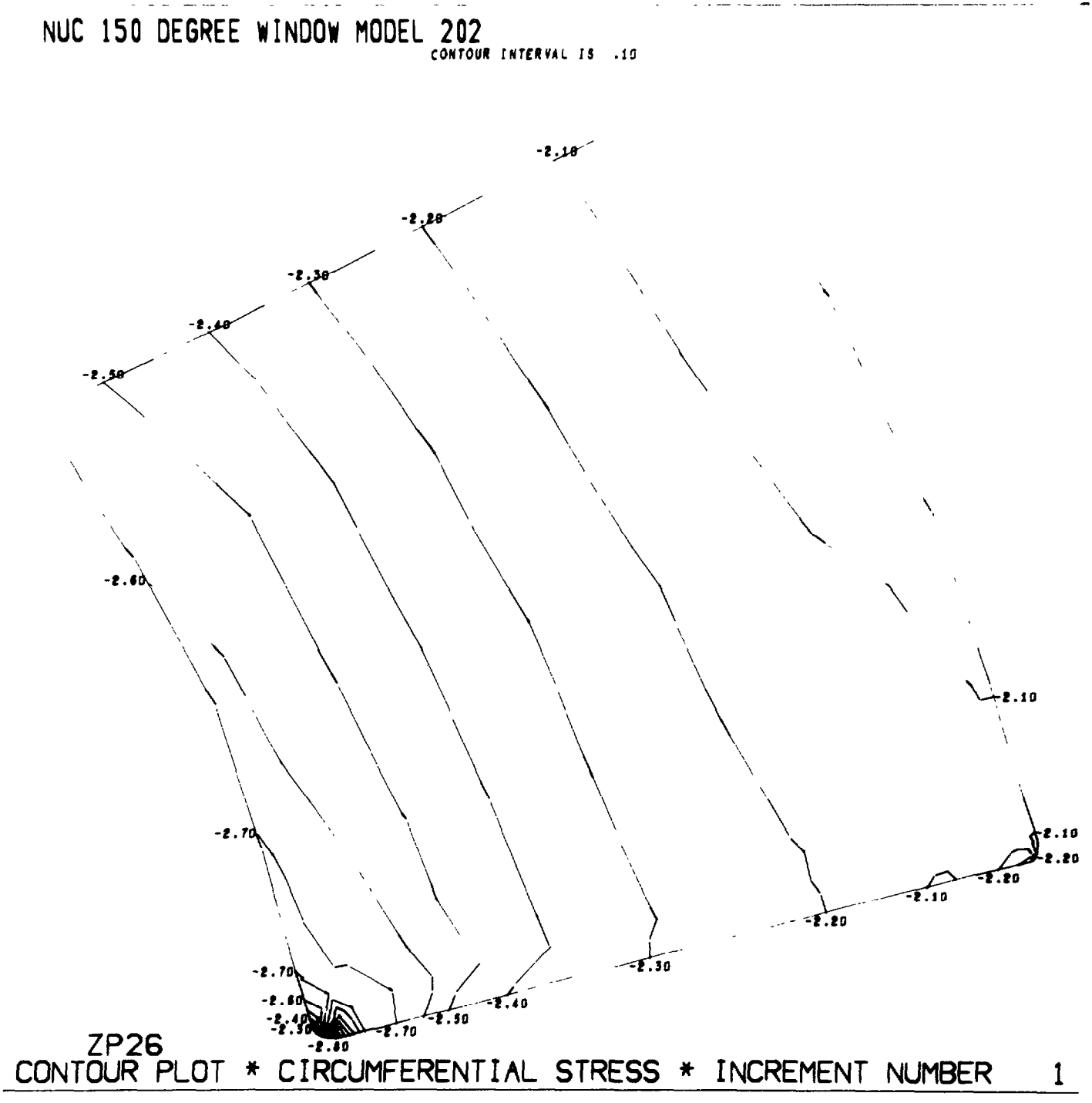

Figure B.10. Magnitude and distribution of stress in window-flange assembly Configuration B utilizing a titanium flange, fiber-reinforced-epoxy gasket, and glass ceramic window (problem 202). (sheet 5 of 8)

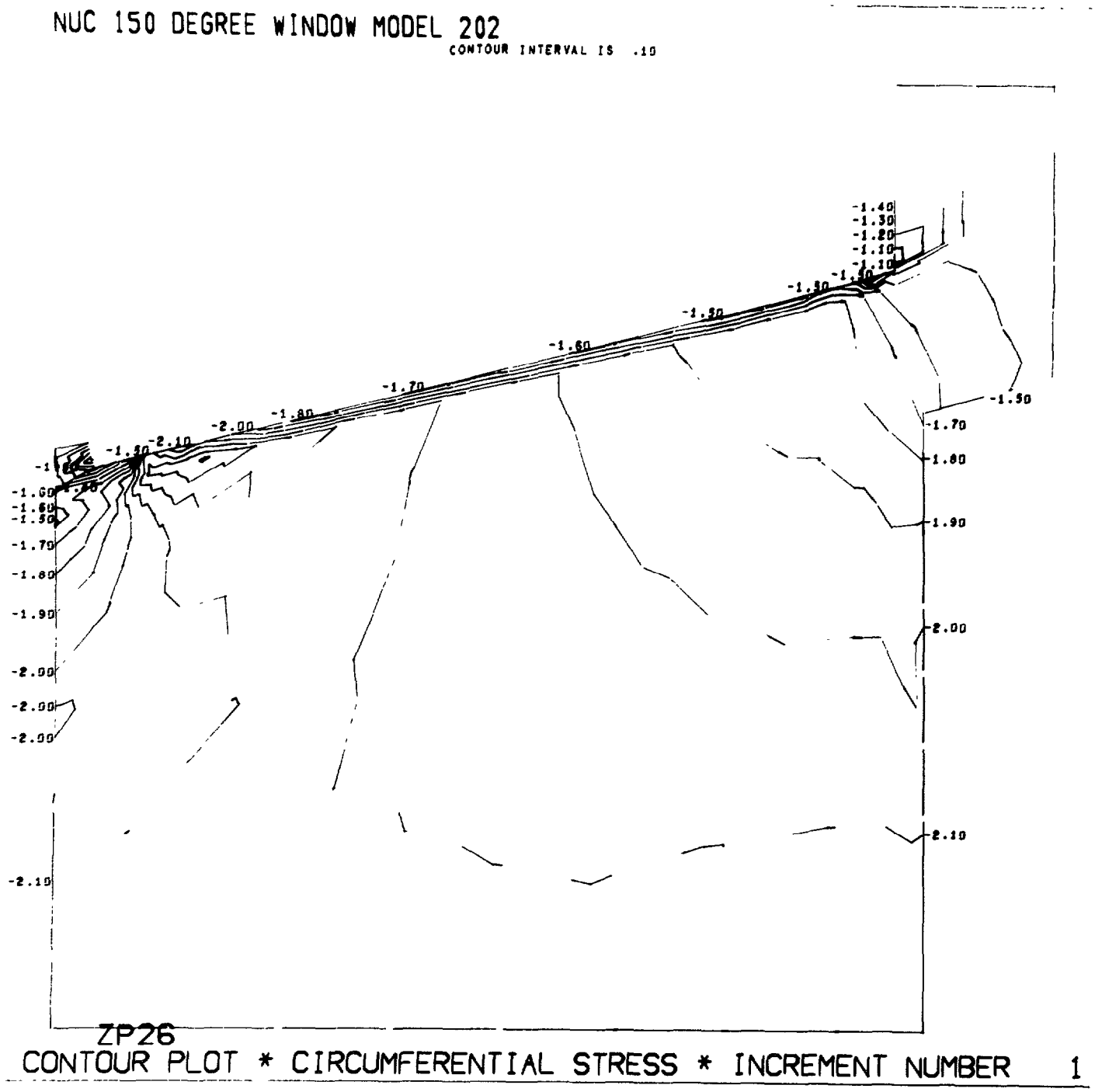

Figure B.10. Magnitude and distribution of stress in window-flange assembly Configuration B utilizing a titanium flange, fiber-reinforced-epoxy gasket, and glass ceramic window (problem 202). (sheet 6 of 8)

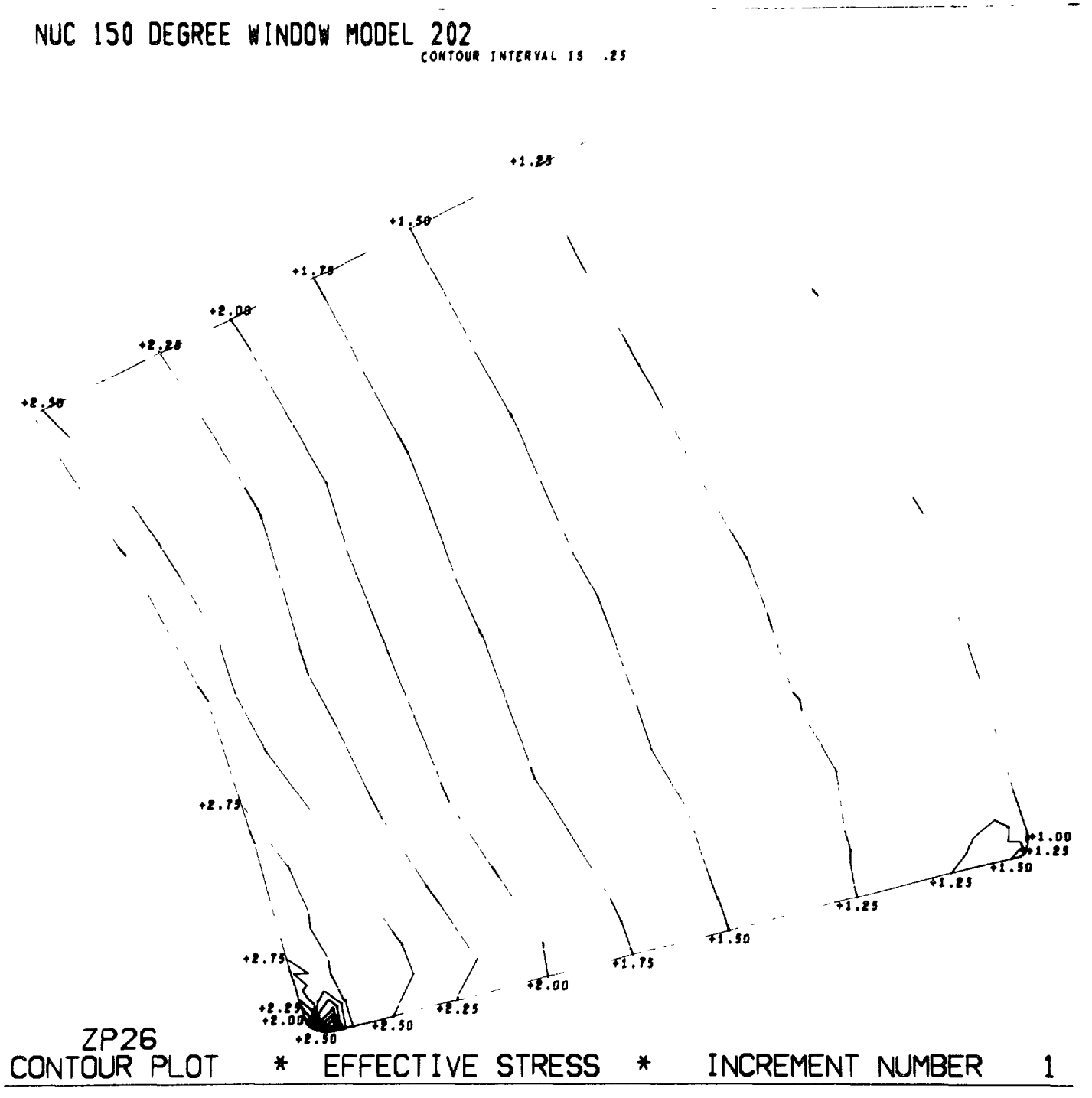

Figure B.10. Magnitude and distribution of stress in window-flange assembly Configuration B utilizing a titanium flange, fiber-reinforced-epoxy gasket, and glass ceramic window (problem 202). (sheet 7 of 8)

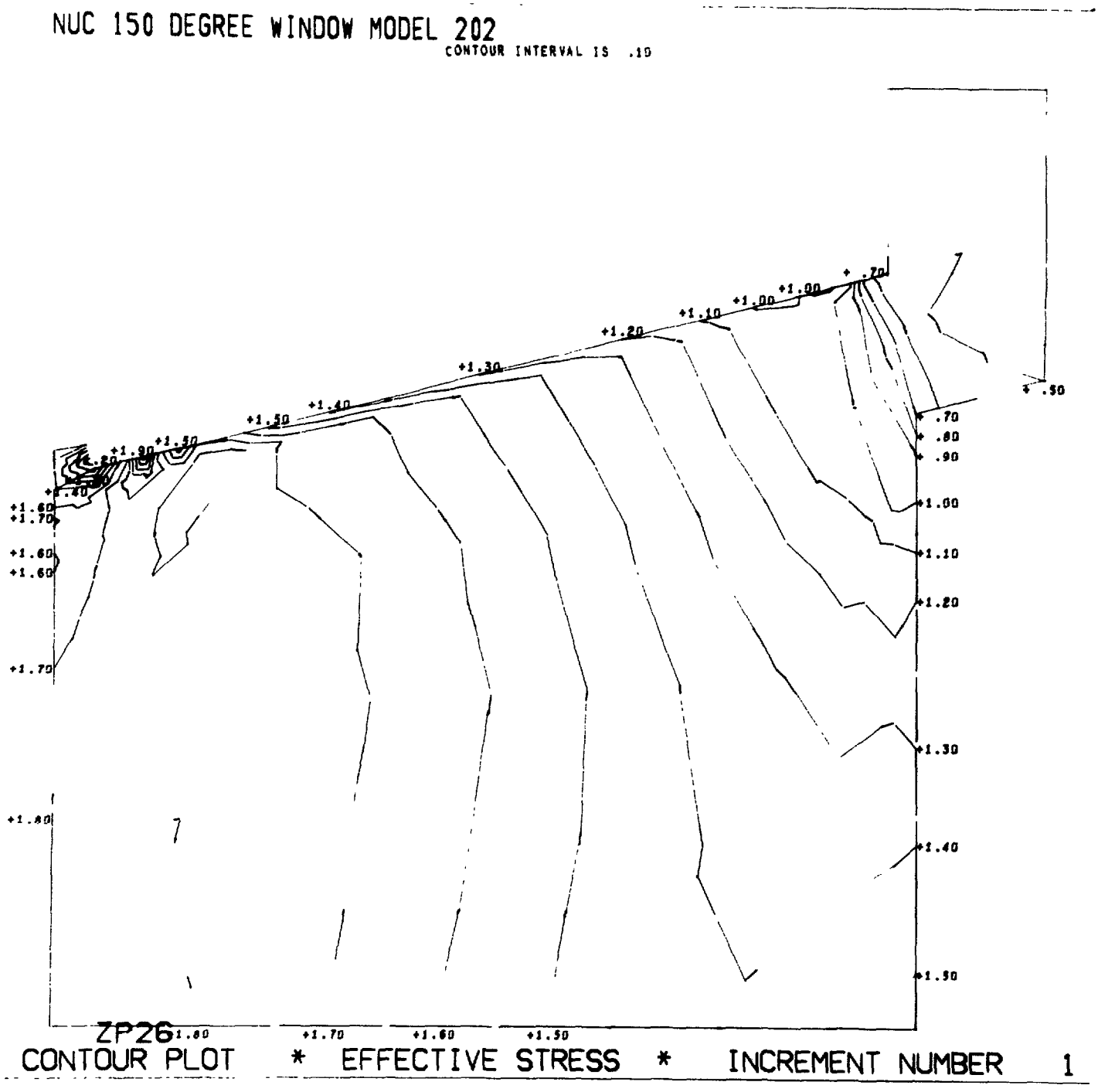

Figure B.10. Magnitude and distribution of stress in window-flange assembly Configuration B utilizng a titanium flange, fiber-reinforced-epoxy gasket, and glass ceramic window (problem 202). (sheet 8 of 8)

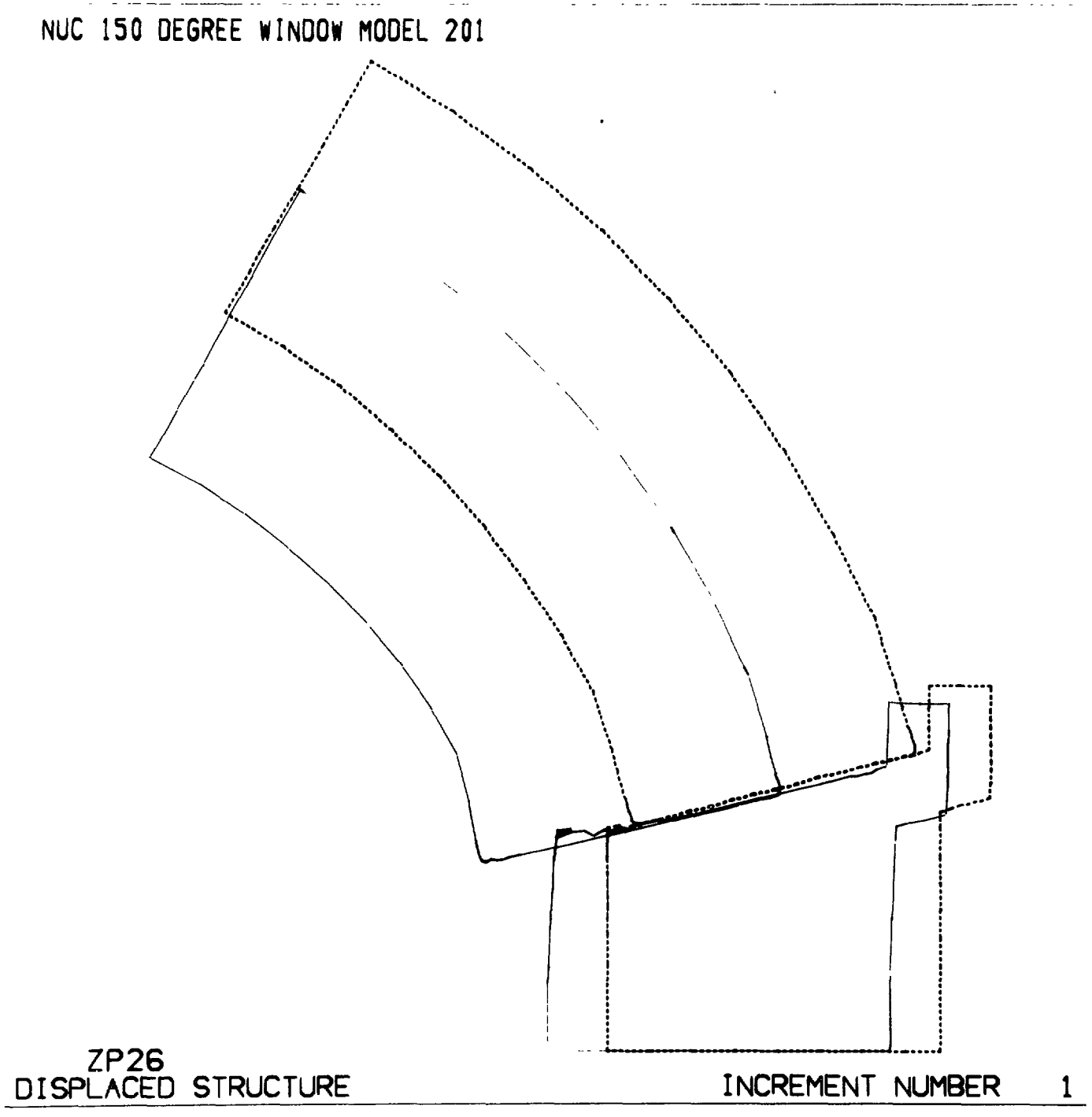

Figure B.11. Radial displacements of window and flange in Configuration B under external hydrostatic loading: problem 201, ceramic on steel.

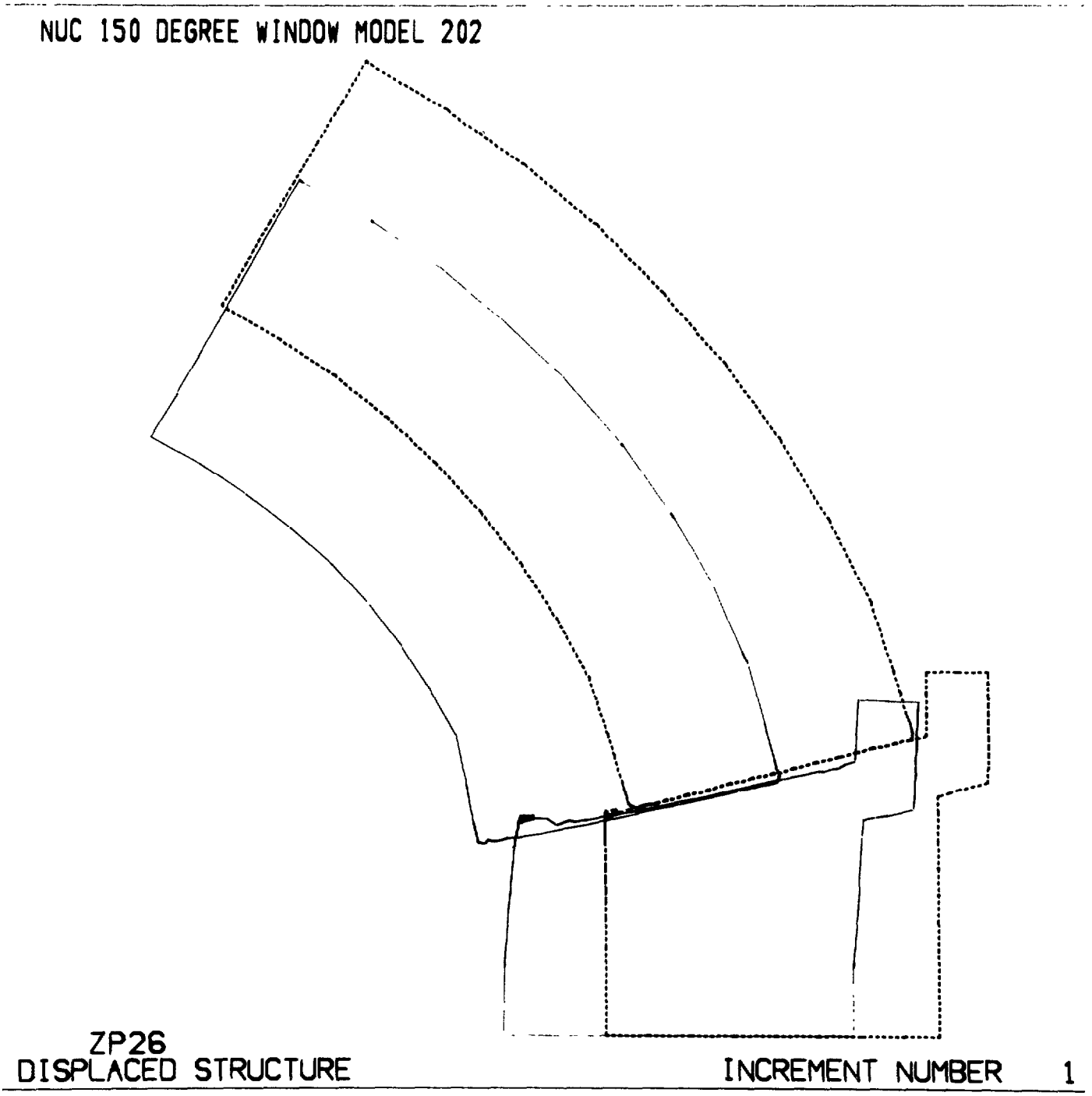

Figure B.11. Radial displacements of window and flange in Configuration B under external hydrostatic loading: problem 202, ceramic on titanium.

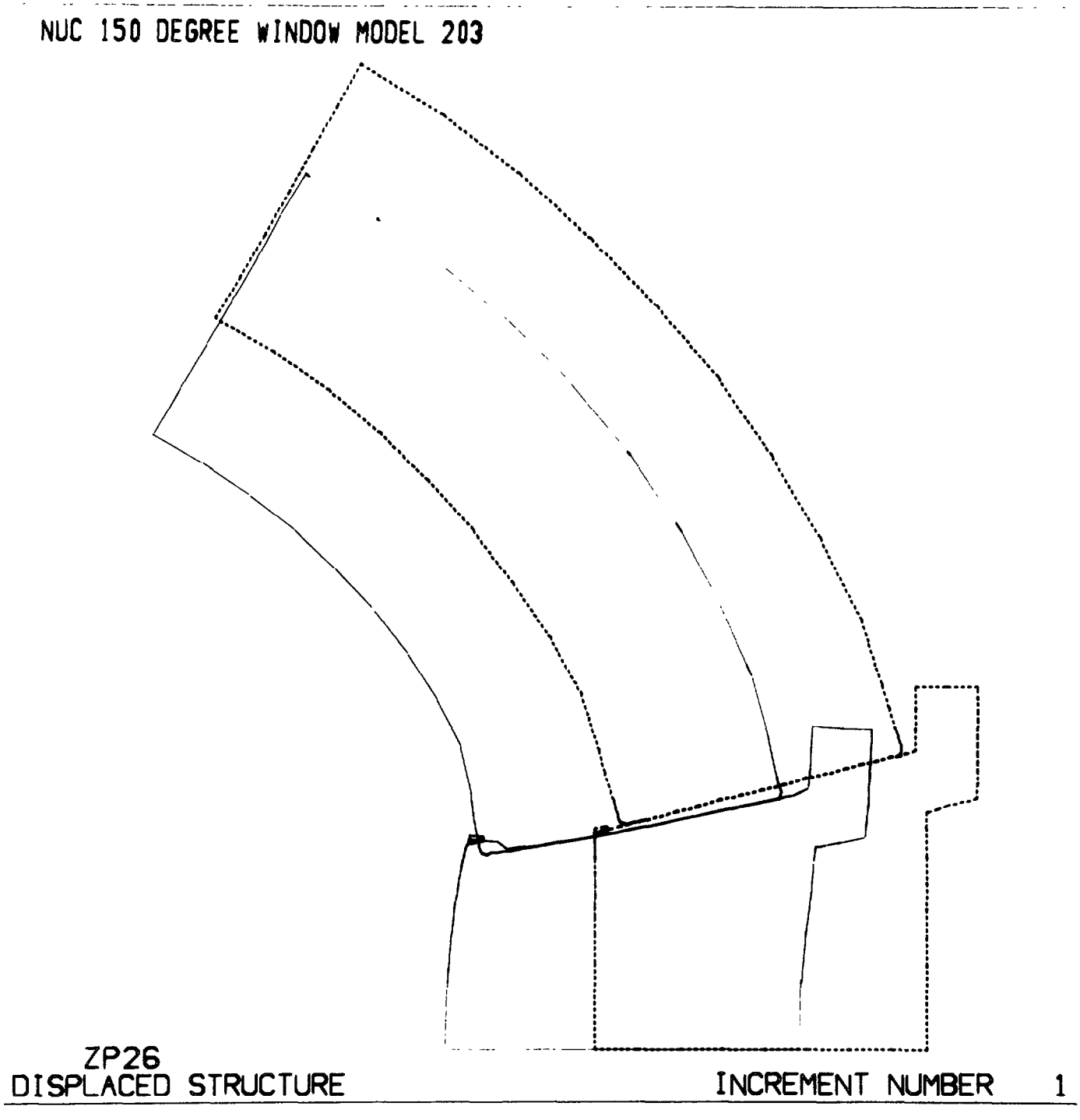

Figure B.11. Radial displacements of window and flange in Configuration B under external hydrostatic loading: problem 203, ceramic on aluminum.

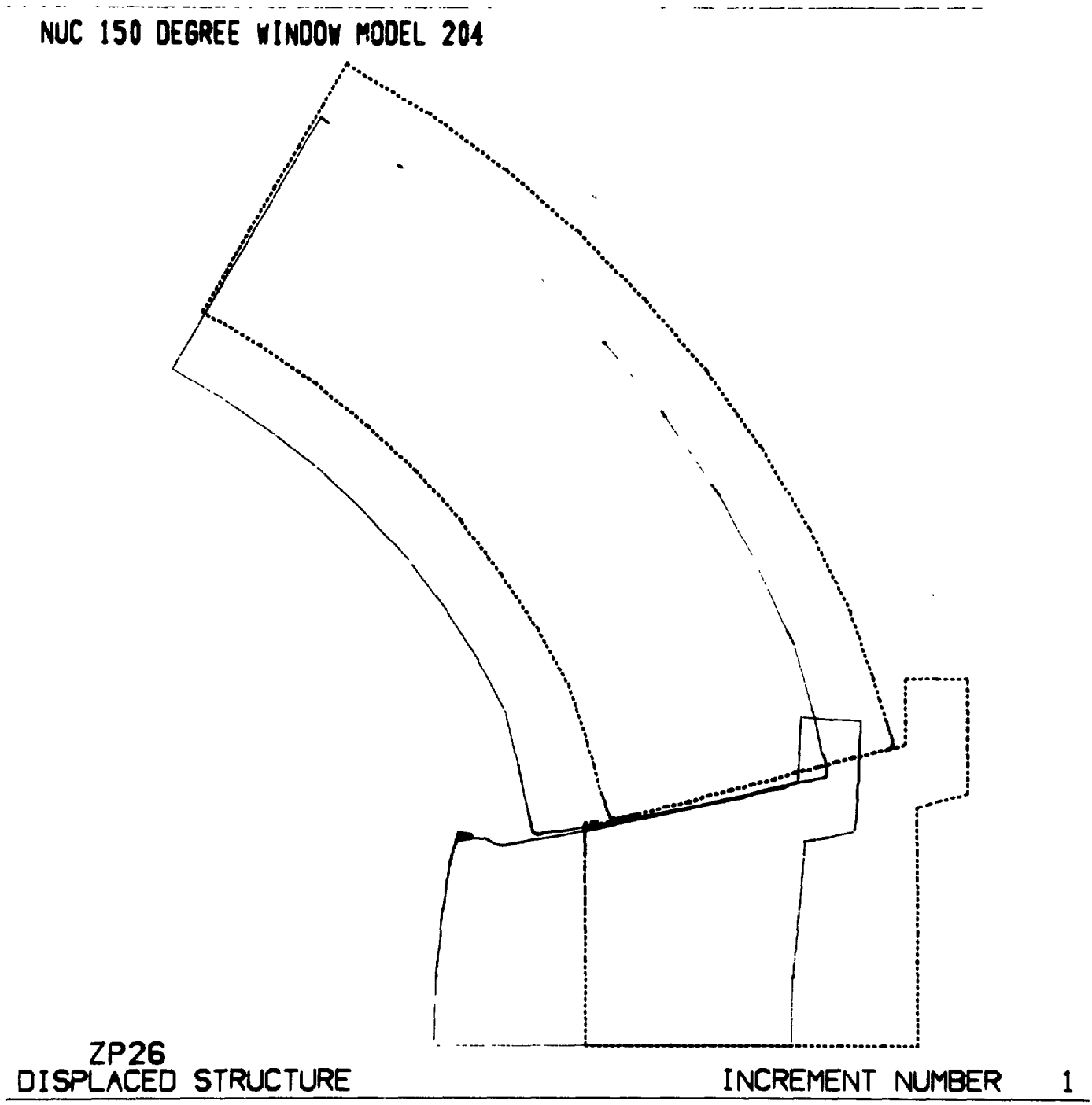

Figure B.11. Radial displacements of window and flange in Configuration B under external hydrostatic loading: problem 204, ceramic on glass-reinforced plastic.

APPENDIX C

FABRICATION OF WINDOWS

Since the windows evaluated in this study were fabricated from four different materials, the fabrication processes differed considerably from one material to another.

The acrylic plastic windows were machined from 4-inch-thick Plexiglas GM sheets using standard metalworking machine-shop equipment. Since the plastic window is much more tolerant to mismatch at the bearing surfaces than glass, the tolerance on the beveled bearing surface was relaxed for plastic windows to ±15 minutes.

After polishing, the windows were annealed to preclude any subsequent crazing during the test program. Since the mechanical and optical properties of Plexiglas GM acrylic plastic are available from the supplier (Cadillac Plastics, Inc.) they will not be discussed here in detail, but are summarized for the reader's convenience in Table C.1.

The optical glass windows were ground from gobs of BK-7 optical glass using standard lens-grinding techniques. The beveled bearing surface on the windows was controlled to within ± 1 minute to eliminate any serious stress raisers. Since the mechanical and optical properties of BK-7 are available from Schott Glass, only a brief summary is given for the reader's convenience in Table C-2.

The glass ceramic windows were pressed in glassy stage (figures C.1 and C.2) by Owens Illinois into graphite molds. The rough hemispherical castings (figure C.3) were subsequently subjected to a controlled heat treatment that converted the glass into nonporous, polycrystalline material exhibiting a high degree of isotropy in all its properties. The resulting Cer-Vit C-101 ceramic hemispheres were ground to final shape (figure C.4) utilizing standard lens-grinding techniques. The transmission of light through the Cer-Vit C-101 window was adequate, but was significantly less than that through the acrylic plastic and BK-7 windows. Mechanical properties of the ceramic are discussed in the body of the report but they are summarized here for the reader's convenience (Table C.3 and figures C.5 through C.13).

The chemically surface-strengthened glass Cer-Vit SSC-201 windows were formed by Owens Illinois in the same molds and from the same glassy material used in the ceramic windows. The major difference was that the cast hemispheres *were not* subsequently subjected to the thermal treatment that would induce crystallization of the glass. After grinding to the final shape by typical lens-grinding

techniques, the windows were subjected to the chemical surface-strengthening process of immersing the finished windows into a bath of $NaNO_3$ salt at 400°C. The depth of ion-exhange in the surface of the glass windows was controlled by the length of immersion in the salt bath, which was approximately 5 hours. The magnitude of the compression stress induced in the surface of the glass by the bath was established experimentally by immersing rod-shaped test coupons of the same material 0.250 inch in diameter and 5.5 inches long in the same salt bath. This procedure showed that the salt bath imparted to the glass an average surface-compression stress of 60,900 psi.

Of the four fabrication processes the most economical was found to be that used for the acrylic plastic window (under $250 in quantities of 20). Also, the local availability of Plexiglas G stock made the procurement time less than one week.

The most expensive fabrication process was found to be the grinding of windows from gobs of optical glass (under $1,000 in quantities of 20). The delivery time is on the order of 4 weeks, since the gobs of glass must be ordered from the fabricator.

The fabrication of Cer-Vit SSC-201 and C-101 windows by pressing and subsequent grinding is slightly less expensive than that of optical glass windows (under $900 in quantities of 20); but it requires considerably more time, since the graphite tooling for pressing the windows must be prepared first. Also, it is only fair to mention that both the Cer-Vit C-101 and SSC-201 windows contain a significant number of inclusions in the form of bubbles, while the optical glass and acrylic plastic ones do not. Also, the absence of tint and higher light transmission noted for the BK-7 and acrylic plastic windows make them more acceptable for applications where the lighting is poor or where true rendition of color is desired.

Table C.1. Properties of Acrylic Plastic G and Plexiglas II UVA.

PROPERTY	ASTM METHOD	UNITS	Plexiglas G and II UVA
Thickness		inches	.250
SPECIFIC GRAVITY	D792-64T	–	1.19
OPTICAL			
Refractive index	D542-50	–	1.49
Light transmittance and haze	D1003-61		
"as received" -parallel		percent	91
-total		percent	92
-haze		percent	1
After 5 years outdoor exposure Bristol, Pa., 45-degree angle facing south			
-parallel		percent	
-total		percent	92
-haze		percent	2
After 240 hours accelerated exposure, carbon arc type, per ASTM E-42-64			
-parallel		percent	90
-total		percent	92
-haze		percent	2
Accelerated weathering, fluorescent sunlamp with dew, 10 cycles, 240 hours exposure	D1501-57T or		
-crazing	LP 406a,	–	none
-warping	method 6024	–	none

Table C.1. Properties of Acrylic Plastic G and Plexiglas II UVA. (Continued)

Instrumental measurement, change in yellowness index after accelerated weathering	(D1925-63T)	–	1.0
Ultraviolet transmission, 320 mμ	Beckman DU-792	percent	0
MECHANICAL			
Tensile strength (¼-inch specimen- 0.2 inch/minute	D638-64T		
Maximum		psi	10,500
Rupture		psi	10,500
Elongation, maximum		percent	4.9
Elongation, rupture		percent	4.9
Modulus of elasticity		psi	450,000
Poisson's ratio			0.35
Flexural strength (span depth ratio 16, 0.1 inch/minute)	D790-63		
Maximum		psi	16,000
Rupture		psi	16,000
Deflection, maximum		inches	0.6
Deflection, rupture		inches	0.6
Modulus of elasticity		psi	450,000
Compressive strength (0.2 inch/minute)	D695-63T		
Maximum		psi	18,000
Modulus of elasticity		psi	450,000
Compressive deformation under load	D621-64		

Table C.1. Properties of Acrylic Plastic G and Plexiglas II UVA. (Continued)

2000 psi at 122°F., 24 hours	conditioned	percent	0.2
4000 psi at 122°F., 24 hours	48 hours at 122°F	percent	0.5
Shear strength	D732-46	psi	9,000
Impact strength			
charpy unnotched	D256-56	ft.lbs/ ½-by ½-in.	3.5
Izod milled notch		ft.lbs./ in. of notch	0.4
Rockwell hardness	(R and H P-20)	—	M-93
Barcol number	(R and H P-79)	—	49
Resistance to stress			
Critical crazing stress	ARTC Mod.		
Isopropyl alcohol	of	psi	2,100
Toluene	MIL-P-6997	psi	1,700
THERMAL			
Hot forming temperature		°F.	290-360
Heat distortion temperature	D648-56		
3.6°F./minute—264 psi		°F.	205
3.6°F./minute—66 psi		°F.	225
Maximum recommended continuous service temperature		°F.	180-200

Table C.1. Properties of Acrylic Plastic G and Plexiglas II UVA. (Continued)

Coefficient of thermal expansion	R and H P4A	$in/in/^{o}F.x10^{-5}$	
-40°F.			2.8
-20			2.9
0			3.1
20			3.3
40			3.6
60			3.9
80			4.2
100			4.6
Coefficient of thermal conductivity	(Cenco-Fitch)	$\frac{BTU}{(hr)\ (sq.ft.)\ (^{o}F./in)}$	1.3
Specific heat at 77°F.	—	$\frac{BTU}{(Lb.)\ (^{o}F.)}$	0.35
ELECTRICAL			
Dielectric strength, short time test	D149-64	volts/mil	500
Dielectric constant	D150-64T		
60 cycles			3.7
1,000 cycles			3.3
1,000,000 cycles			2.5
Power factor	D150-64T		
60 cycles			0.05
1,000 cycles			0.04
1,000,000 cycles			0.03

Table C.1. Properties of Acrylic Plastic G and Plexiglas II UVA. (Continued)

Loss factor	D150-64T		
60 cycles			0.19
1,000 cycles			0.13
1,000,000 cycles			0.08
Arc resistance	D495-61		No tracking
Volume resistivity	D257-61	ohm cm.	6×10^{17}
Surface resistivity	D257-61	ohm/square	2×10^{18}
MISCELLANEOUS			
Flammability (burning rate)	D635-63	in./minute	1.1
Flame resistance, extinguishing Time after second ignition	(SPE Journal, April, 1950)	seconds	–
Water absorption, 24 hours at 73°F.	D570-63		
Weight loss on drying		percent	0.1
Weight gain on immersion		percent	0.2
Soluble matter lost		percent	0.0
Water absorbed		percent	0.2
Dimensional changes on immersion		percent	0.0
Water absorption to saturation			
Weight gain after immersion	D229-49(B)		
1 day	and	percent	0.2
2 days	D570-63	percent	0.3
7 days		percent	0.4

Table C.1. Properties of Acrylic Plastic G and Plexiglas II UVA. (Continued)

28 days		percent	0.8
56 days		percent	1.1
84 days		percent	1.3
Humidity expansion, change in length on going from 20- to 90-percent relative humidity at equilibrium, 74°F.		mils/inch	3

Table C.2. Properties of Borosilicate Crown Glass BK-7*.

Specific gravity	2.51
Coefficient of expansion (-30° to 70°C)	$71 \times 10^{-7}/^{\circ}C$
Specific heat (at 20°C)	$0.205 \frac{cal}{g^{\circ}C}$
Thermal conductivity (at 20°C)	$0.958 \frac{kcal}{mh^{\circ}C}$
Modulus of elasticity	$8310 \frac{kg}{mm^2}$
Modulus of rigidity	$3440 \frac{kg}{mm^2}$
Poisson's ratio	0.208
Micro indentation hardness (Vickers diamond with 136-degree angle 50 g load for 10 seconds)	$633 \frac{kg}{mm^2}$
Index of refraction (N_d)	1.5168

*Schott glass composition

Table C.2. Properties of Borosilicate Crown Glass BK-7. (Continued)

Transmittance of Average Melt

μ (microns)	0.280	0.290	0.300	0.310	0.320	0.330	0.340	0.350	0.360	0.370	0.380	0.390
τ_i at 5-mm thickness		0.06	0.30	0.63	0.805	0.907	0.995	0.972	0.984	0.992	0.995	0.996
τ_i at 25-mm thickness				0.10	0.34	0.61	0.79	0.87	0.92	0.96	0.975	0.980
μ (microns)	0.400	0.420	0.440	0.460	0.480	0.500	0.540	0.580	0.620	0.660	0.700	
τ_i at 5-mm thickness	0.997	0.997	0.998	0.998	0.998	0.998	0.998	0.999	0.999	0.999	0.999	
τ_i at 25-mm thickness	0.984	0.987	0.989	0.990	0.991	0.991	0.993	0.994	0.995	0.995	0.995	

Table C.3. Properties of Cer-Vit Glass-Ceramic C-101.

Density (ρ), g/cc	2.50
Hardness, Knoop (200 g loading)	540
Compressive Strength (psi)	$\geqslant 200 \times 10^3$
Modulus of Rupture (psi)	14.5×10^3

Chemical Properties

(Chemical Durability)	
5 percent HCl at 95°C	17.8 mils/yr
5 percent NaOH at 95°C	204.4 mils/yr
Water at 100°C	15.7 mils/yr

Electrical Properties

Dielectric constant	25°C, 100 Hz	11.7
	25°C, 1 MHz	9.1
	250°C, 1 MHz	14.2
Dissipation factor	25°C, 100 Hz	0.076
	25°C, 1 MHz	0.023
	250°C, 1 MHz	0.093
Volume resistivity (ohm-cm)	25°C	10^{14}
	250°C	10^8
Surface resistivity at 0 percent relative humidity (ohm/sq.)	25°C	10^{13}
	250°C	3×10^{10}

Optical Properties

Index of Refraction (N_D, 25°C)	1.540

Table C.4. Properties of Cer-Vit Material SSC-201.

Mechanical Properties

Modulus of elasticity	12.2×10^6 psi
Shear modulus	5×10^6 psi
Poisson's ratio	$\mu = 0.22$
Coefficient of thermal expansion (0 - 300°C)	44.0×10^{-7}/°C
Density (p), g/cc	2.50
Modulus of Rupture*	60.9×10^3 psi
Compressive Strength	$\geqslant 200 \times 10^3$ psi

Optical Properties**

Wave length, microns	0.30	0.50	0.75	1.00	1.25	1.50	1.75	2.00
Percentage Transmittance	0	92	92	89	89	90	91	91
Wave length	2.25	2.50	2.60	2.70	2.80	2.90	3.00	3.10
Percentage Transmittance	90	90	89	80	36	35	40	45
Wave Length	3.20	3.30	3.40	3.50	3.60	3.70	3.80	3.90
Percentage Transmittance	50	55	60	65	68	68	67	65
Wave Length	4.00	4.10	4.20	4.30	4.40	4.50	4.60	4.70
Percentage Transmittance	60	55	42	35	15	8	6	5
Wave length	4.80	4.90	5.00					
Percentage Transmittance	4	4	3					

* after ion exchange treatment that puts the surface of the specimen into compression.
** sample thickness 0.125 inch.

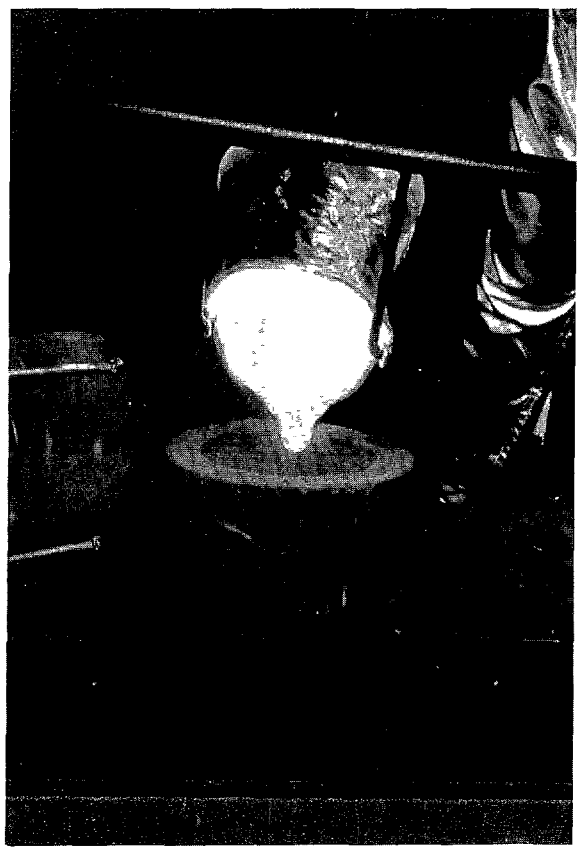

Figure C.1. Molten glass is poured into a graphite male mold.

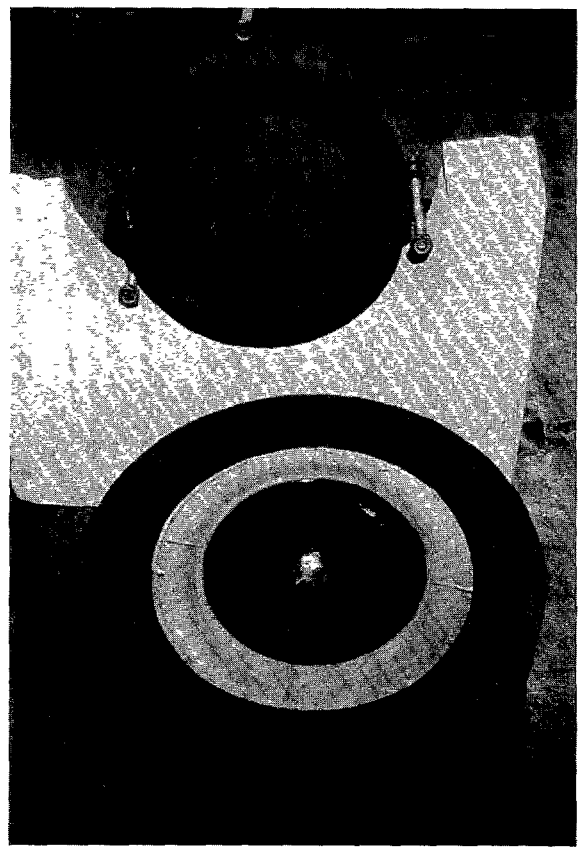

Figure C.2. After the gob of glass has been pressed by the insertion of the male mold it is ready for removal from the female mold.

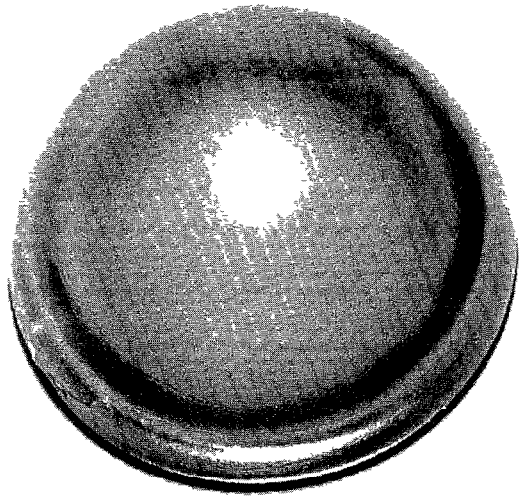

(a) Convex surface

(b) Concave surface

Figure C.3. Rough glass casting.

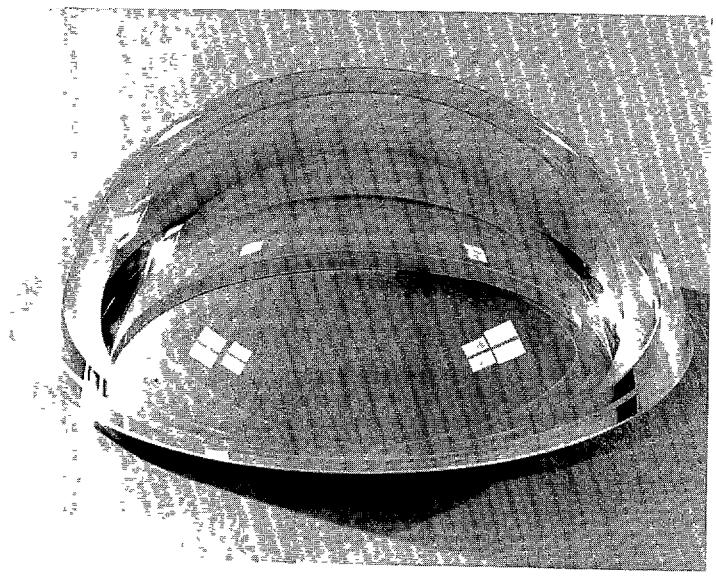

(a) Convex surface

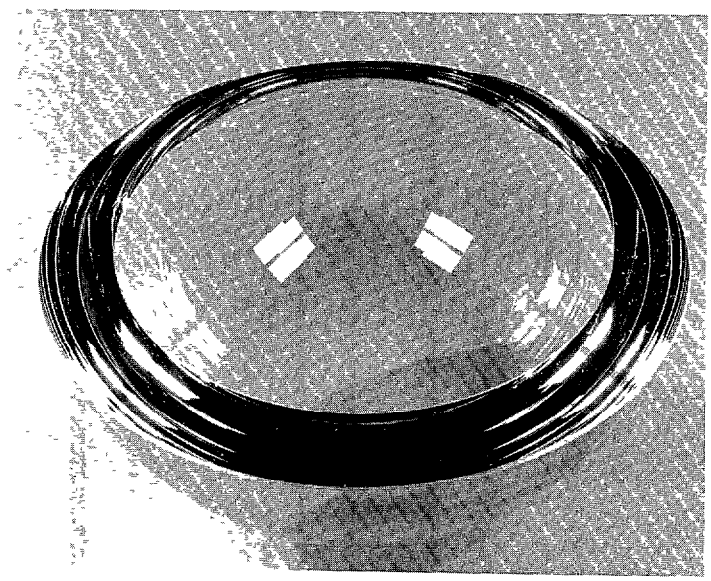

(b) Concave surface

Figure C.4. Ground glass window.

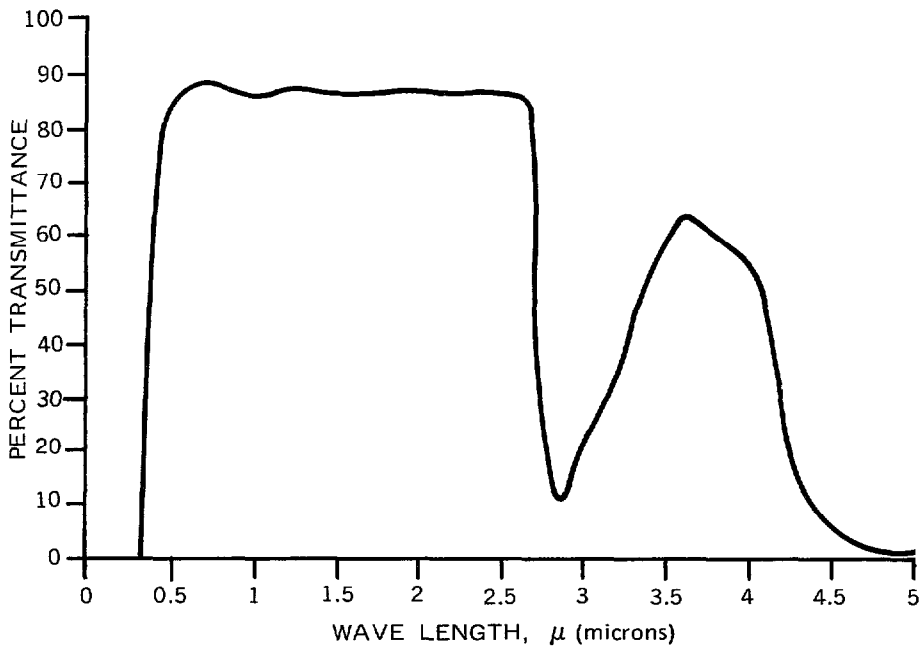

Figure C.5. Transmittance curve typical of Cer-Vit C-101; sample thickness 0.125 inch.

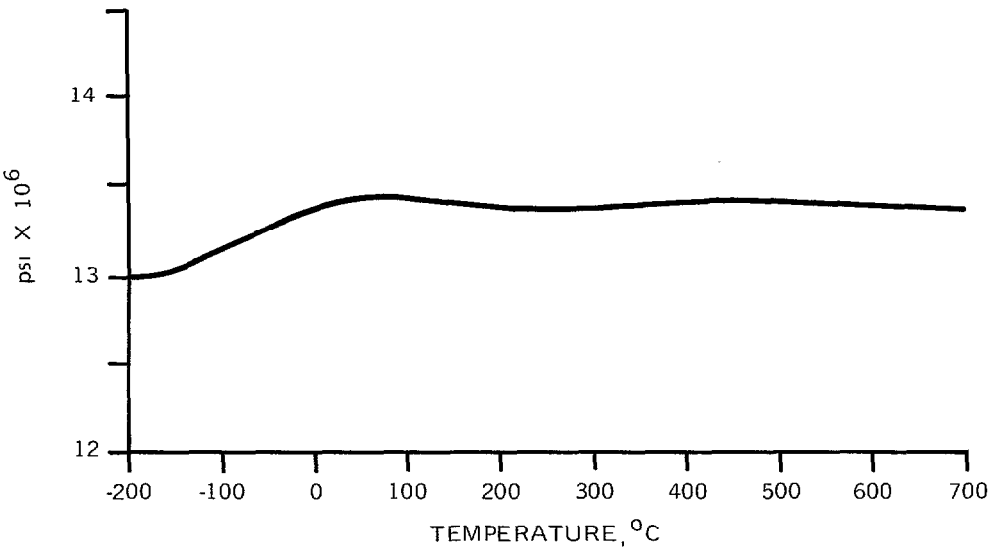

Figure C.6. Young's modulus for Cer-Vit C-101.

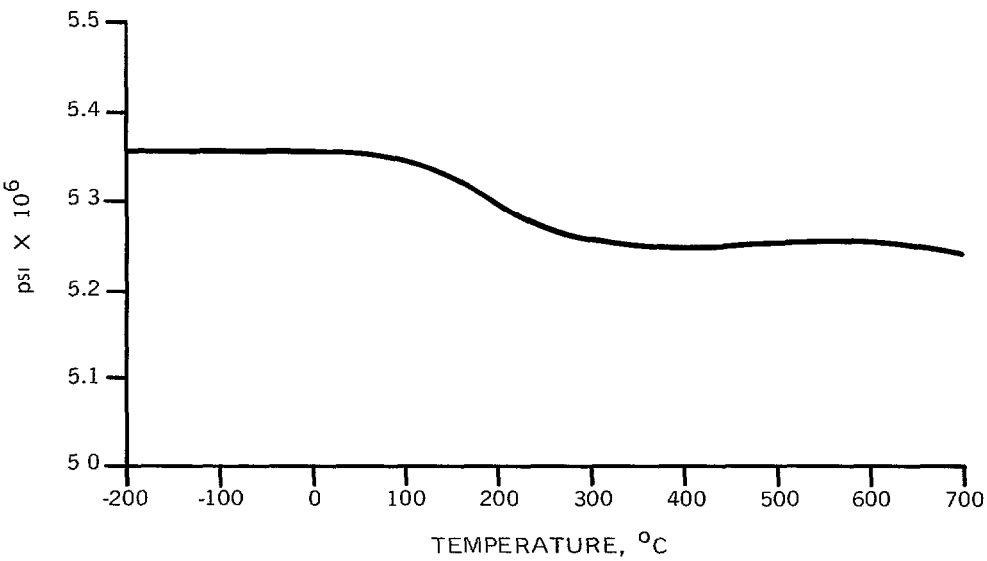

Figure C.7. Shear modulus for Cer-Vit C-101.

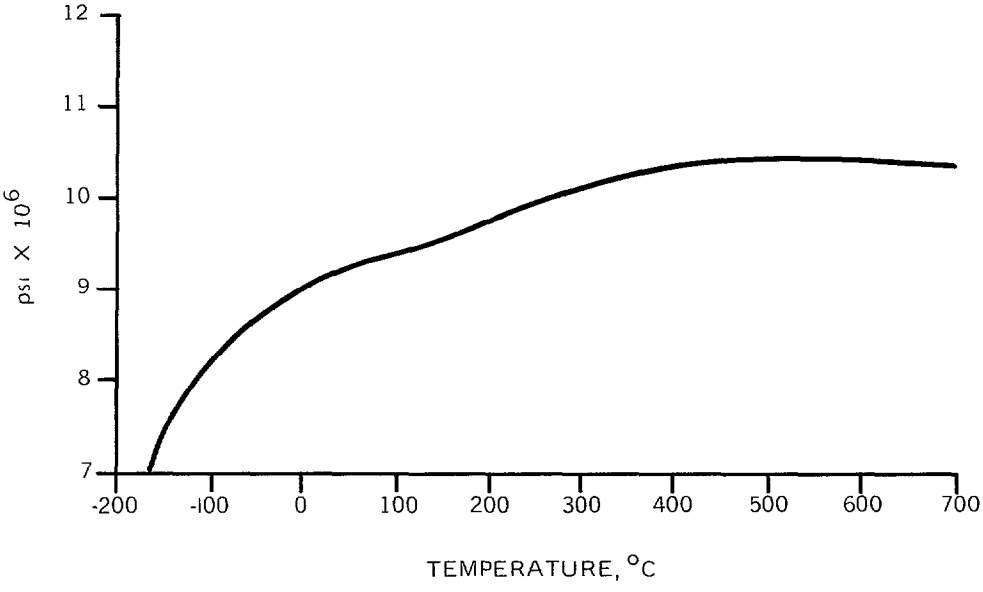

Figure C.8. Bulk modulus (B) for Cer-Vit C-101.

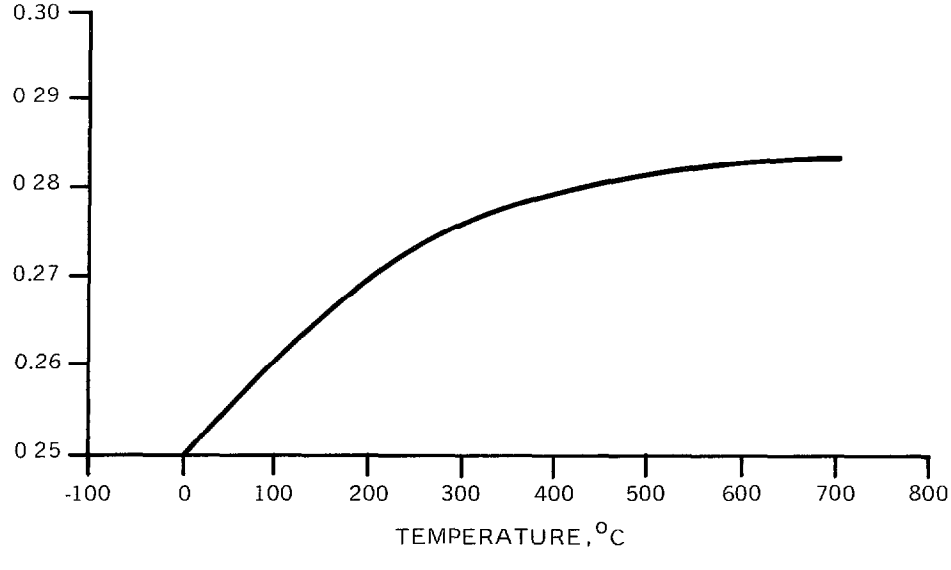

Figure C.9. Poisson's ratio for Cer-Vit C-101.

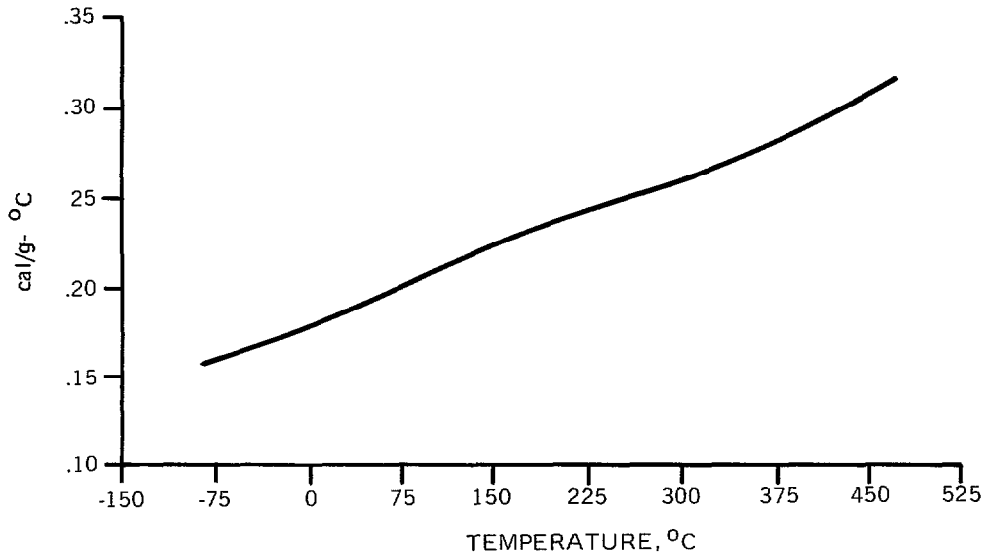

Figure C.10. Specific heat (C) for Cer-Vit C-101.

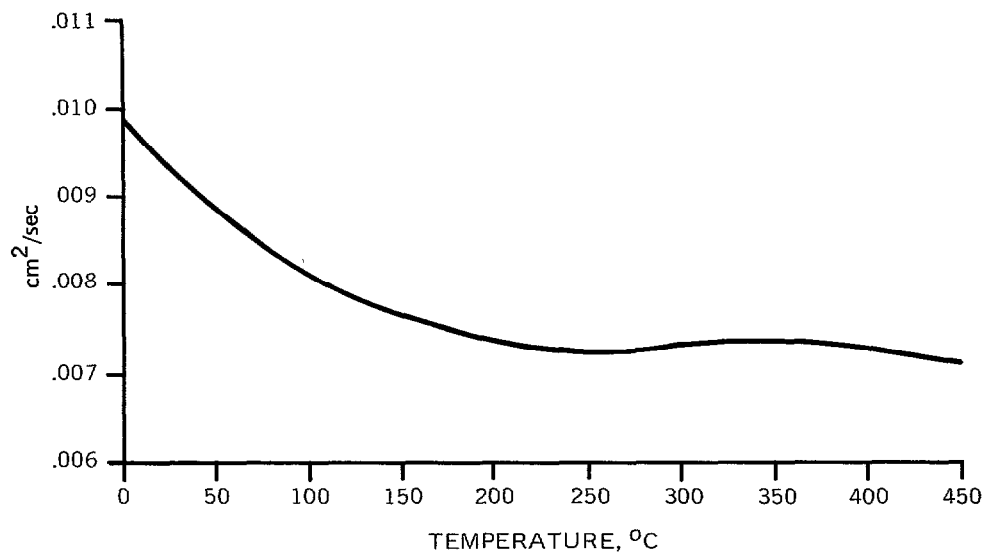

Figure C.11. Thermal diffusivity for Cer-Vit C-101.

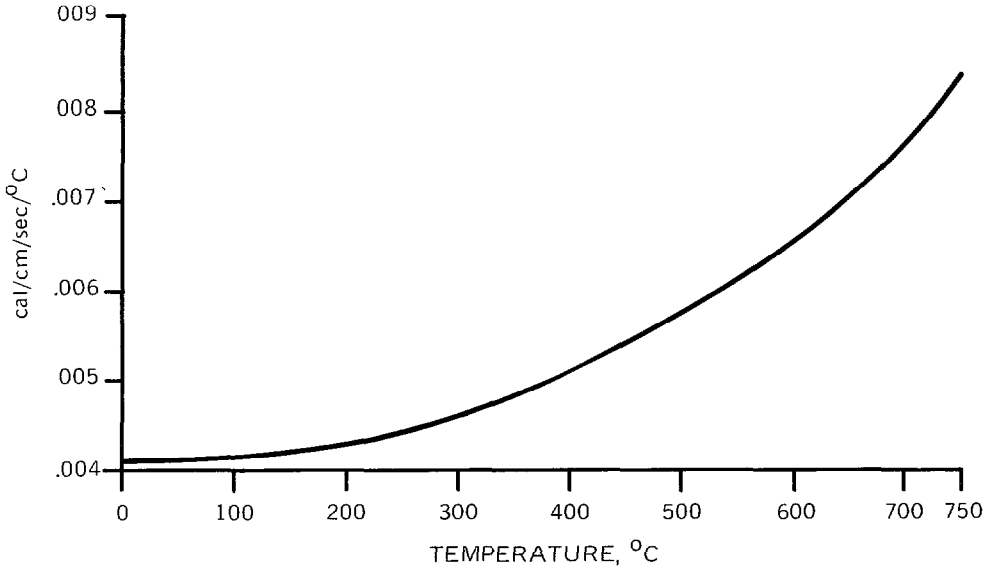

Figure C.12. Thermal conductivity for Cer-Vit C-101.

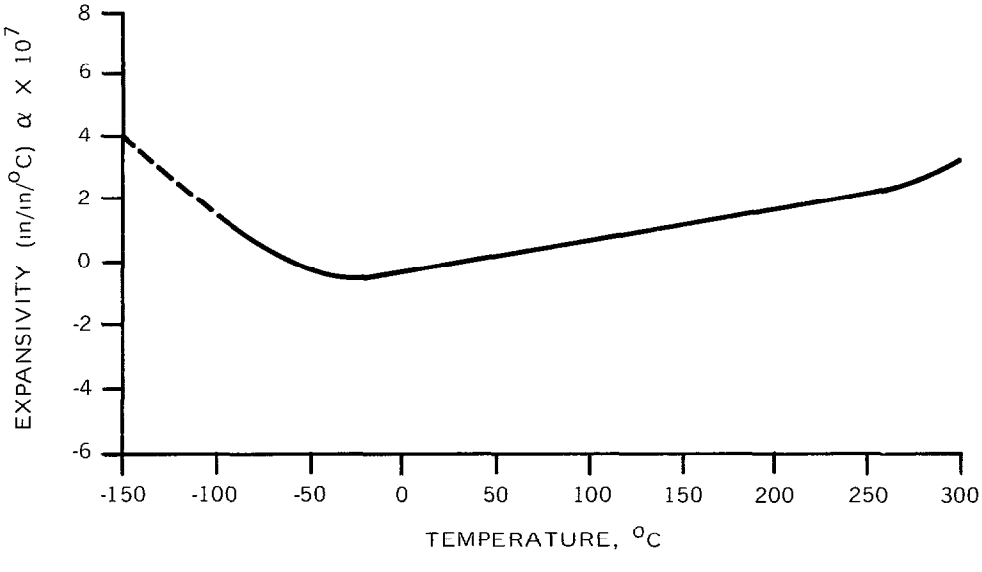

Figure C.13. Thermal expansion coefficient (α) for Cer-Vit C-101.

APPENDIX D

ACOUSTIC EMISSIONS

DISCUSSION

Since recording of acoustic emissions from structural test specimens under load has been found since its inception (reference D.1) to be a valuable research tool (reference D.2), several NUC 150-degree spherical window assemblies were instrumented with accelerometers (160-kHz response) so that their acoustic emissions could be recorded while they were subjected to hydrostatic pressure tests.

As test specimens served glass ceramic Cer-Vit C-101 window specimen 2 and chemically surface-compressed Cer-Vit SSC-201 window specimen 12. They were mounted on regular NUC 150-degree spherical window flanges using Fairprene 5722A bearing gaskets. After the whole window assembly was bolted together, it was placed on a steel bulkhead and locked inside a 10-inch-diameter pressure vessel at the Southwest Research Institute. Steps were taken to isolate the test specimen from the vibrations generated by the pump and the expanding pressure vessel so that the acoustic emissions recorded would represent only the response of the window assembly and bulkhead to increasing external hydrostatic pressure.

The vessel was pressurized at a rate of 500 psi/minute with a small, positive-displacement, air-operated pump. After the vessel was pressurized to 20,000 psi, the pressure was maintained for two hours and then dropped to 0 psi. After 30 minutes of relaxation the vessel was pressurized again to 20,000 psi and held at that pressure for two hours prior to de-pressurization.

RESULTS

Because of the intimate contact between the window and other components of the window test assembly, the recorded acoustic emissions represent a sum of emissions from all of the components. Thus, it is impossible to place a numerical value on the acoustic emissions generated only by the window. Still, comparison of (figure D.1 and D.2) the acoustic emissions from glass and glass ceramic windows generated during the first and second pressure cycles permits certain general observations.

1. The number of emissions generated during the first pressurization was an order of magnitude larger than the number of emissions generated during the second pressurization of the same window test assembly.

2. The number of acoustic emissions generated by the window test assembly incorporating the Cer-Vit C-101 glass ceramic window was several orders of magnitude larger (figure D.1) than the number of acoustic emissions generated by the window test assembly incorporting the Cer-Vit SSC-201 glass window (figure D.2).

3. The rate of acoustic emissions began to increase rapidly only after the pressurization of a window test assembly passed the 16,000-psi pressure value.

4. The rate of acoustic emissions generated by Cer-Vit C-101 glass ceramic window test assembly during sustained pressure loading at 20,000 psi decreased rapidly with time (Table D.1).

5. The number of acoustic emissions generated by Cer-Vit C-101 glass ceramic window test assembly during the first sustained pressure loading (Table D.1) at 20,000 psi was an order of magnitude larger than during that generated during the second sustained pressure loading.

CONCLUSIONS

1. Since identical window test jigs were used to test the C-101 glass ceramic and SSC-201 glass windows, it must be concluded that surface-compressed glass windows are poor sources of acoustic emissions prior to the appearance of macro-cracks. In all probability, the few acoustic emissions recorded during testing of SSC-201 glass windows were generated by the metallic parts of the assembly rather than by the glass window. This substantiates a previously reported finding (reference D.2) that while ceramics are excellent sources of acoustic emissions glass is a very poor one.

2. Since the acoustic emission pattern of glass ceramic exhibits a very pronounced Kaiser effect, it may be concluded that the use of acoustic emission instrumentation during structural tests and analysis of acoustic emission data may be applied to glass ceramic material for detection of incipient failures.

REFERENCES

1. Kaiser, J., "Untersuchungen ueber das Auftreten des gerausches beim Zugversuch", PhD. Thesis, Technische Hochschule, Muenchen, 1950.

2. Graham, L. J., and Alers, G.A., "Investigation of Acoustic Emission From Ceramic Materials", North American Rockwell/Science Center, Final Report, Naval Air Systems Command, Contract No. N000-19-71-C-0344, AD 745000, May 1972.

Table D.1. Acoustic Emission During Sustained Hydrostatic Loading to 20,000 psi.

Test specimen	Material	Cycle number	Duration of sustained pressure loading	Acoustic emission No. of events	Acoustic emission Rate (events/min.)
2	C-101	1st	30 minutes	108,700	3630
			60 minutes	147,300	1290
			90 minutes	163,000	555
			120 minutes	171,300	277
		2nd	60 minutes	19,700	327
			120 minutes	34,700	250
12	SSC-201	1st	60 minutes	1,300	
			120 minutes	1,600	
		2nd	60 minutes	6,200	
			120 minutes	1,900	

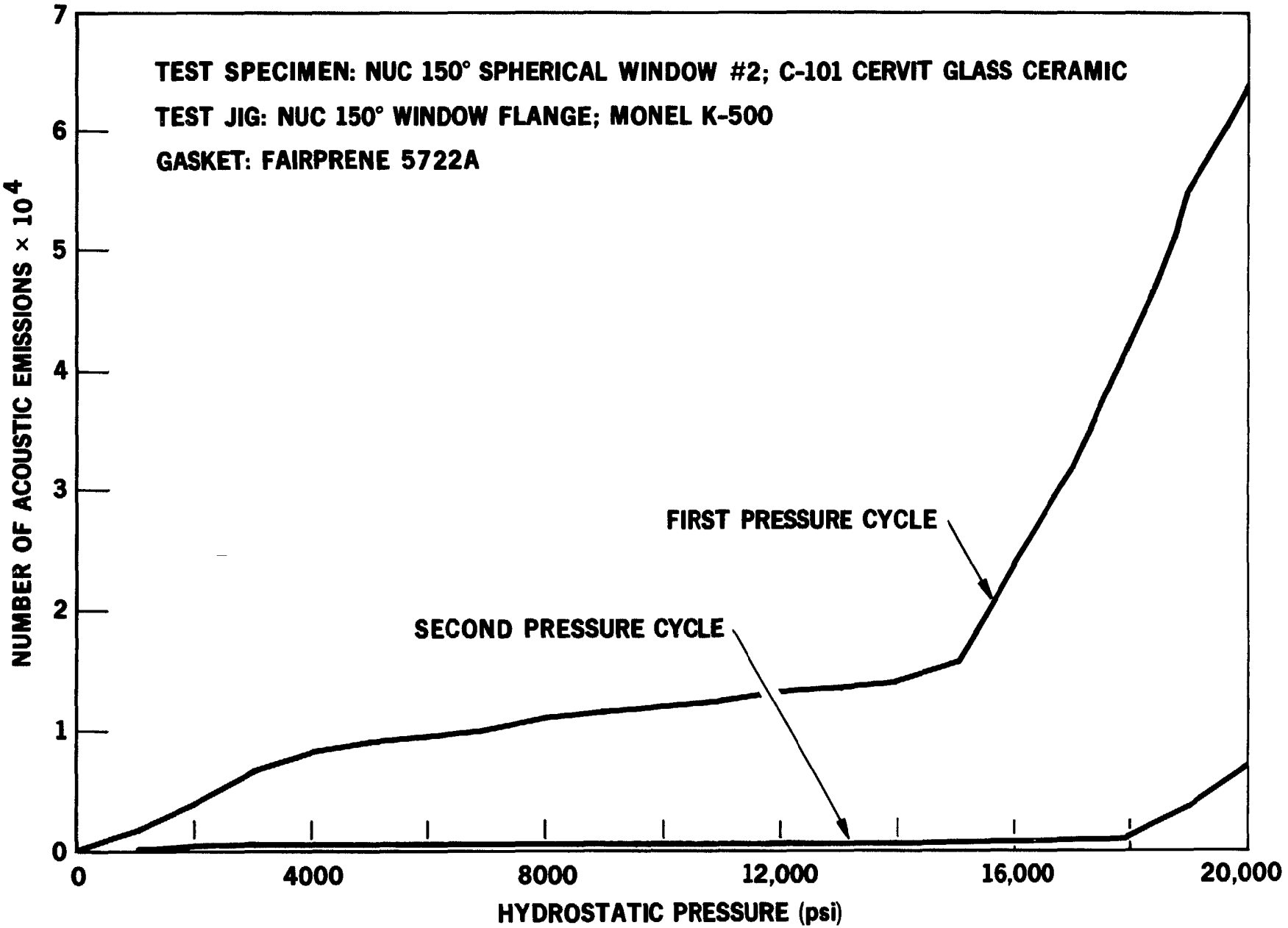

Figure D.1. Cumulative number of acoustic emissions generated by a C-101 glass ceramic, spherical window in NUC 150-degree conical flange seat when subjected to succeeding pressurizations from 0 to 20,000 psi.

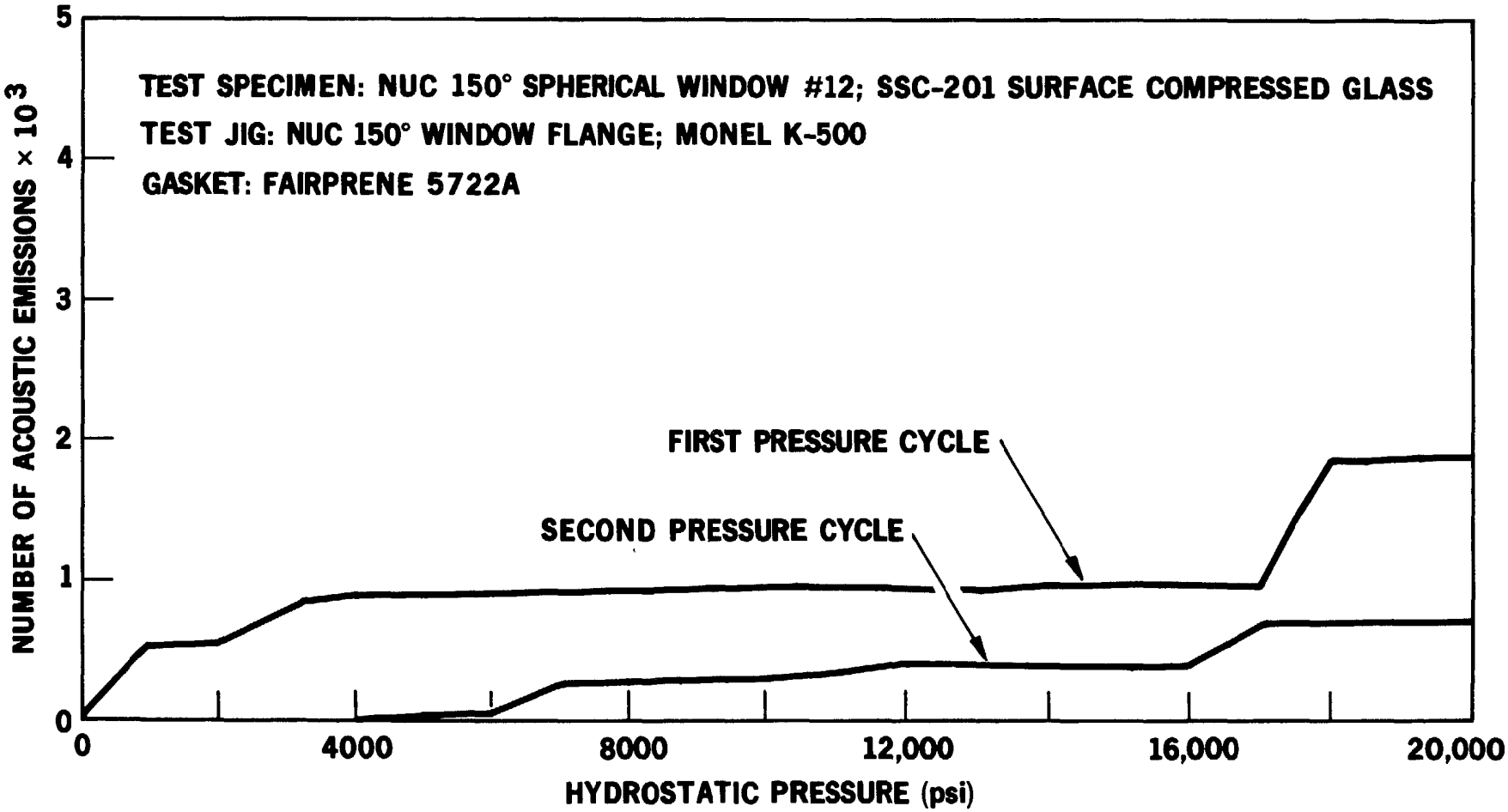

Figure D.2. Cumulative number of acoustic emissions generated by a SSC-201 surface-compressed glass, spherical window in NUC 150-degree conical flange seat when subjected to succeeding pressurizations from 0 to 20,000 psi.

APPENDIX E

COMPARISON OF EXPERIMENTAL AND ANALYTICAL STRESSES

Since during the calculation of stresses an assumption was made that the window flange was going to slide freely upon the hull it was of great interest to find out whether the flange behaved as predicted. For this purpose electric-resistance strain gages were bonded to the interior surfaces of the window and the flange at critical locations and their output was recorded at 100-psi pressure intervals as the external hydrostatic pressure was increased at a rate of 1000 psi/minute from 0 to 20,000 psi.

Several interesting observations can be made on the basis of plotted experimental data.

First, the negative circumferential strains in the window increase with the distance from the contact with the flange. The highest strain is at the apex, while the lowest on is at the bearing surface.

Second, the negative circumferential strains in the flange are about seven times smaller than those in the Cer-Vit C-101 window at the point of contact with the flange (figure E.1).

Third, the axial strains in the window at the point of contact with the flange are not only fifteen times smaller than those at the apex, but are also positive instead of negative (figure E.2).

On the basis of these observations it can be concluded that, contrary to the assumption previously made that sliding is not restrained, very little sliding occurred between the flange and the hull. Sliding between the window and the flange is very pronounced; but it also falls short of the ideal, unrestrained sliding. It can be also concluded that some moments are generated between the window and the flange.

When the experimentally generated stresses (figures E.3 and E.4) are compared to the calculated stresses (figures E.5, E.6, E.7, and E.8), a fair agreement is found between them on the window. On the flange, agreement is good only along the axial direction; in the circumferential direction, the experimental stress is three times lower than the calculated one. The reason for this is, of course, the absence of the assumed free sliding between the flange and the hull.

The sliding that does occur is only about one-third of that predicted (figure E.9) because of friction between the flange and the hull. The net effect is that the flange contracts in the radial direction as if it were made from

a material with a modulus of elasticity of 78 X 10^6 psi rather than 26 X 10^6 psi. Thus, one must conclude that the decision to fabricate the flange from a material with a modulus of elasticity of 26 X 10^6 psi was a sound one, as the friction forces that would have been superimposed on a stiffer flange would have decreased its radial contraction to such a degree that the flange would have failed to support the radially contracting window at its inner edge.

It can be concluded that the chosen design and materials for the window-flange assembly make it function within acceptable stress levels and displacements even at the maximum 20,000-psi hydrostatic pressure loading.

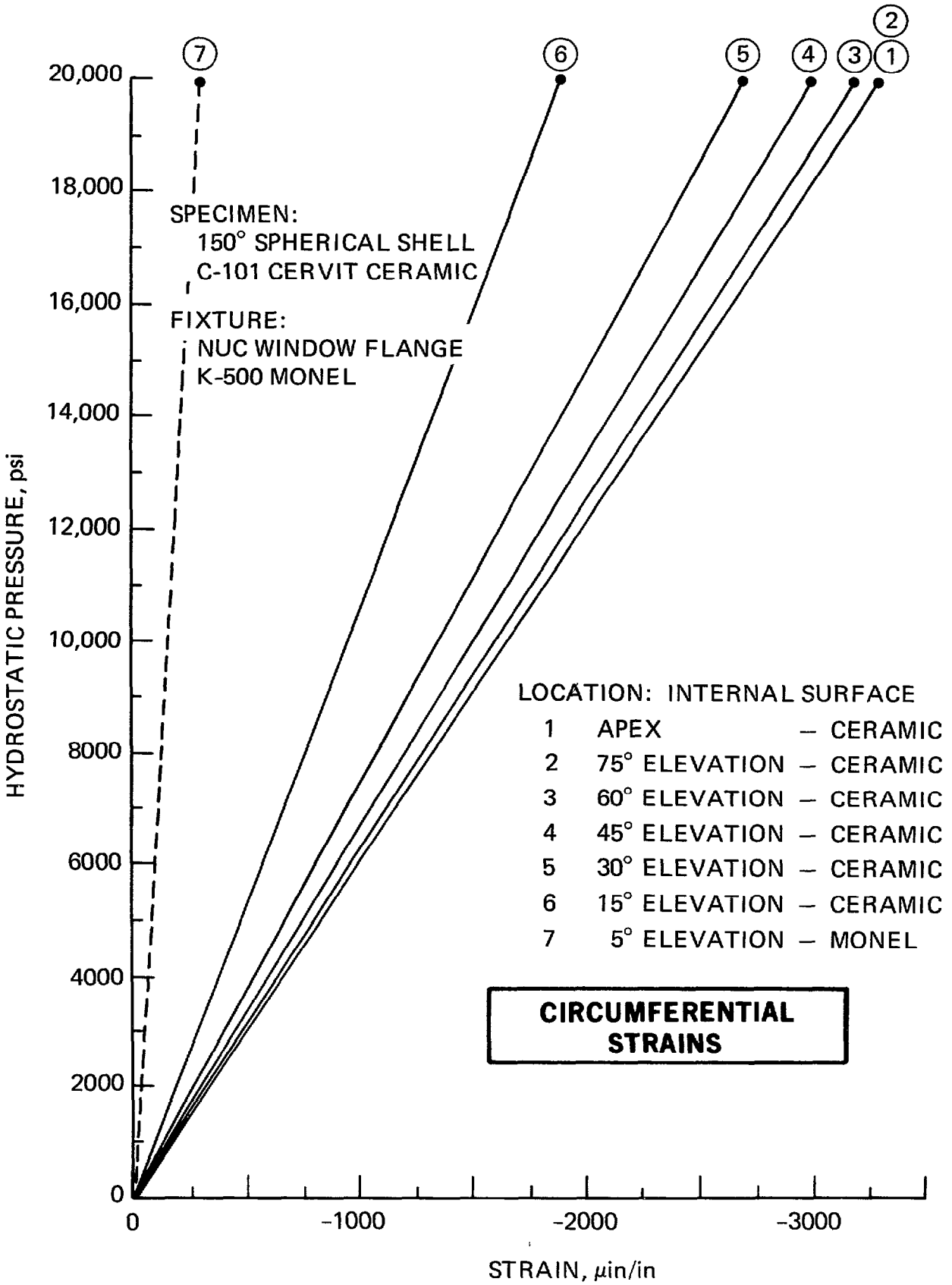

Figure E.1. Comparison of circumferential strains in Cer-Vit C-101 window and Monel K-500 flange.

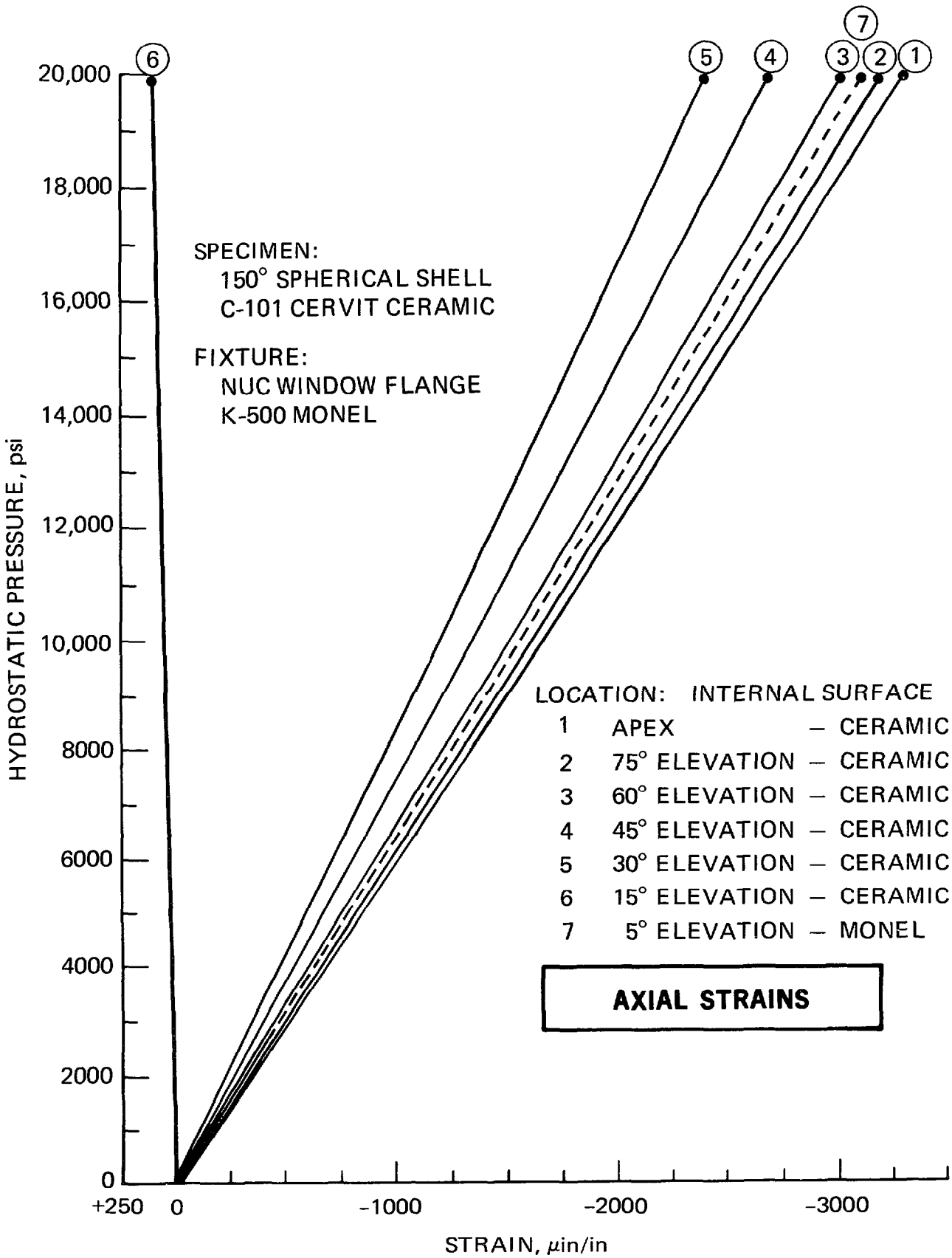

Figure E.2. Comparison of axial strains in Cer-Vit C-101 window and Monel K-500 flange.

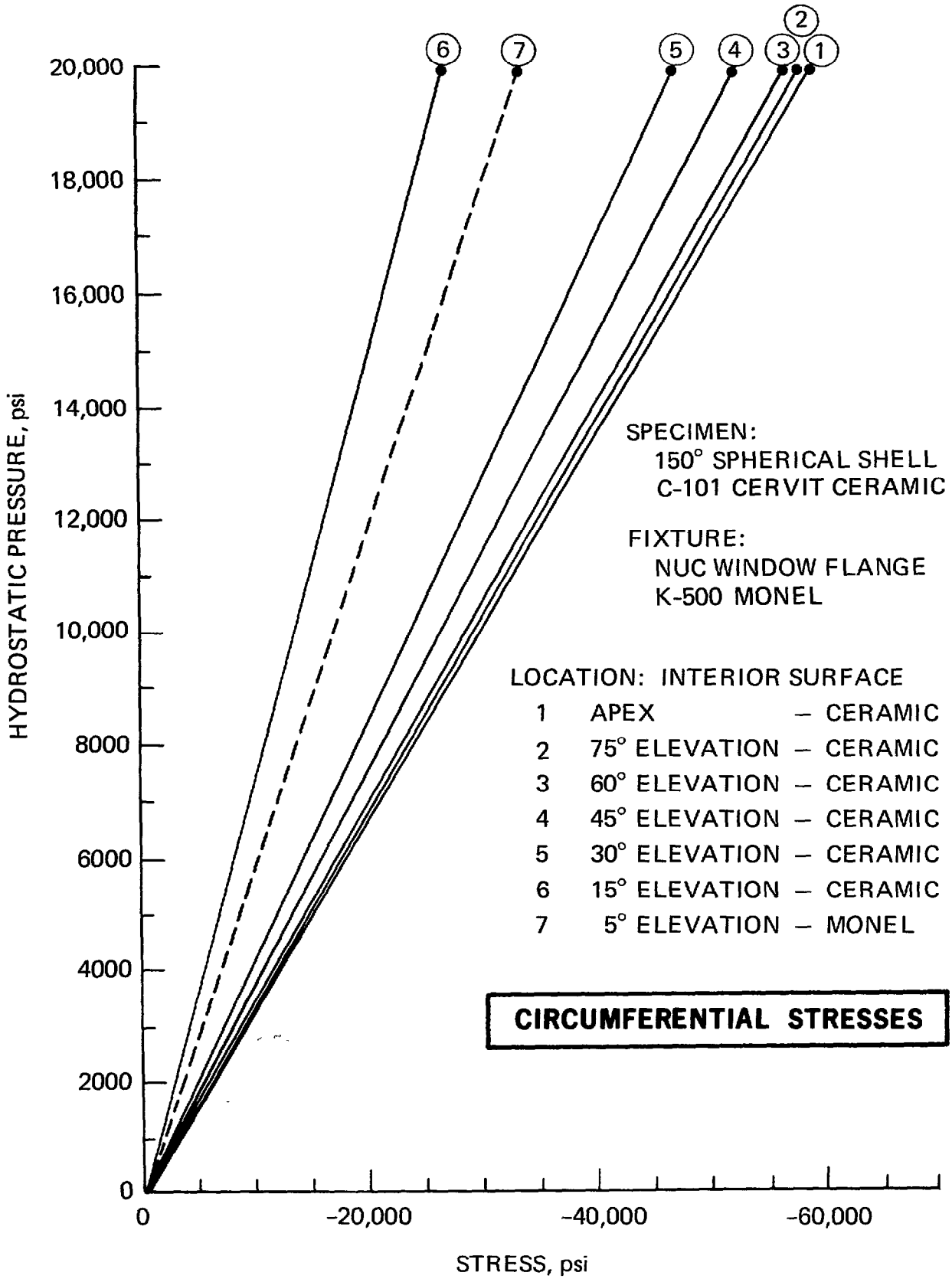

Figure E.3. Experimentally generated stresses in Cer-Vit C-101 window and Monel K-500 flange.

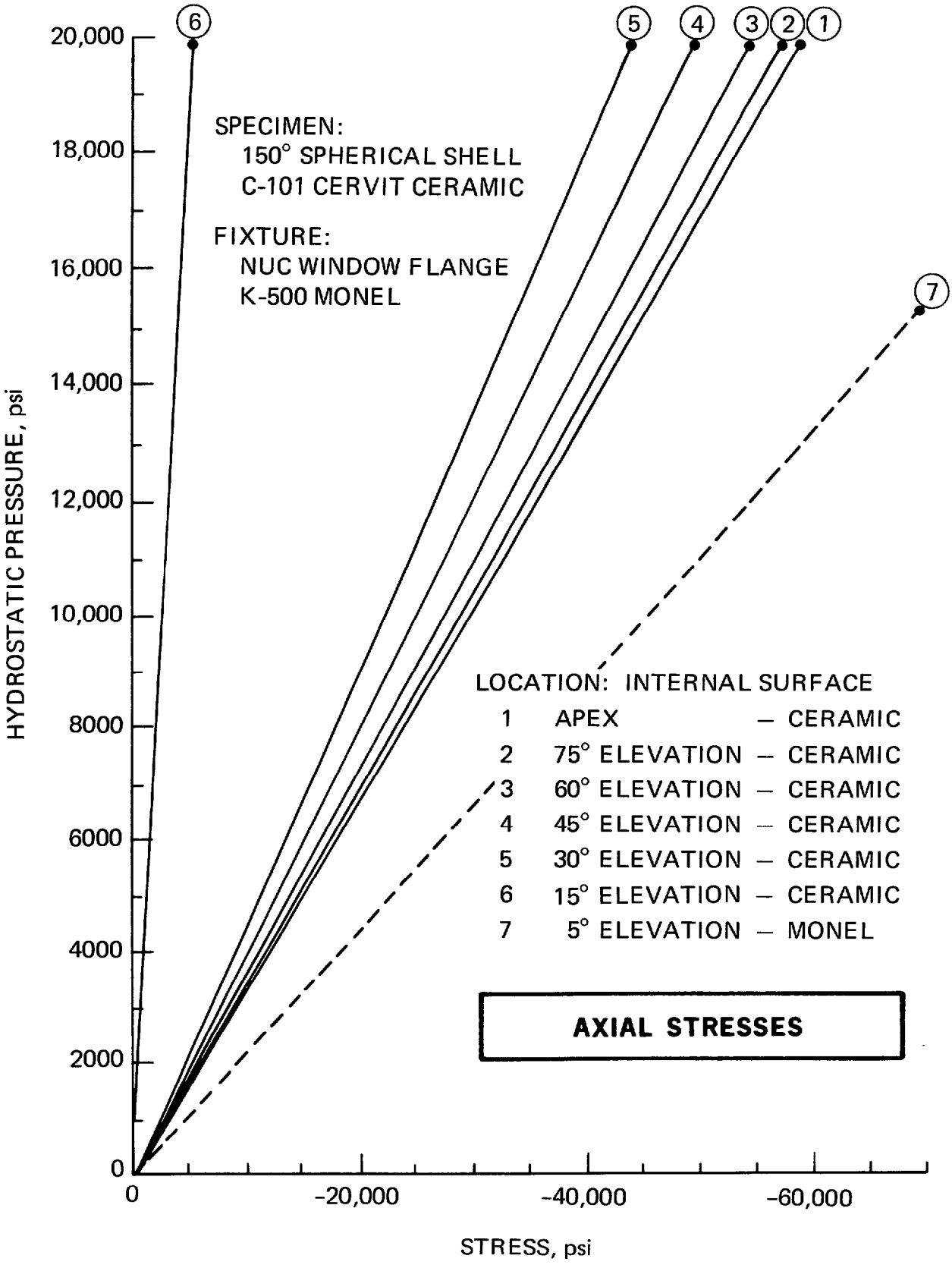

Figure E.4. Experimentally generated axial stresses in Cer-Vit C-101 window and Monel K-500 flange.

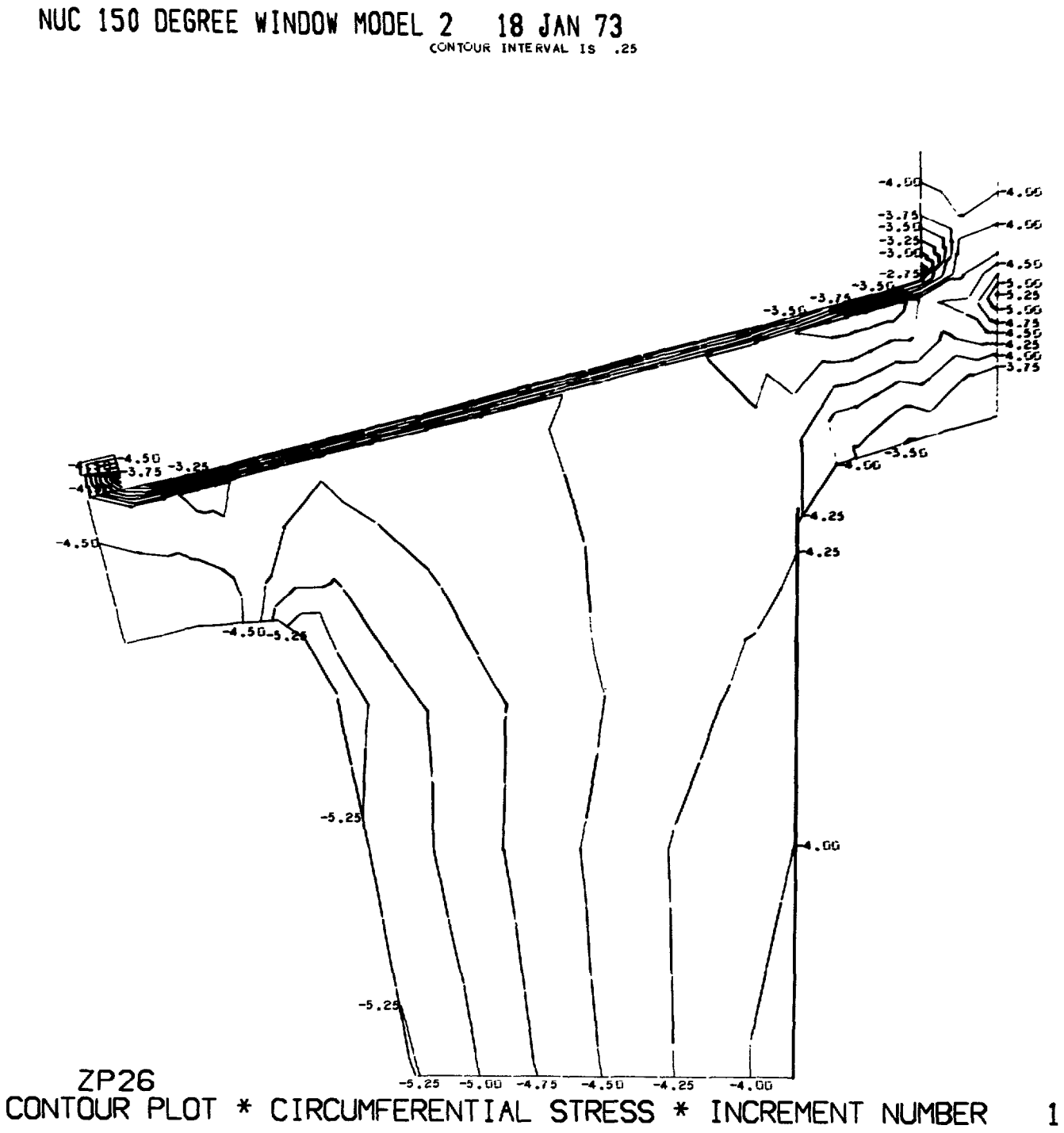

Figure E.5. Calculated circumferential stresses in Cer-Vit C-101 window and Monel K-500 flange. (sheet 1 of 2)

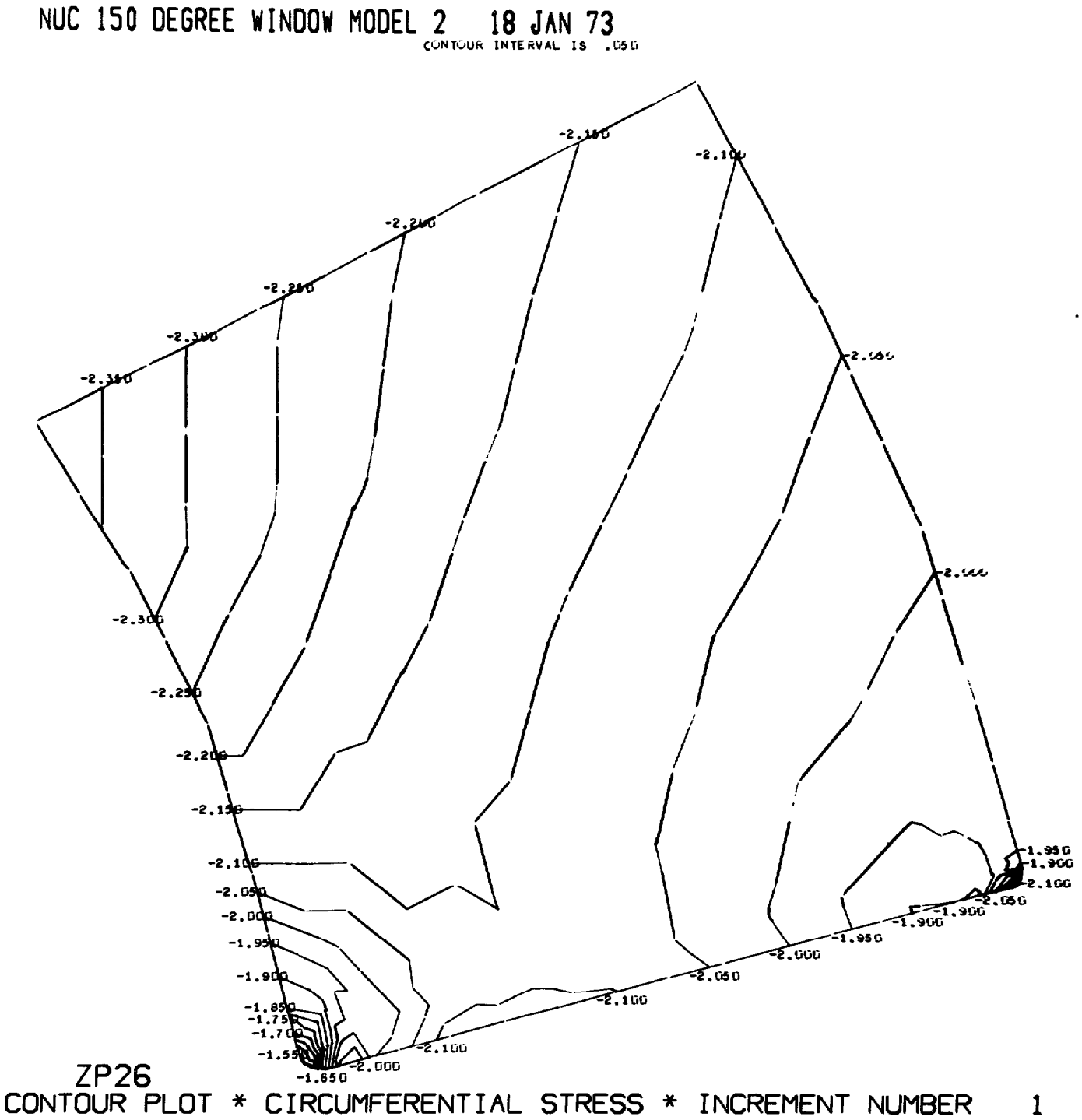

Figure E.5. Calculated circumferential stresses in Cer-Vit C-101 window and Monel K-500 flange. (sheet 2 of 2)

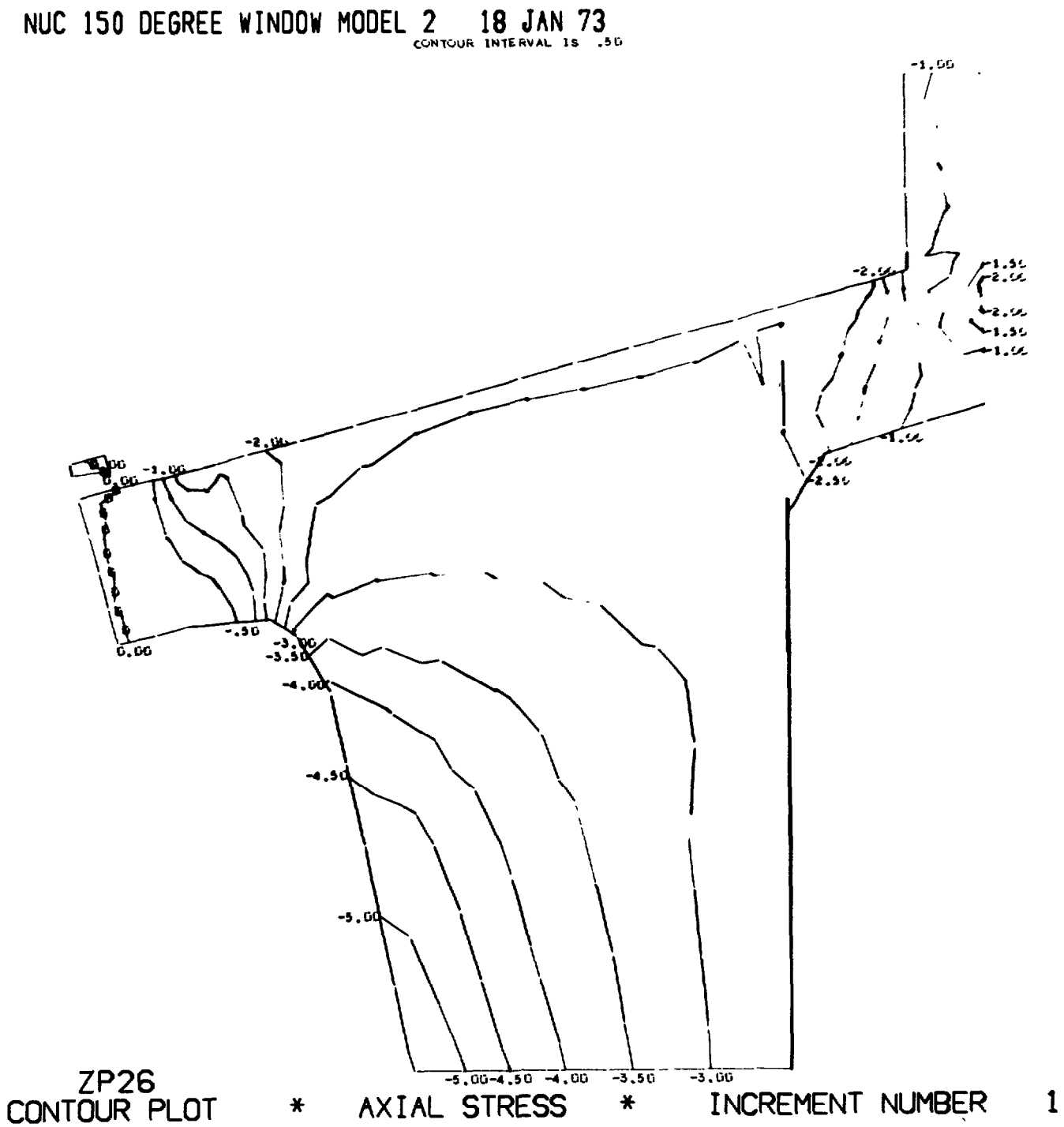

Figure E.6. Calculated axial stresses in Cer-Vit C-101 window and Monel K-500 flange. (sheet 1 of 2)

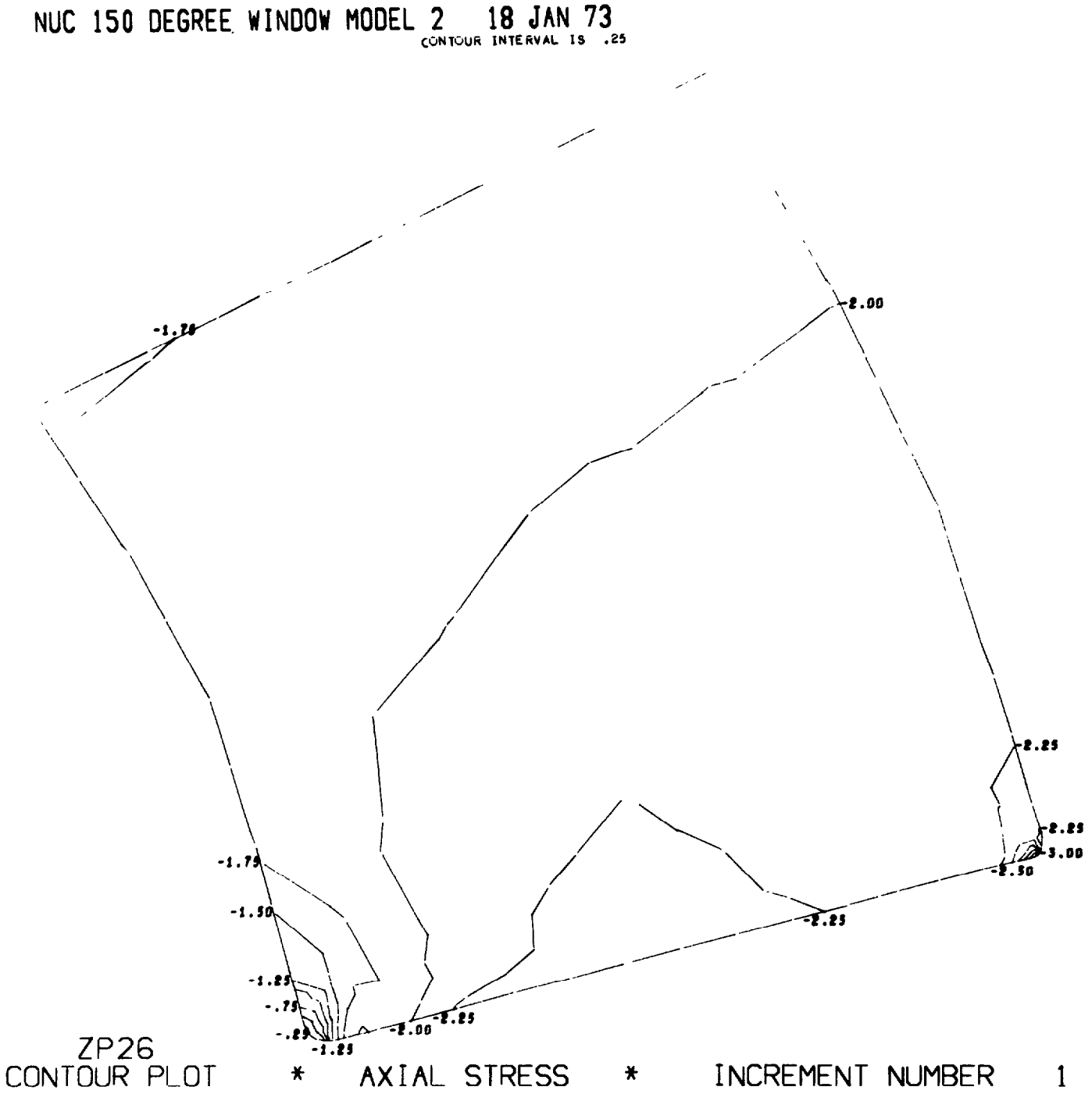

Figure E.6. Calculated axial stresses in Cer-Vit C-101 window and Monel K-500 flange. (sheet 2 of 2)

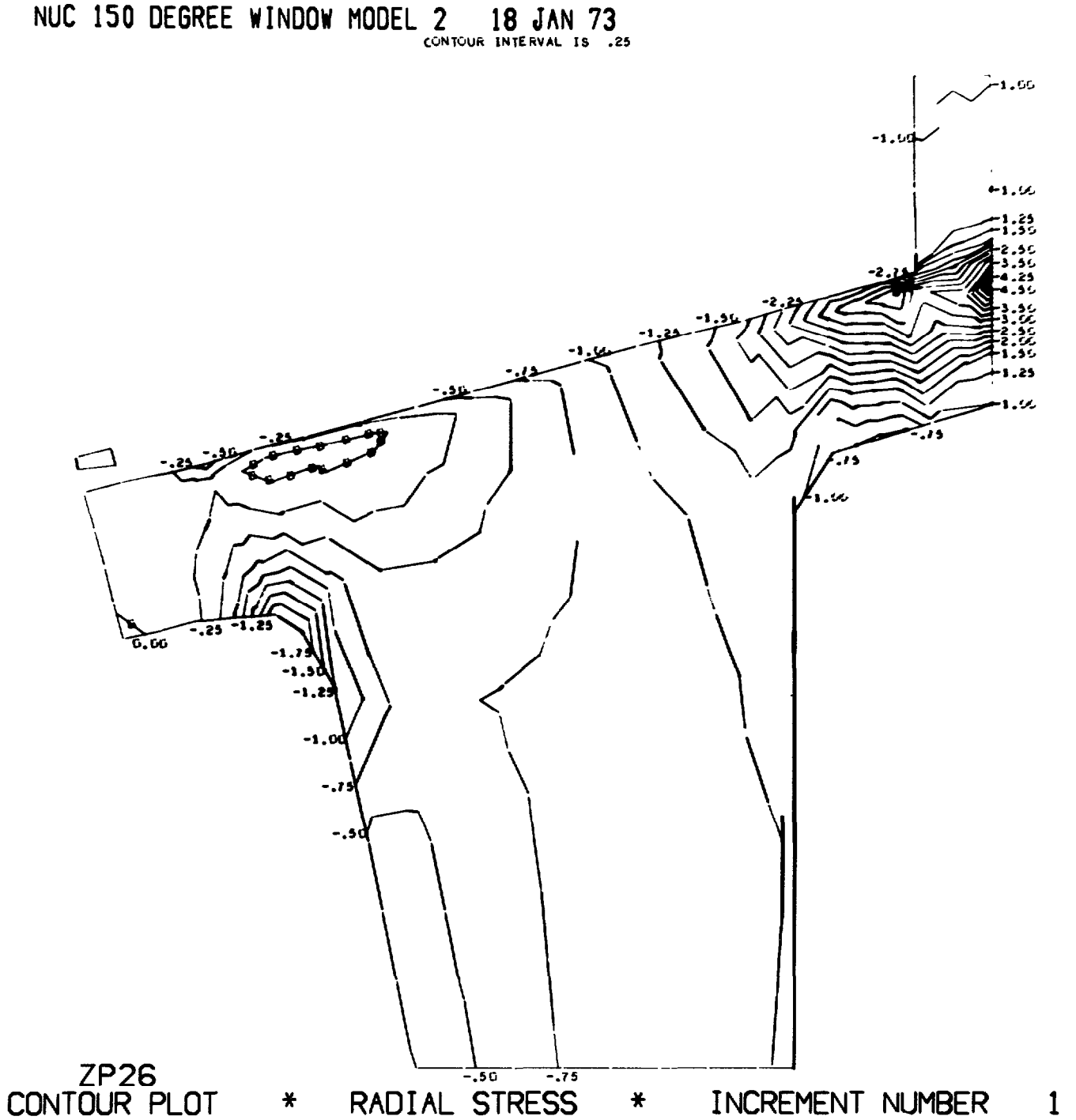

Figure E.7. Calculated radial stresses in Cer-Vit C-101 window and Monel K-500 flange. (sheet 1 of 2)

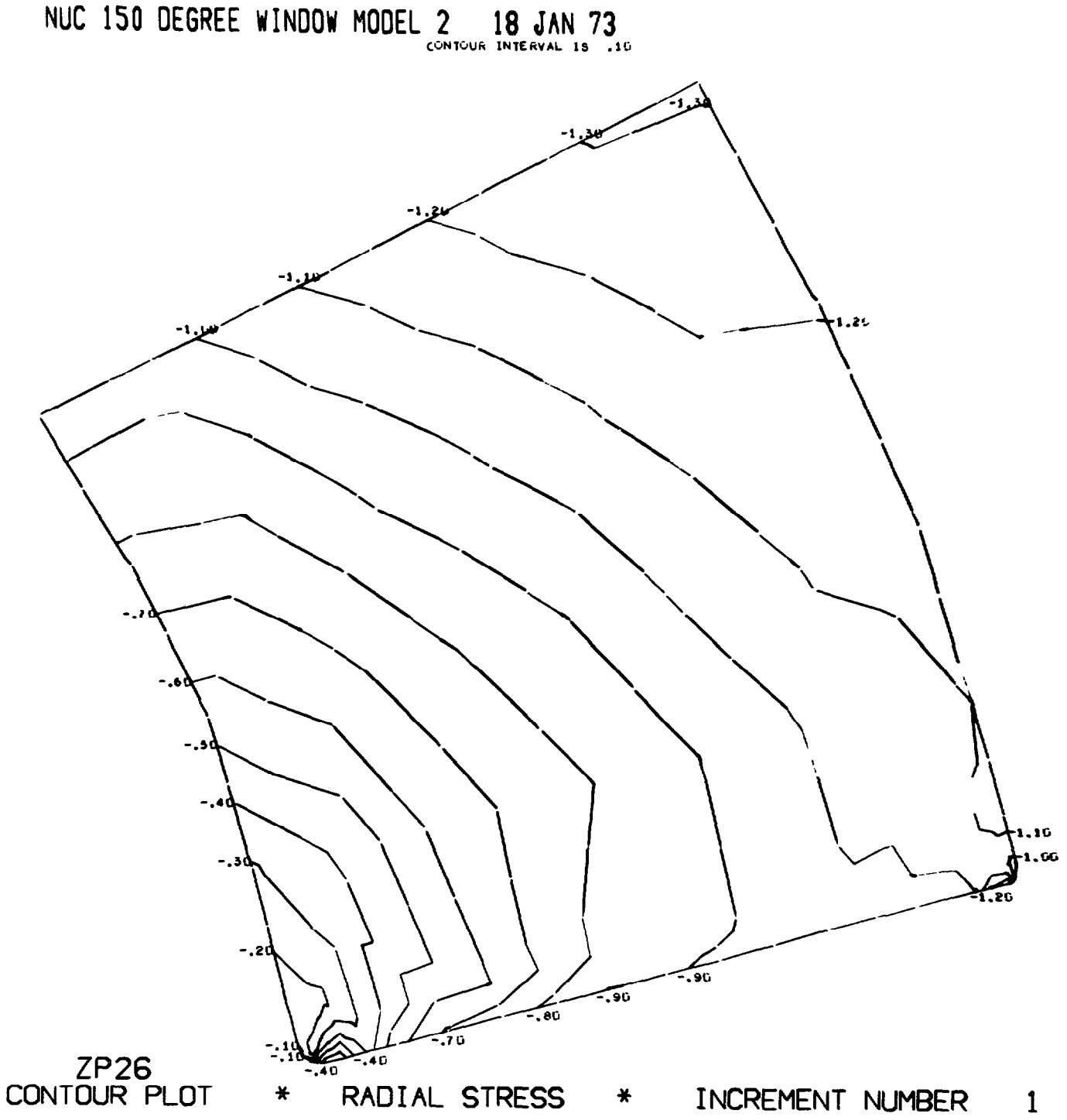

Figure E.7. Calculated radial stresses in Cer-Vit C-101 window and Monel K-500 flange. (sheet 2 of 2)

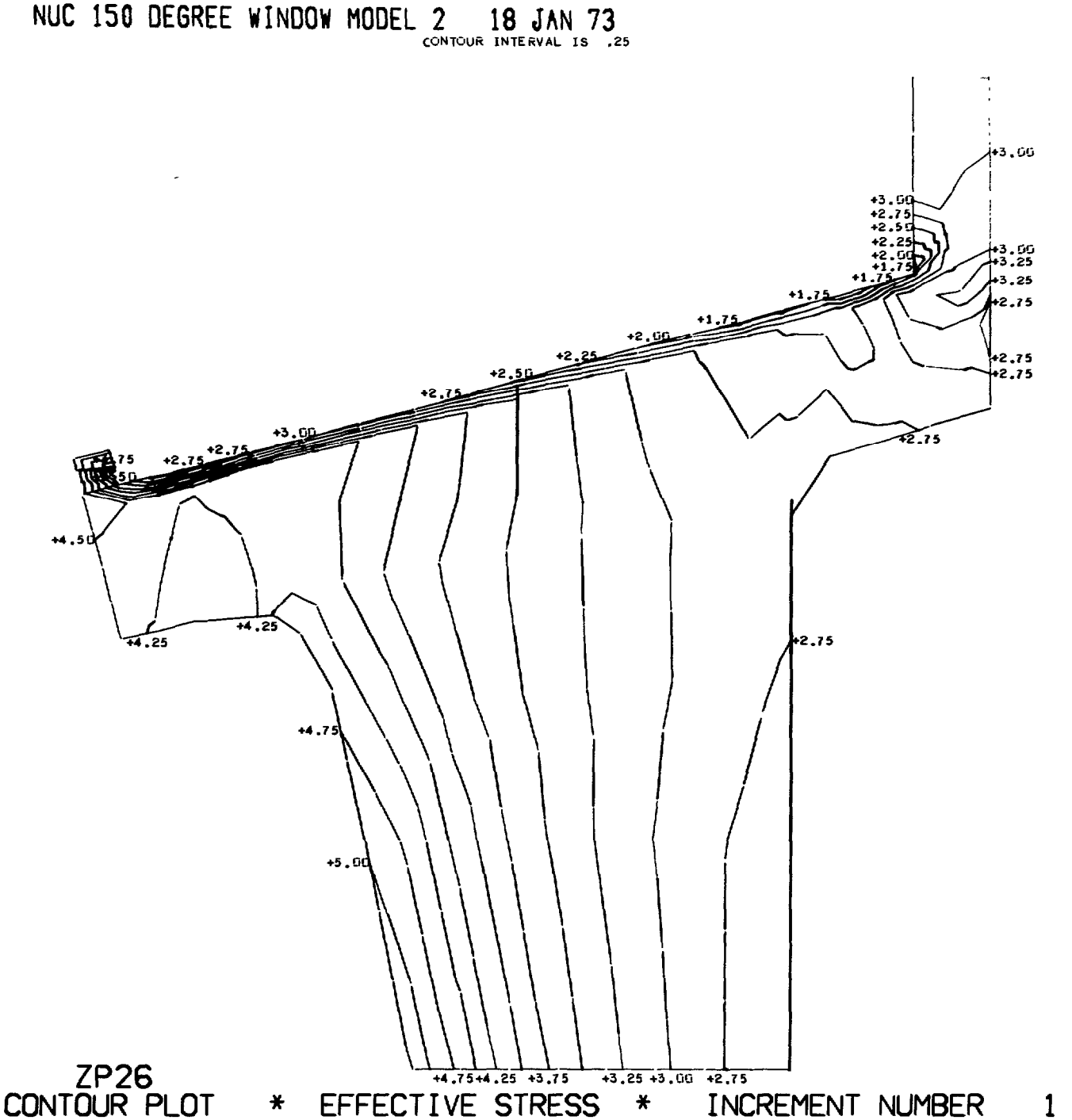

Figure E.8. Calculated effective stresses in Cer-Vit C-101 window and Monel K-500 flange. (sheet 1 of 2)

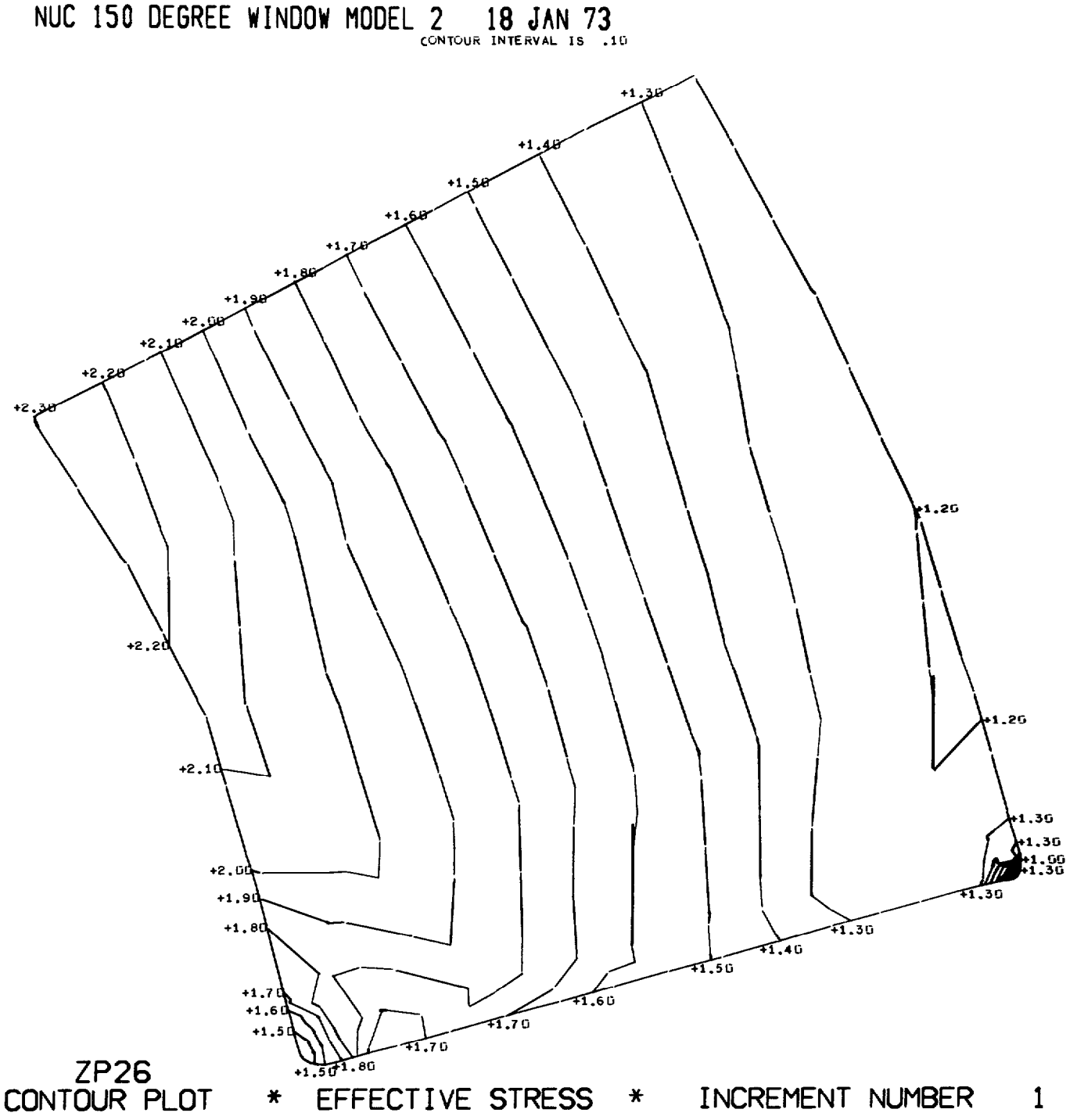

Figure E.8. Calculated effective stresses in Cer-Vit C-101 window and Monel K-500 flange. (sheet 2 of 2)

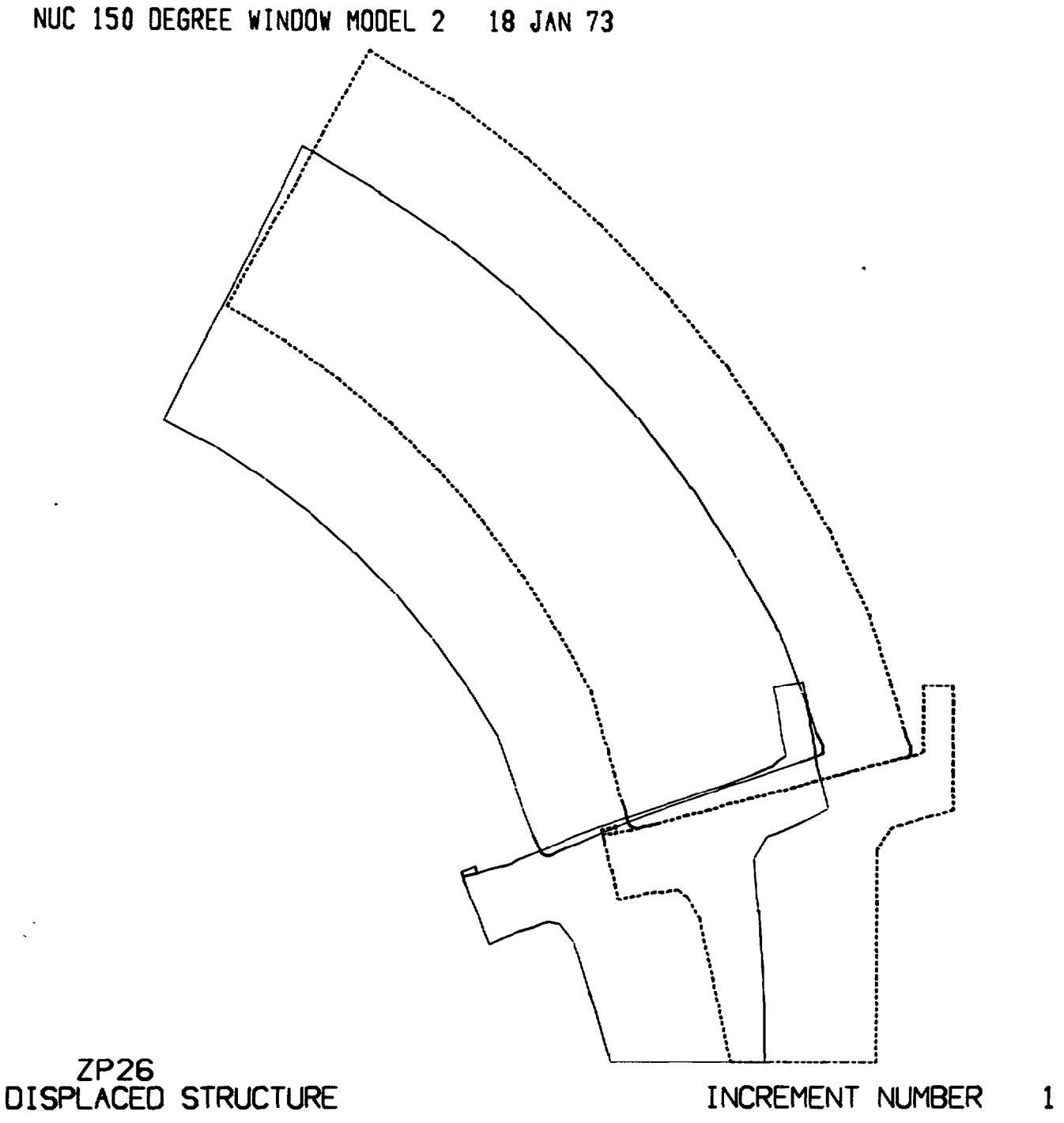

Figure E.9. Calculated displacements of Cer-Vit C-101 window and Monel K-500 flange.